Year: 2024

Brain Derived Extracellular Vesicles for the Stratification and Prediction of Tauopathies

Espourteille Jeanne

Espourteille Jeanne, 2024, Brain Derived Extracellular Vesicles for the Stratification and Prediction of Tauopathies

Originally published at : Thesis, University of Lausanne

Posted at the University of Lausanne Open Archive http://serval.unil.ch
Document URN : urn:nbn:ch:serval-BIB_CBE7569558F04

UNIL | Université de Lausanne
Faculté de biologie et de médecine

Centre de Neurosciences Psychiatriques

Brain Derived Extracellular Vesicles for the Stratification and Prediction of Tauopathies

Thèse de Doctorat en Neurosciences

Présentée à la

Faculté de biologie et de médecine
de l'Université de Lausanne

par

Jeanne Espourteille

Master de l'Université de Lausanne

Jury
Prof. Marlen Knobloch, Présidente
Prof. Nicolas Toni, Directeur de thèse
Dr. Kevin Richetin, Co-directeur de thèse
Prof. Gilles Allali, Expert
Dr. Lavinia Alberi, Experte

Thèse n° 412

Lausanne 2024

Programme Doctoral Interuniversitaire en Neurosciences des Universités de Lausanne et Genève

LEMANIC NEURO SCIENCE DOCTORAL SCHOOL

UNIL | Université de Lausanne

UNIVERSITÉ DE GENÈVE

UNIL | Université de Lausanne
Faculté de biologie et de médecine

Centre de Neurosciences Psychiatriques

Brain Derived Extracellular Vesicles for the Stratification and Prediction of Tauopathies

Thèse de Doctorat en Neurosciences

Présentée à la

Faculté de biologie et de médecine
de l'Université de Lausanne

par

Jeanne Espourteille

Master de l'Université de Lausanne

Jury
Prof. Marlen Knobloch, Présidente
Prof. Nicolas Toni, Directeur de thèse
Dr. Kevin Richetin, Co-directeur de thèse
Prof. Gilles Allali, Expert
Dr. Lavinia Alberi, Experte

Thèse n° 412

Lausanne 2024

Programme Doctoral Interuniversitaire en Neurosciences des Universités de Lausanne et Genève

LEMANIC NEURO SCIENCE DOCTORAL SCHOOL

UNIL | Université de Lausanne

UNIVERSITÉ DE GENÈVE

UNIL | Université de Lausanne

UNIVERSITÉ DE GENÈVE

Programme doctoral interuniversitaire en Neurosciences des Universités de Lausanne et Genève

Imprimatur

Vu le rapport présenté par le jury d'examen, composé de

Président·e	Madame	Prof.	Marlen Knobloch
Directeur·trice de thèse	Monsieur	Prof.	Nicolas Toni
Co-directeur·trice de thèse	Monsieur	Dr	Kevin Richetin
Expert·e·s	Monsieur	Prof.	Gilles Allali
	Madame	Dre	Lavinia Alberti

le Conseil de Faculté autorise l'impression de la thèse de

Madame Jeanne Espourteille

Titulaire d'un Master ès Sciences en biologie médicale
de l'Université de Lausanne

intitulée

Brain Derived Extracellular Vesicles for the Stratification and Prediction of Tauopathies

Lausanne, le 15 août 2024

pour Le Doyen
de la Faculté de Biologie et de Médecine

Prof. Marlen Knobloch

Pour mon Pépé, le premier Dr. Espourteille, qui m'a inspiré toute ma vie à suivre mes rêves, où qu'ils mènent dans le monde, à chérir mes amis comme la famille, et surtout à avoir une passion pour la vie.

Merci pour tout, je t'aime.

Acknowledgements

This thesis is the result of 4 long, difficult years which were also some of the most enriching and rewarding years of my life. It was far from an individual effort; there are many people who played a role in this work. From the bottom of my heart I'd like to thank those who helped me, whether scientifically or personally, to get to the finish line.

First and foremost, I would like to thank my supervisor and thesis co-director, Dr. Kevin Richetin, who first supervised my Master's project and allowed me to continue my project for a PhD afterwards. Thank you for your guidance, your endless ideas and motivation to try new things, and for your enthusiasm to make the lab group not just a group of colleagues, but friends as well. Thank you for pushing me to pursue opportunities I never would have pursued on my own, like going to Baltimore for a new lab collaboration. In a field that is relatively new and a project that is largely exploratory, I had many moments of doubt, frustration, and defeat, but you always motivated me to keep going, try a new angle, and ask important questions along the way. I have no doubt that you'll continue to do great things as a PI, thank you for everything.

I would also like to thank my thesis director, Pr. Nicolas Toni, who also supervised me throughout two degrees over the last 4 years. Thank you for all of your insightful advice, both scientific and about life, for your anecdotes about your time in the US that always made me feel a little piece of home, and for letting me stay in the Tonilab office even though you were worried we would be packed in like sardines as our group grew over the years.

And speaking of the Toni lab, thank you to the lab members for keeping me afloat the last 4 years on the days I wanted to quit science and open a bakery or move to the mountains with a flock of sheep. Thanks to Thomas and Charline for welcoming me all the way back in 2020, fresh out of lockdown, and for your all the insight, advice, and laughs since then. Thanks to Marta, Fabio, and Thibault for bringing amazing energy to the office. Thanks for all the lunches, coffee breaks, snacks, and nights out together. I wouldn't have made it to the end of this thesis without all of you.

And of course, thank you to the Richetin lab members, both past and present. In the beginning it was just Kevin and I, but over the years we've grown to a group of 5 with Luc, Valentin, and Aatmika. We all have quite different scientific and personal backgrounds, and this has made our professional and personal connections so enriching. Thank you for the engaging scientific discussion, for all the fun lab outings, and for all of your help in these last few months on this project. Thank you also to our former Master and Premaster students Lucas, Jean, and Alex for all of your work which contributed to this thesis, and for challenging me and making me a better scientist.

I would also like to thank Dr. Dimitrios Kapogiannis and Dr. Carlos Nogueras-Ortiz for welcoming me into the lab in Baltimore and for your amazing supervision and friendship during such a short time. This project wouldn't be what it is today without all of your help and expertise those 3 months and beyond.

To my family Stateside: thank you for your support from an ocean away. Thank you to Sebastien and Taylor for your encouragement, especially via funny memes and videos, and for actually wanting to read this thing. I hope you have a coffee ready. To Gaga and Poppy Pop, thank you for the daily Wordle updates, holiday cards, and constant love and support you send my way. I look forward to those

conversations and sharing a bit of our day together every day. To Auntie Pam, Uncle Jeff, Sarah, Jeffrey, and Dan, thank you for all of your messages of support and for making the best holiday cookies to look forward to every Christmas when I come home. Thank you all for believing in me through this journey.

To Elle, the one I've talked to probably every day for nearly the last 10 years as we did our Bachelor's together, then moved to Europe and did our Master's and Doctorate degrees together from different countries: thank you for absolutely everything. For countless 12-hour brunch zooms, for always being up for doing a random challenge with me, for amazing memories in Lausanne and Dublin (more still to come), and for your invaluable pep talks on the bad days. You're an absolute ray of sunshine and I couldn't have done this without you. You're so close to your finish line. Keep pushing forward and remember- you're not tired, you're fired up!!

To my friends in Lausanne and elsewhere in Europe, thank you for making this place my home away from home. Thanks for teaching me how to make so many new foods, for indulging my homesickness for events like Thanksgiving, and for always being down to travel, even just for a concert with little to no advanced notice. All the brunches, lake BBQs, dinners, hikes, ski days, river tubing, and nights out in Lausanne are some of my best memories over the last 5 years. Most of you are also PhD students or working in labs, so you understand all the ups and downs that come with this job, and not to expect a coherent answer to the question: "So what are you doing after your thesis?". The simple day-to-day with you guys is what I'll remember most from this period of my life.

To all the Lehigh people who have been a part of this journey, from Boston to California, thank you for staying in touch all these years. Thanks for letting me couch surf every time I come home so I can see as many of you as possible, for your unwavering friendship even through thousands of miles of distance, for amazing trips together, and for even schlepping all the way out here for a visit (or 3) throughout the years. You all have such a special place in my heart.

To the friends from home who have now survived 10-20+ of friendship with me, thanks for sticking around this long. To the Adams clan, Olivia, xxx, and others, thanks for always being up for a quick beach trip or lunch during my brief trips home, and even for coming out here for longer visits throughout the years too. It's amazing to have grown so much together and to still have you in my corner throughout this journey.

Lastly, I would like to thank my parents from the bottom of my heart. You have always supported me on this path of figuring out my passion, both emotionally and financially. From changing my major twice in my Bachelor's, to debating whether or not to move to Lausanne for the Master's, and then stay for the PhD, you have always listened to my doubts and worries, and told me that it's fine to be scared but to try it anyway. It's not easy to live so far away from most of my family, but having supportive parents cheering me on from the other side of the ocean has always calmed my nerves on the tough days. I don't think very many people in this field have parents who can challenge them on the scientific content of their work, but thank you to you both for sending me papers and news articles through the years, for the discussions on the tedious details of mass spectrometry that I have since forgotten, and for all of your questions and interest in my work. Most importantly, thank you for the moral support, particularly these last couple of months. It goes without saying, but I'll say it anyway, this never would have been possible without you.

Table of Contents

List of Abbreviations

3R	3-repeat
4R	4-repeat
AB	Amyloid beta
AD	Alzheimer's disease
AD-EV	Astrocyte derived extracellular vesicle
AF4	Asymmetrical flow field-flow fractionation
AGD	Argyrophillic grain disease
AJ	Adherens junction
AMP1	Astrocytic membrane protein 1
AMP124	Astrocytic membrane proteins 1, 2, 4
AMP2	Astrocytic membrane protein 2
AMP3	Astrocytic membrane protein 3
AMP4	Astrocytic membrane protein 4
AMP5	Astrocytic membrane protein 5
APC	Allophycocyanin
ATP	Adenosine triphosphate
BBB	Blood-brain barrier
BD	Brain derived
BD-EV	Brain derived extracellular vesicle
BP	Biological process
bvFTD	Behavioral variant frontotemporal dementia
CBD	Corticobasal degeneration
CBS	Corticobasal syndrome
CC	Cellular component
CJD	Creutzfeldt-Jakob disease
CN	Cognitively normal
CNS	Central nervous system
CryoEM	Cryogenic electron microscopy
CSF	Cerebrospinal fluid
DAB	Diaminobenzadine
DGUC	Density gradient ultracentrifugation

DMSO	Dimethylsulfoxide
DNA	Deoxyribonucleic acid
DTT	Dithiothretinol
EC	Endothelial cell
EDTA	Ethylenediaminetetraacetic acid
ELISA	Enzyme-linked immunosorbent assay
EM	Electron microscopy
EMA	European medicines agency
EOD	Early onset dementia
ER	Endoplasmic reticulum
ESCRT	Endosomal sorting complexes required for transport
EV	Extracellular vesicle
FC	Fragment crystallizable
FDA	Food and drug administration
FDR	False discovery rate
FFPE	Formalin-fixed paraffin-embedded
FSC	Forward scatter
FT	Flowthrough
FTD	Frontotemporal dementia
FTD-MND	Frontotemporal dementia with motor neuron disease
FTLD	Frontotemporal lobar degeneration
FUS	Fused in sarcoma
GAI	Globular astrocytic inclusion
GFT	Gliofibrillary tangle
GGT	Globular glial tauopathy
GO	Gene ontology
GOI	Globular oligodendroglial inclusion
HABA	4´-hydroxyazobenzene-2-carboxylic acid
HAP	High abundance protein
HC	Healthy control
HCD	Higher energy collisional dissociation
HIV	Human immunodeficiency virus
HPLC	High-performance liquid chromatography

iBAQ	Intensity-based absolute quantification
IHC	Immunohistochemistry
ILV	Intraluminal vesicle
IP	Immunoprecipitation
iPSC	Induced pluripotent stem cell
ISF	Interstitial fluid
JAM	Junctional adhesion molecule
LAP	Low abundance protein
LB	Lewy body
LBD	Lewy body disease
LC-MS/MS	Liquid chromatography with tandem mass spectrometry
LFQ	Label-free quantification
mAb	Monoclonal antibody
MCI	Mild cognitive impairment
MeCN	Methyl cyanide
MF	Molecular function
MISEV	Minimal information for the studies of extracellular vesicles
miST	Modified in-stage tip
MND	Maladies neurodégénératives
MRI	Magnetic resonance imaging
MVB	Multivesicular body
naPPA	Nonfluent variant primary progressive aphasia
NDD	Neurodegenerative disease
NfL	Neurofilament light chain
NFT	Neurofibrillary tangle
NTA	Nanoparticle tracking analysis
NVU	Neurovascular unit
PAF	Protein analysis facility
PART	Primary age-related tauopathy
PBS	Phosphate-buffered saline
PD	Parkinson's disease
PE	Phyocoerythrin
PEG	Polyethylene glycol

PET	Positron emission tomography
PHF	Paired helical filaments
PiD	Pick's disease
PK	Proteinase K
PMSF	Phenylmethylsulfonyl fluoride
PPA	Primary progressive aphasia
PSP	Progressive supranuclear palsy
PSPS	Progressive supranuclear palsy syndrome
P-tau	Phosphorylated tau
PTM	Posttranslational modification
riBAQ	Relative intensity-based absolute quantification
RNA	Ribonucleic acid
ROI	Region of interest
RT	Room temperature
SCX	Strong cation exchange
SDS	Sodium dodecyl sulfate
SEC	Size exclusion chromatography
SMOTE	Synthetic minority over-sampling technique
SNARE	Soluble N-ethylmaleimide-sensitive-factor attachment protein receptor
SSC	Side scatter
svPPA	Semantic variant primary progressive aphasia
TEM	Transmission electron microscopy
TFA	Trifluoroacetic acid
TJ	Tight junction
TMT	Tandem mass tag
TO	Topological overlap
TOM	Topological overlap measure
T-tau	Total tau
UC	Ultracentrifugation
VE	Vésicules extracellulaires
VE-DC	Vésicules extracellulaires dérivées du cerveau
WGCNA	Weighted gene co-expression network analysis

List of Figures

General introduction

Chapter 1: Proteomic Signature of Prefrontal Cortex Derived Extracellular Vesicles Accurately Predicts 3R and 4R Tau Pathology

Chapter 2: A Novel Methodology for the High-Efficiency Isolation of Brain Derived Extracellular Vesicles in Peripheral Biofluids

List of Tables

Chapter 2: A Novel Methodology for the High-Efficiency Isolation of Brain Derived Extracellular Vesicles in Peripheral Biofluids

Abstract

Dementia is an umbrella term which describes the primary characteristic of many neurodegenerative diseases (NDDs): a loss of cognitive function. For example, tauopathies, a family of diseases whereby the protein tau is dysregulated, all feature dementia as one of the main symptoms. Despite important differences in tau propagation and subsequent molecular consequences, many tauopathies are very difficult to differentiate in a clinical setting early in the disease progression. This is one of the main challenges facing clinicians today with an increasingly aging population which is more affected by dementia with each year that passes. The first half of this thesis investigates the potential for brain derived extracellular vesicles (BD-EVs), nanoparticles secreted by all the cells in the brain, to bridge the gap between what we know happens on the molecular level in these diseases and what is measurable in the clinic. By doing an in-depth proteomic analysis of BD-EVs from brain tissue of a tauopathy patient cohort, we were able to identify key features of BD-EV cargo which allow for the histopathological and molecular differences between various tauopathies to be linked with their clinical phenotypes. By looking broadly at the whole proteome of these BD-EVs, we saw patterns of systemic dysregulation reflected from the brain to the EV, highlighting major pathways implicated in disease progression in the brain.

BD-EVs hold much promise in the context of NDD diagnosis, however, there remain many challenges in isolating these particles outside of the brain. BD-EVs are able to cross biological barriers, such as the blood-brain barrier, to enter into peripheral biofluids. They can therefore provide critical information on the health status of the brain without painful or invasive testing. However, isolating only BD-EVs from peripheral fluids, which are full of EVs from all over the body, is challenging. To complicate matters further, EVs are covered in a halo of proteins called the corona. While EVs contain surface proteins indicating the cell type or tissue they come from, the protein corona masks these clues, rendering EVs from all organs almost identical from the outside. To combat this, the second half of this thesis focused on developing a novel method to enzymatically digest the corona, exposing novel tissue-specific proteins at the surface of EVs for immunocapture. This method increases the yield of labeled BD-EVs in peripheral fluids from less than 1% to 30-60%. This project sought to advance our understanding of tauopathies via BD-EVs and to improve upon the existing methodology for BD-EV capture in the periphery. There is still room for improvement, further development, and refinement of these results and concepts, but the work described here has certainly advanced the field of BD-EVs toward something which can one day be clinically relevant to improve patient care in the aging population.

Résumé

La démence est un terme générique qui décrit la caractéristique principale de nombreuses maladies neurodégénératives (MND) : une perte de fonction cognitive. Par exemple, les tauopathies, une famille de maladies où la protéine tau est dysrégulée, présentent toutes la démence comme l'un des principaux symptômes. Malgré des différences importantes dans la propagation de la tauopathie et les conséquences moléculaires ultérieures, les tauopathies sont très difficiles à différencier entre elles dans un contexte clinique au début de la maladie. C'est l'un des principaux défis auxquels sont confrontés les cliniciens aujourd'hui, avec une population vieillissante qui est de plus en plus touchée par la démence chaque année. La première partie de cette thèse explore le potentiel des vésicules extracellulaires dérivées du cerveau (VE-DC), des nanoparticules sécrétées par toutes les cellules du cerveau, pour combler l'écart entre ce que nous savons se passer au niveau moléculaire dans ces maladies et ce qui est mesurable en clinique. En réalisant une analyse protéomique approfondie des VE-DC provenant de tissus cérébraux d'une cohorte de patients atteints de tauopathie, nous avons pu identifier des caractéristiques clés du contenu des VE-DC qui permettent de lier les différences histopathologiques et moléculaires entre diverses tauopathies à leurs phénotypes cliniques. En examinant largement le protéome entier de ces VE-DC, nous avons observé des schémas de dysrégulation systémique reflétés du cerveau aux VE, mettant en évidence des voies majeures impliquées dans la progression de la maladie dans le cerveau.

Les VE-DC offrent beaucoup de promesses dans le contexte du diagnostic des MND, cependant, il reste de nombreux défis dans l'isolement de ces particules en dehors du cerveau. Les VE-DC sont capables de traverser les barrières biologiques, telles que la barrière hémato-encéphalique, pour pénétrer dans les biofluides périphériques. Ils peuvent donc fournir des informations critiques sur l'état de santé du cerveau sans test douloureux ou invasif. Cependant, isoler uniquement les VE-DC des fluides périphériques, qui sont pleins de VE de tout le corps, est difficile. Pour compliquer davantage les choses, les VE sont recouverts d'un halo de protéines appelé la corona. Bien que les VE contiennent des protéines de surface indiquant le type de cellule ou le tissu dont elles proviennent, la corona protéique masque ces indices, rendant les VE de tous les organes presque identiques de l'extérieur. Pour remédier à cela, la seconde moitié de cette thèse s'est concentrée sur le développement d'une nouvelle méthode pour digérer le corona, exposant de nouvelles protéines spécifiques au tissu à la surface des VE pour l'immunocapture. Cette méthode augmente le rendement des VE-DC marqués dans les fluides périphériques de moins de 1 % à 30 à 60 %. Ce projet visait à faire progresser notre compréhension des tauopathies via les VE-DC et à améliorer la méthodologie existante pour la capture des VE-DC en périphérie. Il reste encore des améliorations à apporter, des développements supplémentaires et des affinements de ces résultats et concepts, mais le travail décrit ici a certainement fait progresser le domaine des VE-DC vers quelque chose qui pourrait un jour être cliniquement pertinent pour améliorer les soins aux patients dans la population vieillissante.

General Introduction

Proteinopathies in the Brain

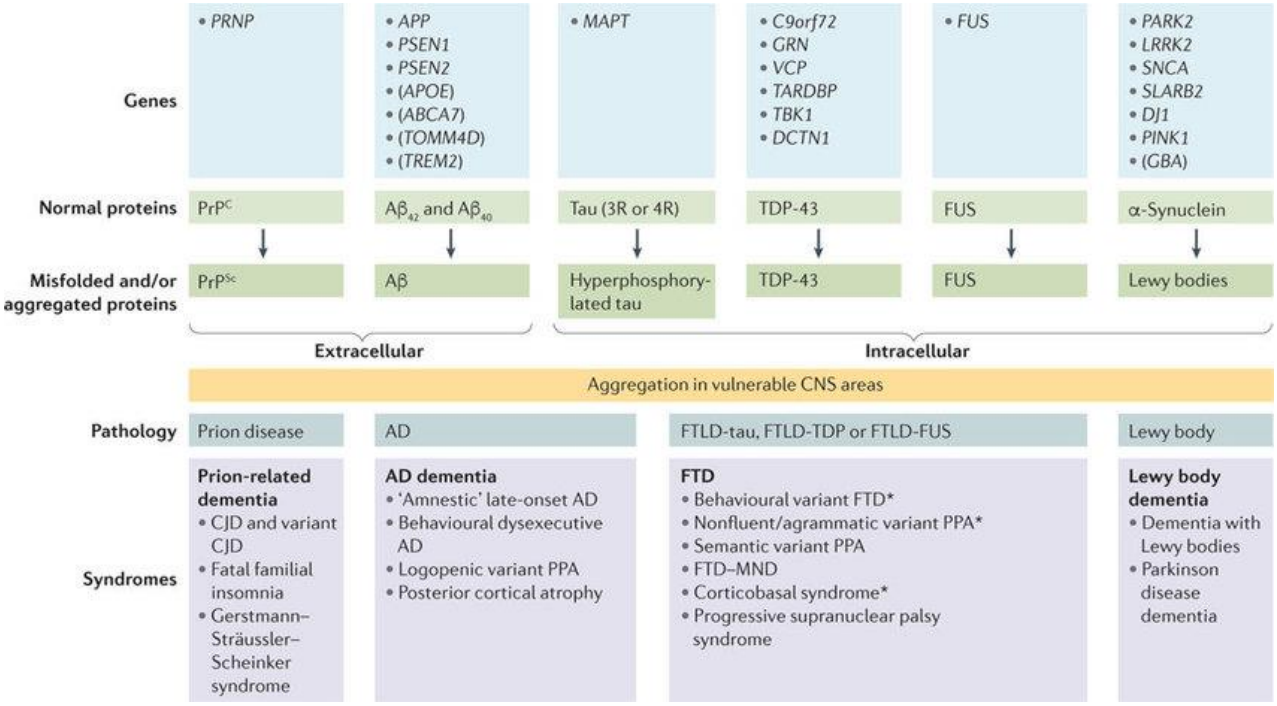

Figure 1 | Clinicopathological spectrum of neurodegenerative proteinopathies

From Elahi & Miller 2017 – Nature Reviews Neurology [1]

Schematic representation of the molecular underpinnings of neurodegenerative diseases and their main clinical manifestations. The figure lists genes with full penetrance that are considered causative and risk genes (in parentheses) that influence molecular processes culminating in the misfolding and/or aggregation of six fundamental proteins: cellular prion protein (PrPC), Aβ42 (and, to a lesser extent, Aβ40), tau, TAR DNA-binding protein 43 (TDP-43), fused in sarcoma (FUS), and α-synuclein. These normal proteins misfold and/or accumulate in intracellular or extracellular compartments in specific areas of the CNS. Four major pathological disease categories are recognized: prion disease, Alzheimer disease (AD), frontotemporal lobar degeneration (FTLD) and Lewy body diseases (LBD). The pathologies can involve multiple molecules; for example, AD is a dual proteinopathy with Aβ and tau aggregates. Also, in some cases of prion disease, Aβ is seen in addition to the principal aggregates of misfolded scrapie prion protein (PrPSc). The majority of FTLD cases are associated with three different proteinopathies: tau, TDP-43 and FUS. Each pathological entity can in turn manifest as a variety of clinical syndromes, sometimes featuring symptoms that bridge syndromes. Asterisks indicate frontotemporal dementia (FTD) syndromes that, in addition to FTLD, can be associated with AD neuropathology. Genetic pleiotropy is also at play: mutations in certain genes have full penetrance for one pathology (FTLD-TDP) and associated FTD syndromes, while representing a risk factor for another pathology (AD). In addition, certain fully penetrant genetic mutations, are associated with additional systemic disease manifestations. The rich and diverse clinical expression of neurodegenerative processes is best illustrated in FTLD, a pathological category with six distinct clinical syndromes. Of note, FUS pathology causing FTLD is typically not associated with FUS mutations, which more often cause amyotrophic lateral sclerosis.

Aβ = amyloid-β, AD = Alzheimer's disease, CJD = Creutzfeldt–Jakob disease, CNS = central nervous system, FTD–MND = frontal temporal dementia with motor neuron disease, FUS = fused in sarcoma, LBD = Lewy body diseases, PPA = primary progressive aphasia

Many neurodegenerative diseases (NDDs) are the result of dysregulation and eventual accumulation of one or more proteins in the brain. Many genes can contribute to the formation of intra- or extracellular protein aggregates within the brain, resulting in a wide variety of pathologies and associated syndromes (**Figure 1**)[1]. Some of these diseases, such as Alzheimer's disease (AD), are dual proteinopathies with two kinds of protein aggregates driving disease. In contrast, others like frontotemporal lobar degeneration (FTLD) can be driven by a number of different proteins, each resulting in a different disease progression and associated syndromes. These diseases often occur sporadically, however, certain genetic factors play into an individual's vulnerability to developing a proteinopathy[2].

The majority of proteinopathies have dementia as one of their earliest-showing and constantly evolving symptoms. However, dementia is not just a simple symptom, it is a complex process which is the result of damage to specific molecular pathways in the brain, leading to inflammation, impaired synaptic transmission, gliosis, and cell death, among other things (**Figure 2**)[1,3,4]. These effects ultimately lead to impaired cognitive functioning, changes in behavior and mood, impaired sensory motor function, and overall loss of autonomy for an individual. The specific location of lesions and aggregates in the brain plays a significant role in the types of symptoms experienced by a patient, as well as the speed of disease progression[5]. Dementia is far from a "one size fits all" term, with much variability and overlap of symptomology between patients, so it's clear why there is difficulty stratifying and diagnosing dementia patients still today.

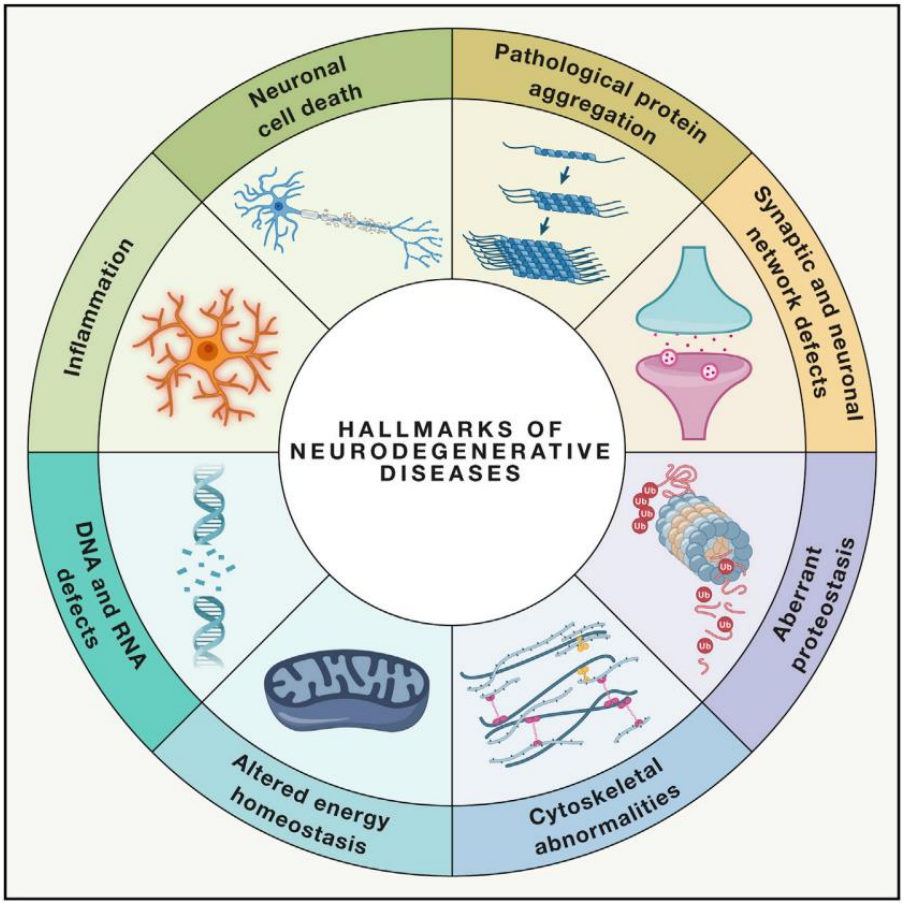

Figure 2 | Hallmarks of neurodegenerative diseases

From Wilson et al., 2022 – Cells [3]

Based on decades of basic, translational, and clinical research, genetic factors and biochemical pathways underlying many NDDs have been identified, resulting in the identification of eight NDD hallmarks: pathological protein aggregation, synaptic and neuronal network dysfunction, aberrant proteostasis, cytoskeletal abnormalities, altered energy homeostasis, DNA and RNA defects, inflammation, and neuronal cell death.

Tauopathies are a subset of proteinopathies explicitly characterized by the abnormal aggregation of tau protein in the brain. Tau, crucial for neuronal health, is best known for maintaining microtubule stability and therefore, cytoskeletal integrity in neurons[6]. Beyond its foundational role, more recent studies have unveiled its involvement in various neuronal functions such as the direct regulation of microtubule dynamics and axonal transport, as well as the indirect promotion of synaptogenesis, neurogenesis, and plasticity (**Figure 3**)[6–8]. However, in pathological conditions, tau undergoes hyperphosphorylation, leading to its detachment from microtubules, accumulation, and eventually aggregation within the cell[9]. Consequently, affected cells experience compromised structural integrity and impaired functionality due to the presence of these pathological protein aggregates.

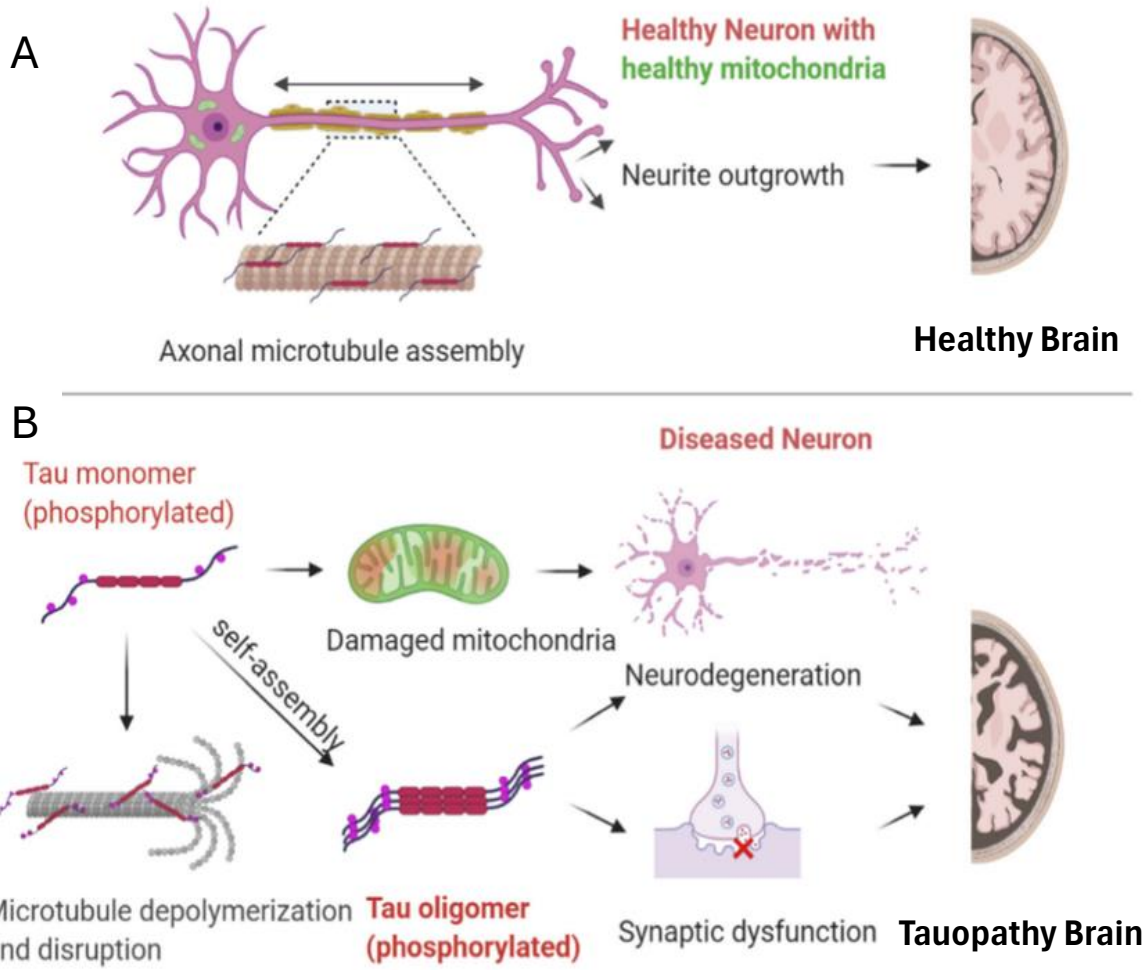

Figure 3 | The function and dysfunction of tau in the brain

Adapted from Guha et al., 2020 – Molecular Neurobiology [8]

Tau in physiological and pathological contexts in the brain

A) In the physiological state, tau plays numerous roles including regulation of axonal microtubule assembly, contributing to neuronal polarity development and outgrowth.

B) In the pathological state, tau with abnormal PTMs exhibits decreased affinity for microtubules and can contribute to mitochondrial damage, as well as impaired synaptic transmission culminating in neurodegenerative processes.

Although tau is relatively small in size, its various forms contribute significantly to the molecular heterogeneity observed in tauopathies. One notable cause for this is alternative splicing, which generates six distinct isoforms of tau (**Figure 4**)[10,11]. Among these, three belong to the 3R group, featuring three microtubule binding domains, while the remaining three make up the 4R group with four microtubule binding domains. Under

normal physiological conditions, 3R and 4R tau are present relatively equally throughout the brain[12]. However, in tauopathies, the accumulation of 3R tau, 4R tau, or a combination of both disrupts this balance, leading to widespread neuronal loss. Beyond isoform variation, tau possesses 85 phosphorylation sites, with only 10 being phosphorylated under normal conditions, compared to up to 55 in Alzheimer's disease alone.[13]. Phosphorylation alters the protein's conformation, particularly hyperphosphorylation, resulting in a myriad of hyperphosphorylated tau forms present in tauopathies.

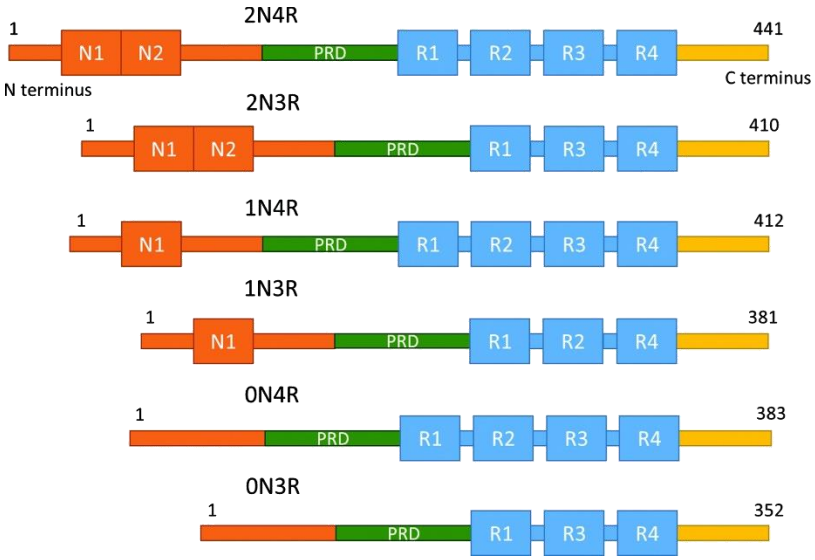

Figure 4 | Isoforms of tau

From Zabik et al., 2017 – Biochemical Cell Biology [11]

Schematic illustration of the six isoforms of the protein tau

Tauopathies can be further classified into different subtypes according to the predominant tau isoform accumulated (3R, 4R, or a mixture of both) and the morphology of tau aggregates present, such as neurofibrillary tangles (NFT) or gliofibrillary tangles (GFT)[14,15]. Moreover, the genetic and molecular mechanisms contributing to tauopathies vary, with mutations in the MAPT gene linked to certain tauopathies but not all[16].

Given the considerable molecular diversity within tauopathies, it's unsurprising that they also manifest differences in clinical presentation and neuropathological features.[17,18]. For instance, while Alzheimer's disease and progressive supranuclear palsy predominantly impact cortical brain regions, others like corticobasal degeneration and Pick's disease primarily affect subcortical areas (**Figure 5**)[5]. These topographical differences result in distinct clinical symptoms; Alzheimer's patients typically present with memory deficits and mood disturbances, whereas those with Pick's disease often experience initial changes in personality and decision-making, with memory decline occurring later[19]. Understanding the heterogeneity

among tauopathies is critical for accurate diagnosis and treatment and for advancing our knowledge of the molecular underpinnings of these complex diseases.

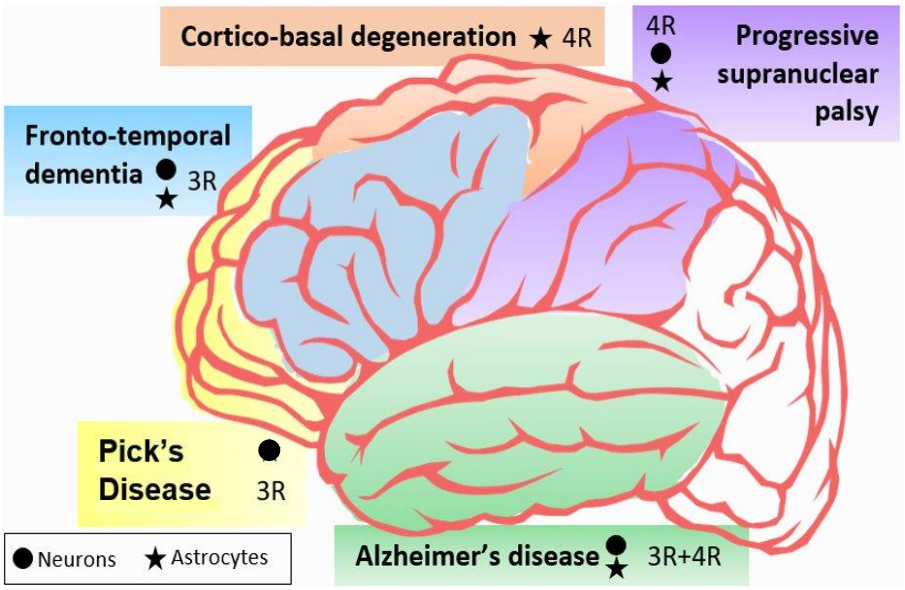

Figure 5 | Topographical distribution and cellular heterogeneity of various primary and secondary tauopathies
Figure designed by Valentin Zufferey

Schematic illustration depicting the brain regions most impacted by different tauopathies. Included is also the cell type which primarily accumulates tau in each disease.

Diagnosing tauopathies

The current strategy for diagnosing tauopathies and related diseases combines patient or proxy self-reporting of symptoms, neuropsychological testing to evaluate cognitive and memory function, biofluid testing when proteinopathy is suspected, and brain imaging in the form of magnetic resonance imaging (MRI) to look for regional atrophy or lesions and/or positron emission tomography scan (PET) for specific pathological protein or aggregate presence, such as amyloid beta (Aβ) or phosphorylated tau (P-Tau). There are no definitive diagnostic tests yet for these diseases, and many of the physical symptoms of tauopathies are also present in other neurological conditions, making precise diagnosis difficult, particularly in earlier stages of disease progression[19,20]. Additionally, the progression of the disease can be slow and subtle, which can delay diagnosis and diminish efficacy of any potential treatments such as monoclonal antibody treatment targeting amyloid beta plaques in the case of AD[21]. Despite their many differences, tauopathies can often present with similar clinical and neuropathological features in earlier stages but require different treatments or symptom management (**Figure 6**)[22–25]. This complicates diagnosis and often leaves patients and clinicians without clear answers for months or years as the pathology evolves.

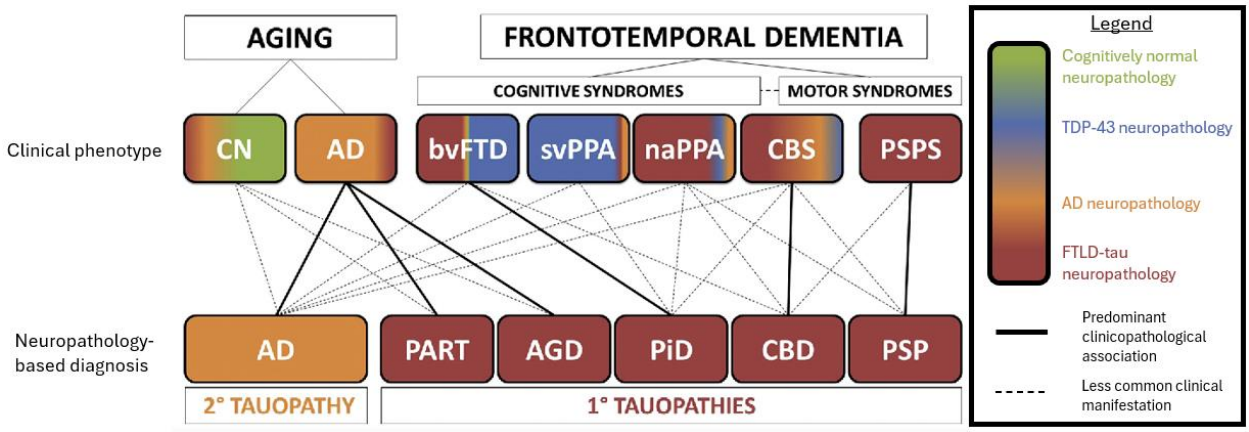

Figure 6 | Clinicopathological correlations in tauopathies

From Irwin 2016 – Parkinsonism & Related Disorders [25]

The scheme portrays (top) the relative frequencies of neuropathological subtypes of FTLD-Tau (i.e. primary tauopathies-red) and AD (i.e. secondary tauopathy-yellow) seen at autopsy in clinical phenotypes in FTD-spectrum disorders and aging by the color-coding of each box. Unremarkable neuro- pathological findings are shaded in green and TDP-43 protienopathies in blue (this schematic does not account for cerebrovascular changes, co-morbid pathology or less common neurodegenerative diseases). FTD clinical phenotypes are divided by cognitive and motor syndromes; the dashed line represents the clinical overlap between FTD cognitive and motor syndromes and CBS is placed intermediate to these categories as this clinical syndrome has aspects of both cognitive and motor dysfunction. AD neuropathology (yellow) is found in approximately a third of older patients who are cognitively normal and is seen in the majority amnestic AD clinical phenotype. FTLD-Tau (red) is found in virtually all PSPS cases and the majority of naPPA. FTLD-Tau is also found in a significant proportion of CBS and relatively rare in svPPA. Roughly half of bvFTD cases harbor FTLD-Tau while a small percentage can have AD neuropathology (yellow). Solid lines represent the predominant clinicopathological association for each specific tauopathy (bottom) while dashed lines represent less common clinical manifestations of each tauopathy. AD neuropathology is most commonly associated with the amnestic AD clinical phenotype but may also present as bvFTD, PPA variants and CBS. PART and AGD are largely associated with late onset (>80 years) amnestic syndrome similar to clinical AD and less commonly in CN individuals. PiD is most commonly found in association with bvFTD but can present with PPA variants or CBS. CBD tauopathy is primarily associated with CBS but also can manifest as bvFTD, naPPA or PSPS, while PSP is predominantly associated with PSPS and less commonly associated with naPPA or CBS.

CN = cognitively normal, AD = Alzheimer's disease, bvFTD = behavioral variant frontotemporal dementia, svPPA = semantic variant primary progressive aphasia, naPPA = non-fluent variant primary progressive aphasia, CBS = corticobasal syndrome, PSPS = progressive supranuclear palsy syndrome, PART = primary age-related tauopathy, AGD = argyrophilic grain disease, PiD = Pick's disease, CBD = corticobasal degeneration, PSP = progressive supranuclear palsy

Different forms of tau are currently used to inform on the disease status of patients in clinics. For example, in the cerebrospinal fluid (CSF), P-tau181 (tau hyperphosphorylated at threonine181) and total tau (T-tau) can act as biomarkers of mild cognitive impairment (MCI), early onset dementia (EOD), and AD[26–28]. In the blood, however, P-tau217 (tau hyperphosphorylated at threonine217) has been shown to most accurately reflect Aβ plaque and tau tangle load in AD patients in various Braak stages[29,30]. P-tau181 and P-tau231 are also measured in the blood with success, though they appear to correlate slightly less well with Aβ plaque and tau tangle load than P-tau217[29,31]. Tau PET has also recently shown promise as a reliable way to measure NFTs in the brain. Second generation tau tracers have improved upon first generation tracers in their affinity for NFT tau and their specificity, binding less frequently to Aβ plaques[32]. While some tau tracers have been approved by the food and drug administration (FDA) for research purposes, they are not yet approved for clinical and diagnostic purposes. Additionally, the best tau tracers, along with the best tau markers in CSF and blood, only

work for AD pathology, meaning they rely on the presence of Aβ increasing the amount of detectable tau[27,32]. Some tau PET tracers do work specifically for 4R tau NFTs, meaning they can be used for tauopathies such as progressive supranuclear palsy (PSP) and corticobasal degeneration (CBD), which primary feature aggregates of 4R tau.

Aβ is also used as a biomarker of proteinopathies which feature Aβ plaque deposition (typically AD). More specifically, the $A\beta_{42}/A\beta_{40}$ ratio is often used. This is the ratio of Aβ peptides which are 42 or 40 peptides long. This ratio is highly informative on Aβ plaque load in patients both via the CSF and the blood, though $A\beta_{42}$ alone can also be measured in the blood[27]. Several Aβ PET tracers also exist with high specificity and sensitivity to detecting Aβ plaques in vivo[32]. Multiple tracers have been approved by both the FDA and the European Medicines Agency (EMA) for clinical use. Of course as the name suggests, Aβ measurements and PET are only useful for diseases with Aβ pathology, eliminating primary tauopathies for the list of diseases these methods can diagnose.

General neurodegeneration can also be measured, irrespective of tau and Aβ pathology. Neurofilament light chain (NfL), which can be measured in both plasma and CSF, has emerged as a strong marker of general neurodegeneration[27,30]. NfL is particularly strong for detecting neurodegeneration in frontotemporal, vascular, and HIV-associated dementias. Neurodegeneration is often also assessed by MRI in order to detect atrophy or lesions associated with pathology in the brain. Finally, a newer marker which is still being validated I the context of AD is glial fibrillary acidic protein (GFAP), a potential marker of altered astrocytic homeostasis[30,33,34].

There has been a staggering amount of progress in the field of biomarker research for neurodegenerative disease in the last decade alone. There now exist multiple protein markers which can be measured in the blood, CSF, or by PET scan. However, even with all of these improvements, most markers today are validated only for AD and AD-related pathologies. Some, such as tau PET, can now detect specifically 4R tau, however this is not clinically validated yet. Primary tauopathies still lack in protein biomarkers, with most being diagnosed based on neuropsychological testing, MRI, and measurement of general markers of neurodegeneration. The clinical feasibility of tau PET tracers is still being studied, however these are a promising step for 4R tauopathies[35,36].

Proteomics of tau isoforms

One method which can accurately distinguish between 3R and 4R tau inclusions in the human brain is proteomics. Targeted proteomics using tandem mass tag labeling (TMT) is a method which relies on analyzing a pure sample of the protein(s) of interest as a standard, along with the sample which is being analyzed for those proteins, on order to compare the relative quantities based on the "standard" sample[37]. It can be a time consuming and expensive technique, however it is highly accurate in distinguishing these small differences such as between isoforms of proteins or post translational modifications (PTMs) which can have significant consequences on pathological proteins such as tau.

One group investigated this exact question of stratifying primary tauopathies using proteomics of the different kinds of tau inclusions found in control, corticobasal degeneration (CBD, a 4R tauopathy), frontotemporal lobar degeneration 4R or 3R (FTLD-4R; FTLD-3R), Pick's disease (PiD, a 3R tauopathy), and AD (a mixed 3R/4R tauopathy)[38]. In this study, they found that targeted TMT mass spectrometry could indeed differentiate between the isoforms and specific PTMs associated with inclusions from each of these pathologies, however that there is a very big difference between the insoluble tau which aggregates within cells and the soluble tau which is secreted into biofluids and used currently for diagnostic purposes. While the 3R/4R ratio of insoluble tau could differentiate these disease groups (3R, 4R, 3R or 4R, and 3R and 4R), the same measure in soluble tau could not differentiate any groups. This may shed some light on why soluble tau can only be used to diagnose AD and AD-related pathologies, which have Aβ pathology in addition to tau pathology. The Aβ pathology drives the soluble tau levels up in a way which distinguishes AD from primary tauopathies, but in primary tauopathies the soluble tau levels are lower and in the same 3R/4R ratio regardless of the specific disease.

Extracellular vesicles

Extracellular vesicles (EVs) are nanoparticles which are secreted by all the cells of the body. They range widely in size, and are typically grouped into 3 categories: exosomes, microvesicles, and apoptotic bodies (**Figure 7**)[39]. All three of these EV subtypes have a unique biogenesis, size range, and function.

Exosomes are EVs which are formed with endosomal origin, budding inward from the membrane of early endosomes and later maturing into multivesicular bodies (MVB)[40]. These early endosomes are involved in protein sorting, recycling, storage, transport, and release, and resultant MVBs are typically sent to the lysosome for degradation or fused with the plasma membrane to release their content (exosomes) into the extracellular space[41]. Exosomes range in size from about 30-150nm[42].

Microvesicles differ from exosomes primarily in size and origin. They are typically larger than exosomes, ranging from about 100nm – 1um in diameter[43]. They are formed through an outward budding of the plasma membrane and are "shed" into the extracellular space surrounding the cell[44]. Like exosomes, microvesicles participate in intercellular communication and material transport. They are, however, made up more of typical cytosolic and plasma membrane proteins rather than the more specific endosomal sorting complex required for transport (ESCRT) machinery which signifies a biogenesis through the MVB[40].

Apoptotic bodies have the largest size range of any EV subtype, measuring anywhere from 50nm to 5um[40]. This population of EVs does tend to be on the larger end of that range, however. Apoptotic bodies are formed by a separation of the plasma membrane from the cytoskeleton of a cell and are released only by dying cells as their name suggests. These EVs can contain intact organelles, chromatin, and other material vital to cell survival.

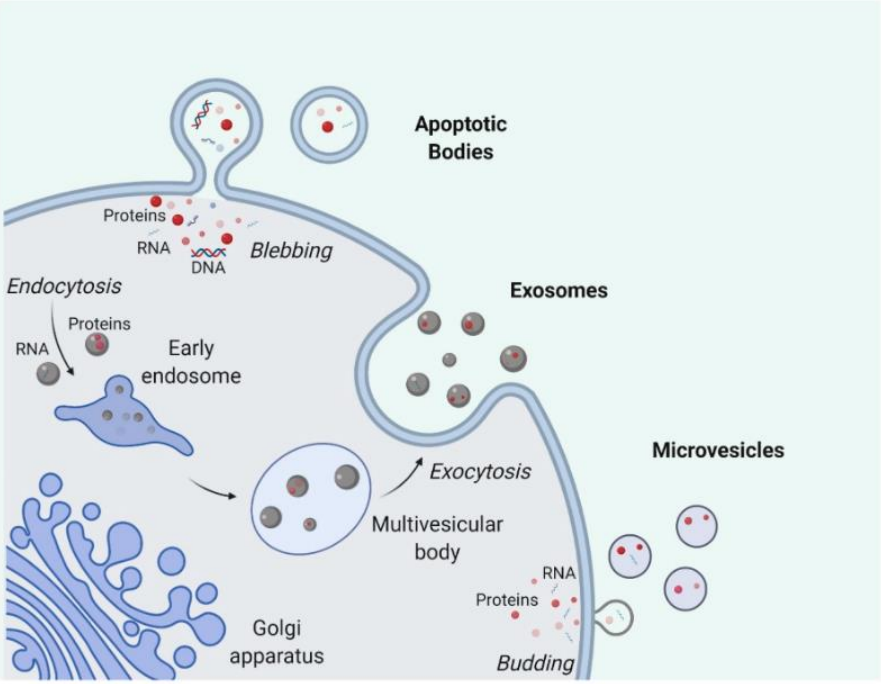

Figure 7 | Biogenesis of extracellular vesicle subtypes

From Dang et al., 2020 – Cells [39]

Exosomes are intraluminal vesicles which are released when a multivesicular body fuses with the cell membrane through exocytosis. Microvesicles are formed by outward shedding of the cell membrane into extracellular space. Apoptotic bodies are generated when cells undergo apoptosis.

Long thought to just be the “trash bags” of cells, studies in the last decade have shown that EVs participate in much more than cellular waste disposal. Indeed, they are critical in roles of intercellular communication, cell maintenance, tumor progression, and the transportation of biological material from one cell to another[40,42]. They are known to transport a wide variety of biological material, including proteins, DNA, RNA, lipids, and even whole functioning organelles like mitochondria (**Figure 8**)[40,45–47].

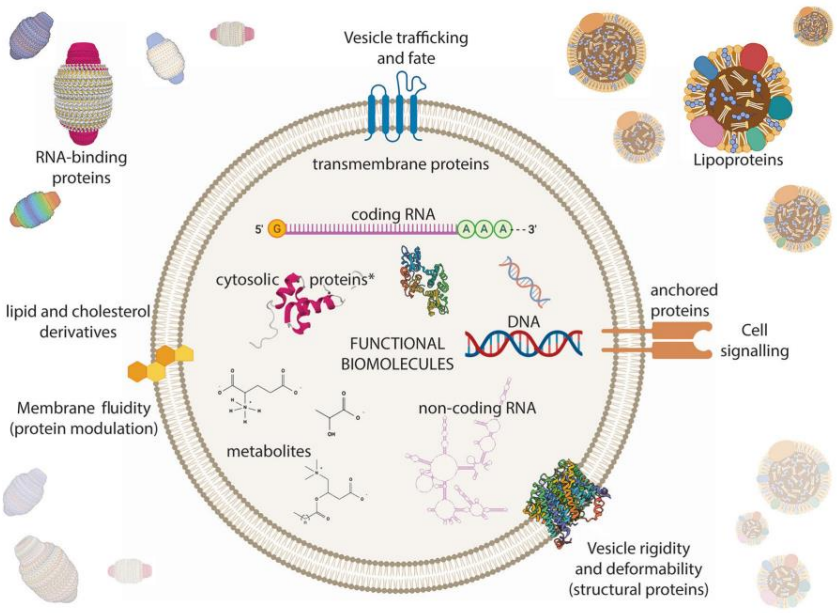

Figure 8 | Extracellular vesicle composition in the context of biological solutions
From Veziroglu & Mias 2020 – Frontiers in Genetics [47]

EVs carry all biomolecule classes that have been associated with cells. DNA and RNAs (both coding and non-coding) are found within EVs. Proteins can be freely soluble, membrane-associated, membrane-anchored, and trans-membrane. Metabolites and other small molecules are also found within EVs. The membrane bilayer is composed of phospholipid and cholesterol derivatives. EVs cannot be purely isolated and other non-vesicular molecular chaperones such as RNA-binding proteins and lipoproteins often contaminate EV preparations.

EVs involved in cell-cell communication must be capable of reaching the cell(s) they are targeting. Not much is known about how this process works in detail, but certain overarching themes have been demonstrated. Most importantly, EVs released by cells in distress tend to express “don’t eat me” molecules at their surface (such as CD47) in order to delay their uptake by phagocytic cells and increase their time in circulation, and tissues which are in distress tend to express more adhesion molecules in order to receive more EVs[48]. Together, these two concepts illustrate the importance of EVs in cell and tissue reparation, presumably by providing molecules which are beneficial to the cells in need which are sending out distress signals. Additionally, the quantity of EVs secreted by cells is dependent on the physiological state of the cell, with injured or distressed cells releasing more EVs than normal cells[48]. This likely helps activate more healthy cells in the immediate surroundings to secrete EVs which contain beneficial molecules. There is some evidence of EV from certain cell types being preferentially taken up by other cell types, such as this study on the uptake of oligodendrocytic EVs by microglia, however this kind of evidence is quite rare and there is still a large knowledge gap in the specifics of this topic in the field of EVs[49].

While the mechanisms of EV homing are not yet well understood, the various mechanisms of EV uptake are well-documented (**Figure 9**). EV content can enter recipient cells in a number of ways, such as phagocytosis (typically apoptotic bodies), pinocytosis (exosomes or microvesicles), direct membrane fusion or cell surface receptor interaction to empty cargo into the cytoplasm of the cell, or clathrin or caveolin-mediated endocytosis for delivery to the endosome (and subsequently re-secretion by MVB or destruction by the lysosome)[42,50]. The mechanism of EV uptake is largely dictated by the content and surface proteins present on an EV, indicating its biological purpose to the cell.

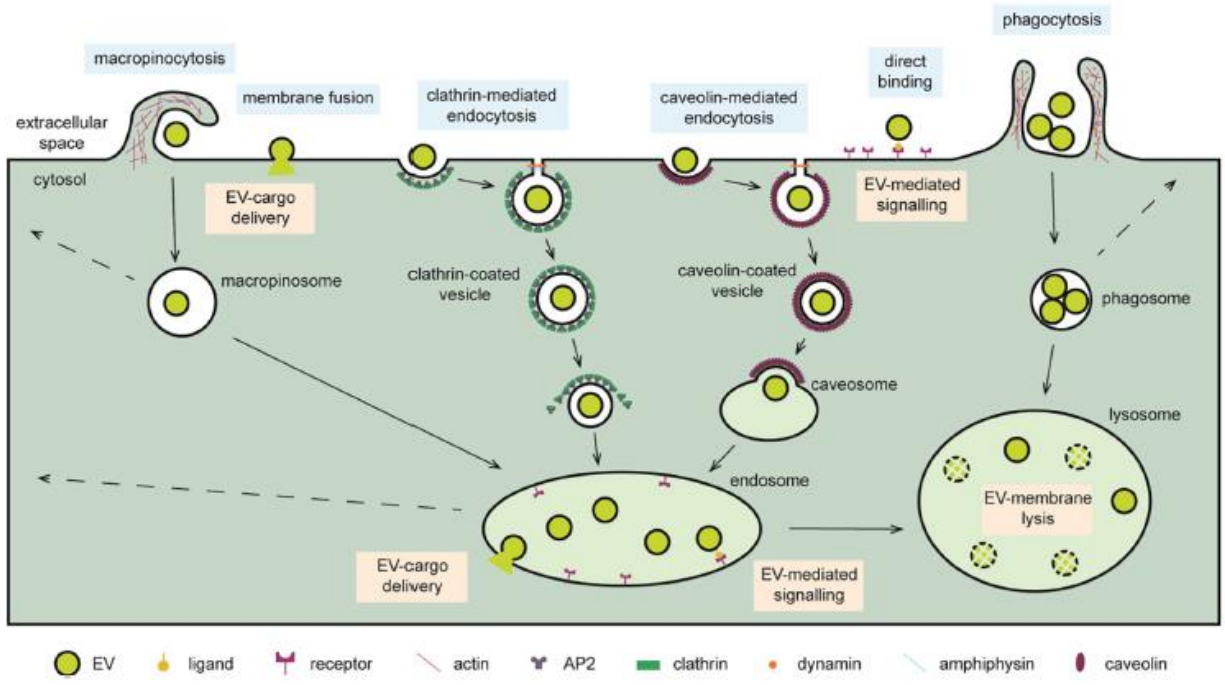

Figure 9 | Cellular pathways exploited for the delivery of EV cargo

From Pedrioli & Paganetti 2021 – Frontiers in Cell and Developmental Biology [50]

EVs reaching recipient cells can interact with cell surface receptor or fuse with the limiting membrane and deliver the soluble cargo directly to the cytosol. Alternatively, EVs are internalized through macropinocytosis, micropinocytic processes such as clathrin-mediated endocytosis, and caveolin-mediated endocytosis or phagocytosis. Internalized EVs transit through endosomal compartments when directed to lysosomes. Within endo-lysosomal organelles, ligands present on the EV surface can induce an intracellular signaling cascade through a ligand–receptor mechanism. Moreover, cytosolic delivery of EV cargo may occur by fusion with the membrane of these organelles. The action of acidic hydrolases may liberate the EV cargo for degradation, interaction with other endo-lysosomal components, or recycling to the extracellular milieu by back fusion with the cell membrane. Symbols used are specified in the legend on the bottom of the scheme.

The surface of extracellular vesicles

One factor which likely plays a large role in how and by which cells EVs are taken up is the surface proteome of the EV. Much like their cargo, the proteins at the surface of the EV membrane tell a story about where it came from and where it can go[51]. EVs are known to have many kinds of functional molecules at their surface, including receptors, receptor ligands, and transmembrane proteins[52]. Many groups are interested in decoding

the surface proteome of EVs in order to study specific subpopulations of interest, though this remains a big challenge which has not yet been fully overcome. To complicate matters further, EVs attract a protein corona around the proteins in their membrane. This corona is full of soluble proteins which have a high affinity for the surface proteins of the EV[53]. The complexity and affinity of the corona to the EV depends on the biofluid in which the EV is circulating, as well as how long it is circulating before being internalized.

Isolation of extracellular vesicles

The method of EV isolation chosen for an experiment depends heavily on several variables, such as the biofluid containing the EVs, the type of analysis which will be performed on the EVs, whether or not EVs should be functional, the yield and purity desired, and others. There is no one correct way to isolate EVs; several examples are provided in **Figure 10**[54,55]. Researchers must consider the questions they seek to answer, the kind of EV sample they require, and the tools at their disposal. There are currently two "gold standard" approaches to EV isolation commonly accepted within the EV community, each offering different advantages and disadvantages. Ultracentrifugation (UC) is used primarily for high yield experiments, often at a cost of sample purity[54]. UC is widely used because isolating a large enough amount of EVs for certain analyses can be challenging, and this technique tends to produce high particle yield. The downside to UC is that it is often less pure than other methods. Extremely high-speed centrifugation (>100,000g) can arbitrarily stick free floating proteins to EVs in suspension, meaning the EV sample will contain proteins which are not associated with EVs. UC can be made more pure by using different variations, such as discontinuous or continuous density gradient ultracentrifugation (DGUC). On the other hand, size exclusion chromatography (SEC) is often used when high sample purity is needed, often at the expense of the overall yield[54]. SEC efficiently separates EVs from free proteins and small contaminating lipoproteins by pore size on resin columns, eluting EVs more quickly than free proteins. Other methods such as precipitation kits, microfluidics, and immunocapture offer their own advantages for specific kinds of studies.

Extracellular vesicles in peripheral biofluids

EVs are found in all biofluids of the body, including the blood, saliva, urine, tears, brain interstitial fluid (ISF), CSF, lymphatic fluid, and amniotic fluid[40]. Not only are EVs found in the biofluid in which they are secreted, they are capable of crossing biological barriers such as the blood-brain barrier or the choroid plexus[56]. This means that EVs from specific organs and tissues can be found in biofluids far from where they originated. This is particularly pertinent for brain derived EVs (BD-EVs), which can be found in blood, saliva, CSF, urine, and other fluids[57]. Thanks to their brain derived biological cargo, BD-EVs in peripheral biofluids remain a critical element of the search for noninvasive brain biomarkers in the form of a "liquid biopsy".

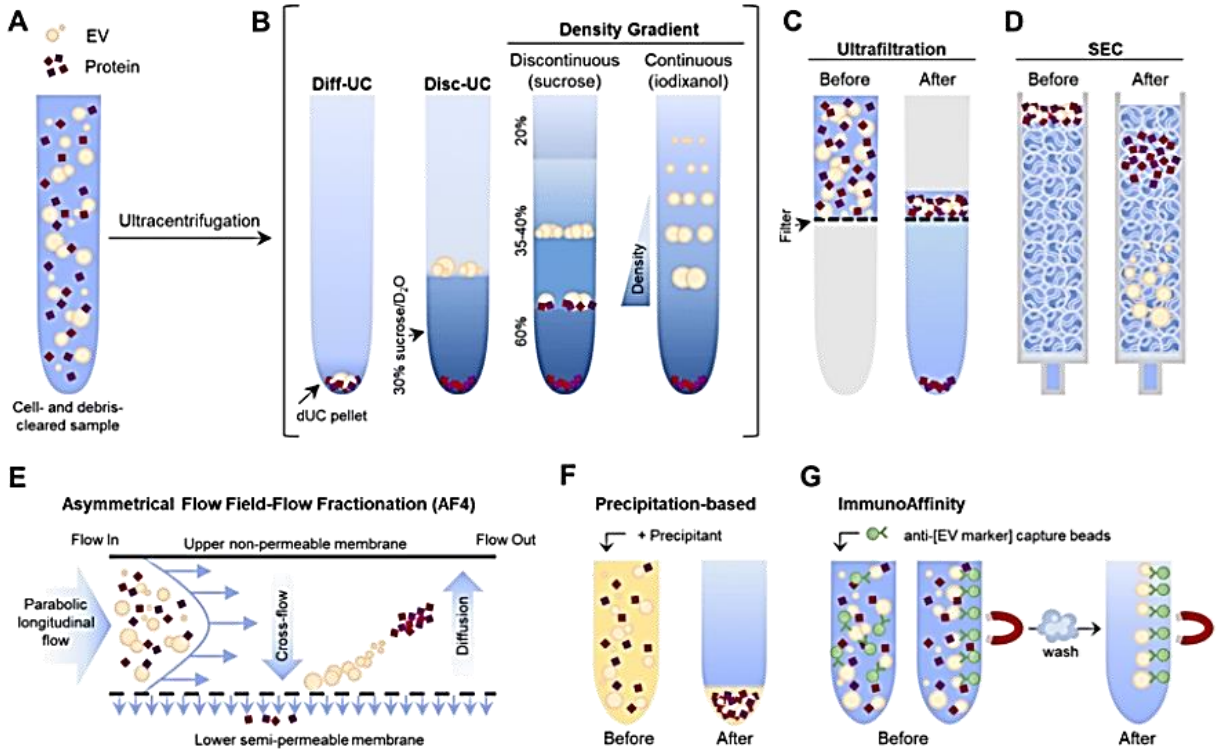

Figure 10 | Graphical summary of EV isolation methods

From Monguio-Tortajada et al., 2019 – Cellular and Molecular Life Sciences [55]

A) The starting sample is a cell- and debris-cleared biofluid containing EVs and proteins in suspension.

B) Ultracentrifugation renders an EV pellet that also contains proteins (dUC pellet), which can be further purified by discontinuous ultracentrifugation (disc-UC), like floatation in a sucrose cushion, or by density gradient (DG) ultracentrifugation: in a discontinuous gradient using different sucrose solutions or in a continuous, self-making gradient using solutions of iodixanol (optiprep). Proteins and the different EV populations are separated by their density.

C) Ultrafiltration is a dead-end filtration system that allows the separation of molecules according to the molecular weight cutoff (size) of the filter pore used. It renders a mixed sample of EVs and proteins but allows great sample volume reduction. It separates molecules by their hydrodynamic radius.

D) Size-exclusion chromatography (SEC) separates molecules by their hydrodynamic radius. The first to elute are the molecules bigger than the matrix pores (EVs), while smaller particles within the fractionation range (proteins) get slowed down by entering the matrix bead pores and so elute later.

E) Asymmetrical flow field-flow fractionation (AF4) separate molecules by their hydrodynamic radius (size). In AF4, a crossflow (field) perpendicular to the longitudinal laminar flow forces particles towards the semipermeable membrane. Particles smaller than the membrane pore are removed through the membrane. Retained ones migrate away due to diffusion and flow in the equilibrium position of the two forces (field and diffusion) according to their size. The velocity of the longitudinal flow increases parabolically, thus smaller particles, in the center of the flow, are carried faster and elute before bigger ones. This way, proteins and differently sized EV populations are separated.

F) Precipitation-based isolation relies on the addition of water-excluding precipitants like PEG (polyethylene glycol) to concentrate all particles in one pellet.

G) Immunoaffinity isolation is based on EV capture using a specific antibody that recognizes an EV-specific marker coupled to beads that can be separated by centrifugation or magnetically. Given the lack of pan-EV markers, not all EVs are isolated. Original graphical artwork from the publishing authors

Extracellular vesicles in pathology

As described above, EVs are known to play crucial roles in intercellular communication and can transport many different biological materials, including proteins, RNA, and lipids, between cells[42,58]. In the context of

pathology, however, EVs have been implicated in the propagation of pathological material. The earliest evidence of this comes from the field of oncology, where EVs have been shown for decades to play a role in tumor growth and metastasis[59–63]. They are also known to propagate viral infection throughout the body[64]. It should come as no surprise, then, that EVs can take on this role in the brain as well. EVs can be particularly efficient at propagating diseases which spread in a prion-like fashion throughout the brain, like proteinopathies (**Figure 11**)[5,65]. EVs carry, whether as cargo or stuck in the protein corona, pathological proteins from one cell to another, actively spreading and "seeding" these proteins in previously healthy cells[5,66]. It is likely this mechanism which is responsible, to a certain degree, for tau aggregation in glial cells, which normally have little to no endogenous tau[67]. Indeed, we have previously demonstrated that free form tau secreted extracellularly is not taken up by astrocytes. Rather it is tau contained within or stuck to EVs which is internalized by astrocytes[68]. Furthermore, EVs derived from various cell types, such as astrocytes and microglia, can have unique cargo profiles which may contribute to the pathogenesis of specific neurodegenerative diseases[69–71].

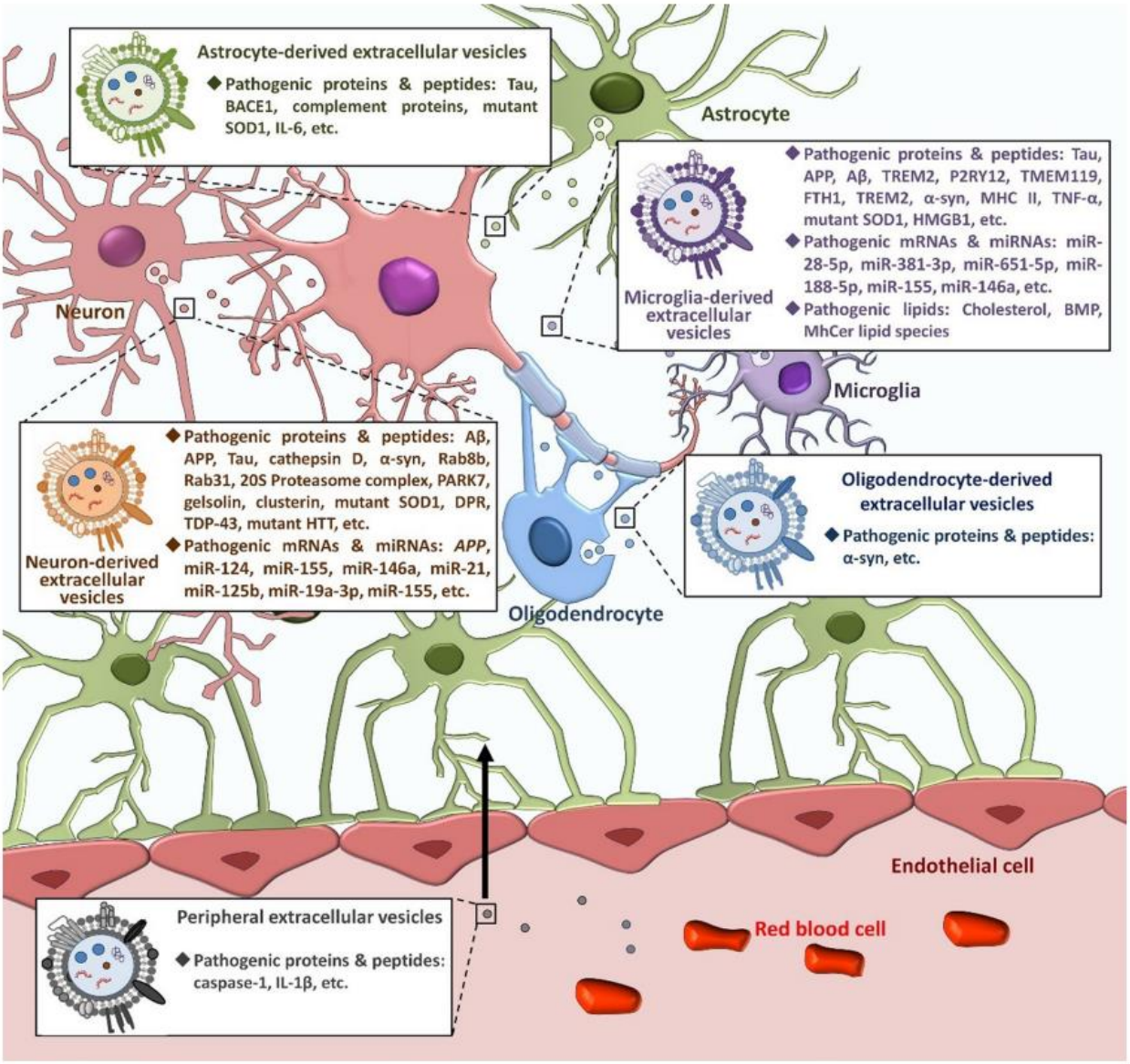

Figure 11 | The pathological effects of extracellular vesicles on neurodegenerative diseases

From Xia et al., 2022 – Translational Neurodegeneration [65]

In the brain, there are EVs released from brain cells (e.g., neurons, astrocytes, microglia, and oligodendrocytes) and peripheral EVs that enter the brain through the BBB. Under pathological conditions, these EVs carry pathogenic factors including proteins/peptides, coding and non-coding RNAs, and lipids that contribute to the onset and progression of NDDs through facilitating the spreading and aggregation of pathogenic molecules, enhancing cell death, stimulating inflammatory responses, and disrupting the BBB.

BBB = blood-brain barrier, EV = extracellular vesicle, NDD = neurodegenerative disease

The role of glial cells in neurodegenerative disorders

Despite making up 50% of the cells in the brain, for more than a century, glial cells were thought to be merely the glue which held neurons together. They are now recognized for their integral role in actively maintaining a cognitively healthy and functioning brain, providing structural, metabolic, and immune support to neurons and

other glia[72]. From the very beginning of central nervous system (CNS) development, microglia are responsible for synaptic pruning, phagocytosing apoptotic neurons, and providing immune defense[73]. Radial glia also facilitate the radial migration of neurons during this early brain development and throughout adult neurogenesis as well[74]. Astrocytes are largely involved in the maintenance of homeostasis in the brain. They support neurons in a variety of ways, including structurally by actively participating in synaptic remodeling[75]. The brain is an organ which demands a lot of energy, and most of that goes to keeping neurons firing as needed. Astrocytes are ideally positioned between neurons and cerebral capillaries and are uniquely adapted to regulating the metabolic needs of neurons by facilitating the flow of glucose from vessels to be supplied to neurons in the form of glutamate, and even releasing vasoactive molecules which can control their access to glucose as needed[76]. Astrocytes also promote both neurogenesis and synaptogenesis, aiding in the proliferation of adult neural stem cells, the integration of new neurons into the neural network, and synaptogenesis through secreted factors[77–79]. They are even critical players in processes such as attention and memory through the synchronization of neuronal activity into neuronal oscillations[80,81]. Finally, astrocytes are also key structural members of the blood-brain barrier, helping to control what leaves, and more importantly, what enters the brain from the periphery[82,83].

A similarly outdated mindset about glial cells plagued the study of neurodegenerative diseases until somewhat recently. Even the name neurodegenerative disease implies that neurons are the only cell type affected by these pathologies, but this couldn't be further from the truth. Inflammation is common to most neurodegenerative diseases. It is also a major factor in kickstarting glial reactivity, a major event which propels neurodegeneration[84]. Reactive astrocytes and microglia also possess the ability to assume a loss-of-function phenotype for tasks such as synapse maintenance and metabolic support of neurons, as well as a gain-of-function phenotype which is destructive to neural networks and glia alike (**Figure 12**)[85–88]. This typically happens later in disease progression, with astrocytes and microglia participating in the clearance of aggregates early in pathology[86]. It is clear, however, that once more and more glial cells become reactive and begin not only failing to maintain but even "attacking" neurons, the process of neurodegeneration is swiftly accelerated.

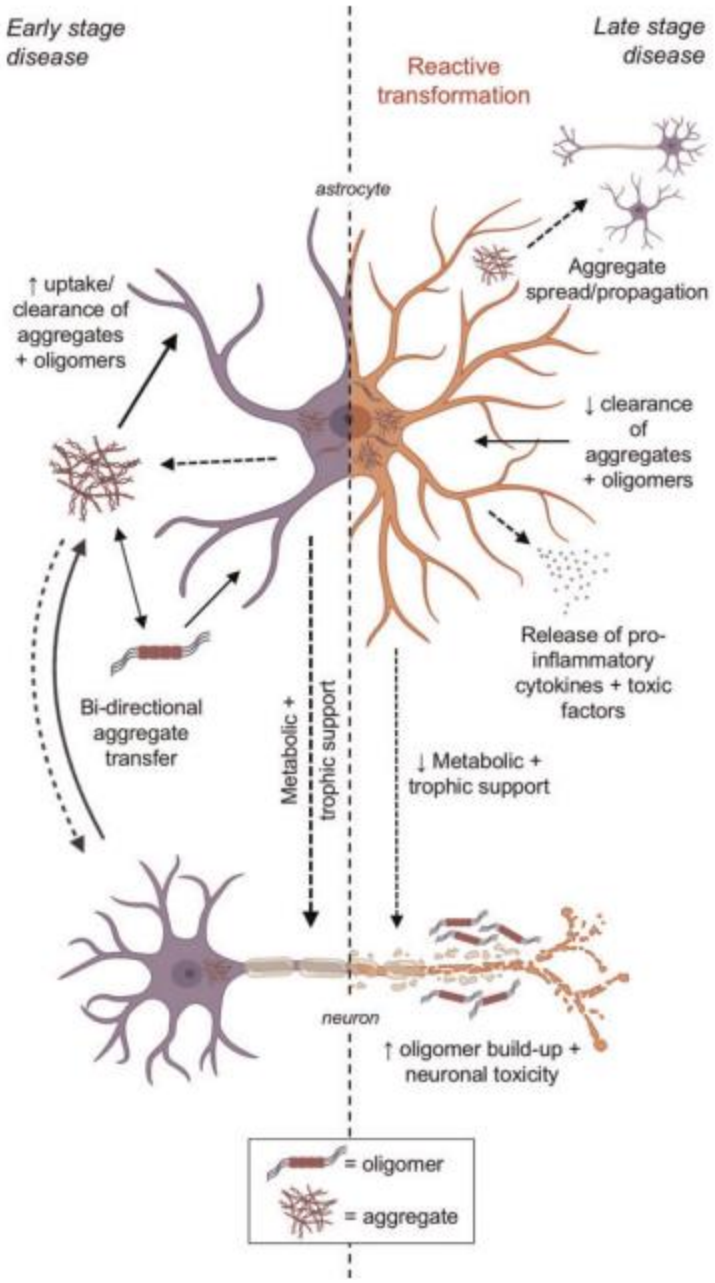

Figure 12 | Representation of hypothetical astrocytic involvement in prion-like mechanisms of early- and late-stage neurodegenerative disease

From Smethurst et al., 2022 – Brain [86]

The early stage represents an increased spread, uptake and clearance of aggregates and oligomers from neurons for degradation with continued metabolic and trophic support. Late-stage disease represents a decrease in aggregate and oligomer uptake, degradation, and clearance, increased reactive astrocyte transformation, increased aggregate spread and propagation to other neurons and astrocytes and increased oligomer build up resulting in increased neuronal toxicity.

Additionally, numerous studies point to an active role played by astrocytes in the propagation of prion-like proteins, such as pathological tau[89–91]. It has been shown that astrocytes contain aggregated tau in patients diagnosed with different tauopathies[15,92], and that astrocytes are known to internalize this tau from BD-EVs rather than freely secreted tau[68].

In addition to metabolic consequences of glial reactivity in NDDs, the position of astrocytes on the blood-brain barrier (BBB) has major importance for the permeability both into and out of the brain during disease. It is well-established that the BBB becomes more permeable and less selective as it breaks down, leaving the brain increasingly vulnerable to outside attacks and releasing pathological material from the brain into the periphery (**Figure 13**)[93].

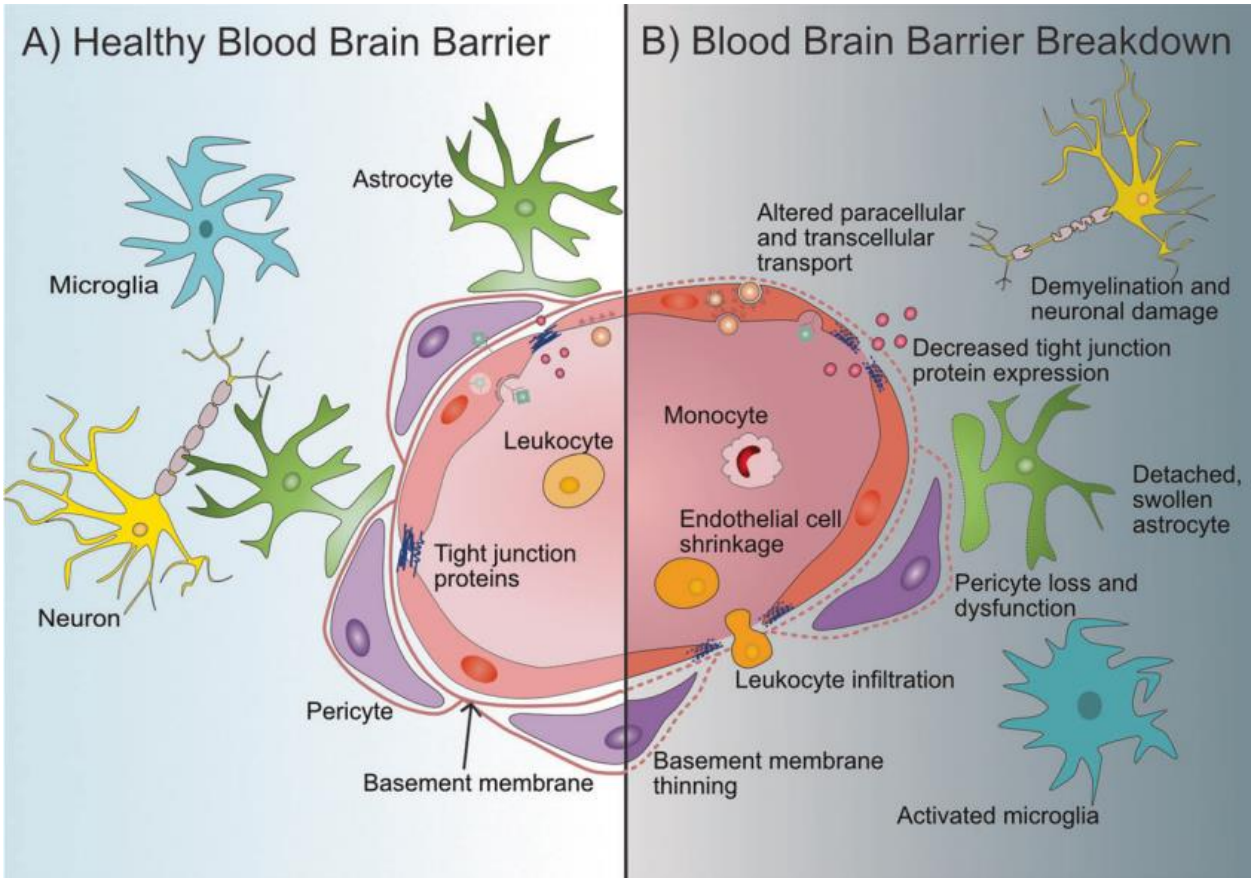

Figure 13 | Schematic representation of the BBB in a healthy state and during BBB breakdown

From Knox et al., 2022 – Molecular Psychiatry [93]

A) Healthy, intact BBB structure and surrounding cells and key components. Endothelial cells form the main physical barrier lining the blood vessels in the brain with tight junction proteins between them. Leukocytes are in constant circulation. Endothelial cells are encompassed by the basement membrane, which also encompasses pericytes in close contact to the endothelial cells. Astrocytic endfeet interact closely with the endothelial cells and pericytes and help maintain BBB integrity. Inactivated microglia and functional neurons are present in a healthy neurovascular unit.

B) During breakdown, BBB integrity can become compromised at various levels. Characteristics of disruption of the BBB include endothelial cell alterations such as loss of tight junction proteins, endothelial cell shrinkage, changes in molecular transport at the paracellular level, and transcellular level in some cases, and increased leukocyte infiltration. In some disruption models, pericyte dysfunction or loss is apparent. Astrocyte changes such as swollen or detached endfeet are also typical. Microglia can become activated, while neurons may experience demyelination or become damaged.

BBB = blood-brain barrier

Major pathways affected in neurodegenerative disorders

Several biochemical pathways are implicated, to different degrees, in most neurodegenerative diseases. Commonly dysregulated systems include cellular metabolism and energy homeostasis, proteostasis, synaptic transmission, inflammation, and axonal transport[3,94,95]. Generally speaking, neurodegenerative diseases all feature a marked increase in inflammation, decreased synaptic connectivity, decreased mitochondrial function, and decreased cytoskeletal integrity. What remains unknown is in what order these problems appear. Most groups studying the matter believe that inflammation is one of the first dominos to fall, however what comes next is unclear, and it's likely the exact sequence of events varies between pathologies and individuals. These pathways are all interconnected, so it is unsurprising that they are all implicated in many pathologies. For example, tau protein, normally a cytoskeleton stabilizer, dissociates and begins to aggregate within the cell. This causes axonal instability, decreased axonal transport of critical biomolecules and even mitochondria, and therefore reduced metabolic function. In parallel, intracellular aggregation of tau will also begin to increase inflammation, triggering reactive glia which will fail to provide metabolic support to synapses in need, leading to decreased synaptic function. While it is impossible to map an exact time course of the progression of these diseases, we are aware of the major pathways involved and the cellular and systemic consequences of this dysregulation.

Aims of the Thesis

This thesis has two aims, split into two chapters. The first aim is to perform an in-depth proteomic analysis on BD-EVs from the cortex of healthy and tauopathy patients to assess whether or not the content of BD-EVs reflects the molecular changes associated with different kinds of tauopathies (3R vs. 4R). This will be done by comparing the proteomic output with histopathological staining of sections of brain taken from the same region of the same patients as the BD-EVs and performing a correlative analysis between the two. The second aim is to develop a novel methodology for isolating BD-EVs from peripheral biofluids (plasma, saliva) whereby the protein corona of EVs is subjected to enzymatic digestion to reveal surface epitopes for immunocapture. This method also involved a thorough search for novel surface markers of BD-EVs to increase the efficiency of isolation in peripheral biofluids.

Summary of Publications

jove

Live-imaging of Mitochondrial System in Cultured Astrocytes

Jeanne Espourteille[1], Valentin Zufferey[1], Jean-Honoré Laurent[1], Kevin Richetin[1]

[1] Department of Psychiatry, Center for Psychiatric Neurosciences, Lausanne University Hospital (CHUV) and University of Lausanne

November 2021

Abstract

While much attention has been given to mitochondrial alterations at the neuronal level, recent evidence demonstrates that mitochondrial dynamics and function in astrocytes are implicated in cognition. This article describes the method for time-lapse imaging of astrocyte cultures equipped with a mitochondrial biosensor: MitoTimer. MitoTimer is a powerful and unique tool to assess mitochondrial dynamics, mobility, morphology, biogenesis, and redox state. Here, the different procedures for culture, image acquisitions, and subsequent mitochondrial analysis are presented.

Key Points:

- A novel methodology for the longitudinal live-imaging of the mitochondrial system in cultured astrocytes, and eventually other cell types, is proposed.
- The biosensor MitoTimer is used to visualize mitochondria and to determine their relative redox state at baseline and after H_2O_2 treatment.
- Based on MitoTimer visualization, mitochondrial morphological (elongation, sphericity, area, etc.) and motility (tracking of movement paths) metrics are analyzed alongside the redox state in order to assess the overall effect of treatment on the mitochondrial network.
- This methodology improves upon the existing standards of live-imaging in that microscope automation allows for the return to and imaging of the exact same cell(s) over multiple days. Therefore, researchers can compare the effect of a treatment to a cell's own baseline rather than to an average baseline over an entire well or ROI.
- This method also does not require high levels of light exposure, avoiding photobleaching of the cells of interest.

See Annex 1 for full publication[96]

Molecular Therapy
Original Article

Extracellular vesicles: Major actors of heterogeneity in tau spreading among human tauopathies

Elodie Leroux,[1,5] Romain Perbet,[1,5] Raphaëlle Caillierez,[1] Kevin Richetin,[2,3,4] Sarah Lieger,[1] **Jeanne Espourteille,[2]** Thomas Bouillet,[1] Séverine Bégard,[1] Clément Danis,[1] Anne Loyens,[1] Nicolas Toni,[2] Nicole Déglon,[3,4] Vincent Deramecourt,[1] Susanna Schraen-Maschke,[1] Luc Buée,[1] and Morvane Colin[1]

[1]Université de Lille, INSERM, CHU-Lille, Lille Neuroscience & Cognition, 59000 Lille, France

[2]Department of Psychiatry, Center for Psychiatric Neurosciences, Lausanne University Hospital (CHUV) and University of Lausanne, 1011 Lausanne, Switzerland

[3]Lausanne University Hospital (CHUV) and University of Lausanne, Neuroscience Research Center (CRN), Laboratory of Cellular and Molecular Neurotherapies, 1011 Lausanne, Switzerland

[4]Lausanne University Hospital (CHUV) and University of Lausanne, Department of Clinical Neuroscience (DNC), Laboratory of Cellular and Molecular Neurotherapies, 1011 Lausanne, Switzerland

February 2022

Abstract

Tauopathies are neurodegenerative diseases characterized by tau inclusions in brain cells. Seed-competent tau species have been suggested to spread from cell to cell in a stereotypical manner, indicating that this may involve a prion-like mechanism. Although the intercellular mechanisms of transfer are unclear, extracellular vesicles (EVs) could be potential shuttles. We assessed this in humans by preparing vesicles from fluids (brain-derived enriched EVs [BD-EVs]). These latter were isolated from different brain regions in various tauopathies, and their seeding potential was assessed in vitro and in vivo. We observed considerable heterogeneity among tauopathies and brain regions. The most striking evidence was coming mainly from Alzheimer's disease where the BD-EVs clearly contain pathological species that can induce tau lesions in vivo. The results support the hypothesis that BD-EVs participate in the prion-like propagation of tau pathology among tauopathies, and there may be implications for diagnostic and therapeutic strategies.

Key Points:

- BD-EVs from AD patients contain seed-competent tau species, whereas PiD and PSP patient BD-EVs contain less seed-competent tau.
- The tau species which are shuttled by BD-EVs are very heterogenous in isoform and in seeding capacity.

See Annex 2 for full publication[66]

cells

MDPI

Article

Tau Transfer via Extracellular Vesicles Disturbs the Astrocytic Mitochondrial System

Romain Perbet [1], Valentin Zufferey [2], Elodie Leroux [1], Enea Parietti [2], **Jeanne Espourteille [2]**, Lucas Culebras [2], Sylvain Perriot [3], Renaud Du Pasquier [3], Séverine Bégard [1], Vincent Deramecourt [1], Nicole Déglon [4], Nicolas Toni [2], Luc Buée [1], Morvane Colin [1,*,†] and Kevin Richetin [2,*,†]

[1] Univ. Lille, Inserm, CHU Lille, LilNCog—Lille Neuroscience & Cognition, 59000 Lille, France; vincent.deramecourt@chu-lille.fr (V.D.)

[2] Department of Psychiatry, Center for Psychiatric Neurosciences, Lausanne University Hospital (CHUV) and University of Lausanne, 1011 Lausanne, Switzerland

[3] Laboratory of Neuroimmunology, Neuroscience Research Centre, Department of Clinical Neurosciences, CHUV, 1011 Lausanne, Switzerland

[4] Lausanne University Hospital (CHUV) and University of Lausanne, Neuroscience Research Center (CRN), Laboratory of Neurotherapies and Neuromodulation, 1011 Lausanne, Switzerland

* Correspondence: morvane.colin@inserm.fr (M.C.); kevin.richetin@chuv.ch (K.R.)

† These authors contributed equally to this work.

March 2023

Abstract

Tauopathies are neurodegenerative disorders involving the accumulation of tau isoforms in cell subpopulations such as astrocytes. The origins of the 3R and 4R isoforms of tau that accumulate in astrocytes remain unclear. Extracellular vesicles (EVs) were isolated from primary neurons overexpressing 1N3R or 1N4R tau or from human brain extracts (progressive supranuclear palsy or Pick disease patients or controls) and characterized (electron microscopy, nanoparticle tracking analysis (NTA), proteomics). After the isolated EVs were added to primary astrocytes or human iPSC-derived astrocytes, tau transfer and mitochondrial system function were evaluated (ELISA, immunofluorescence, MitoTracker staining). We demonstrated that neurons in which 3R or 4R tau accumulated had the capacity to transfer tau to astrocytes and that EVs were essential for the propagation of both isoforms of tau. Treatment with tau-containing EVs disrupted the astrocytic mitochondrial system, altering mitochondrial morphology, dynamics, and redox state. Although similar levels of 3R and 4R tau were transferred, 3R tau-containing EVs were significantly more damaging to astrocytes than 4R tau-containing EVs. Moreover, EVs isolated from the brain fluid of patients with different tauopathies affected mitochondrial function in astrocytes derived from human iPSCs. Our data indicate that tau pathology spreads to surrounding astrocytes via EVs-mediated transfer and modifies their function.

Key Points:

- A proposition of new mechanisms of tau transfer from neurons to astrocytes.
- Most soluble neuronal tau is secreted in free form, however the majority of neuronal tau which is internalized by astrocytes is contained to large EVs.
- 3R and 4R tau have different effects on the astrocytic mitochondrial network, with 3R tau inducing more oxidation and smaller, fragmented mitochondria and 4R tau inducing reduction with longer, filamentous mitochondria.
- These differences between 3R and 4R tau are confirmed with BD-EVs from PiD and PSP patients, representing 3R and 4R tauopathies respectively, suggesting that BD-EVs carry isoform-specific species of tau from neurons to astrocytes.

See Annex 3 for full publication[68]

Karger OPEN ACCESS

Neurodegenerative Diseases

Circulating Biomarkers for Alzheimer's Disease: Unlocking the Diagnostic Potential in Low- and Middle-Income Countries, Focusing on Africa

Luc Nwamekang Belinga[1,2,3] MD, **Jeanne Espourteille[1]**, Yembe Wepnyu Njamnshi [3,4,5] MD, Ariole Zafack Zeukang[3], Olivier Rouaud[2] MD, Alfred Kongnyu Njamnshi [3,4,6+] MD, Gilles Allali[2+] MD & Kevin Richetin[1,2*] PhD

[1] Department of Psychiatry, Center for Psychiatric Neurosciences, Lausanne University Hospital (CHUV) and University of Lausanne, 1011 Lausanne, Switzerland

[2] Leenaards Memory Center, Department of Clinical Neurosciences, Lausanne University Hospital, University of Lausanne, 1011 Lausanne, Switzerland.

[3] Department of Translational Neuroscience, Brain Research Africa Initiative (BRAIN), 1226 Thonex-Geneva, Switzerland & 25625 Yaoundé, Cameroon

[4] Neuroscience Lab, Faculty of Medicine & Biomedical Sciences, The University of Yaoundé I, 337 Yaoundé, Cameroon.

[5] Division of Health Operations Research, Ministry of Public Health, 3038 Yaoundé III, Cameroon.

[6] Department of Clinical Neuroscience and Neurology, Yaoundé Central Hospital, 87 Yaoundé, Cameroon

+Equal contribution *Corresponding

March 2024

Abstract

Background: Alzheimer's disease (AD) is emerging as a significant public health challenge in Africa, with predictions indicating a tripling in incidence by 2050. The diagnosis of AD on the African continent is notably difficult, leading to late detection that severely limits treatment options and significantly impacts the quality of life for patients and their families.

Summary: This review focuses on the potential of high-sensitivity specific blood biomarkers as promising tools for improving AD diagnosis and management globally, particularly in Africa. These advances are particularly pertinent in the continent, where access to medical and technical resources is often limited.

Key Messages: Identifying precise, sensitive, and specific blood biomarkers could contribute to the biological characterization and management of Alzheimer's disease in Africa. Such advances promise to improve patient care and pave the way for new regional opportunities in pharmaceutical research and drug trials on the continent for Alzheimer's disease.

Key Points:

- Lower-middle income countries rely heavily on clinicoradiological evidence for the diagnosis of Alzheimer's disease, however this approach carries a relatively high risk of misdiagnosis and excludes many potential patients from clinical trials due to limited patient characterization and a very strict biological definition of AD.
- Focusing on blood biomarkers in LMIC, particularly many countries in Africa, could help address these challenges and lead to a more comprehensive patient characterization and diagnostic effort.
- The combination of blood biomarkers associated with neuroinflammation and vascular modulation provides a noninvasive and cost-effective diagnostic approach which could increase clinical trial participation in LMIC.
- It is essential, however, to standardize measurement techniques and conduct validation studies which consider confounding factors in order for this to be implemented properly

See Annex 4 for full publication[33]

Cold Spring Harbor Laboratory
bioRxiv
THE PREPRINT SERVER FOR BIOLOGY

Inverse and Postponed Impacts of Extracellular Tau PHF on Astrocytes and Neurons' Mitochondrial Function

Valentin Zufferey[1], Enea Parietti[1], Aatmika Barve[1], **Jeanne Espourteille[1]**, Yvan Varisco[2], Kerstin Fabbri[2], Francesca Capotosti[2], Nicolas Preitner[2], Kevin Richetin[1,3*]

[1] Centre des Neurosciences Psychiatriques (CNP), Centre Hospitalier Universitaire Vaudois (CHUV) - Université de Lausanne (UNIL)

[2] AC Immune SA, Lausanne, Switzerland

[3] Centre Leenaards de la mémoire, Centre Hospitalier Universitaire Vaudois (CHUV) - Université de Lausanne (UNIL)

Abstract

Background: Tauopathies encompass a spectrum of neurodegenerative disorders which are marked by the pathological aggregation of tau protein into paired helical filaments (PHF-tau), neurofibrillary tangles (NFTs) and Glial-fibrillary tangles (GFTs). These aggregates impair cellular, mitochondrial, and synaptic functions. The emergence of extracellular tau (ePHF-tau), featuring a myriad of isoforms and phosphorylation states, presents a challenge in comprehending its nuanced effects on neural cells, particularly concerning synaptic and mitochondrial integrity.

Methods: We studied the impact of ePHF-tau (2N4R) on different states and ages of primary cultures of rat neuroglia. Using confocal microscopy and proteomic analysis of synaptosomes, we studied the impact of ePHF-tau on neurite and synapse number. We monitored mitochondrial responses in neurons and astrocytes over 72 hours using advanced fluorescence microscopy for dynamic, high-throughput analysis.

Results: Treatment with ePHF-tau has a strong effect on the neurites of immature neurons, but its toxicity is negligible when the neurons are more mature. At the mature stage of their development, we observed a substantial increase in the density of the PSD-95/vGlut1 zone in neurite, suggesting altered synaptic connectivity and ePHF-tau excitotoxicity. Proteomics revealed significant changes in mitochondrial protein in synaptosomes following exposure to ePHF-tau. In the neuronal compartment, real-time imaging revealed rapid and persistent mitochondrial dysfunction, increased ATP production, and reduced mitochondrial turnover. In contrast, we observed increased mitochondrial turnover and filamentation after treatment in the astrocyte processes, indicating cell-specific adaptive responses to ePHF-tau.

Conclusions: This study sheds light on the intricate effects of extracellular tau aggregates on neuronal and astrocytic mitochondrial populations, highlighting how tau pathology can lead to mitochondrial disturbances and synaptic alterations. By delineating the differential responses of neurons and astrocytes to ePHF-tau, our findings pave the way for developing targeted therapeutic interventions to mitigate the detrimental impacts of tau aggregates in neurodegenerative diseases.

Key Points:

- This study highlights the differences between the toxic effects of extracellular tau aggregates on neurons and astrocytes, specifically looking at mitochondrial and synaptic function.

- The mitochondria of neurons are affected rapidly and progressively, while mitochondria of astrocytes are not initially strongly affected by tau aggregates but show reaction a few days later.
- Extracellular tau aggregates induce an increase in neuronal excitability at the synapse.

See Annex 5 for full publication[97]

Chapter 1

Proteomic Signature of Prefrontal Cortex Derived Extracellular Vesicles Accurately Predicts 3R and 4R Tau Pathology

Proteomic Signature of Prefrontal Cortex Derived Extracellular Vesicles Accurately Predicts 3R and 4R Tau Pathology

Jeanne Espourteille[1], Aatmika Barve[1]*, Valentin Zufferey[1]*, Elodie Leroux[4], Nicolas Toni[1], Luc Buée[4], Morvane Colin[4], Kevin Richetin[1,2,3]

[1] Department of Psychiatry, Center for Psychiatric Neurosciences, Lausanne University Hospital (CHUV) and University of Lausanne, 1011 Lausanne, Switzerland

[2] Lausanne University Hospital (CHUV) and University of Lausanne, Neuroscience Research Center (CRN), Laboratory of Cellular and Molecular Neurotherapies, 1011 Lausanne, Switzerland

[3] Lausanne University Hospital (CHUV) and University of Lausanne, Department of Clinical Neuroscience (DNC), Laboratory of Cellular and Molecular Neurotherapies, 1011 Lausanne, Switzerland

[4] Université de Lille, INSERM, CHU-Lille, Lille Neuroscience & Cognition, 59000 Lille, France

Keywords: Tauopathy; extracellular vesicles; glia; neuron; proteomics; 3R tau; 4R tau; prefrontal cortex

Graphical Abstract

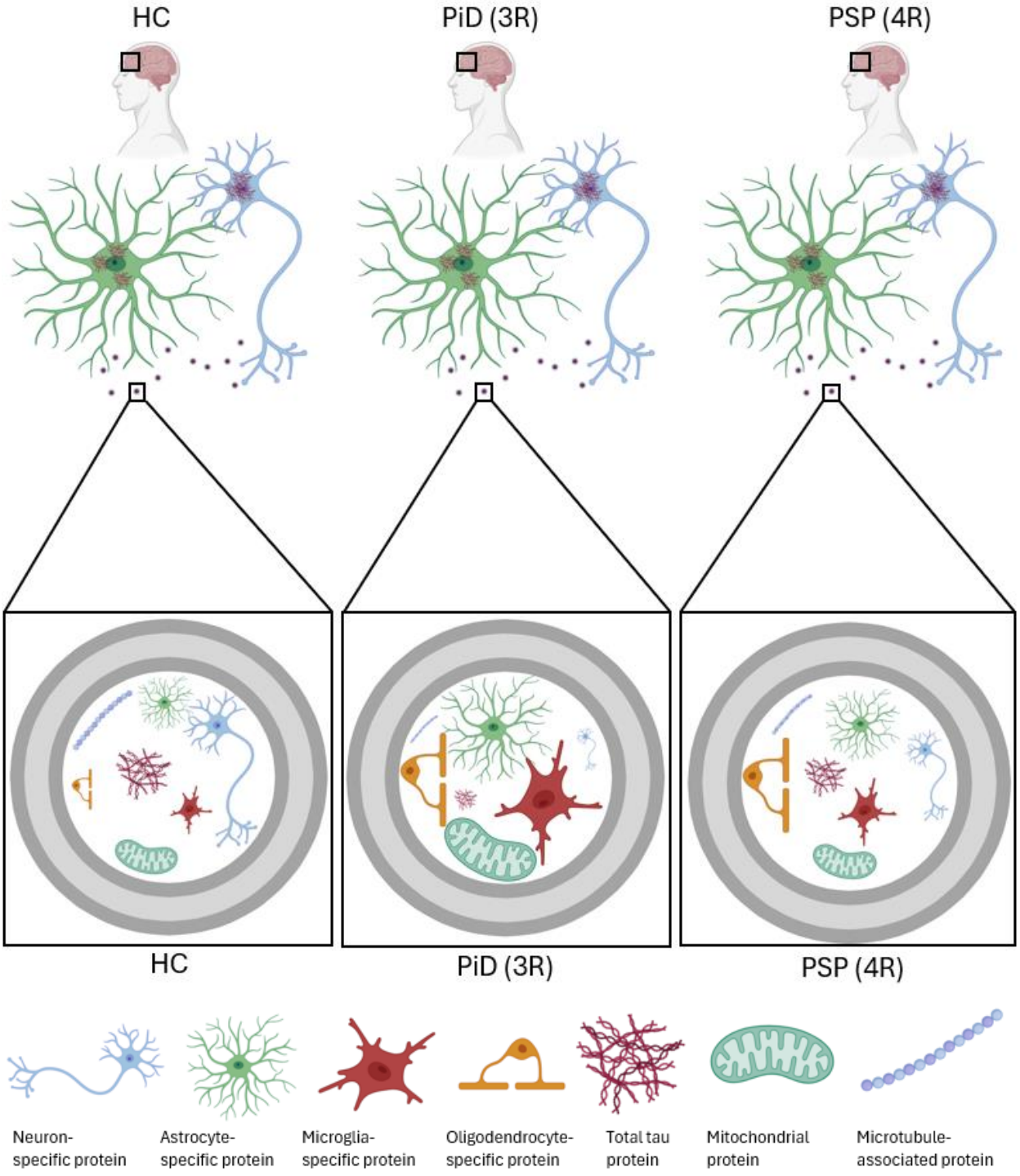

BD-EVs from patient frontal cortex reflect isoform-specific differences in aggregates which are not revealed with AT8 and AT100 histopathology. Icon size within BD-EVs is proportional to corresponding protein abundance in BD-EVs

Abstract

Currently, the field of neuroscience is lacking in biomarkers which can reveal the subtle differences between neurodegenerative diseases, such as tauopathies, which are not apparent in clinical evaluation. Such markers would improve diagnostic efforts, allow for earlier and more specific treatment options, and overall improve patient care. We know from histopathological analysis of post-mortem brain tissue that there are many molecular differences between tauopathies, from the isoform of tau which aggregates, to the cell types affected, to the size and shape of inclusions, but these differences are not visible to clinicians treating living patients. Brain derived extracellular vesicles (BD-EVs), however, contain biological cargo from their parent cells which can provide insight into the health status of the brain. Indeed, we have found that the proteomic content of EVs from tauopathy patients' frontal cortex correlates to the pathological tau accumulation within the cortex and can even be used to accurately predict disease status, differentiating between 3R (PiD) and 4R (PSP) tau pathology. Features such as glial, mitochondrial, and microtubule-associated protein abundances varied in relation to the tau inclusions present in patient brains. Knowing that their cargo reflects cellular nuances in the tauopathy brain, and that BD-EVs can cross biological barriers to be isolated in peripheral biofluids, they are ideal carriers of cerebral biomarkers which could be used to aid in patient screening or diagnosis.

Introduction

In the intricate tapestry of the human brain, tau protein plays a pivotal role in maintaining neuronal integrity. In its healthy state, tau stabilizes microtubules, vital components of the neuronal cytoskeleton, aiding in nutrient transport and cellular communication[6,98,99]. However, when tau becomes dysfunctional, it gives rise to a class of neurodegenerative diseases known as tauopathies[18].

The heterogeneity of tauopathies is striking; they manifest in a spectrum of clinical presentations and neuropathological profiles. Each tauopathy has distinct clinical and pathological features but shares the commonality of tau dysfunction. The mechanisms leading to tau aggregation are complex and not yet fully understood. They involve abnormal phosphorylation of tau, which reduces its affinity for microtubules and increases its propensity to form intracellular aggregates[9,100]. The specific pattern of tau deposition, the isoforms of tau which aggregate, and the regional brain involvement vary across different tauopathies, which can influence the clinical presentation and progression of the disease (**Figure 1**)[14,15,17,18]. For instance, Pick's disease (PiD) is typically characterized by the presence of "Pick bodies", large inclusions of 3R tau in neurons

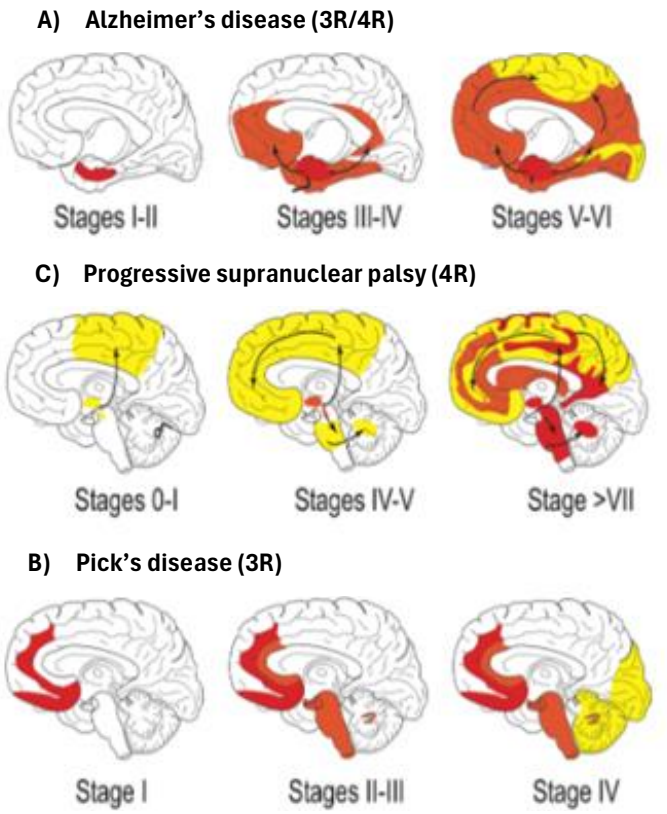

Figure 1 | Progression of tau pathology through the brain

Modified from Colin et al., 2020 - Acta Neuropathologica [5]

A) Staging of tau pathology in AD. Topographic distribution of tau lesions at the different stages of tau pathology in schemes of brains in medial views. Stages I and II, tau lesions invade entorhinal and transentorhinal regions. Stages III and IV: lesions involve the associative areas of the neocortex, and finally, during stages V and VI, tau lesions invade all the primary and secondary neocortical areas. (From Braak et al., 2013).

B) Staging of tau pathology in PSP. Topographical distribution of tau lesions at the different neuropathological stages of PSP in schematic brain representations in medial views. Stages 0/I—Only the pallido-luyso-nigral complex shows tau pathology with weak involvement of the premotor cortex. Stage II/III—Tau pathology reaches the basal ganglia, pedunculopontine nucleus and dentate nucleus. Stages IV/V—Frontal and temporal lobes are involved. Stages VI/VII—Subthalamic nucleus, substantia nigra, internal globus pallidus, neocortical areas, pedunculopontine nucleus and cerebellum are more severely affected. (Modified from Williams et al., 2007).

C) Staging of tau pathology in PiD. Topographical distribution of Pick bodies at the different stages of tau pathology evolution in schematic brain representations in medial views. Stage I Tau pathology is deposited in the limbic and neocortical frontotemporal regions as well as the angular gyrus. Stages II/III—White matter tracts, subcortical structures, serotonergic/noradrenergic brainstem nuclei are affected, followed by the primary motor cortex and pre-cerebellar nuclei. Finally, in stage IV, tau is deposited in the visual cortex as well as in the cerebellar granular layer and brainstem white matter.

AD = Alzheimer's disease, PSP = progressive supranuclear palsy, PiD = Pick's disease

of the prefrontal cortex, whereas progressive supranuclear palsy (PSP) and corticobasal degeneration (CBD) are characterized by glial inclusions of 4R tau, often resulting in a "tufted" or "thorny" astrocyte phenotype (**Figure 2**)[101,102]. This diversity in tauopathies suggests that while tau is a common pathological thread, disease-specific factors determine the more subtle phenotypes of this family of diseases. Indeed, knowing the impact of pathological tau on the mitochondrial system, our group sought to investigate whether the mitochondria of human iPSC derived astrocytes were sensitive to different forms of tau[68]. Free form soluble tau is not taken up by astrocytes, so we seeded extracellular vesicles containing either 3R tau or 4R tau from neurons which had been virally infected to overexpress either tau 1N3R or tau 1N4R. The 3R and 4R tau affected astrocytic mitochondria differently, with 3R tau causing oxidation and significant reduction of mitochondrial length and 4R tau having the exact opposite effect. Importantly, this phenomenon was again observed when astrocytes were treated with EVs from patients with 3R tau pathology (PiD) or 4R tau pathology (PSP), suggesting that BD-EVs from tauopathy patients carry isoform-specific tau seeds which impact the mitochondrial system of astrocytes differently[68]. Interestingly, the opposite effect was previously observed in neurons, where 4R tau impacted mitochondrial axonal transport more severely[103].

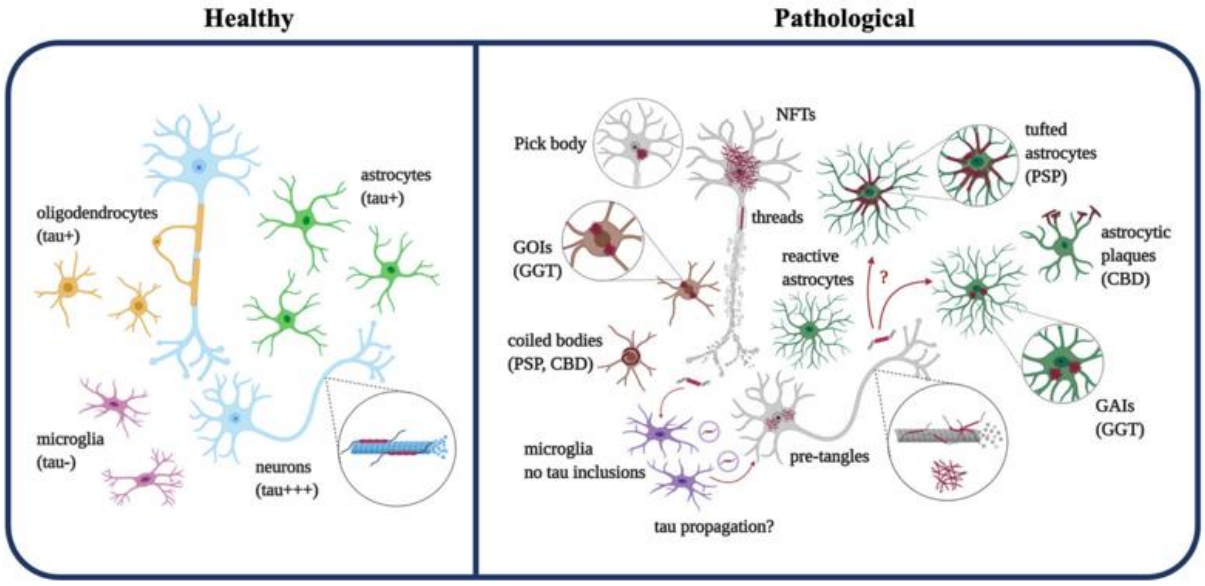

Figure 2 | Kinds of pathological tau lesions in different tauopathies

From Chung et al., 2021 – Molecular Degeneration [67]

In the healthy brain (left), microtubule-binding protein tau interacts with neuronal microtubules to promote stability and facilitate axonal transport. While neurons have the highest expression level of tau, oligodendrocytes and astrocytes also express endogenous tau, albeit at lower levels. Microglia do not express endogenous tau. In a pathological condition (right), tau becomes aberrantly aggregated in the form of various inclusions, impaired in its physiological functions, such as supporting microtubule stability. In neurons, tau can accumulate in the forms of NFTs, neuropil threads, or Pick bodies. Tau also accumulates in astrocytes, mostly in primary tauopathies such as PSP, CBD, and GGT, in the form of tufted astrocytes, astrocytic plaques, and GAIs. Moreover, tau aggregates in oligodendrocytes in the form of coiled bodies or GOIs. Microglia do not form tau inclusions, while accumulating studies have suggested that they may contribute to tau propagation.

PSP = progressive supranuclear palsy, CBD = corticobasal degeneration, GGT = globular glial tauopathy, NFT = neurofibrillary tangle, GOI = globular oligodendroglial inclusion, GAI = globular astrocytic inclusion

Clinicians today still struggle to differentiate and diagnose tauopathies early in the disease progression. This is particularly true of primary tauopathies, for which the main protein driver is tau. Circulating biomarkers like phosphorylated tau (P-tau) in blood and cerebrospinal fluid (CSF) are increasingly accurate at reflecting tau pathology in the brain at earlier timepoints in disease progression, but they are often only validated for pathologies like AD which have amyloid beta as a pathology driver as well[27]. Some tau positron emission tomography (PET) tracers can differentiate 4R tau inclusions and thus can identify diseases like PSP and CBD, however these tracers are not yet validated for clinical use[32]. Interestingly, proteomic analysis of tau inclusions in human 3R and 4R pathology is able to distinguish specific tauopathies based on posttranslational modifications present in the insoluble tau aggregates obtained from brain tissue[38]. While the insoluble tau showed specific phenotypes for each pathology, insoluble tau from the same aggregates could not differentiate between these pathologies. Different forms of soluble hyperphosphorylated tau are measured in blood and CSF for diagnostic purposes currently, but this study reinforces what is already known about these measurements: they cannot diagnose primary tauopathies.

Extracellular vesicles (EVs), once considered mere cellular debris, have now gained prominence as a potential diagnostic tool[42]. Brain derived EVs (BD-EVs), shed by cells into the brain's interstitial spaces, encapsulate a cargo that reflects the physiological and pathological state of the parent cell. EVs, therefore, hold a snapshot of the cellular environment and could serve as a window into the brain's health[56]. What is lacking most in today's biomarkers is something which can reflect the specific tau landscape of the brain. Total tau (T-tau) and P-tau inform clinicians about how much tau is present and how much of it is hyperphosphorylated, but not which isoform or whether it is aggregating in neurons or glia. With their vast proteomic cargo, BD-EVs may hold the clues necessary for precise tauopathy diagnosis. Indeed, there are many other groups with this line of thinking, trying to use BD-EVs as biomarkers for a wide variety of NDDs[104–108].

Results

Challenges in distinguishing 3R and 4R tauopathies in prefrontal cortex: insights from detailed tau aggregation analysis

We questioned whether tau protein aggregation could differentiate the prefrontal cortex of patients diagnosed with 3R tauopathy (Pick's disease (PiD)) or 4R tauopathy (progressive supranuclear palsy (PSP)) from healthy controls (HC). To this end, we examined the post-mortem prefrontal cortex of diagnosed patients using AT8 antibodies for the early stages of tau aggregation[109–114] and AT100 antibodies for the later stages[109,115]. We conducted complete tissue sections for each patient and performed an automated multiparametric analysis (**Figure 1A**). This analysis aimed to quantify the densities of small inclusions (sized between 2 and 5um) and globular and flame-shaped neurofibrillary tangles (NFTs) for each form of tau aggregate (AT8 and AT100), (**Figure 1B**). Although AT8 and AT100 coverage measurements revealed apparent individual elevations in some PSP and PiD patients, in group terms, we observed no significant difference in the number of total tau lesions observed between healthy controls and the different types of tauopathy (**Figure 1C-D**). Analysis of the distribution of different types of inclusions across the sections showed that the AT8 and AT100 inclusions observed in patients and controls were predominantly small (**Figure 1E-F**). Regardless of size, tau aggregates did not differentiate healthy controls from 3R and 4R tauopathies in their early (AT8) forms (**Figure 1E**). However, in the advanced forms of aggregates (AT100), small aggregates were more abundant in PiD and PSP patients, while globular aggregates were less frequent in both tauopathies than in healthy controls (**Figure 1F**). Despite a multiparametric approach, these results demonstrate the difficulty of distinguishing between different types of 3R and 4R tauopathy in the prefrontal cortex according to the tau hyperphosphorylation and aggregation level.

The isoform of tau aggregated in frontal cortex does not impact the number or quality of cortical BD-EVs

Serial parts of prefrontal cortex samples (adjacent to samples used for histopathological characterization) were prepared to isolate brain derived (BD)-fluids according to the protocol described by Leroux and colleagues[66]. Then, BD fluid-derived EVs (BD-EV) were isolated from human BD fluid using differential centrifugation and size exclusion chromatography (SEC). BD-EVs were then subjected to nanoparticle tracking analysis (NTA) to evaluate their size and concentration, as

well as liquid chromatography tandem mass spectrometry (LC-MS/MS) to evaluate their protein content (**Figure 2A**).

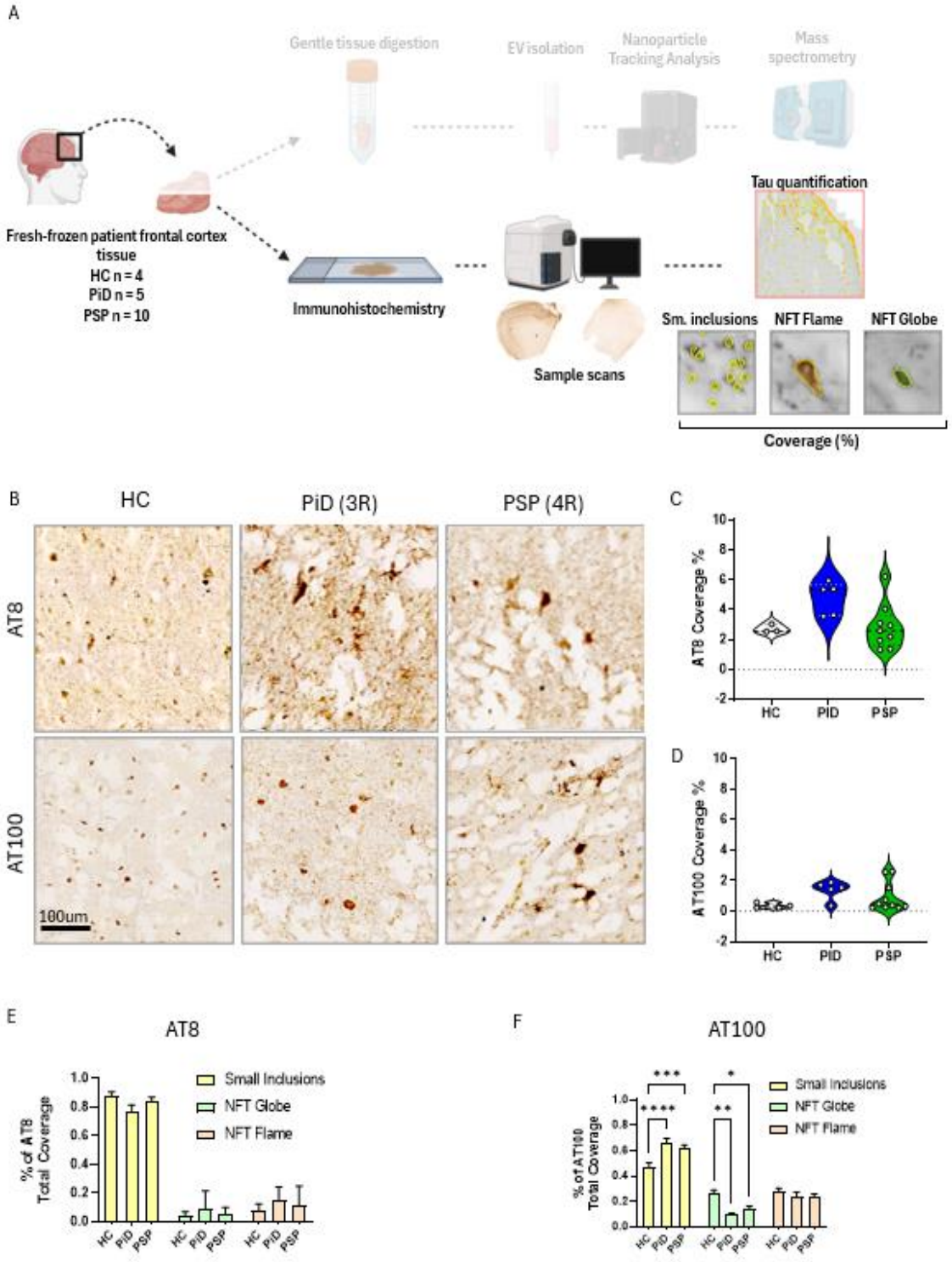

Figure 1 | Analysis of aggregated tau in human prefrontal cortex cannot differentiate tauopathies from each other

A) Illustration of the procedure to investigate how BD-EVs reflect brain tau pathology. Highlighted is the tau IHC portion.
B) Micrographs of patient tissues stained for phopho-tau. Scale bar: 100um
C) Violin plot of the percent coverage of AT8 by patient group. Each dot represents one patient. Kruskal-Wallis test with Dunn's multiple comparisons test revealed no significant differences between groups.
D) Violin plot of the percent coverage of AT100 by patient group. Each dot represents one patient. Kruskal-Wallis test with Dunn's multiple comparisons test revealed no significant differences between groups.
E) Shares of the different type of inclusions (within total coverage) of AT8. Ordinary two-way ANOVA with Tukey's multiple comparisons test with single pooled variance did not reveal any significant differences between groups.
F) Shares of the different types of inclusions (within total coverage) of AT100. Ordinary two-way ANOVA with Tukey's multiple comparisons test with single pooled variance was run. * $p < 0.05$, ** $p < 0.01$, *** $p < 0.001$, **** $p < 0.0001$

HC = healthy control, PiD = Pick's disease, PSP = progressive supranuclear palsy, NFT = neurofibrillary tangle

Firstly, measurements with NTA indicated that PiD and PSP pathology do not affect the concentration of BD-EVs circulating in the patient's prefrontal cortex fluids (**Figure 2B-C**). PiD pathology does, however, shift the size distribution of the EV sample towards having a higher ratio of small EVs (<150nm) and to large EVs (>150nm) than HC (**Figure 2C-D**). We also used proteomic analysis to evaluate the quality of BD-EV isolations. We revealed that the majority of proteins detected in patient BD-EVs are shared among healthy and pathological samples, while a small number of proteins are detected only in PiD or PSP **(Figure 2E**). Using the MISEV2018 guidelines, we then annotated all proteins according to their known association with EVs as potential EV markers or potential contaminants of EV isolation[54]. This analysis revealed a significantly higher abundance of EV-associated proteins than components of non-EV associated co-isolated structures **(Figure 2F**) in all three patient groups, indicating that EV samples are highly enriched in vesicular material and relatively pure of contaminating intracellular material. Taken all together, these results indicate that tau pathology does not influence the quantity or quality of BD-EVs secreted into the interstitial fluid (ISF) of patients but may affect other aspects of the proteomic makeup of BD-EVs as well as the size distribution.

Then, we investigated whether size distribution, EV protein abundance and particle count could be used in machine learning to predict patient disease status. To do this, we used OneVsRest classifier model to evaluate the abilities of the features described in Figure 2A-F to differentiate between disease classes. We used the F1 score to evaluate the model's prediction accuracy, as both precision and recall were critically important. In this first round of machine learning, the model could only reliably predict HC patients on the basis of the percentage of large EVs present in the sample (**Figure 2G**). This further corroborates the conclusion of the findings in Figure 2A-F that none of these features differ importantly between the patient groups except the ratio of small and large EVs in the

sample. Even so, this feature was not specific enough to differentiate between PiD and PSP, only HC from pathology (**Figure 2G**). Finally, we investigated whether these criteria correlated with the level of pathophysiology assessed by multiparametric quantification of tau aggregation on the serial brain sections (evaluated in Figure 1). Indeed, we observed that the ratio of small and large EVs correlates significantly with certain histopathological features, such as the percentage of AT100 inclusions which are globular NFTs or small inclusions **(Figure 2H**). If we look more closely at this relationship, we see that while the correlation is significant, these parameters do not efficiently separate the three groups (**Figure 2I-J**).

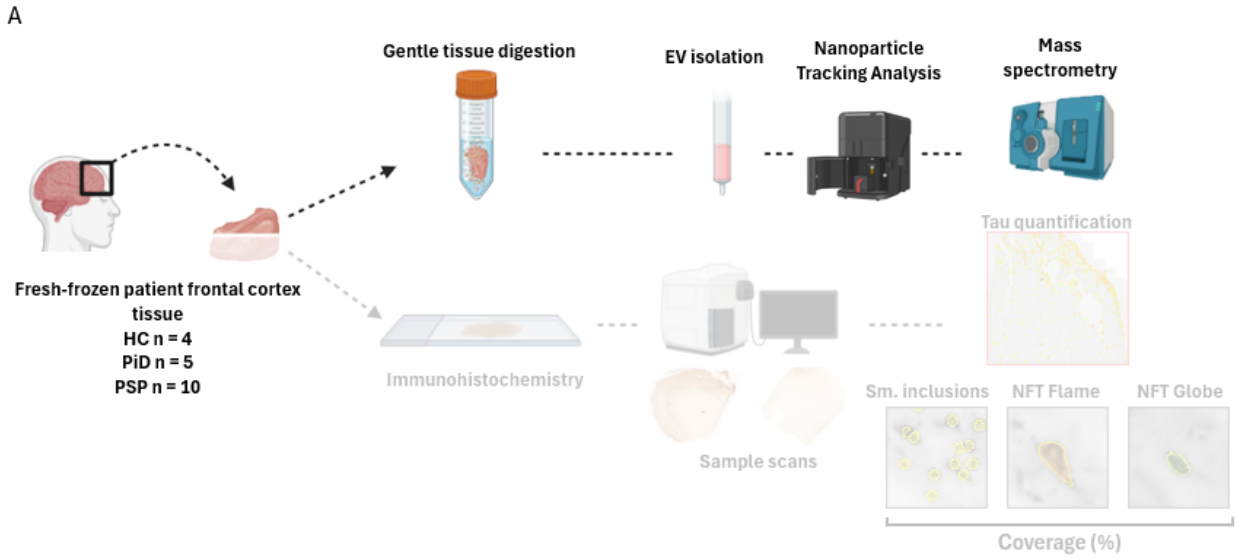
A
Gentle tissue digestion
EV isolation
Nanoparticle Tracking Analysis
Mass spectrometry
Fresh-frozen patient frontal cortex tissue
HC n = 4
PiD n = 5
PSP n = 10
Immunohistochemistry
Tau quantification
Sm. inclusions
NFT Flame
NFT Globe
Sample scans
Coverage (%)

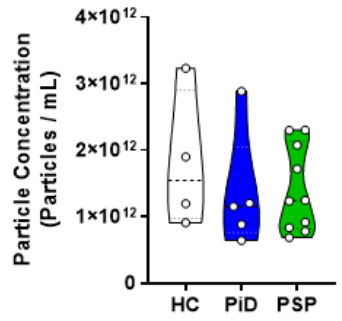
B
Particle Concentration (Particles / mL)
HC
PiD
PSP

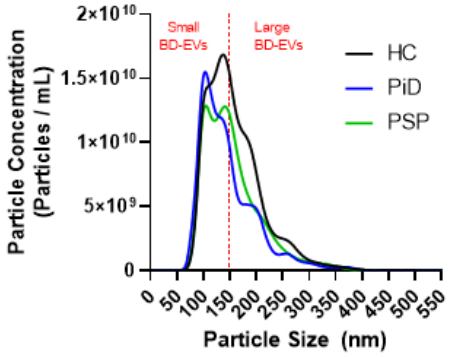
C
Particle Concentration (Particles / mL)
Small BD-EVs
Large BD-EVs
HC
PiD
PSP
Particle Size (nm)

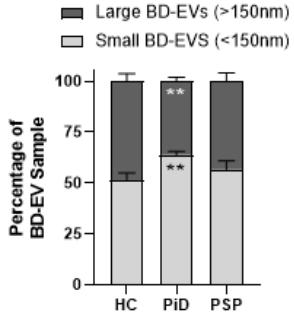
D
Large BD-EVs (>150nm)
Small BD-EVS (<150nm)
Percentage of BD-EV Sample
HC
PiD
PSP

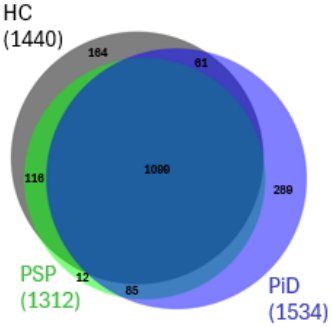
E
HC (1440)
PSP (1312)
PiD (1534)

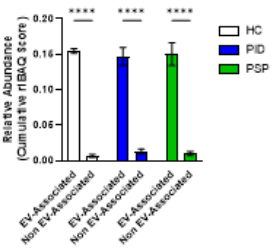
F
Relative Abundance (Cumulative riBAQ score)
HC
PiD
PSP

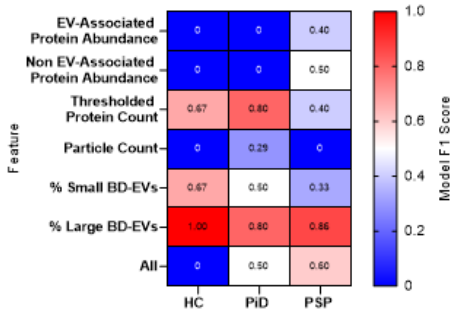
G
EV-Associated Protein Abundance
Non EV-Associated Protein Abundance
Thresholded Protein Count
Particle Count
% Small BD-EVs
% Large BD-EVs
All
Feature
HC
PiD
PSP
Model F1 Score

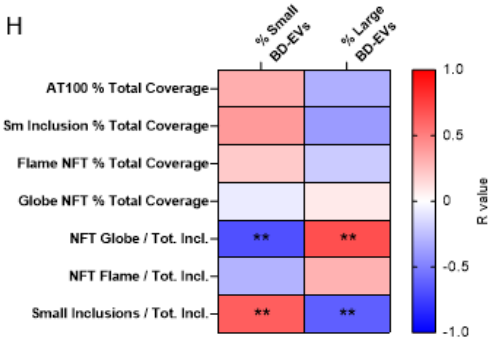
H
% Small BD-EVs
% Large BD-EVs
AT100 % Total Coverage
Sm Inclusion % Total Coverage
Flame NFT % Total Coverage
Globe NFT % Total Coverage
NFT Globe / Tot. Incl.
NFT Flame / Tot. Incl.
Small Inclusions / Tot. Incl.
R value

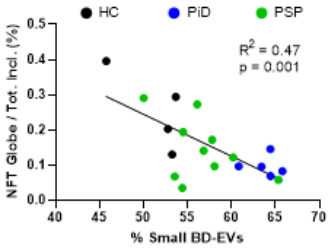
I
HC
PiD
PSP
R² = 0.47
p = 0.001
NFT Globe / Tot. Incl. (%)
% Small BD-EVs

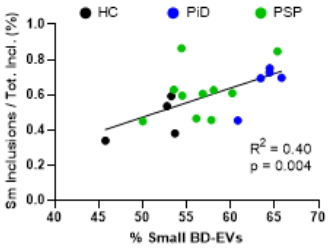
J
HC
PiD
PSP
R² = 0.40
p = 0.004
Sm Inclusions / Tot. Incl. (%)
% Small BD-EVs

Figure 2 | Tau pathology does not impact concentration or quality of cortex BD-EVs

A) Illustration of the procedure to investigate how BD-EVs reflect brain tau pathology. Highlighted is the BD-EV analysis portion.
B) Violin plot depicting the concentration of BD-EVs detected by NTA by patient group. Each dot represents one patient.
C) Area graph depicting the size and number of EVs in each patient group. Numbers have been normalized by tissue weight prior to EV extraction.
D) Stacked bar graph showing the ratio of small (<150nm) to large (>150nm) EVs by patient group. Kruskal-Wallis test with Dunn's multiple comparisons test revealed a significant difference between PiD and HC. ** $p < 0.01$
E) Venn diagram showing the number of proteins present after threshold filtration in the BD-EV of HC, PiD and PSP patients.
F) Bar graph quantifying the abundance of protein associated with EVs vs. potentially contaminating protein of EV isolation according to MISEV2018 guideline categories. Two-way ANOVA was run with Sidak's multiple comparisons test with a single pooled variance. **** $p<0.0001$
G) Confusion matrix depicting the performance of a classification model based on BD-EV quality control features from parts B-F.
H) Heatmap derived from correlation matrix comparing aspects of EV quality with histological findings from Figure 1. R values are plotted, two-tailed Pearson's correlation test was run with 95% confidence interval. ** $p<0.01$
I) Scatter plot showing the details of Small BD-EV % and NFT Globe interaction from part G. Each dot represents one patient.
J) Scatter plot showing the details of Small BD-EV % and Small inclusion coverage from part G. Each dot represents one patient.

HC = healthy control, PiD = Pick's disease, PSP = progressive supranuclear palsy, EV = extracellular vesicle, BD-EV = brain derived extracellular vesicle, NFT = neurofibrillary tangle

Abundance of MAPT in cortex BD-EVs can differentiate 3R tau pathology

BD-EVs contain a wide array of proteins both as cargo and at their surface, including some proteins which have already been established as markers of neurodegenerative disease (NDD)[1]. We analyzed proteomic dataset for these established literature markers and found several to be present in samples (**Figure 3A-C**). Tau (MAPT) abundance decreases significantly in BD-EVs from PiD patients relative to both HC and PSP (**Figure 3A**), indicating that the quantity of total tau in BD-EVs could be a marker for PiD and 3R tauopathy. Interestingly, although none of these diseases are primary synucleinopathies, alpha synuclein (SNCA) follows the same pattern as MAPT in patient BD-EVs and is about ten times more abundant than MAPT in each group (**Figure 3B**). Conversely, amyloid precursor protein (APP) is generally only present in very low amounts, even in patient groups, indicating that it is not a relevant marker in this context (**Figure 3C**). Using the same machine learning model as previously described, we observed that none of these markers on their own is robust enough to be able to reliably predict disease status (**Figure 3D**). We do see that combining their scores allows the model to once again predict HC patients with 100% accuracy, however it still cannot reliably predict pathological groups. Interestingly, the quantity of MAPT in BD-EVs does correlate significantly with the percentage of inclusions which are globular NFTs in histological

staining (**Figure 3E**), indicating that it is perhaps the form of tau which aggregates into the AT100+ globular NFTs which is present in or on BD-EVs. Looking more closely at the correlation, we see that indeed PiD patients are nicely separated from the other two groups, while there is much overlap between HC and PSP patients (**Figure 3F**).

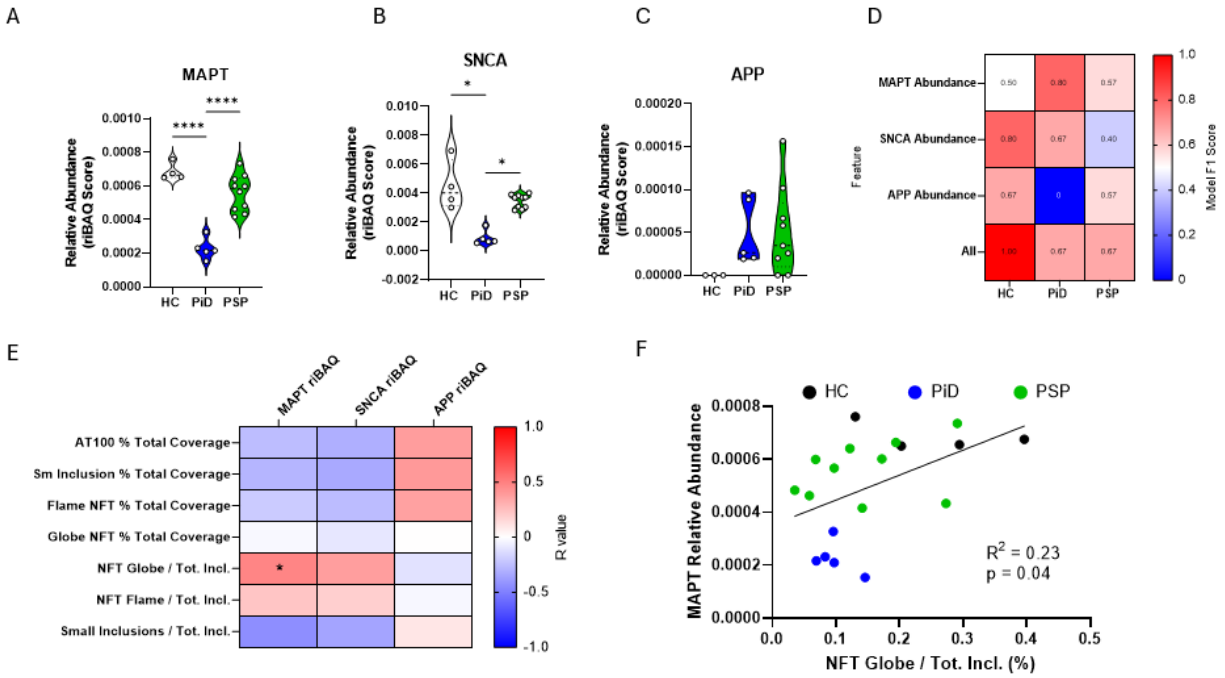

Figure 3 | Markers of neurodegenerative disease are not relevant markers in the context of BD-EVs

A-C) Violin plots represent the comparative abundance of established markers of neurodegenerative disease in BD-EVs. Each dot represents one patient. Ordinary one-way ANOVA was run with Tukey's multiple comparison test and single pooled variance. *** p<0.001, **** p<0.0001. Proteins pictured are:

A) Tau protein (MAPT)
B) Alpha synuclein (SNCA)
C) Amyloid precursor protein (APP)
D) Confusion matrix depicting the performance of a classification model based on abundance of markers in A-C.
E) Heatmap derived from correlation matrix comparing abundance of established NDD markers with histological findings from Figure 1. R values are plotted, two-tailed Pearson's correlation test was run with 95% confidence interval. * p<0.05
F) Scatter plot showing the details of MAPT abundance and NFT Globe interaction from part D. Simple linear regression was performed. Each dot represents one patient.

HC = healthy control, PiD = Pick's disease, PSP = progressive supranuclear palsy, EV = extracellular vesicle, BD-EV = brain derived extracellular vesicle, NFT = neurofibrillary tangle

Isoform of tau aggregated in cortex affects the ratio of neuronal and glial material in BD-EVs

Given the distinct impact of various tauopathies on different brain cells, we explored if these differences extend to the cell type-specific protein content of BD-EVs in samples. Generally, all patient groups were found to have the same proportion of "brain specific" not "nonspecific" material in BD-EVs, with each group having 41% of all protein being brain specific (**Figure 4A**). In this case, "brain specific" refers to the cumulative abundance of proteins which are specific to one cell type of the brain (i.e.: neurons, astrocytes, oligodendrocytes, microglia, or endothelial cells), within the context of the brain, according to the database curated by McKenzie and colleagues[116]. Utilizing this same cell-type specificity database, analysis indicated a consistent reduction in neuron-specific proteins in PiD and PSP compared to HC, while proteins specific to oligodendrocytes were consistently significantly more abundant in these groups relative to HC (**Figure 4B**). Using the Human Protein Atlas database[117], we differentiated between excitatory and inhibitory neuron-specific proteins and saw that PiD EVs contain significantly less material from both categories of neuronal protein than HC (**Figure 4B**). Notably, only PiD samples showed a significant increase in proteins identified as astrocyte specific, microglia specific, and endothelial cell specific compared to HC EVs (**Figure 4B**). Interestingly, combining the different glial cell type abundances together (astrocyte + microglia + oligodendrocyte) reveals a significant difference in the overall abundance of neuronal vs. glial material in both PiD and PSP relative to HC (**Figure 4C**). Interestingly, there is also a significant difference between the amount of glial material in PiD and PSP, suggesting that this parameter can differentiate between 3R and 4R pathology (**Figure 4C**). These findings suggest that alterations in cell type-specific material in BD-EVs could be indicative of brain pathology, particularly changes to the balance of overall neuronal and glial protein abundance which is observed in HC BD-EVs.

Knowing there are many systems which are differently dysregulated in different tauopathies, we also sought to investigate whether this was reflected in BD-EV content. Weighted Gene Co-Expression Network Analysis (WGCNA) was performed in order to determine the modules of proteins which are most driving the variance between patient groups. This analysis revealed four modules of interest: M1-Endoplasmic Reticulum, M2-Mitochondrion, M3-Microtubule, and M4-Trivalent Inorganic Cation Transport (**Figure 4D**). Looking more closely at the proteins contained within these modules, we see differences in their abundance between patient groups. For example, endoplasmic reticulum and mitochondrial proteins are significantly more present in PiD BD-EVs than in HC or PSP, while conversely, microtubule proteins are significantly less present in PiD than in PSP or HC, and

significantly less present in PSP than HC as well (**Figure 4E**). After observing similar profiles in WGCNA and the cell type specificity analysis, we investigated whether some of these proteins could be driving both groups. In this case, we analyzed the overlap between the proteins contained in each WGCNA module and those in each cell type specificity list and performed a Fisher's exact test with Benjamini Hochberg correction. This revealed a significant overlap between some groups, such as astrocytic and mitochondrial proteins, neuronal and microtubule proteins, oligodendrocytic and microtubule proteins, and endothelial and mitochondrial proteins (**Figure 4F**). In applying the same machine learning model to the WGCNA features of this figure, only mitochondrion and microtubule could successfully identify a group with 100% accuracy, and it was only PiD for both (**Figure 4G**). However, looking at the abundance of glial vs. neuronal material, we saw one which overwhelmingly outperformed the previous models. Using the glial protein abundance feature, the model was able to predict the disease state of the EV samples with 100% accuracy for each group (**Figure 4H**). We also tested the different cell types separately, which showed that microglial proteins on their own achieved this same result, while other cell types only identified one group with 100% accuracy (**Figure S1A**). Together, these results indicate that the increase in abundance of glial proteins, and particularly microglial proteins, can be predictors of disease in the context of BD-EVs and tauopathies. Because microglial proteins are not very abundant in BD-EVs, it would likely be beneficial to consider all glial proteins as this will exacerbate the difference between PiD and PSP patients and create a buffer of extra proteins which can be relied upon.

We correlated these features with the histopathological analysis from Figure 1 and found again that microglial and glial protein abundance correlates significantly with the percentage of inclusions which are globular NFTs, among a few other correlations (**Figure 4I**). Looking specifically at the cell type correlations, we see that the three patient groups are nicely separated from each other, indicating that these are important features for distinguishing not only between HC and pathology but between the pathologies themselves (**Figure 4J-L**).

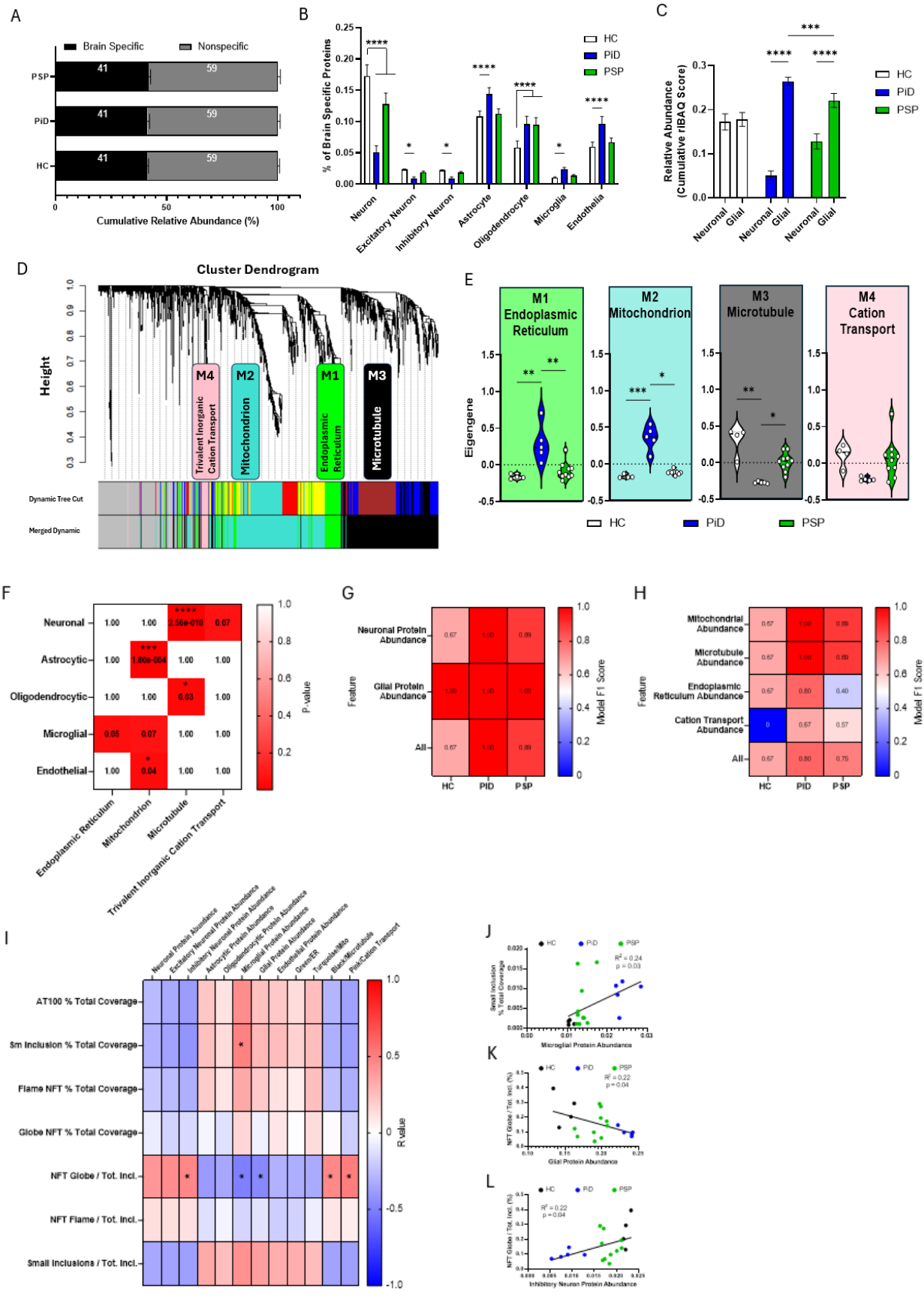
A
Brain Specific
Nonspecific
PSP
PiD
HC
41
59
Cumulative Relative Abundance (%)
B
% of Brain Specific Proteins
HC
PiD
PSP
Neuron
Excitatory Neuron
Inhibitory Neuron
Astrocyte
Oligodendrocyte
Microglia
Endothelia
C
Relative Abundance (Cumulative riBAQ Score)
Neuronal
Glial
D
Cluster Dendrogram
Height
M4
Trivalent Inorganic Cation Transport
M2
Mitochondrion
M1
Endoplasmic Reticulum
M3
Microtubule
Dynamic Tree Cut
Merged Dynamic
E
M1 Endoplasmic Reticulum
M2 Mitochondrion
M3 Microtubule
M4 Cation Transport
Eigengene
F
Neuronal
Astrocytic
Oligodendrocytic
Microglial
Endothelial
Endoplasmic Reticulum
Mitochondrion
Microtubule
Trivalent Inorganic Cation Transport
P-value
G
Neuronal Protein Abundance
Glial Protein Abundance
All
Feature
Model F1 Score
H
Mitochondrial Abundance
Microtubule Abundance
Endoplasmic Reticulum Abundance
Cation Transport Abundance
I
AT100 % Total Coverage
Sm Inclusion % Total Coverage
Flame NFT % Total Coverage
Globe NFT % Total Coverage
NFT Globe / Tot. Incl.
NFT Flame / Tot. Incl.
Small Inclusions / Tot. Incl.
R value
J
Microglial Protein Abundance
K
Glial Protein Abundance
L
Inhibitory Neuron Protein Abundance

Figure 4 | Cell type specific proteins can predict isoform specific tau pathology

A) Stacked bar plot depicting the proportion of brain-specific and non-specific proteins present in EV samples. "Specificity" was determined by a database generated by McKenzie and colleagues for brain cell type specific proteins (specific to neurons, astrocytes, oligodendrocytes, microglia, and endothelial cells).

B) Bar graph showing the percentage of brain specific proteins which can be categorized as neuronal, astrocytic, oligodendrocytic, microglial, and endothelial. Within the neuronal category, we also compared excitatory and inhibitory neuron-specific proteins according to the Human Protein Atlas. Ordinary two-way ANOVA was run with Dunnett's multiple comparison test and single pooled variance. * $p<0.05$, **** $p<0.0001$.

C) Bar graph depicting the overall relative abundance of neuron-specific and glia-specific material. Glial abundance was determined by summing the abundance of astrocytic, oligodendrocytic, and microglial material according to McKenzie et al database. Ordinary two-way ANOVA was run with Sidak's multiple comparisons test and a single pooled variance. **** $p<0.0001$.

D) Weighted gene co-expression network analysis emphasizing 4 modules of proteins which account for variance between patient groups: Endoplasmic Reticulum, Mitochondrion, Microtubule, and Trivalent Inorganic Cation Transport.

E) Violin plots of the abundance of the proteins contained within each of the 4 highlighted modules in WGCNA. Ordinary one-way ANOVA was run with Tukey's multiple comparisons test and a single pooled variance. ** $p<0.01$, **** $p<0.0001$.

F) Heatmap depicting the p values of Fisher's Exact Test with Benjamini Hochberg correction of the overlapping proteins within each WGCNA module and each cell type specificity database from McKenzie et al. * $p<0.05$, *** $p<0.001$, **** $p<0.0001$.

G) Confusion matrix depicting the performance of a classification model based on abundance of WGCNA module proteins from parts D-E.

H) Confusion matrix depicting the performance of a classification model based on abundance of glial and neuronal proteins from part C.

I) Heatmap derived from correlation matrix comparing abundance of cell type-specific material and WGCNA module proteins with histological findings from Figure 1. R values are plotted, two-tailed Pearson's correlation test was run with 95% confidence interval. * $p<0.05$.

J) Scatter plot showing the details of microglial protein abundance and small inclusion coverage interaction from part H. Simple linear regression was performed. Each dot represents one patient.

K) Scatter plot showing the details of glial protein abundance and NFT Globe interaction from part H. Simple linear regression was performed. Each dot represents one patient.

L) Scatter plot showing the details of inhibitory neuron protein abundance and NFT Globe interaction from part H. Simple linear regression was performed. Each dot represents one patient.

HC = healthy control, PiD = Pick's disease, PSP = progressive supranuclear palsy, EV = extracellular vesicle, BD-EV = brain derived extracellular vesicle, NFT = neurofibrillary tangle, riBAQ = relative intensity-based absolute quantification, ER = endoplasmic reticulum

Discussion

Despite the field of biomarker discovery for neurodegenerative diseases making progress in the last decade, there remains a lack of noninvasive biomarkers which can truly inform on the molecular nuances of these diseases which often present similarly in the clinic[22]. Current circulating biomarkers are not validated for primary tauopathies, so there are dozens of NDDs which still lack accurate biomarkers[27]. The proteomic content of BD-EVs, which themselves may contain isoform specific tau seeds based on previous work, may provide enough of a broad view of the cellular landscape of the tauopathy brain to be able to distinguish between them reliably in a clinical context[68]

In this study, we first sought to investigate to what extent we could differentiate 3R and 4R pathology by looking at the source: tau inclusions in the frontal cortex of HC, PiD (3R), and PSP (4R) patients. We assessed AT8 (early aggregation) and AT100 (late aggregation) for this question but found the only differences to be relative to HC, not between the two pathologies. This suggests that while the isoforms and posttranslational modifications may differ greatly between 3R and 4R tauopathies, the overall coverage of inclusions, and even the distribution of small inclusions vs. large NFTs is not impacted by isoforms. This indicates that without isoform-specific staining, it is not possible to differentiate between tauopathies in the frontal cortex with just histopathological staining alone.

Several EV qualities were assessed for dependence on pathology. While there was a significant difference in the ratio of small (<150nm) and large (>150nm) EVs in PiD patients, other parameters such as the overall concentration and the abundance of EV-associated material did not differ with pathology. The shift in EV size in PiD could indicate a shift in the mechanism of EV secretion in cells which are not apoptotic. For example, this could indicate a shift away from microvesicle blebbing from the plasma membrane and toward MVB-mediated release of exosomes. However, this is purely speculative. A more thorough analysis on exosome markers present in the different samples would need to be done to confirm this.

We also investigated the presence of established markers of NDDs in the three groups. To this end, we were interested to see if these markers were relevant in the context of BD-EVs. Interestingly, the two markers (MAPT, SNCA) which showed significance only separated PiD, not PSP from HC patients. They also separated PiD and PSP, suggesting that they may be relevant markers for identifying 3R pathology. SNCA not only differentiating 3R and 4R pathology, but being present at 10x the abundance as MAPT was rather unexpected. Upon consulting the literature, however, it has been shown in the frontal cortex and the dentate gyrus that neurons which contain Pick bodies may also acquire Lewy bodies (LBs) during disease progression[118,119]. It has also been shown in AD that neurons with tau aggregates are more susceptible to LB formation[120]. Whether the presence of aggregated tau induced LB formation, or cells with NFTs are simply too overwhelmed to clear other aggregating proteins isn't exactly clear, but the presence of alpha synuclein in addition to tau aggregation likely implies a very advanced stage of pathology. While we cannot confirm the presence of LB in this patient cohort, if the MAPT trend is any indication, PiD patients likely have alpha

synuclein aggregation alongside the tau aggregates in frontal cortex. Furthermore, alpha synuclein in neuron derived EVs has been shown to be a potential biomarker for Parkinson's disease (PD)[121,122]. While PiD is not a synucleinopathy, alpha synuclein may be worth measuring in tandem with other protein markers to assess likelihood of primary tauopathy pathology.

Lastly, we looked at the cellular signatures present in the BD-EVs. We looked at brain cell type specificity, as well as cellular pathway dysregulation. In cell type specificity, we found a significant difference in the ratio of neuronal and glial material in pathological BD-EVs compared to HC BD-EVs. Importantly, we also saw a significant difference in the amount of glial material between PiD and PSP, indicating that this could be a measure which can differentiate primary tauopathies. Recently, glial fibrillary acidic protein (GFAP) has emerged as a potential biomarker for different neurodegenerative diseases, including AD and PD[30,33,123]. Given that circulating GFAP is typically present in low levels in healthy individuals, its presence in NDD patients indicates astrogliosis and a likely advanced stage of pathology in the brain[124]. While circulating GFAP does not appear to be linked to a specific disease, the glial content of BD-EVs may provide more context to be able to more precisely predict pathology. Indeed, that is exactly what the model was able to do in this case, using the glial protein abundance to predict HC, 3R, or 4R pathology with 100% accuracy. It is worth noting that the small group sizes in this model resulted in high variance and overfitting of the model. More testing would need to be done with a larger patient cohort to confirm these results, though they are very promising.

In the molecular pathway analysis by WGCNA, we saw that microtubule-associated proteins could differentiate PiD from HC and PSP, but could not separate PSP from HC. This suggests that while there are differences in the effects of 3R and 4R tau accumulation on the cytoskeleton and mitochondria, these differences cannot necessarily be directly observed in BD-EVs in this study. The mitochondrial profile observed supports previous work done which showed that EVs from PiD patients had a more deleterious effect on human iPSC derived astrocytes than EVs from PSP patients[68].

Many of the features we analyzed, from the size of EVs to different aspects of their proteomic content, correlated with features of histopathology in the same patients. This is one of the more important aspects of this study, in that it demonstrates that BD-EVs can reflect the molecular landscape of the tauopathy brain. The protein tau itself correlated with the percentage of AT100 inclusions which were globular NFTs, suggesting that the kind of tau which makes up this type of inclusion may be similar to the tau which is found in BD-EVs in late stage tauopathy. It's possible that tauopathy EVs contain pieces of aggregates: insoluble tau which would not otherwise have been secreted by cells in free form. This has been demonstrated in AD, but not other tauopathies[125]. Interestingly, this same group even saw that the aggregates in advanced AD EVs were globular in nature.

A concept which is both daunting and rewarding in the field of EVs is that the proteome of the cell which secretes them is not the same as the proteome of the EVs which are secreted. This has been well demonstrated by You and colleagues, with their study comparing proteomics of iPSC derived astrocytes, neurons, microglia, and oligodendrocytes to the cell type specific EV they secreted in culture[71]. Indeed, even in this simplified comparison, the EVs often did not contain typical cell type specific markers which would be expected in EVs whose origin is certain to be from one cell type. EVs from human brains are sure to be much more complex, containing information not just from one cell but from the many intricate systems of the brain. In this sense, it can be difficult to draw conclusions on the presence or absence of specific proteins of interest, particularly in the context of late-stage pathology when so many of these systems are under stress.

The purpose of this study was not to propose a "one-size-fits-all" biomarker for the stratification of 3R and 4R tauopathies, but rather to highlight the importance of looking at the bigger picture in the brain. This is something we can see more clearly via BD-EVs, which contain lots of relevant material to evaluate the overall health status of the brain. Indeed, it was not a single protein that allowed us to separate the three groups and predict the disease state in this study. Instead, it was a group of interconnected proteins that can provide more context than a single marker. Given that glial cells are impacted differently by the accumulation of different tau isoforms[68], it may not seem surprising that this difference is reflected in BD-EV content. It must be noted, however, that not all cellular differences are directly reflected in the cargo of BD-EVs. Some, like the quantity of tau protein itself,

is reflected inversely. EVs can sometimes reflect exactly what is happening at the cellular level, sometimes the opposite, and sometimes do not reveal a clear picture of a system in struggle. This study of course has limitations. We have assigned the weight of an entire category of diseases to one representative disease (PiD for 3R tau, PSP for 4R tau). In this sense, some results may be overinterpreted by saying that all primary tauopathies can be stratified using this method. Additionally, more data is needed on the proteomic content of BD-EVs from other NDDs. We cannot be sure that the effects we have seen in this study are unique to tauopathies and not common to general neurodegeneration or another form of pathological aging. Lastly, the brain tissue and EV samples which were used for this study are from late-stage tauopathy patients. We therefore cannot yet confirm that these findings would hold true in preclinical stages of these diseases, however it gives a starting point for what kinds of changes to look for in early-stage tau pathology.

While EVs can be complicated to investigate, this type of exploratory study demonstrates the wealth of information which can be obtained from their cargo. Here we only evaluated the proteomic signature of these particles, but it has also been well established that EVs carry DNA, RNA, and metabolites which could be equally informative[40]. Not only are BD-EVs rich in brain material, they also have the capacity to cross biological barriers such as the blood-brain barrier to enter into peripheral biofluids, making this material accessible noninvasively[56]. This study has improved our understanding of the relationship between molecular nuances and observable phenotypes of disease, as well as our understanding of what may make a successful biomarker for families of diseases such as tauopathies.

Materials and Methods

Patient Cohort

Brain extracts were obtained from the CHUV Biobank and Lille Neurobank, fulfilling requirements concerning biological resources and declared to the competent authority. Samples were managed by the CRB/CIC1403 Biobank (BB-0033-00030 for Lille Neurobank) and CNP (BB-0063 for CHUV biobank). The demographic data are listed in Leroux et al., 2022[66].

Brain Derived Fluid Isolation from Patient Brain Tissue

In collaboration with the group of Morvane Colin (Lille, FR). Brain derived fluids (BD-fluids) were isolated as previously described[126]. Briefly, roughly 1.5g of fresh-frozen patient prefrontal cortex was gently cut into smaller pieces. These were then incubated in a Papain/Hibernate-E solution to gently digest the tissue and release interstitial fluid, theoretically avoiding cellular lysis. After tissue digestion, differential centrifugations at 300g for 10min, 2,000g for 10min, and 10,000g for 30min were performed at 4ºC to remove cells, membranes, and debris respectively and the supernatant of the 10,000g centrifugation was then stored at -80ºC until EV isolation was performed. To avoid bias in the results, normalization according to the weight of the brain extracts was systematically done.

Brain Derived EV Isolation from Patient Brain Derived Fluid

In collaboration with the group of Morvane Colin (Lille, FR). The procedures to isolate the brain derived EVs (BD-EVs) from the human BD-fluid were carried out in accordance with the Minimal information for the studies of extracellular vesicles (MISEV) guidelines that were established and updated in 2018 by the International Society for Extracellular Vesicles[54]. Various controls were applied to validate the enrichment and the content of the BD-EVs, as recommended in these guidelines. However, the procedure described above to recover BD-fluids may still lead to some cell lysis and therefore some intracellular contamination. The presence of intraluminal vesicles (ILVs) in the preparations cannot be fully excluded. 500uL of BD-fluid was loaded on the top of a size exclusion chromatography (SEC) column (10mL column, CL2B Sepharose, pore size 75 nm, Millipore)[127]. A mean of 7.94×10^{10} ($\pm 3.36 \times 10^{9}$ vesicles/g of tissue in F1–4 (n = 36 samples) was recovered for each sample. Isolation was carried out in phosphate-buffered saline (PBS) with a flow

of 36–48 s/mL. The first 3mL was eliminated, and the following 20 fractions were recovered (with 500uL per fraction).

Measurement of BD-EV Size and Concentration

In collaboration with the group of Morvane Colin (Lille, FR). Nanoparticle tracking analysis (NTA) was performed on individual fractions diluted in PBS with a NanoSight NS300 (Malvern Panalytical). To generate statistical data, five videos of 90 s were recorded and analyzed using NTA software (camera level, 15; detection threshold, 4).

Label-Free LC MS/MS Analysis of BD-EV Samples

Sample Preparation and Protein Digestion: miST

In collaboration with Protein Analysis Facility (PAF) of Until: Manfredo Quadroni and Patrice Waridel.

Protein digestion: F1-4 fractions were digested according to a modified version of the iST method (named miST method)[128]. Briefly, 50 ml solution in PBS were supplemented with in 50 ml miST lysis buffer (1% Sodium deoxycholate, 100 mM Tris pH 8.6, 10 mM DTT) and heated at 95°C for 5 min. Samples were then diluted 1:1 (v:v) with water and reduced disulfides were alkylated by adding 1 /4 vol of 160 mM chloroacetamide (final 32 mM) and incubating at 25°C for 45 min in the dark. Samples were adjusted to 3 mM EDTA and digested with 0.5 mg Trypsin/LysC mix (Promega #V5073) for 1h at 37°C, followed by a second 1h digestion with a second and identical aliquot of proteases. To remove sodium deoxycholate and desalt peptides, two sample volumes of isopropanol containing 1% TFA were added to the digests, and the samples were desalted on a strong cation exchange (SCX) plate (Oasis MCX; Waters Corp., Milford, MA) by centrifugation. After washing with isopropanol/1% TFA, peptides were eluted in 250 ml of 80% MeCN, 19% water, 1% (v/v) ammonia.

Liquid chromatography-tandem mass spectrometry: Tryptic peptide mixtures were injected on an Ultimate RSLC 3000 nanoHPLC system interfaced via a nanospray Flex source to a high resolution Orbitrap Exploris 480 mass spectrometer (Thermo Fisher, Bremen, Germany). Peptides were loaded onto a trapping microcolumn Acclaim PepMap100 C18 (20 mm x 100 µm ID, 5

µm, Dionex) before separation on a C18 custom packed column (75 µm ID × 45 cm, 1.8 µm particles, Reprosil Pur, Dr. Maisch), using a gradient from 4 to 90 % acetonitrile in 0.1 % formic acid for peptide separation (total time: 140 min). Full MS survey scans were performed at 120,000 resolution. A data-dependent acquisition method controlled by Xcalibur software (Thermo Fisher Scientific) was used that optimized the number of precursors selected ("top speed") of charge 2+ to 5+ while maintaining a fixed scan cycle of 2 s. Peptides were fragmented by higher energy collision dissociation (HCD) with a normalized energy of 30 % at 15,000 resolution. The window for precursor isolation was of 1.6 m/z units around the precursor and selected fragments were excluded for 60s from further analysis.

MS and MS data analysis: Data files were analyzed with MaxQuant 1.6.14.0[129] incorporating the Andromeda search engine[130]. Cysteine carbamidomethylation was selected as fixed modification while methionine oxidation and protein N-terminal acetylation were specified as variable modifications. The sequence databases used for searching were the human (Homo sapien) reference proteome based on the UniProt database and a "contaminant" database containing the most usual environmental contaminants and enzymes used for digestion (keratins, trypsin, etc.). Mass tolerance was 4.5 ppm on precursors (after recalibration) and 20 ppm on MS/MS fragments. Both peptide and protein identifications were filtered at 1% FDR relative to hits against a decoy database built by reversing protein sequences.

Categorical Annotation of Proteins

Proteins were annotated according to several databases in order to better classify them in later analyses. These databases included the Gene Ontology (GO) Human database[131,132], further split into the categories of cellular component (CC), biological process (BP), and molecular functions (MF), the MISEV guidelines for EV-associated and potential contaminant proteins[54], a database generated by McKenzie and colleagues in their publication for brain cell type specificity[116], and the Human Protein Atlas databases for cell type specificity and predicted subcellular localization[117].

WGCNA

In collaboration with Aatmika Barve. Protein co-expression network analysis was performed with the R package WGCNA[133] on the preprocessed proteomic data of all identified proteins with their respective riBAQ scores for each disease group. At first, a correlation matrix for all pair-wise

correlations of proteins across all samples was generated and then transformed into a matrix of connection strengths, i.e., a weighted adjacency matrix with soft threshold power β = 16. Then the topological overlap (TO) was calculated using the connection strengths. TOM is a robust, pairwise measure which indicates two proteins' similarity based on their co-expression relationships with all other proteins in the network. Proteins were further hierarchically clustered using 1-TOM as the distance measure to generate a cluster dendrogram, and modules of proteins with similar co-expression relationships were identified by using dynamic tree-cutting algorithm with parameters set to: minimal module size = 30, deepSplit = 2, and merge cut height = 0.15. Within each module, the module eigenprotein was defined as the first principal component, which serves as a weighted summary of protein expression within the module and accounts for the greatest variance among all module proteins. These proteins are assigned with a color representing each module. Further, module membership (kME) was assigned by calculating Pearson's correlation between each protein and each module eigenprotein and the corresponding p-values. Proteins were reassigned to the module for which they had the highest module membership with a reassignment threshold of $p < 0.05$. Again, colors are assigned to the new merged modules to signify a robust group of proteins. From each module, hub proteins were found using the signedkME function which explains the membership of protein with its module and strong association within the module.

Gene Ontology

In collaboration with Aatmika Barve. Through WGCNA, specific modules were assigned a color. To understand each module in detail, a detailed genetic annotation of each protein within the module was needed. It could then be understood how the proteins might be interacting and which kind of molecular pathways they could be associated with. These differentially expressed proteins and co-expressed proteins were characterized based on their gene ontologies, using GO Elite (version 1.2.5) python package[134]. The entire set of proteins identified and included in the network analysis served as the background dataset. The presence of significantly overrepresented ontologies within a module was gauged using a Z-score, while the significance of Z-scores was evaluated using a one-tailed Fisher's exact test, with adjustments for multiple comparisons via the Benjamini-Hochberg FDR method. Threshold analysis included a Z-score cut off of 2, a p-value threshold of 0.05, and a minimum requirement of 5 genes per ontology before ontology pruning was performed. The best

gene ontology term which explains the molecular and cellular function of each module was used to name it.

Brain cell type enrichment

In collaboration with Aatmika Barve. To investigate the cell type specificity of the proteins within each module, the method of adapting the function called geneListFET in R was used[135,136]. The cell type specific gene list from RNA-seq in human brain was used[116]. The total list of identified protein group was used in background and the cell-type specific gene list was filtered for presence in the total proteins list prior to cross-referencing. One tailed Fisher's exact test was performed and correction for multiple comparison by the FDR (Benjamini Hochberg) method was applied to evaluate the significance of cell type enrichment of each module.

Machine Learning

In collaboration with Aatmika Barve. Machine learning was used to support the traditional statistical results. The data is relatively too small to make the machine learn, so the data was split into 60% training set and 40% testing set. Since the study classes were not balanced, the split was stratified and performed 42 times with different random seeds. Then, Borderline SMOTE (Synthetic Minority Over-sampling Technique) was performed on the training set to balance the classes before training the model. OneVsRestClassifier model[137] performed upon XGBClassifier model[138] was used with parameters set to multi:softprob for objective and mlogloss for evaluation metric. The model was trained with the training set for the classification of data into three classes for each individual feature. The model was evaluated on the testing set and its performance was assessed using F1-score as the metrics for evaluation. F1-score was chosen as the metric because it provides a more balanced and nuanced view of model's performance. In this study, precision and recall both are critically important, therefore the F1-score was chosen as it is the harmonic mean of precision and recall. The F1-score for each individual feature for three classes was represented in a heatmap. The closer the score is to 1, the better the model's performance is.

Due to the very small data size, there were some challenges to be faced to develop a generalized model. High variance and overfitting of model had to be taken into account. The effective model evaluation metric score also had to be carefully considered. As a result, a generalized model using

XGBoost classifier, SMOTE and OneVsRest classifiers was built. The model was also evaluated with cross-validation.

Histopathological Staining of Frontal Cortex Sections

In collaboration with the group of Morvane Colin (Lille, FR). Automated immunohistochemistry (IHC) was performed using 4-mm-thick formalin-fixed, paraffin-embedded (FFPE) tissue on a BenchMark Ultra (Roche Tissue Diagnostics) with the UltraView diaminobenzidine (DAB) IHC detection kit (Ventana) and the primary Ab AT8 (dilution 1:500) or AT100 (dilution 1:500). The monoclonal Ab (mAb) AT8 recognizes the phosphoserine 202, phosphoserine 208, and phosphothreonine 205 residues of tau (MN1020; Thermo Scientific, Illkirch, France)[139]. The mAb AT100 (MN1060; Thermo Scientific, Illkirch, France) recognizes phosphothreonine 212 and phosphoserine 214 and allowed the detection of insoluble/aggregated tau[140–142].

Histopathological Analysis

In collaboration with Valentin Zufferey. A slide scanner was used to acquire images of entire section (Zeiss Axioscan Z1, ~5mm^2 of scan area, 20X magnification). Scans were processed using FIJI (v1.54f) for image corrections and conversions and Nikon General Analysis 3 (GA3; NIS-Elements AR v5.21.03) module for advanced image quantifications. As entire scans were analyzed, detection of the section was first performed to define boundaries of analysis area and for further density and coverage calculations. Detection of punctual features (contrast-based spot detection for typical diameter of ~5um) was performed to quantify small inclusions. Larger objects (NFTs) were segmented by image-thresholding and categorized based on their circularity. High circularity objects (>0.7) were classified as "globular NFTs" and the rest (more elongated) as "flame NFTs". We measured the integrated area, number (density) and mean neighbor distance for each type of inclusion. Both stainings were analyzed similarly, with refinements made to optimize the detection of different objects.

Correlation Analyses

Correlation matrices were created to compare various BD-EV features with histopathological findings. R values were plotted. Two-tailed Pearson's correlation test was run with 95% confidence interval. Significance was denoted with stars: * $p < 0.05$, ** $p < 0.01$, *** $p < 0.001$, **** $p < 0.0001$.

Supplementary Information

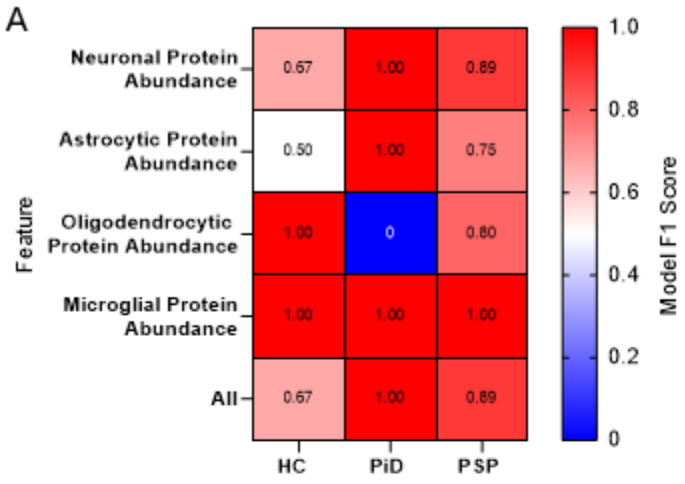

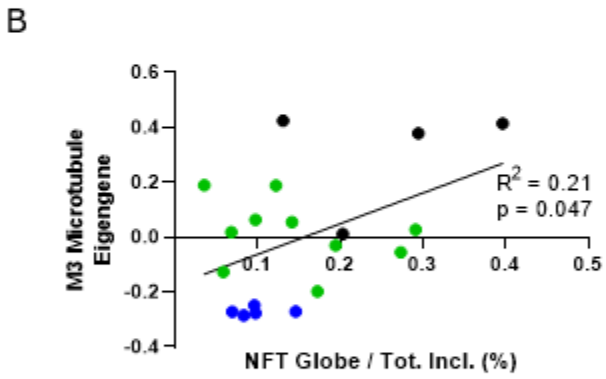

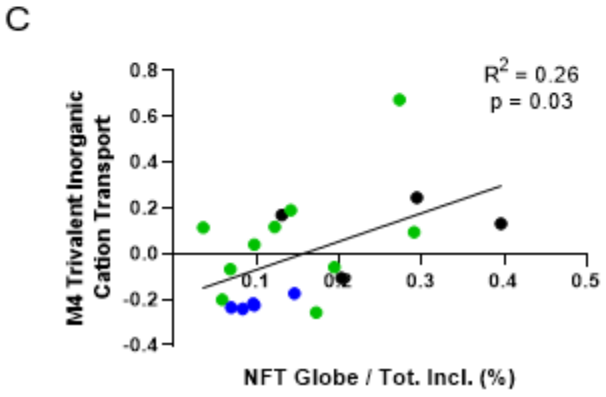

Supplementary Figure 1 | Additional Features of Cell Type Specificity and WGCNA

A) Confusion matrix depicting the performance of a classification model based on abundance of all brain cell type proteins from Figure 4C.

B) Scatter plot showing the details of M3 Microtubule Eigengene and NFT Globe interaction from Figure 4H. Simple linear regression was performed. Each dot represents one patient.

C) Scatter plot showing the details of M4 Trivalent Inorganic Cation Transport Eigengene and NFT Globe interaction from Figure 4H. Simple linear regression was performed. Each dot represents one patient.

Chapter 2

A Novel Methodology for the High-Efficiency Isolation of Brain Derived Extracellular Vesicles in Peripheral Biofluids

A Novel Methodology for the High-Efficiency Isolation of Brain Derived Extracellular Vesicles in Peripheral Biofluids

Jeanne Espourteille[1], Kevin Richetin[1,2,3]

[1] Department of Psychiatry, Center for Psychiatric Neurosciences, Lausanne University Hospital (CHUV) and University of Lausanne, 1011 Lausanne, Switzerland

[2] Lausanne University Hospital (CHUV) and University of Lausanne, Neuroscience Research Center (CRN), Laboratory of Cellular and Molecular Neurotherapies, 1011 Lausanne, Switzerland

[3] Lausanne University Hospital (CHUV) and University of Lausanne, Department of Clinical Neuroscience (DNC), Laboratory of Cellular and Molecular Neurotherapies, 1011 Lausanne, Switzerland

Keywords: Extracellular vesicle ; protein corona ; plasma ; saliva ; brain derived EV ; surface marker ; astrocyte

Graphical Abstract

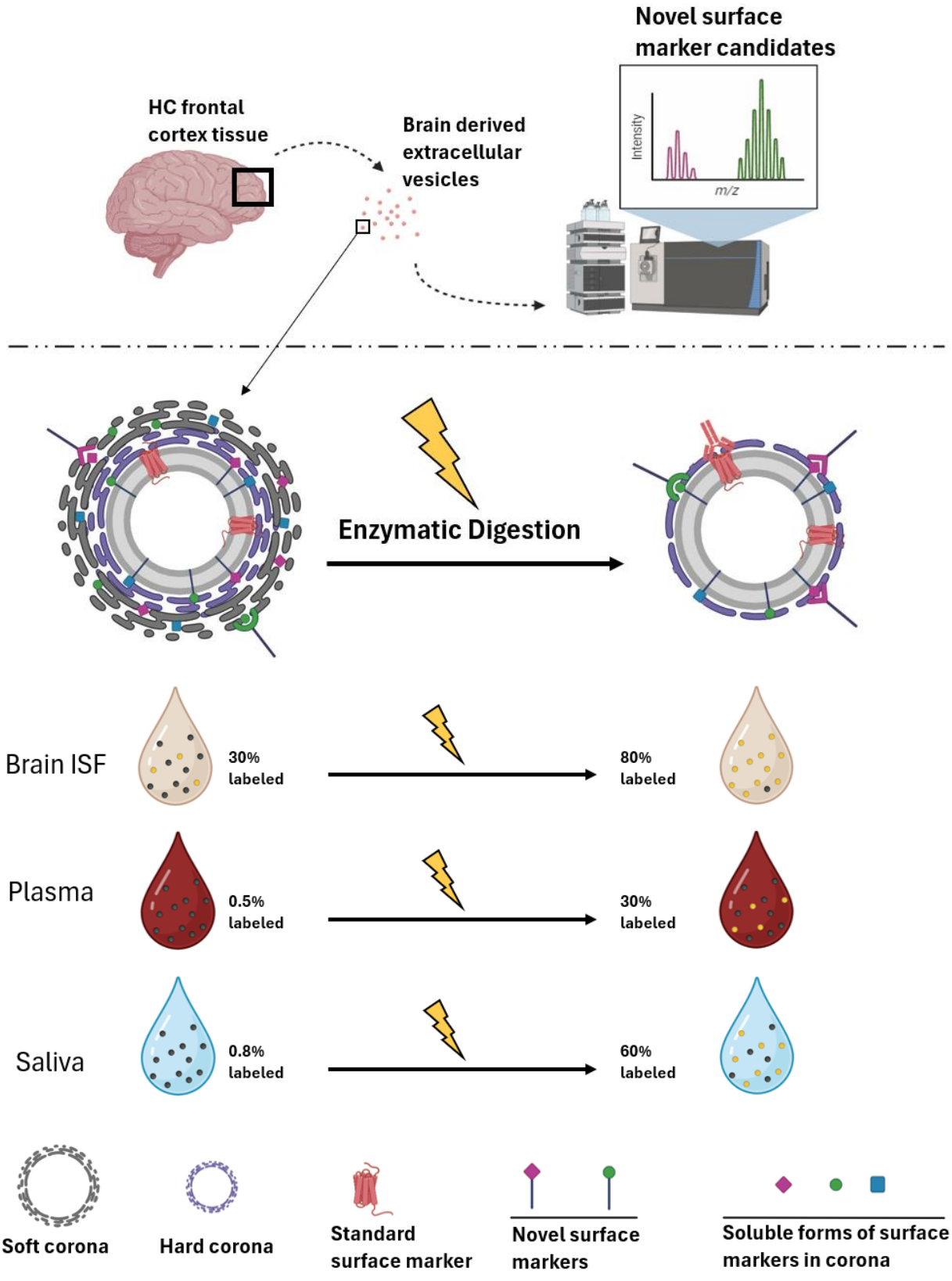

Abstract

Circulating brain-derived extracellular vesicles (BD-EVs) offer considerable potential for diagnosing central nervous system (CNS) disorders. However, specific isolation and enrichment of these vesicles remain extremely challenging among the many other circulating extracellular vesicles (EV) and proteins in peripheral biofluids. Based on an in-depth proteomic analysis of the vesicular secretome isolated from patient brain tissue, we have identified candidate epitopes for the specific isolation of BD-EVs. Combining isolation by size exclusion, enzymatic digestion of the EV protein corona, and capture by a novel antibody cocktail, we have created a novel methodology for isolating BD-EVs from various peripheral biofluids. By combining this novel cocktail with the enzymatic treatment of the protein corona to liberate EV surface epitopes and increase their accessibility to antibodies, we have increased the efficiency of capture of brain-derived EVs in plasma and saliva from less than 1% to 30% and 60% respectively. This technique improves upon established EV capture techniques in the EV yield and overall particle specificity to the brain.

Introduction

Extracellular vesicles (EVs) are nanoparticles which are secreted by all cells of the body. Brain derived EVs (BD-EVs) are secreted directly into the interstitial fluid surrounding the cells that secrete them. However, they can also cross biological barriers to enter peripheral biofluids such as plasma, saliva, cerebrospinal fluid, urine, and others[56]. Once they have crossed these barriers into circulating biofluids, the difficulty is in differentiating them from the rest of the circulating EVs. This is further complicated by our lack of knowledge surrounding how these EVs actually cross biological barriers and to what extent they are modified in the process. While there are several ideas about the mechanisms of EV crossing, particularly of the blood-brain barrier (BBB) (**Figure 1**)[143,144], it remains unclear whether EVs which cross biological barriers are heavily modified by cells which make up the barriers or are left relatively untouched in the process. For this reason, it is difficult to know what kind of surface proteins are most relevant to target for immunocapture of brain derived EVs in fluids like blood.

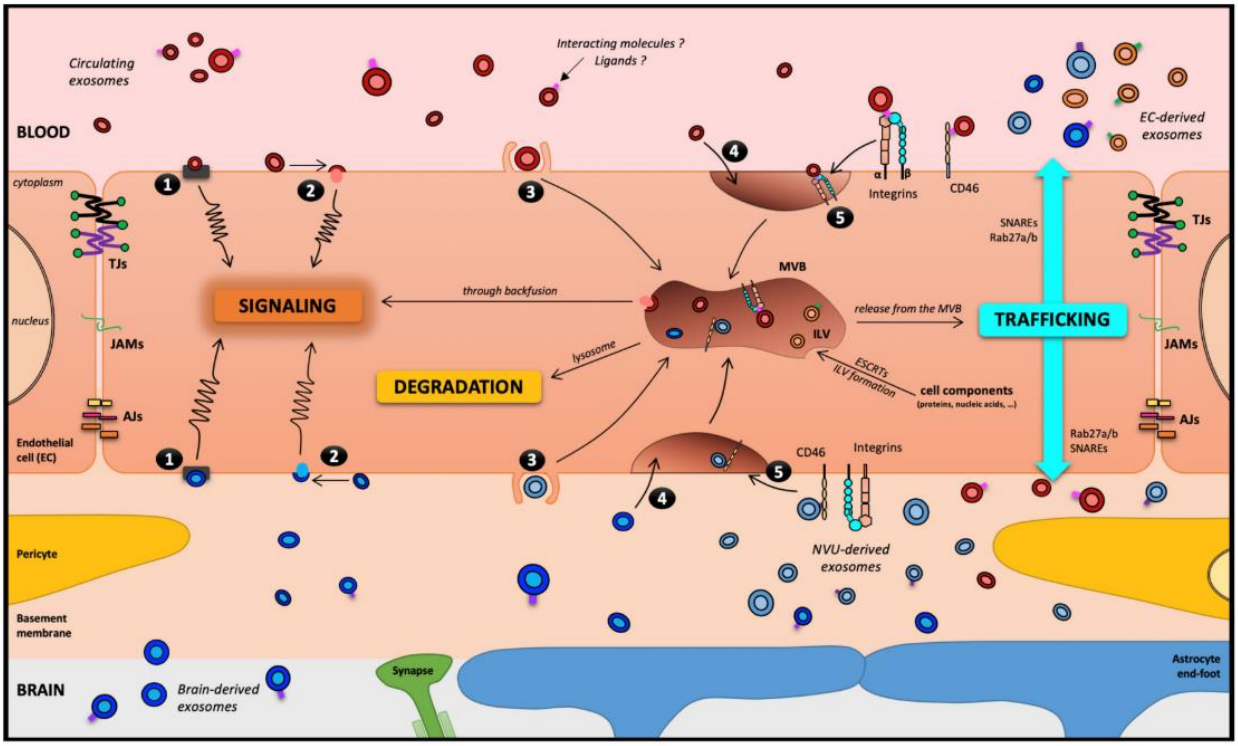

Figure 1 | Potential mechanisms of blood-brain barrier crossing by exosomes

Adapted from Saint-Pol et al., 2020 - Cells [143]

The blood–brain barrier, theoretically a motorway for a melting-pot of exosomes. Five routes have been described for exosomes interacting with a receiving cell (exosomes have been more widely studied than general EVs):

(1) Association with a protein G-coupled receptor on the cell surface, inducing a signaling cascade
(2) Adhesion to the cell surface and fusion, releasing the exosome content in the cytoplasm, which can lead to several types of events, including cell signaling
(3) Macropinocytosis
(4) Nonspecific/lipid raft
(5) Receptor-mediated transcytosis, leading to its entry into the cell through the endocytic pathway and its storage in the MVB.

Then, three outcomes remain possible for exosomes: (i) degradation by lysosomes; (ii) signaling induction through a back fusion event in the MVB releasing its content in the cytoplasm; or (iii) trafficking from the MVB to the plasma membrane as neo-formed ILVs in the receiving cell. It is worth noting that except in pathological models, EVs and exosomes have not been described to cross the BBB through the paracellular pathway.

AJs: adherens junctions; EC: endothelial cells; ESCRT: endosomal sorting complexes required for transport; ILV: intraluminal vesicles; JAMs: junctional adhesion molecules; NVU: neurovascular unit; SNARE: soluble N-ethylmaleimide-sensitive-factor attachment protein receptor; TJs: tight junctions

The blood is perhaps one of the most popular choices for BD-EV isolation in the periphery, though it is quite a complex fluid. The vast majority of blood is a small group (~22 proteins) of highly abundant proteins such as albumin, immunoglobulins, and complement components (**Figure 2**)[145]. These proteins often make immunocapture and analyses such as mass spectrometry incredibly difficult, as it is nearly impossible to fully deplete the blood of these "contaminating" proteins to capture or analyze proteins of interest such as biomarkers.

Saliva is also a highly complex biofluid with over 1400 proteins identified within it[146]. Contrary to plasma, however, saliva EVs can be easily isolated using a number of different techniques, without need of further purification or depletion of contaminating proteins[146].

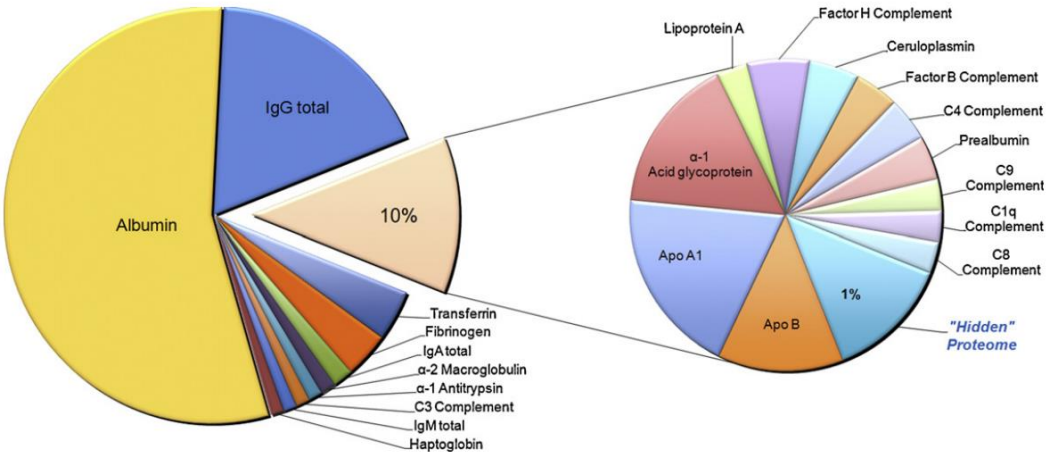

Figure 2 | Proteomic composition of blood

From Lista et al., 2013 – Progress in Neurobiology [145]

A significant portion of the total protein content in plasma and serum is comprised of just a few proteins. Plasma and serum include a narrow population of different high-abundance proteins (HAPs). The 10 most abundant proteins represent approximately 90% of the total protein content in human plasma/serum; the 22 most abundant proteins are supposed to embrace about 99% of the total protein mass. As a result, the tens of thousands of other different proteins and peptides, that should encompass all possible biomarkers of diseases, result to be buried and hidden under such few predominant HAPs. The ''hidden proteome'' expression refers to the low- and very low-abundance proteins (LAPs). They constitute less than 1% of the total protein content.

HAPs = high-abundance proteins, LAPs = low-abundance proteins, IgA Total = Immunoglobulin A Total, IgM Total = Immunoglobulin M Total, Apo A1 = Apolipoprotein A1, Apo B = Apolipoprotein B

Embedded in the membrane of EVs are anywhere from dozens to hundreds of membrane-associated proteins which are often active molecules or functional receptors which play a role in EV homing, targeting, and uptake by recipient cells[52]. These surface proteins often also carry characteristics of their cells and tissues or origin, making them useful for the study of specific subpopulation of EVs in the context of pathology[51]. Currently, many groups are attempting to decode exactly which proteins can be found at the surface of different classes of EVs. In recent years, this question has advanced new techniques for mapping the surface of the EV, including proteolytic digestion of surface proteins[147,148], targeted and untargeted mass spectrometry[147,149], antibody microarray platforms[150], proximity barcoding assays[51], proximity ligation assays[151], flow cytometry[151–153], single EV microscopy imaging[154–157], and others. Together, these techniques all seek to identify which proteins can be found at the surface of the EV and in which context, often with the goal of isolating specific subpopulations of EVs from circulating biofluids.

This is a particularly pertinent question for EVs of the central nervous system (CNS), as they are being more and more widely used in questions of diagnostics, stratification of disease, and targeted molecule delivery to the brain[56,158–160]. These EVs can provide information about the pathological state of an organ system which is incredibly difficult to physically access in routine clinical settings. As EVs can cross biological barriers such as the blood-brain barrier, they can provide information about the brain without invasive biofluid sampling like a lumbar puncture. This is only possible, however, if we can separate brain derived EVs from all the other EV subpopulations which circulate in peripheral biofluids.

Many groups have been working on this subject for years, attempting to isolate brain specific EVs from blood, urine, saliva, and other peripheral biofluids to answer various biological and medical questions. Different groups have isolated neuron derived EVs[160–164], astrocyte derived EVs[164–166], microglia derived EVs[167–169], and oligodendrocyte derived EVs[164,170], mostly from human plasma. To do this, they identified proteins at the

surface of these EVs which they could target in some form of immunocapture. Table 1 summarizes some of the current markers used for the capture of different subpopulations of EVs being targeted in the plasma, as well as general EV markers which have been established for many years. While there is a consensus on some of these markers, others have become the subject of debate in recent years. For example, the relevance of L1CAM to isolate neuron derived EVs has been contested by Norman and colleagues[171], who argue that L1CAM is not actually in the membrane of neuronal EVs but rather is secreted in a soluble form and then stuck to the protein corona of circulating EVs. Furthermore, it has been shown that L1CAM is expressed in many tissues of the body and is therefore not specific to the brain. Other proteins, such as GLAST for astrocyte derived EVs and CD63 as a general EV marker are not present at high levels in brain derived EVs, leaving room for improvement to find markers which are more abundant and relevant to the target population. As newer studies are contesting some of these "standard" EV markers, more groups are looking for novel markers which are more specific to their subpopulations of interest, more abundant, and more likely to be found in the EV membrane rather than in the EV corona.

Marker Type	Surface Protein	Publication
General EV	CD9	Théry et al., 2018
	CD63	Théry et al., 2018
	CD81	Théry et al., 2018
	CD47	Théry et al., 2018
	ADAM10	Théry et al., 2018
Neuron-Derived EV	L1CAM	Guha et al., 2019; Nogueras-Ortiz et al., 2020
	SNAP25	Ohmichi et al., 2019
Astrocyte-Derived EV	GLAST1	Goetzl et al., 2019; Ohmichi et al., 2019
	GFAP	Goetzl et al., 2019; Zhang et al., 2019
Microglia-Derived EV	ANXA1	Lemaire et al., 2019
	TMEM119	Winston et al., 2021; Visconte et al., 2023
Oligodendrocyte-Derived EV	OMG	Ohmichi et al., 2019
	PLP	López-Guerrero et al., 2020

The protein corona is not a new concept in the field of EVs, however it has only begun to be seriously investigated in the last 5 years or so. The corona is a group of proteins which surround circulating EVs once they have been secreted from a cell. These proteins are typically soluble proteins circulating in biofluids which have high affinity for EVs and the proteins at their surface[172]. In more complex biofluids like plasma, different layers of the corona can form. Typically, within seconds to minutes, a first "hard corona" will form, made up of high affinity proteins (**Figure 3**)[53]. Then within minutes to hours, a second layer will form around the hard

corona. This layer is called the soft corona and is made up of lower affinity proteins[53]. The soft corona can be more easily changed and digested, while proteins of the hard corona are typically irreversibly bound to the EV[173]. These layers of proteins can mask EV surface proteins, effectively disguising their cell or tissue of origin from immunocapture efforts. In the blood, proteins such as albumin, immunoglobulins, and other lipoproteins tend to form the protein corona (**Figure 4**)[53,174]. In more filtered biofluids such as saliva, the EV corona appears to be less complex and with a lower affinity for the EV[175]. The biogenesis of the EV, its size, shape, charge, and the proteins at its surface, as well as the biofluid in which it is circulating all help determine the proteins which will make up its corona[53].

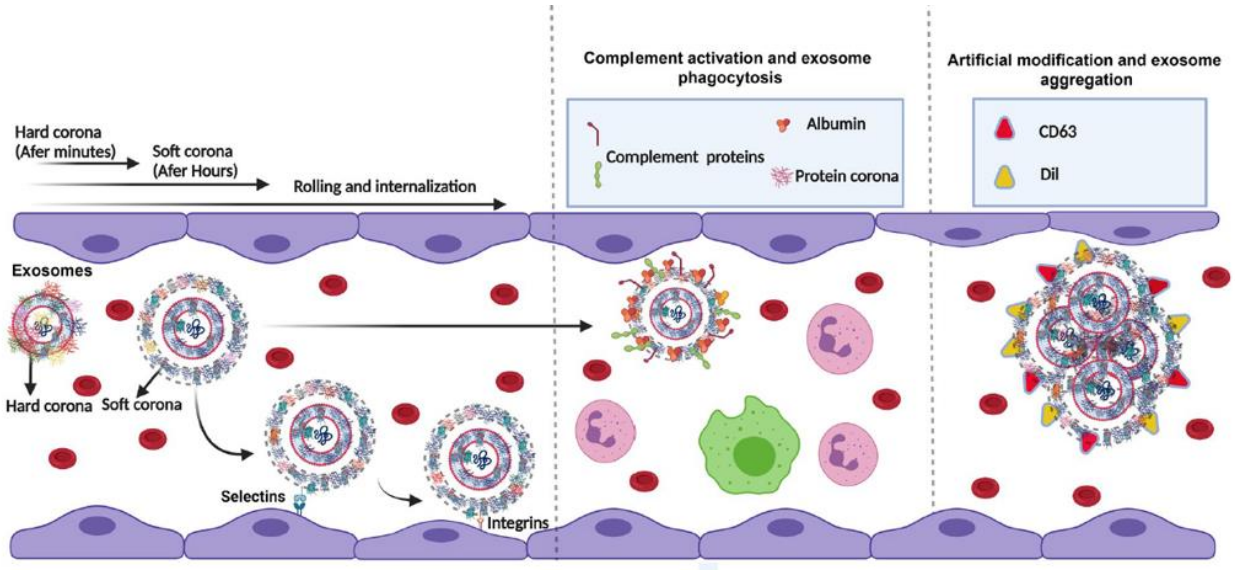

Figure 3 | Formation of the EV protein corona in plasma

Adapted from Heidarzadeh et al., 2023 – Cell Communication and Signaling [53]

Protein corona formation on the surface of EVs inside in vivo conditions. Both hard and soft protein corona layers are generated around EVs as a result of non-specific interactions and ligand-receptor affinity. The binding of different serum proteins on the vesicular surface can affect the hydrodynamic size, biodistribution, colloidal stability, and ligand-receptor interaction between EVs and acceptor cells.

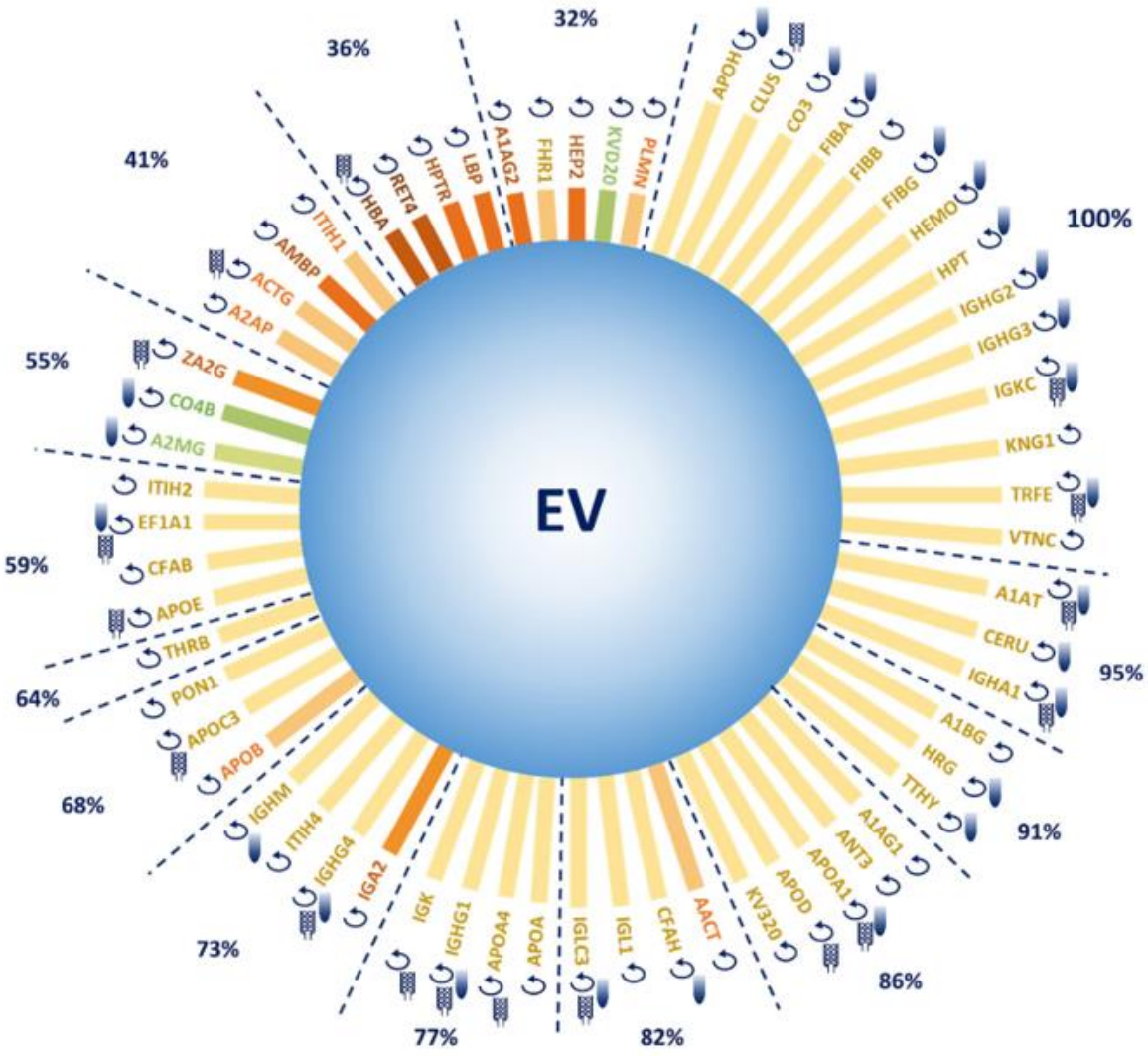

Figure 4 | Components of the EV protein corona in plasma

Adapted from Toth et al., 2021 - Journal of Extracellular Vesicles [174]

The protein corona is most often made up of common blood proteins such as albumin, apolipoproteins, and immunoglobulins.

In order to access true surface proteins of EVs, the protein corona must be bypassed. This is most often done by enzymatic digestion, partially or fully removing the protein corona from a group of EVs. There are several ways that the protein corona can be digested or dissociated from the EV. Proteolytic digestion, such as with Proteinase K (PK), Trypsin, and Trypsin Lys-C are common methods used depending on the desired outcome of the digestion[147,148]. Proteinase K will digest the proteins into peptides <4 amino acids in length, making them undetectable by techniques such as mass spectrometry. Conversely, Trypsin will cut proteins into peptides between 7 and 10 amino acids in length, allowing them to be separated from the EV population and run in mass

spectrometry to determine the identity of the digested proteins. Antimicrobial peptides may also be used to remove the outer corona proteins[176].

Removal of the protein corona can help show the "true" size of EVs, which can be increased substantially by the aggregation of proteins to the surface[53]. It can also serve to remove "contaminating" proteins for techniques such as mass spectrometry, where particularly blood proteins in large quantities can mask proteins of interest in small quantities in a sample[148]. Perhaps most importantly in this context, removal of the protein corona can reveal surface proteins embedded in the EV membrane and increase their access to immunocapture by specific antibodies (**Figure 5**).

Previously, we have demonstrated the ability of the proteomic signature of brain derived EVs to predict tau pathology and differentiate between 3R and 4R tauopathies. This work was done in brain derived EVs isolated from patient frontal cortex samples, but in order for this finding to be relevant for patient screening or diagnosis, we need to be able to isolate these EVs from peripheral biofluids noninvasively. For this reason, we have designed a study which uses in an in-depth proteomic analysis of cortex BD-EVs to identify novel surface markers which can be targeted in biofluids such as blood and saliva in order to enrich cerebral material for further analysis. We then propose an improved protocol for immunocapture of brain derived EVs in patient interstitial fluid (ISF), plasma, and saliva which features enzymatic digestion of the EV corona.

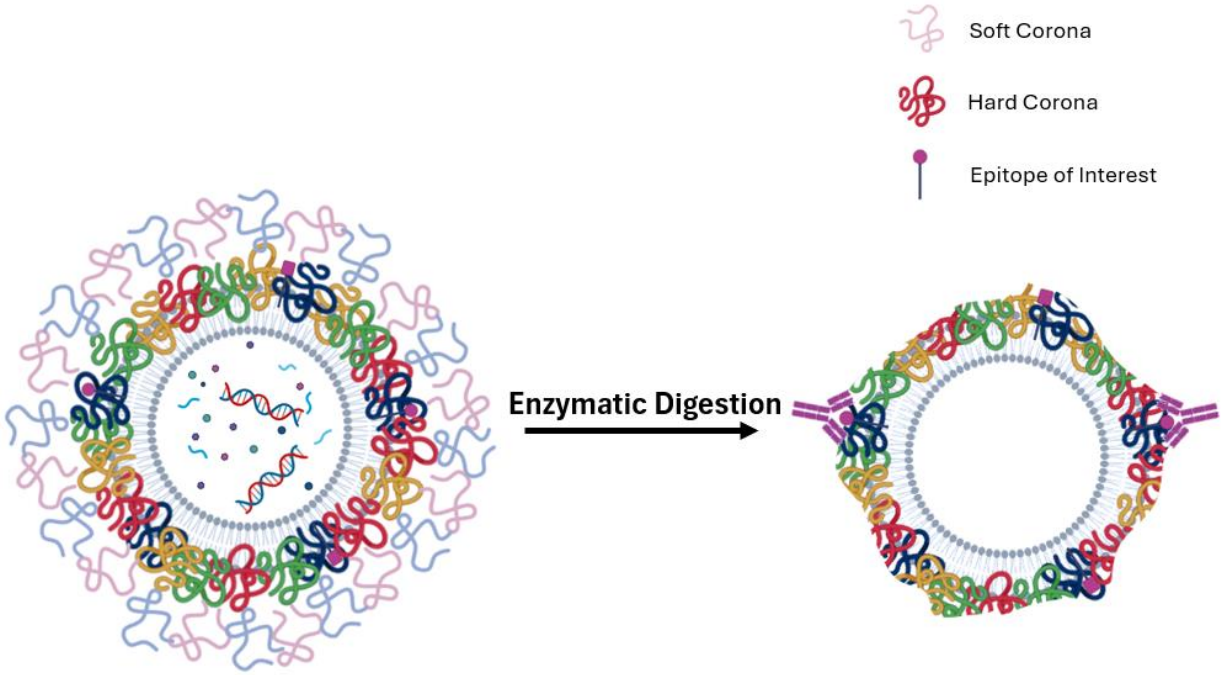

Figure 5 | Digesting the protein corona
Original graphic modified from BioRender

Schematic illustrating the hard and soft protein corona of extracellular vesicles both before and after enzymatic digestion. Soft corona proteins have a lower affinity for the vesicle complex and thus are more easily disturbed and removed. Hard corona proteins are typically irreversibly bound to the EV membrane, only to be removed by strong enzymatic digestion. Gentle enzymatic digestion can reveal surface proteins embedded in the plasma membrane and improve their access for immunocapture.

Results

In silico analysis reveals novel surface markers of BD-EVs

In order to determine the target proteins present on the surface of BD-EVs, the proteomic data obtained from the analysis of BD-EVs from 36 patients with a controlling or neurodegenerative disease (described previously in Chapter 1) was used for an in-depth in silico analysis. Using the Human Protein Atlas database for predicted subcellular localization[117], 380 proteins were identified as being associated to the plasma membrane (**Table S1**). Of these, 124 were identified as having an elevated abundance in brain tissue according to the Human Protein Atlas tissue specificity tool[117] (**Table S1**). In the top 50 membrane proteins by abundance, 33 are considered to be elevated in the brain (**Table 2**). Using the brain cell specificity database curated by McKenzie and colleagues[116], these proteins were annotated according to their cell type specificity within the context of only the brain. Of the top 33 brain membrane proteins, 8 were identified as being neuronal, 10 as astrocytic, and 3 as oligodendrocytic (**Table 2**). Some proteins were identified through the McKenzie database as being brain cell type specific, while not having an elevated abundance in brain tissue according to Human Protein Atlas. These cell type specificities have been highlighted in red to indicate that these proteins are likely not specific to that brain cell type when taking the whole body into consideration.

Table 2 | Top 50 EV predicted membrane proteins ranked by abundance

Rank	Elevated in Brain	Brain Cell Specificity
1	Elevated in Brain	Astrocytic
2	Elevated in Brain	Neuronal
3		Neuronal
4	Elevated in Brain	Neuronal
5	Elevated in Brain	Astrocytic
6	Elevated in Brain	Neuronal
7	Elevated in Brain	Neuronal
8	Elevated in Brain	
9	Elevated in Brain	Neuronal
10	Elevated in Brain	
11	Elevated in Brain	Astrocytic
12	Elevated in Brain	
13	Elevated in Brain	
14		
15		Oligodendrocytic
16		
17	Elevated in Brain	Astrocytic
18	Elevated in Brain	
19		
20	Elevated in Brain	Astrocytic
21		
22	Elevated in Brain	Oligodendrocytic
23	Elevated in Brain	Astrocytic
24	Elevated in Brain	
25	Elevated in Brain	Oligodendrocytic
26	Elevated in Brain	
27		Oligodendrocytic
28	Elevated in Brain	
29	Elevated in Brain	Astrocytic
30		Endothelial
31		
32	Elevated in Brain	Neuronal
33		

34	Elevated in Brain	Neuronal
35	Elevated in Brain	
36		Endothelial
37	Elevated in Brain	Astrocytic
38	Elevated in Brain	
39		
40	Elevated in Brain	
41		Neuronal
42	Elevated in Brain	
43		Endothelial
44	Elevated in Brain	Neuronal
45		Astrocytic
46	Elevated in Brain	Astrocytic
47		
48	Elevated in Brain	
49	Elevated in Brain	Astrocytic
50		Astrocytic

Previous work has established that astrocytes are highly sensitive to pathological tau accumulation. In particular, the mitochondrial network of astrocytes responds differently to 3R and 4R tau accumulation[68]. Given this quantifiable sensitivity, it's likely that astrocytes also secrete molecules, freely and in EVs, which reflect their reaction to tau aggregation. Therefore, astrocyte derived EVs may inform more on the specific pathology in the brain than EVs from other cell types. Additionally, considering the proximity of astrocytes to the blood vessels of the brain, it is highly likely that they are involved in the process of secreting EVs from the brain into the blood. This suggests that many EVs which pass from the brain to the blood will likely have passed through or been modified in some way by astrocytes, so they will likely enter the blood containing some astrocytic material. For these reasons, we decided to focus on astrocytic surface markers for this study, but this concept could easily be expanded to include surface proteins from neurons, oligodendrocytes, and microglia as targets to increase the yield and diversity of the brain EVs captured in other biofluids.

Plotting the relative abundance in HC patients against the percent sequence coverage of the 10 astrocytic membrane proteins, three emerged as more abundant and with a higher sequence coverage than the current literature standard for astrocyte derived EV isolation (SLC1A3) (**Figure 1A**). These three candidates were, in order of abundance, astrocytic membrane protein 1, 2, and 3 (AMP1, AMP2, and AMP3). All 10 proteins were

subjected to more stringent brain specificity using the Human Protein Atlas tissue specificity tool. Only proteins which were expressed only in the brain or expressed highly in the brain and only at lower levels in other tissues were considered. Beyond this point, only five candidates remained relevant: AMP1, AMP2, AMP3, AMP4, and AMP5 (**Figure 1B-F**). In this ranking, AMP4 is the literature standard SLC1A3. Dark yellow bars in Figure 2B-F correspond to brain tissue abundance. All other eliminated candidates are shown in Supplementary Figure 2. Pictured as well, for context, is the current literature standard for isolating neuron derived EVs in the plasma: L1CAM (**Figure S2**).

Finally, the candidate proteins were assessed for whether they were affected by pathology by comparing their abundance in patients with PSP and PiD. The most notable difference was for AMP1, though even in pathologies where the abundance is lowest for this protein, it remains more abundant than the other candidates (**Figure 1G**). AMP3 also becomes diminished in the presence of PiD pathology relative to HC (**Figure 1G**)

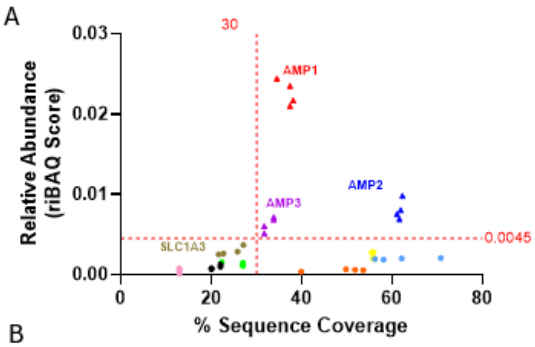
A
30
AMP1
AMP2
AMP3
SLC1A3
0.0045
Relative Abundance (riBAQ Score)
% Sequence Coverage


B
All other organs
AMP1

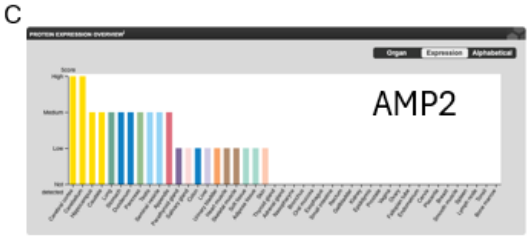
C
AMP2

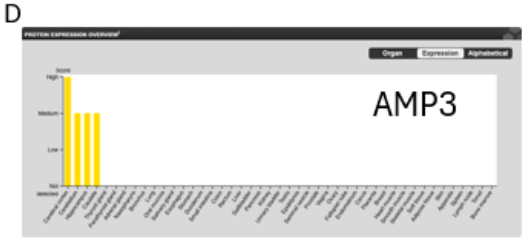
D
AMP3


E
AMP4


F
AMP5

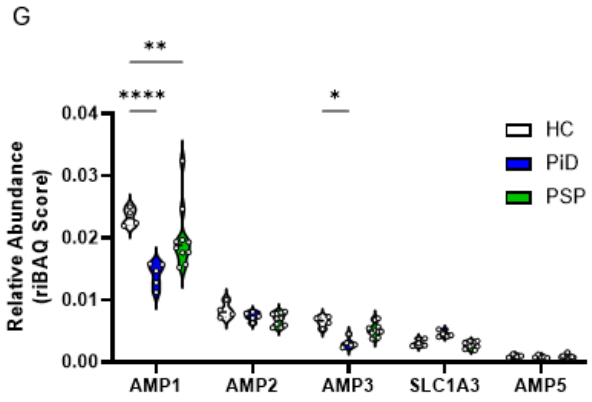
G
**
****
*
Relative Abundance (riBAQ Score)
HC
PiD
PSP
AMP1
AMP2
AMP3
SLC1A3
AMP5

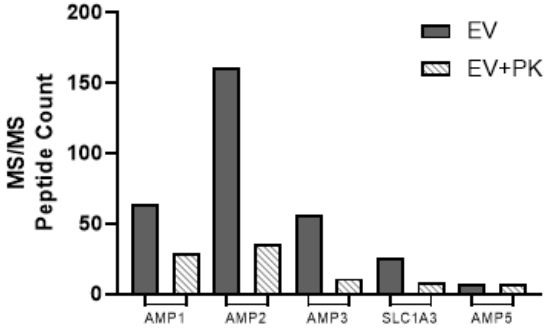
H
MS/MS Peptide Count
EV
EV+PK
AMP1
AMP2
AMP3
SLC1A3
AMP5

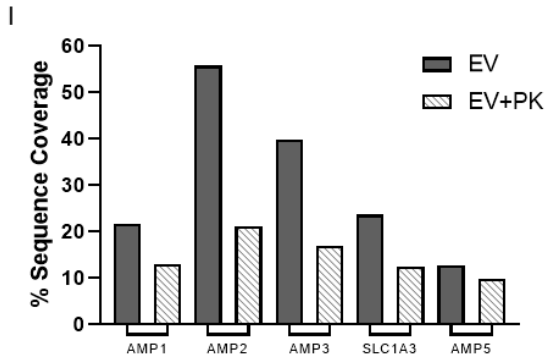
I
% Sequence Coverage
EV
EV+PK
AMP1
AMP2
AMP3
SLC1A3
AMP5

Figure 1 | Discovery of novel astrocytic surface markers of frontal cortex-derived EVs

A) Scatter plot showing the relative abundance vs. sequence coverage of the top 8 most abundant astrocytic membrane proteins in n=4 HC patients. Highlighted are the top 3 proteins by abundance (AMP1, AMP2, and AMP3), as well as the current literature standard for isolation of astrocyte-derived EVs in peripheral biofluids (SLC1A3). Each point represents 1 patient, each protein is represented by a different color and has n=4 patients

B) Human Protein Atlas diagram depicting the level of protein expression in 45 tissue systems for AMP1

C) Human Protein Atlas diagram depicting the level of protein expression in 45 tissue systems for AMP2

D) Human Protein Atlas diagram depicting the level of protein expression in 45 tissue systems for AMP3

E) Human Protein Atlas diagram depicting the level of protein expression in 45 tissue systems for AMP4

F) Human Protein Atlas diagram depicting the level of protein expression in 45 tissue systems for AMP5

G) Violin plot depicting the top 4 remaining candidates across 6 patient pathology groups (HC: n=4, PSP: n=10, PiD: n=5, AD I-II: n=3, AD III-IV: n=4, AD V-VI: n=10). Ordinary two-way ANOVA with Dunnette's multiple comparison test and single pooled variance was run. * $p < 0.05$, *** $p < 0.001$, **** $p < 0.0001$

H) Bar graph depicting the change in MS/MS Peptide Count (estimate of abundance) in n=1 HC patient from the untreated EV sample (grey) to the PK-treated EV sample (white and grey)

I) Bar graph depicting the change in % Sequence Coverage (amount of protein sequence detected) in n=1 HC patient from the untreated EV sample (grey) to the PK-treated EV sample (white and grey)

Subcellular localization to the membrane was confirmed using Protter[177]. This tool was used to confirm that proteins had the expected confirmation at the vesicle membrane, or conversely that they displayed a "flipped" orientation, a phenomenon described by Cvjetkovic and colleagues[147]. From this analysis, AMP5 was eliminated as not being transmembrane, leaving AMP1, AMP2, AMP3, and AMP4 (**Figure S1**).

Enzymatic digestion of EV protein corona confirms several novel markers

In order to test the validity of the astrocytic membrane proteins, and particularly the top 5 mentioned above, an experimental validation was designed whereby the protein at the exterior of the EVs was digested, without disturbing the EVs' structure or the protein contained within them. This experiment was designed following a similar protocol published by Cvjetkovic and colleagues[147]. Briefly, a purified EV sample from the frontal cortex of a HC patient was treated with Proteinase K to digest all the proteins of the EV corona and extravesicular portions of transmembrane proteins. After PK digestion a 30-75% decrease in MS/MS Peptide Count and % Sequence Coverage was observed for the top four remaining candidate proteins (**Figure 2H-I**). The substantial decrease, without total elimination, of peptide count and sequence coverage in these four candidates indicates that they have both extravesicular and intravesicular portions, confirming that they are likely embedded in the EV membrane.

Subcellular localization to the membrane was confirmed using Protter[177]. This tool was used to confirm that proteins had the expected confirmation at the vesicle membrane, or conversely that they displayed a "flipped" orientation, a phenomenon described by Cvjetkovic and colleagues[147]. From this analysis, TTYH was eliminated as not being transmembrane, leaving AMP1, AMP2, AMP3, and AMP4 as the most relevant candidates (**Figure S1**).

Enzymatic digestion of protein corona impacts immunocapture of BD-EVs in ISF, plasma, and saliva

EVs from plasma, saliva, and cortex ISF were stained with antibodies targeting the candidate surface markers established above. AMP1, AMP2, and AMP4 were combined into an astrocytic antibody cocktail (AMP124) for the following experiments. In cortex ISF, nearly 30% of EV particles were positive for AMP124 (**Figure 2A,C**). A PK treatment was then tested to examine whether this would increase staining efficiency by increasing access to EV surface proteins underneath the protein corona. Indeed, the percentage of antibody-positive EV particles in cortex ISF increased to 78% after PK treatment (**Figure 2B,B**). In plasma, without PK treatment only about 0.5% of EV particles were antibody stained (**Figure 2D,F**). However, with PK treatment this was increased to 32% (**Figure 2E,F**). These results suggest that not only are there fewer astrocyte derived EVs in the plasma than the ISF, but that the corona is likely more inhibiting in the plasma than in brain ISF. Similarly, in saliva only 0.8% of EV particles were antibody stained without PK treatment (**Figure 2G,I**), but with PK treatment this increased to 60% (**Figure 2H,I**). These results suggest that the surface proteins are more accessible in ISF than in plasma and saliva, or that the EV corona in ISF is made up largely of astrocytic proteins compared to the corona in plasma and saliva. In ISF, PK treatment is not necessary to reveal EVs with astrocytic proteins at their surface membrane, but in plasma and saliva PK treatment is necessary to achieve this result.

With the same dose of PK treatment, very different levels of antibody staining were observed in the three biofluids tested. A likely reason for this is the probable difference in the amount of astrocyte derived EVs (AD-EVs) in these different fluids. A range of PK doses also revealed different effects on antibody staining in each biofluid. In ISF, antibody-positive EVs seemed to reach a dose plateau, where increasing the dose no longer affected the AD-EV population. Even at a low dose of 2ug/mL, a maximum population of 80% of particles was attained (**Figure S3A**). In plasma, however, a higher dose of 500ug/mL PK revealed the most AD-EVs, with the highest dose lowering the percentage of AMP124-positive EVs (**Figure S3B**). The percentage of AD-EVs remained steady in saliva for the low and mid dose of PK, while at the high dose the population increased by 20% (**Figure S3C**). This difference between the biofluids could indicate that the protein corona of brain EVs is less complex than in other biofluids, and any dose will liberate surface proteins, or even that the PK treatment was permeabilizing the EVs in ISF and saliva, meaning antibodies were staining cargo rather than surface proteins.

This second hypothesis was at least partly supported by another test, whereby a second PK treatment after antibody staining was done in order to test the ability of PK to digest the antibodies at the EV surface. In plasma, this second PK treatment was highly efficient, reducing the antibody-positive population back down to <1%

(**Figure S3E**). However, in both saliva and brain ISF, the second PK treatment had almost no effect (**Figure S3D,F**). This indicates that it's possible the EVs were partially permeabilized and that the antibodies were in fact staining cargo within the EVs rather than proteins at the surface of EVs.

Immunoprecipitation (IP) was used as the primary method to isolate the AD-EV population. The IP in was tested in both plasma and saliva, using mass spectrometry and CryoEM as readouts. In both biofluids, the purified samples were treated with PK, then antibody stained and magnetically immunoprecipitated. AD-EVs from both biofluids were sent to mass spectrometry, where the cell type specificity database was used as an evaluation of the efficiency of the immunoprecipitation.

Overall in the plasma, more astrocytic proteins were observed after IP than proteins of other cell types such as neurons and oligodendrocytes (**Figure 2J**). However, there was not a considerable increase in the amount of astrocytic material between the immunoprecipitated sample and the flowthrough sample in the plasma. Rather an equal amount was left in the flowthrough, meaning either the immunoprecipitation was not very efficient in the plasma or that plasmatic EVs also contain a lot of astrocytic material as cargo, not just at the surface. In saliva EVs, however, the vast majority of astrocytic material was in the immunoprecipitated sample, with almost none left in the flowthrough sample (**Figure 2K**). Then, astrocytes were the most represented cell

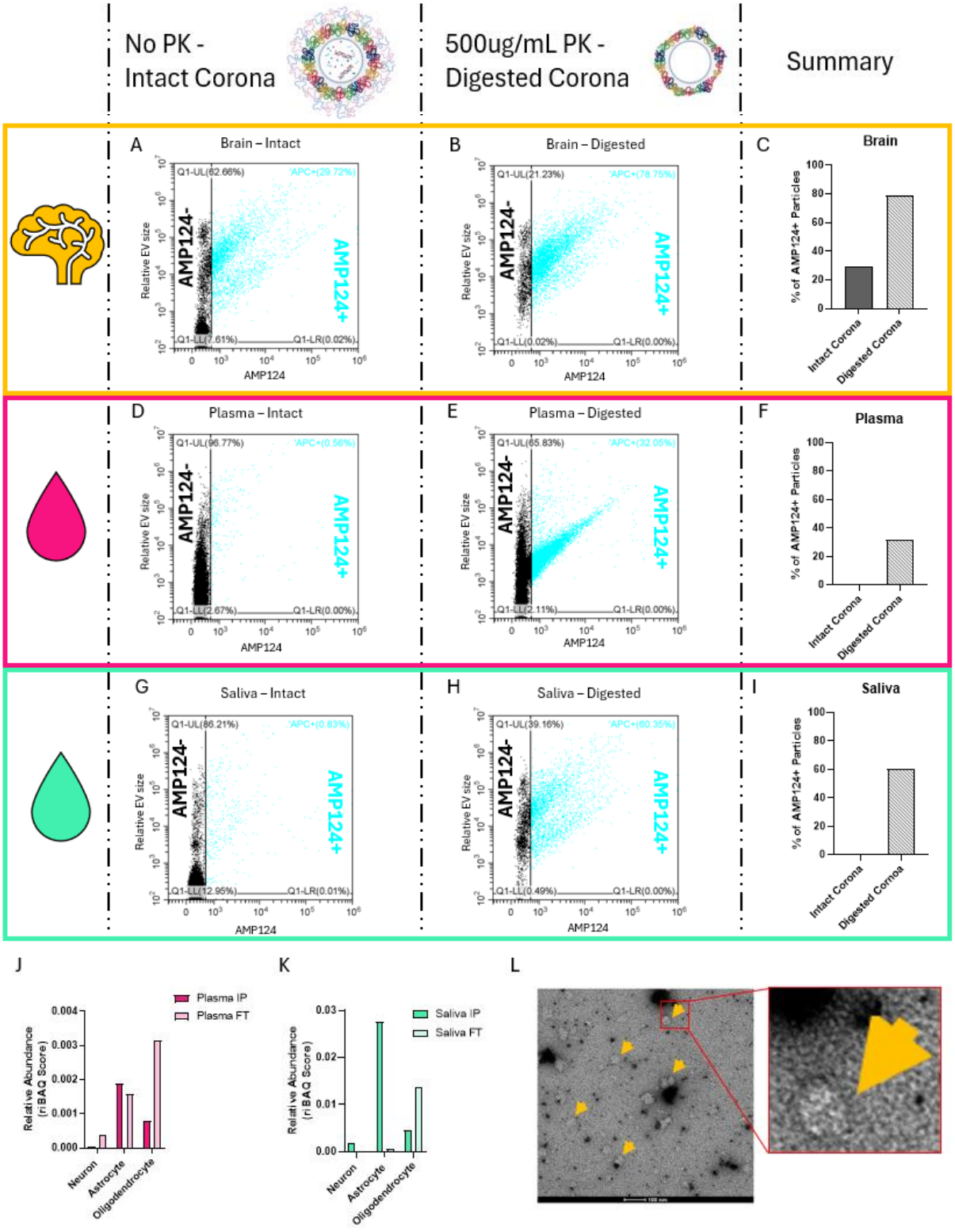
No PK -
Intact Corona
500ug/mL PK -
Digested Corona
Summary
A
Brain – Intact
Q1-UL(62.66%)
APC+(29.72%)
AMP124-
AMP124+
Q1-LL(7.61%)
Q1-LR(0.02%)
Relative EV size
AMP124
B
Brain – Digested
Q1-UL(21.23%)
APC+(78.75%)
Q1-LL(0.02%)
Q1-LR(0.00%)
C
Brain
% of AMP124+ Particles
Intact Corona
Digested Corona
D
Plasma – Intact
Q1-UL(96.77%)
APC+(0.56%)
Q1-LL(2.67%)
Q1-LR(0.00%)
E
Plasma – Digested
Q1-UL(65.83%)
APC+(32.05%)
Q1-LL(2.11%)
Q1-LR(0.00%)
F
Plasma
G
Saliva – Intact
Q1-UL(86.21%)
APC+(0.83%)
Q1-LL(12.95%)
Q1-LR(0.01%)
H
Saliva – Digested
Q1-UL(39.16%)
APC+(60.35%)
Q1-LL(0.49%)
Q1-LR(0.00%)
I
Saliva
J
Plasma IP
Plasma FT
Relative Abundance (riBAQ Score)
Neuron
Astrocyte
Oligodendrocyte
K
Saliva IP
Saliva FT
L

Figure 2 | Novel astrocytic surface markers are present on EVs in peripheral biofluids

A) Flow cytometric plot depicting human cortex ISF EV sample with no PK treatment. In blue: AMP124+ EVs make up 29.72% of total particles
B) Flow cytometric plot depicting human cortex ISF EV sample after PK treatment. In blue: AMP124+ EVs make up 78.75% of total particles
C) Bar plot summarizing the percentage of AMP124+ EVs before and after PK treatment in cortex ISF EVs
D) Flow cytometric plot depicting human plasma EV sample with no PK treatment. In blue: AMP124+ EVs make up 0.56% of total particles
E) Flow cytometric plot depicting human plasma EV sample after PK treatment. In blue: AMP124+ EVs make up 32.05% of total particles
F) Bar plot summarizing the percentage of AMP124+ EVs before and after PK treatment in plasma EVs
G) Flow cytometric plot depicting human saliva EV sample with no PK treatment. In blue: AMP124+ EVs make up 0.83% of total particles
H) Flow cytometric plot depicting human saliva EV sample after PK treatment. In blue: AMP124+ EVs make up 60.35% of total particles
I) Bar plot summarizing the percentage of AMP124+ EVs before and after PK treatment in saliva EVs
J) Bar graph showing the abundance of neuron-specific, astrocyte-specific, and oligodendrocyte-specific proteins in plasma EVs in IP and flowthrough fractions after immunoprecipitation with AMP124
K) Bar graph showing the abundance of neuron-specific, astrocyte-specific, and oligodendrocyte-specific proteins in saliva EVs in IP and flowthrough fractions after immunoprecipitation with AMP124
L) Negative stain of AMP124+ EVs after immunoprecipitation and bead removal. Scale bar is 100nm

type in the immunoprecipitated sample, indicating that the IP was highly efficient in the saliva. To confirm the presence of EVs after immunoprecipitation, the plasma IP sample was analyzed by CryoEM. Here, many intact EVs were observed in the typical size range of 50-100nm (**Figure 2L**). These images also confirmed that the PK treatment did not destroy EVs in the sample.

Discussion

In a technical context, in this study we found ourselves limited by the capabilities of flow cytometers to sort nanoparticles. In our proof-of-concept experiment (see methods section), we saw that the machine is indeed capable of detecting and sorting single nanoparticles when they are highly fluorescent. In our actual experiment with antibody staining, we saw a much less efficient sorting of EV populations, likely due to the lower intensity fluorescence of the antibodies compared to the general protein dye. On smaller EVs, we can expect a maximum of 2-3 antibodies to fix to the EV surface, meaning only 2-3 fluorescent molecules per particle. On the other hand, many dye molecules can pass the EV membrane and activate within the EV. This means that the whole particle fluoresces from within rather than only having a few fluorescent points on its periphery. This, combined with the fact that we had far fewer APC+ particles than PE+ particles means the machine likely had trouble detecting these particles which are not overly fluorescent and are lost in a cloud of more-fluorescent particles. This is evidenced by the fact that the “impurity” in the APC+ sort is not from PE+ particles, but simply from EVs that are not positive for any antibody and only have violet dye at their interior (**Figure 3J**). These antibody negative EVs account for 90% of the sorted particles, indicating that the machine likely has trouble differentiating negative particles from slightly positive ones.

While this technology has advanced a lot in recent years, and more and more groups are using flow cytometry to visualize EV subpopulations[151,153], we are still not at a point of being able to use flow cytometry sorting to separate out these subpopulations efficiently. Even aside from the difficulty in obtaining pure populations, this process takes far longer than is viable for routine experimentation. To sort 3mL of sample took close to 12 hours, also requiring changing sheath fluid for the machine mid-run. This is not sustainable for groups who use these machines at a platform or who have multiple samples to sort from the same experiment. Techniques such as immunoprecipitation have the advantage of being much faster (in our case, we can run up to 16 samples in an afternoon, though this number could be increased) and of providing a better working volume at the end. Sorting dilutes the sample significantly by the end, sometimes requiring reconcentration before further analysis such as mass spectrometry can be run.

By exploiting the BD-EV proteomics dataset already at our disposal, we were able to identify proteins which were present in our EV samples and which could likely be found at the EV membrane. Many identified surface proteins have come from the study of EV surface proteins in other fields (such as immunology and cancer) or from the concept that these proteins are present at the membrane of certain brain cell types, without doing comprehensive tests to show that these proteins are indeed at the surface of brain derived EVs and not simply in the protein corona. For example, L1CAM is commonly used to isolate neuron derived EVs from fluids such as plasma, but recently its presence in the EV membrane has been called into question[71,171]. In the Norman article, they claim that L1CAM is not actually associated with EV membranes, but rather that cleaved, soluble L1CAM gets stuck in the protein corona after EV secretion. The article by You and colleagues supports this notion, having not detected L1CAM in EVs from iPSC derived neurons. Indeed, when we performed the PK treatment of cortex EVs, we saw that the little amount of L1CAM which was present before treatment was completely digested (**Figure S4**). Additionally, the portion which was present in our sample before PK treatment did not include the transmembrane portion of the protein (**Figure S4**). This is why we found it critical to identify the proteins present in our samples which were confirmed to be surface proteins and highly abundant as a starting off point for our novel AD-EV surface markers, rather than taking literature standards as a starting point.

The complexity of the protein corona in different biofluids is a major factor in the efficiency of the immunocapture of circulating EVs. Corona complexity will determine the dose of PK digestion which is necessary to liberate access to surface proteins for capture. As such, it is necessary to go further into the biofluid analysis than we were able to within the scope of this study. Ideally, we should perform a PK digestion at several doses and observe the EVs before and after PK treatment by CryoEM or a similar technique in each

biofluid. With the correct concentration of EVs, this would allow us to potentially see the effect of the digestion on the protein corona itself, as well as any effects that a strong treatment may have on the structural integrity of the EV. We should also perform an immunoGold antibody staining and CryoEM visualization to visualize nanobeads either at the surface or the interior of EVs. This would allow us to be sure of the dose of PK that we are using to clear the corona without permeabilizing the EVs. This test is absolutely critical to show that a. we increase staining efficiency with PK treatment as observed in flow cytometry and b. that we are still staining surface proteins and not EV cargo, meaning that the increase in staining efficiency is true.

The efficiency of AD-EV immunoprecipitation was not the same in plasma and saliva as seen by the amount of astrocytic material which remained in the flowthrough of both biofluids after IP. While it's possible that there are more AD-EVs in saliva than in plasma, it's also possible that AD-EVs in plasma are better "protected" than those in the saliva. There is evidence in BD-EVs of small EVs existing within larger EVs[178–180]. It's therefore possible that plasma has a higher proportion of these multiple EV particles than other fluids like saliva. If small AD-EVs were to be found within larger plasma or endothelial EVs, this would mean that even with a PK treatment, we would not capture all the AD-EVs in the plasma. It's also possible that in the process of crossing the BBB, AD-EVs may be broken down within cells of the BBB and "repackaged" into new EVs which maintain astrocytic cargo but now contain endothelial markers at their surface[143]. In this case, we would see results similar to what we observed in proteomics where we have a similar amount of astrocytic material in the IP fraction as the flowthrough (FT) fraction. Because we still don't know the exact mechanisms by which BD-EVs cross the BBB (and it's likely there are different mechanisms for different types of EVs), it's difficult to know in what capacity these EVs exist in the blood.

There are many groups to this day which isolate BD-EVs in the blood, whether they capture neuron derived EVs[161], astrocyte derived EVs[165], or EVs derived from other brain cell types[164,169]. It has been shown in many different ways that this capture works, so it's very likely that some EVs pass the BBB without much modification. However, it's equally likely that many are modified and that elucidating the mechanisms of crossing would shed a lot of light on how we could improve the targeting of these particles in the blood. The current literature on the subject hypothesizes several mechanisms of action, including transcytosis, macropinocytosis, clathrin-mediated endocytosis, caveolae-mediated endocytosis, and adsorptive-mediated endocytosis[143,144]. There are groups who also isolate BD-EVs in other biofluids, such as saliva and urine[181,182]. Given the proteomic complexity of the blood, other biofluids may prove simpler for immunocapture of BD-EVs. That being said, most groups who use salivary EVs as biomarkers for CNS disorders do not separate out BD-EVs but rather take the whole EV population and dose brain-specific proteins within all EVs[183]. If, as our

results suggest, up to 60% of salivary EVs contain brain material at their surface, this could be a much simpler way of profiling proteomic changes in the context of CNS pathology, without prior immunocapture of BD-EVs.

The main goal of the second half of this thesis project was to improve the capture of BD-EVs in the periphery. Here I say BD-EVs rather than AD-EVs because the methods we used for AD-EVs can be applied to any cell type. The goal was to create a methodology to efficiently and reproducibly isolate a specific subset of EVs, but by changing the target proteins, this methodology could realistically be applied to any subset of EVs. The specifics of this set of experiments still leave room for improvement. We can improve the actual cocktail we are using by eliminating candidate proteins which may be less specific than we want (AMP2), or by adding another highly specific candidate which is more abundant than the current literature standard (AMP3), among others. Additionally, the decision to begin digesting the corona of EVs to better access their surface proteins was made to improve the overall isolation of specific EVs in the plasma. It's well established that the EV corona is highly complex, particularly in a biofluid such as plasma[53]. Other groups have investigated this concept of PK digestion of the corona in order to "clean" the contaminating plasmatic proteins from the sample[148]. This is particularly relevant for analyses such as mass spectrometry, where blood proteins present in high quantities will mask the proteins present in low quantities, heavily biasing untargeted proteomics approaches.

This novel capture method we have developed is an improvement upon the existing techniques for several reasons. First, the use of Proteinase K to digest the protein corona around the EV increases the yield of positive EVs by making surface proteins more accessible to antibody capture. This also makes us more confident that EVs are astrocytic in nature as they contain these proteins at their surface and not just in the surrounding corona. Furthermore, the Proteinase K digestion also serves to clean the EV samples of contaminating proteins and aggregates which may co-precipitate with EVs during the isolation process. Additionally, we did not take the literature standard for AD-EV isolation (SLC1A3) at face value. Instead, we tested it like the other candidate proteins and found that while it is still a valid marker which held up against PK digestion and maintains its brain specificity in the context of other organs, there were three other candidate proteins which may capture more EVs as they were more abundant in EV samples. Finally, this method is applicable to a wide range of EV subpopulations. The developed cocktail may be substituted for a cocktail or single antibody of choice for a different EV subpopulation and the PK digestion will still likely aid in the capture of these EVs.

Materials & Methods

Determination of Brain Derived Surface Proteins

Using the proteomic dataset described in Chapter 1, all proteins in HC patients were annotated according to three different databases.

The first database was from the Human Protein Atlas[117]. This database provides the predicted subcellular localization of proteins (intracellular, secreted extracellularly, transmembrane, etc.). It was used to identify proteins which were predicted to be located at the plasma membrane to determine which proteins may also be located at the membrane of EVs.

The membrane proteins were then annotated for tissue specificity to the brain. Again using the Human Protein Atlas[117], proteins which showed an elevated abundance in the brain were noted. The Human Protein Atlas assigns a protein expression level of "high", "medium", "low", or "not" to each protein in 45 different tissues within 15 organ systems. A given protein was characterized as being brain-specific if it was a. only expressed in tissues of the brain or b. highly expressed in tissues of the brain, while only expressed at lower levels in other tissues.

Finally, a cell type specificity database generated by McKenzie and colleagues[116] was used. Briefly, this database identifies proteins which are specific to different cell types of the brain, within the context of the brain only, at different thresholds defined by the authors. The authors considered 6 brain cell types in this analysis: neurons, astrocytes, microglia, oligodendrocytes, endothelial cells, and oligodendrocyte precursor cells. Using RNA expression data from five studies, the authors defined cell type specificity as the minimum fold change in expression between the cell type of interest and each of the other cells, cell type enrichment as the fold change in expression when comparing the cell type of interest to all of the other cells at once, and cell type absolute expression as the expression in a particular cell type irrespective of that in other cell types (McKenzie et al., 2018). Cell type specificity is the strictest definition in this study, and this is the metric which was used to annotate the proteins specific to certain brain cell types in this dataset.

Lastly, the remaining candidates were evaluated for the effect of pathology on their abundance. The abundance of each candidate protein in our proteomic dataset was compared across HC, PiD, and PSP patients.

Experimental Validation of Surface Candidates by Digestion of the Protein Corona

EVs were subjected to digestion by Proteinase K (New England Biolabs, P8111S) in order to digest the protein corona around the EVs, leaving only cargo proteins intact within the EVs. EVs were treated with various doses of PK ranging from 2ug/mL to 1000ug/mL depending on the biofluid and biological question being tested. PK-treated EVs were incubated at 37ºC for 1hr, and then PK was inactivated by heating samples to 60ºC for 10min. Samples were then washed by ultrafiltration at 100kD (Merck Millipore, Amicon Ultra-4, UFC810024) to eliminate the remaining small peptides from the EV samples.

**Note, for the first PK treatment (experimental validation of in silico candidate selection), 5mM PMSF (Sigma-Aldrich, 93482-50mL-F) was added to the sample to inhibit the PK activity rather than using heat deactivation. PMSF was then deactivated (so that mass spectrometry digestion would not be inhibited) by bringing the sample pH to 11 with NaOH.

After enzymatic digestion, subcellular localization was confirmed with the free online tool Protter[177]. This website shows the configuration of most proteins encoded by the human genome at the amino acid level, including showing which amino acids are extracellular, intracellular, and embedded in the membrane for transmembrane proteins.

Label-Free LC MS/MS Analysis of BD-EV Samples

In collaboration with Protein Analysis Facility (PAF) of UNIL: Manfredo Quadroni and Partrice Waridel.

Protein Digestion: miST

F1-4 fractions were digested according to a modified version of the iST method (named miST method)[128]. Briefly, 50 ml solution in PBS were supplemented with in 50 ml miST lysis buffer (1% Sodium deoxycholate, 100 mM Tris pH 8.6, 10 mM DTT) and heated at 95°C for 5 min. Samples were then diluted 1:1 (v:v) with water and reduced disulfides were alkylated by adding 1 /4 vol of 160 mM chloroacetamide (final 32 mM) and incubating at 25°C for 45 min in the dark. Samples were adjusted to 3 mM EDTA and digested with 0.5 mg

Trypsin/LysC mix (Promega #V5073) for 1h at 37°C, followed by a second 1h digestion with a second and identical aliquot of proteases. To remove sodium deoxycholate and desalt peptides, two sample volumes of isopropanol containing 1% TFA were added to the digests, and the samples were desalted on a strong cation exchange (SCX) plate (Oasis MCX; Waters Corp., Milford, MA) by centrifugation. After washing with isopropanol/1% TFA, peptides were eluted in 250 ml of 80% MeCN, 19% water, 1% (v/v) ammonia

See Table 3 for details of which experiments used miST protein digestion

Protein Digestion: SP3

Samples were digested following the SP3 method (Huges, et al., 2019) using magnetic Sera-Mag Speedbeads (Cytiva 45152105050250, 50 mg/ml). Briefly, samples were diluted with SP3 buffer (2% SDS, 10mM DTT, 50 mM Tris, pH 7.5) and heated 10 min at 75°C. Proteins were then alkylated with 32mM (final) iodoacetamide for 45 min at room temperature (RT) in the dark. Beads were added at a ratio of 10:1 (w:w) to samples, and proteins were precipitated on beads with ethanol (final concentration: 60 %). After 3 washes with 80% ethanol, beads were digested in 50ul of 100 mM ammonium bicarbonate with 1.0 ug of trypsin (Promega #V5073). After 1h of incubation at 37°C, the same amount of trypsin was added to the samples for an additional 1h of incubation. Supernatant were then recovered, transferred to new tubes, acidified with formic acid (0.5% final concentration), and dried by centrifugal evaporation. In order to remove traces of SDS, two sample volumes of isopropanol containing 1% TFA were added to the digests, and the samples were desalted on a strong cation exchange (SCX) plate (Oasis MCX; Waters Corp., Milford, MA) by centrifugation. After washing with isopropanol/1%TFA and 2% acetonitrile/0.1% FA, peptides were eluted in 200ul of 80% MeCN, 19% water, 1% (v/v) ammonia, and dried by centrifugal evaporation.

See Table 3 for details about which experiments used SP3 protein digestion

Liquid chromatography-tandem mass spectrometry: Tryptic peptide mixtures were injected on an Ultimate RSLC 3000 nanoHPLC system interfaced via a nanospray Flex source to a high resolution Orbitrap Exploris 480 mass spectrometer (Thermo Fisher, Bremen, Germany). Peptides were loaded onto a trapping microcolumn Acclaim PepMap100 C18 (20 mm x 100 µm ID, 5 µm, Dionex) before separation on a C18 custom packed column (75 µm ID × 45 cm, 1.8 µm particles, Reprosil Pur, Dr. Maisch), using a gradient from 4 to 90 % acetonitrile in 0.1 % formic acid for peptide separation (total time: 140 min). Full MS survey scans were performed at 120,000 resolution. A data-dependent acquisition method controlled by Xcalibur software

(Thermo Fisher Scientific) was used that optimized the number of precursors selected ("top speed") of charge 2+ to 5+ while maintaining a fixed scan cycle of 2 s. Peptides were fragmented by higher energy collision dissociation (HCD) with a normalized energy of 30 % at 15,000 resolution. The window for precursor isolation was of 1.6 m/z units around the precursor and selected fragments were excluded for 60s from further analysis.

MS and MS data analysis: Data files were analyzed with MaxQuant 1.6.14.0[129] incorporating the Andromeda search engine[130]. Cysteine carbamidomethylation was selected as fixed modification while methionine oxidation and protein N-terminal acetylation were specified as variable modifications. The sequence databases used for searching were the mouse (Homo sapien) reference proteome based on the UniProt database, and a "contaminant" database containing the most usual environmental contaminants and enzymes used for digestion (keratins, trypsin, etc.). Mass tolerance was 4.5 ppm on precursors (after recalibration) and 20 ppm on MS/MS fragments. Both peptide and protein identifications were filtered at 1% FDR relative to hits against a decoy database built by reversing protein sequences

Table 3 | Summary of mass spectrometry protocols by experiment

Experiment	Protein Digestion
Base cohort - Lille HC, PiD, PSP patients	miST
Proteinase K digestion of HC EVs	miST
Plasma & Saliva BD-EV IP	SP3

Proteinase K Proteomics Analysis

For this analysis, MS/MS Peptide Counts and Unique Razor Peptide Counts were used as measures of protein abundance rather than any of the abundance scores previously discussed (LFQ, iBAQ, riBAQ). Due to the difference in dynamic range of the sample without PK and with PK, the normalized abundance scores were not reliable. If a protein contained at least 2 MS/MS Peptide Counts **and** at least 2 Unique Razor Peptide Counts, it was considered to be present for this analysis.

Antibody Labeling

Antibodies against 4 candidate surface markers were tested in plasma, saliva, and cortex ISF. EVs were purified by SEC using Izon 35nm columns (Izon, ICO35-11550). After purification, some EVs from each biofluid were subjected to PK treatment at a concentration of 500ug/mL and then washed by ultrafiltration at 100kD (Merck Millipore, Amicon Ultra-4, UFC810024). EVs were then dyed with the esterase-activated protein dye

CellTrace Violet (Thermo Fisher, C34571) at a concentration of 20uM and incubated at 37ºC for 90min. EVs were washed again by ultrafiltration at 100kD and incubated for 30min at RT with human FC receptor blockers (Miltenyi Biotec, 130-059-901). Finally, EVs were stained with relevant antibodies. First, antibodies were directly conjugated to the fluorophore of choice using the FlexAble kit (Proteintech, KFA003 / KFA002) according to the kit's instructions. Once conjugated, antibodies were added to samples at a concentration of 0.2ng/uL and incubated overnight at 4ºC with rotation. The following day, samples were cleaned by adding 100uL of CaptoCore400 beads (Cytiva, 17372401) and incubating at RT for 30min with rotation. Samples were then centrifuged at 2000g for 2min and supernatant was gently removed from bead pellet and stored in a clean tube at 4ºC until further analysis.

Flow Cytometry of Fluorescently Labeled EVs

In collaboration with Dr. Dimitrios Kapogiannis and Dr. Carlos Nogueras-Ortiz (Baltimore, USA). EVs which were dyed and antibody stained were analyzed by flow cytometry (CytoFlex LX2). Briefly, several control samples were run before the EV samples in order to set up proper gating, including buffer only (filtered PBS), buffer+dye without EVs, buffer+antibodies without EVs, and unstained EVs. Detecting particles by fluorescence, EV samples were then run. A first gating determined the EV population among all the particles of the sample. This population was fluorescent in violet, whereas non-EVs (or particles not containing esterases) were not fluorescent and fell outside of the determined gate. From this EV population, the relevant fluorphore(s) (PE/AF555 and/or APC/AF647) were gated for antibody positivity in order to obtain the subpopulation of EVs which were positive for the antibodies of choice.

Machine settings used were the following: FSC Gain ~190, SSC Gain ~120, APC ~400, Violet450 ~350, PE ~400. Trigger channel (Violet450) threshold: manual 1300 height.

Fluorescence-Assisted Sorting of EVs

In collaboration with Dr. Dimitrios Kapogiannis and Dr. Carlos Nogueras-Ortiz (Baltimore, USA). After successfully analyzing single EVs by flow cytometry, an attempt was made to sort EVs as a replacement for immunoprecipitation. EV samples were processed in the same way as described above, and the machine was then set to sort specified populations according to antibody fluorescence. Three populations were sorted each time: violet EVs which were also PE+, violet EVs which were also APC+, and violet EVs which were both PE+ and APC+. This process took about 12 hours per sample.

A proof-of-concept experiment was set up to assess the machine's true ability to analyze and sort single EVs. Using the same live dye as described above, multiple colors were used simultaneously on EV samples to mimic single and double positive EVs. For this experiment, violet, PE, and APC dyes were used and the samples were set up as follows: sample 1 contained EVs colored with both the violet and PE simultaneously to mimic violet-dyed EVs positive for one antibody, sample 2 was the same but with violet and APC, to mimic single positivity for a different antibody, sample 3 had all three dye colors added simultaneously to mimic violet-dyed, double positive EVs, and sample 4 was a mixture of samples 1 and 2, mixed just before placing in the machine for analysis to prevent dye mixing (**Figure 3A**). The idea here was that sample 3 should have EVs which are tri-colored, whereas sample 4 should have two distinct populations of bi-colored EVs (violet/APC and violet/PE), but the EVs should not appear triple positive if the machine is in fact visualizing single EVs. Indeed, this was exactly what was observed. Panels b-k of Figure 1 all show the population of violet particles (EVs) as the total population, with PE and APC-positive EVs as subsets of the total EV population. Sample 1 showed over 99% violet/PE positive particles (**Figure 3B**), and sample 2 showed 94% violet/APC positive particles, with about 6% of particles leaking into the PE channel as double positives (**Figure 3C**). Sample 3 showed about 96% violet/PE/APC positive particles (**Figure 3D**). Sample 4, the one which can demonstrate the machine's ability to distinguish single EVs, showed 70% PE positive particles, 27% APC positive particles, and only 2% of particles appeared positive for all three colors (**Figure 3E**). This means that only 2% of the population was falsely identified, likely as a result of analyzing multiple EVs as one particle. When sample 4 was sorted to see if the machine could also sort individual EVs as well as analyzing them, results again confirmed the machine's capabilities. The 70% PE positive EVs were sorted separately from the 27% APC positive EVs from panel e, and the purity for the PE positive EVs was over 99% (**Figure 3F**), while the purity for APC positive EVs was over 95% (**Figure 3G**)

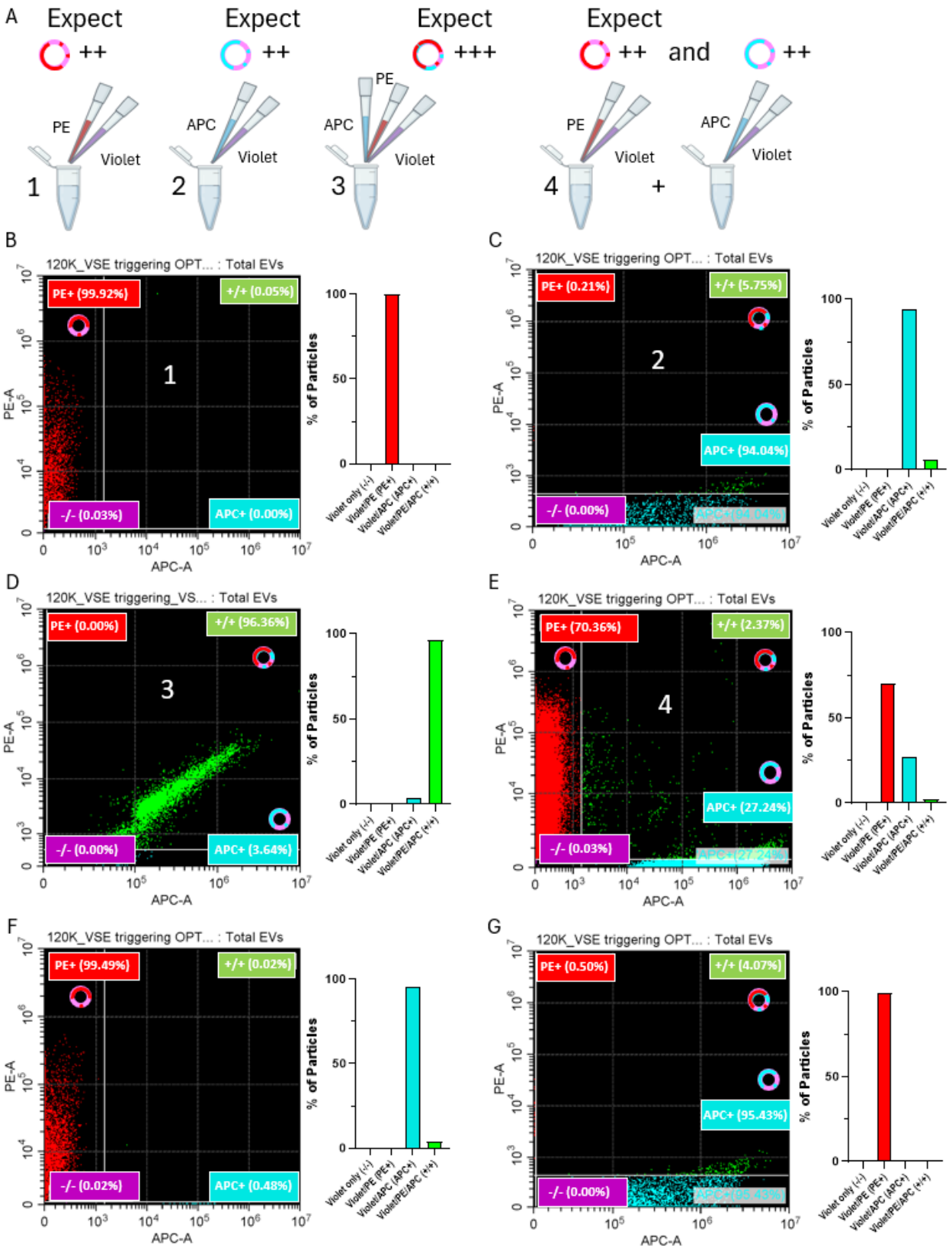
A
Expect
++
PE
Violet
1
Expect
++
APC
Violet
2
Expect
+++
PE
APC
Violet
3
Expect
++
PE
Violet
4
+
and
++
APC
Violet
B
120K_VSE triggering OPT... : Total EVs
PE+ (99.92%)
+/+ (0.05%)
1
-/- (0.03%)
APC+ (0.00%)
PE-A
APC-A
% of Particles
Violet only (-/-)
Violet/PE (PE+)
Violet/APC (APC+)
Violet/PE/APC (+/+)
C
120K_VSE triggering OPT... : Total EVs
PE+ (0.21%)
+/+ (5.75%)
2
APC+ (94.04%)
-/- (0.00%)
APC+ (94.04%)
D
120K_VSE triggering_VS... : Total EVs
PE+ (0.00%)
+/+ (96.36%)
3
-/- (0.00%)
APC+ (3.64%)
E
120K_VSE triggering OPT... : Total EVs
PE+ (70.36%)
+/+ (2.37%)
4
APC+ (27.24%)
-/- (0.03%)
APC+ (27.24%)
F
120K_VSE triggering OPT... : Total EVs
PE+ (99.49%)
+/+ (0.02%)
-/- (0.02%)
APC+ (0.48%)
G
120K_VSE triggering OPT... : Total EVs
PE+ (0.50%)
+/+ (4.07%)
APC+ (95.43%)
-/- (0.00%)
APC+ (95.43%)

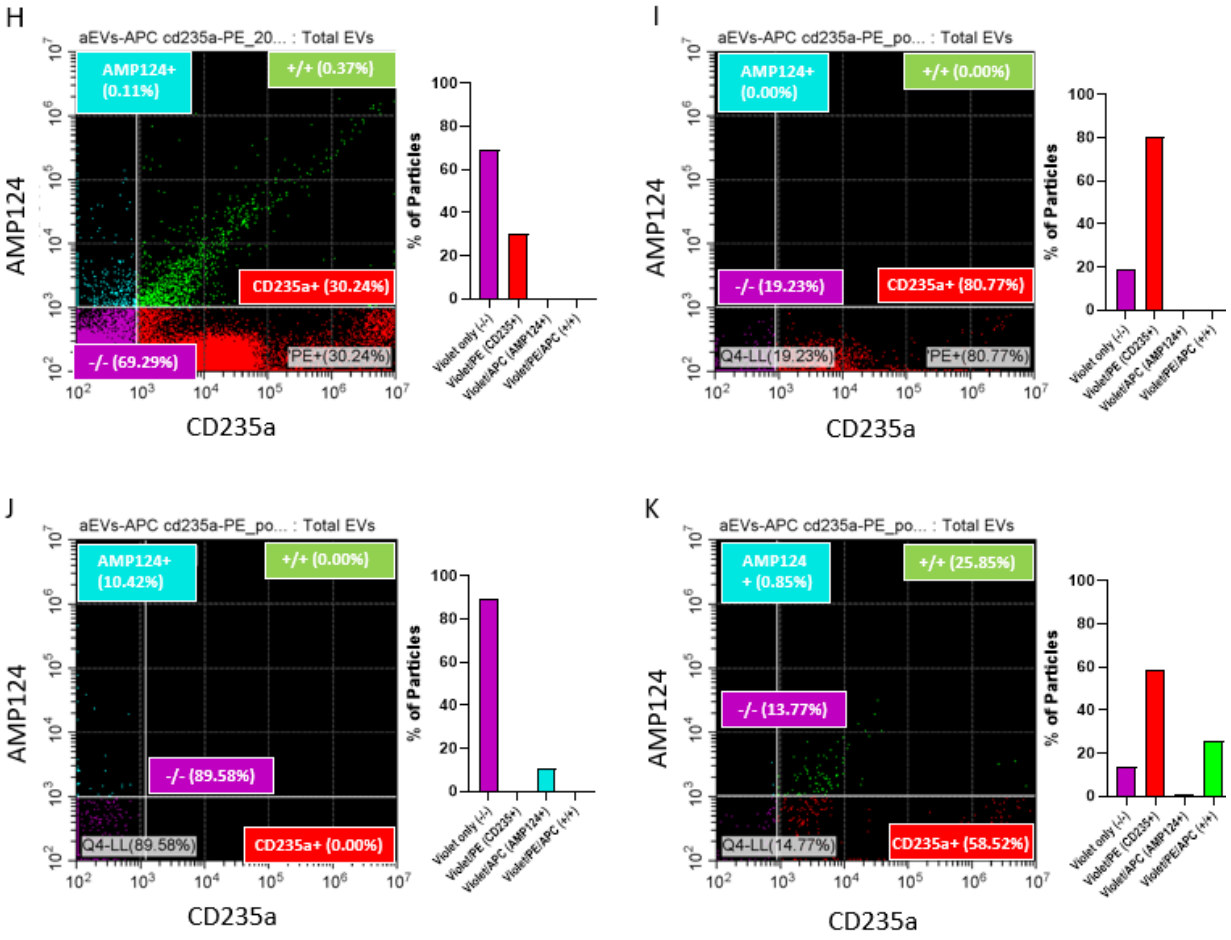

Figure 3 | Methodological proof-of-concept: flow cytometry sorting of single extracellular vesicles

A) Schematic detailing the proof-of-concept experiment setup

B) Flow cytometric plot depicting sample 1 of proof-of-concept: In red: EVs dyed both violet and PE. Violet/PE double positive EVs make up 99.92% of total EVs

C) Flow cytometric plot depicting sample 2 of proof-of-concept: In blue: EVs dyed both violet and APC. Violet/APC double positive EVs make up 94.04% of total EVs

D) Flow cytometric plot depicting sample 3 of proof-of-concept: In green: EVs dyed violet, PE, and APC. Violet/PE/APC triple positive EVs make up 96.36% of total EVs

E) Flow cytometric plot depicting sample 4 of proof-of-concept: a combination of samples 1 and 2 with EVs dyed both violet and PE in red and EVs dyed both violet and APC in blue. Violet/PE double positive EVs make up 70.36% of total particles, violet/APC double positive EVs make up 27.24% of total particles, and violet/PE/APC triple positive EVs in green make up 2.37% of total EVs

F) Post-sort analysis of sample 4 violet/PE double positive population (70.36% in panel e). In red: violet/PE double positive EVs make up 99.49% of post-sort total EV population

G) Post-sort analysis of sample 4 violet/APC double positive population (27.24% in panel e). In blue: violet/APC double positive EVs make up 95.43% of post-sort total EV population

H) Flow cytometric plot depicting human plasma EV sample. In red: CD235a single positive EVs make up 30.24% of total EVs. In blue: AMP124 single positive EVs make up 0.11% of total EVs. In green: CD235a/AMP124 double positive EVs make up 0.37% of total EVs

I) Post-sort analysis of panel h CD235a single positive population (30.24% in panel h). In red: CD235a single positive EVs make up 80.77% of post-sort total EV population

J) Post-sort analysis of panel h AMP124 single positive EV population (0.11% in panel h). In blue: AMP124 single positive EVs make up 10.42% of post-sort total EV population

K) Post-sort analysis of panel h CD235a/AMP124 double positive EV population (0.37% in panel h). In green: CD235a/AMP124 double positive EVs make up 25.85% of post-sort total EV population

EV = extracellular vesicle

These results were very promising, so EVs stained with the astrocytic antibody cocktail (AMP124) were then tested. AMP124 was in the APC channel and CD235a, a surface marker of erythrocytes, was in the PE channel. The initial analysis of this sample revealed 30% of particles were single positive for CD235a, only 0.1% were single positive for AMP124, and 0.37% were double positive for CD235a and AMP124 (**Figure 3H**). When these populations were sorted, there was 80% purity in the PE positive particles **(Figure 3I**), 10% purity in the APC positive particles (**Figure 3J**), and 25% purity in the double positive particles, with most of the particles in this sorted population being single positive for PE (**Figure 3K**). This sort was far less efficient than the proof of concept, particularly for the APC positive particles.

AD-EV Immunoprecipitation

In collaboration with Dr .Dimitrios Kapogiannis and Dr. Carlos Nogueras-Ortiz (Baltimore, USA). As EV sorting was an exceptionally long process, a standard immunoprecipitation of the AD-EV population was also used. EVs were processed as described in the antibody labeling section, however instead of fluorescent antibodies, in-house biotin-conjugated antibodies with streptavidin linkers were used on the EVs (protocol below). Following their incubation, streptavidin-affinity magnetic beads (Thermo Fisher, 65602) were incubated with the EV samples. Using a magnetic tube rack (Thermo Fisher, 12321D), EVs bound to the magnetic beads were then precipitated out for mass spectrometry and CryoEM analysis.

Antibody Biotinylation

Antibodies were conjugated to biotin using EZ-Link NHS-SS-PEG_4 kit (Thermo Fisher, 21442) following kit instructions. Briefly, a solution of 10mM biotin in DMSO was prepared. Solution was added to antibodies according to kit instructions to achieve desired molar excess (in this case 20-fold) and incubated for 30min at RT. Non-reacted NHS-SS-PEG_4-biotin and hydrolysis byproducts were removed using ultrafiltration with 3kD filters (Merck Millipore, Amicon Ultra-4, UFC800324) To cleave the disulfide bond in the spacer arm, samples were then incubated for 30min at 50ºC.

All biotinylations were verified using a HABA assay for biotin quantitation (Thermo Fisher, 28005) following kit instructions.

Cryogenic Electron Microscopy

In collaboration with group of Pr. Matteo Dal Peraro (EPFL). Cryo-EM grids were prepared with an EM GP2 Automatic Plunge Freezer (Leica Microsystems). Three different grids were screened: UltrAuFoil R1.2/1.3 Holey Gold foil on Gold 300 mesh grids (Quantifoil), Nickel-Titanium Holey Foil grids (ANTcryo™) and 300-mesh holey carbon grid (Au 1.2/1.3 Quantifoil Micro Tools). Grids were glow-discharged for 30s at 15 mA using the GloQube Plus Glow Discharge System from Quorum. 4.0 µL of sample at 1mg/mL was applied to the glow-discharged grids, back-blotted for 3 s under blot force 10 at 95% humidity and 10 °C in the sample chamber and plunge-frozen in liquid ethane, cooled by liquid nitrogen. After vitrification the grid was stored under liquid nitrogen until further use. Grids were loaded in a TFS Glacios microscope (200 kV) and screened for vesicle presence and ice quality.

Negative Staining Electron Microscopy

In collaboration with group of Pr. Matteo Dal Peraro (EPFL). For negative staining EM, 15 µL of diluted sample at 0.1 mg/mL and 0.05 mg/mL was applied on glow discharged 400 mesh copper grids on carbon film. The grids were incubated with 2% (w/v) uranyl acetate for 30 s for staining. Grids were imaged on a Talos F200S (TEM) microscope.

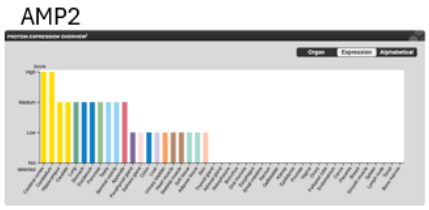

Supplementary Figure 1 | Human protein atlas protein expression by tissue for 10 astrocytic membrane proteins and L1CAM

Dark yellow bars indicate brain tissue presence

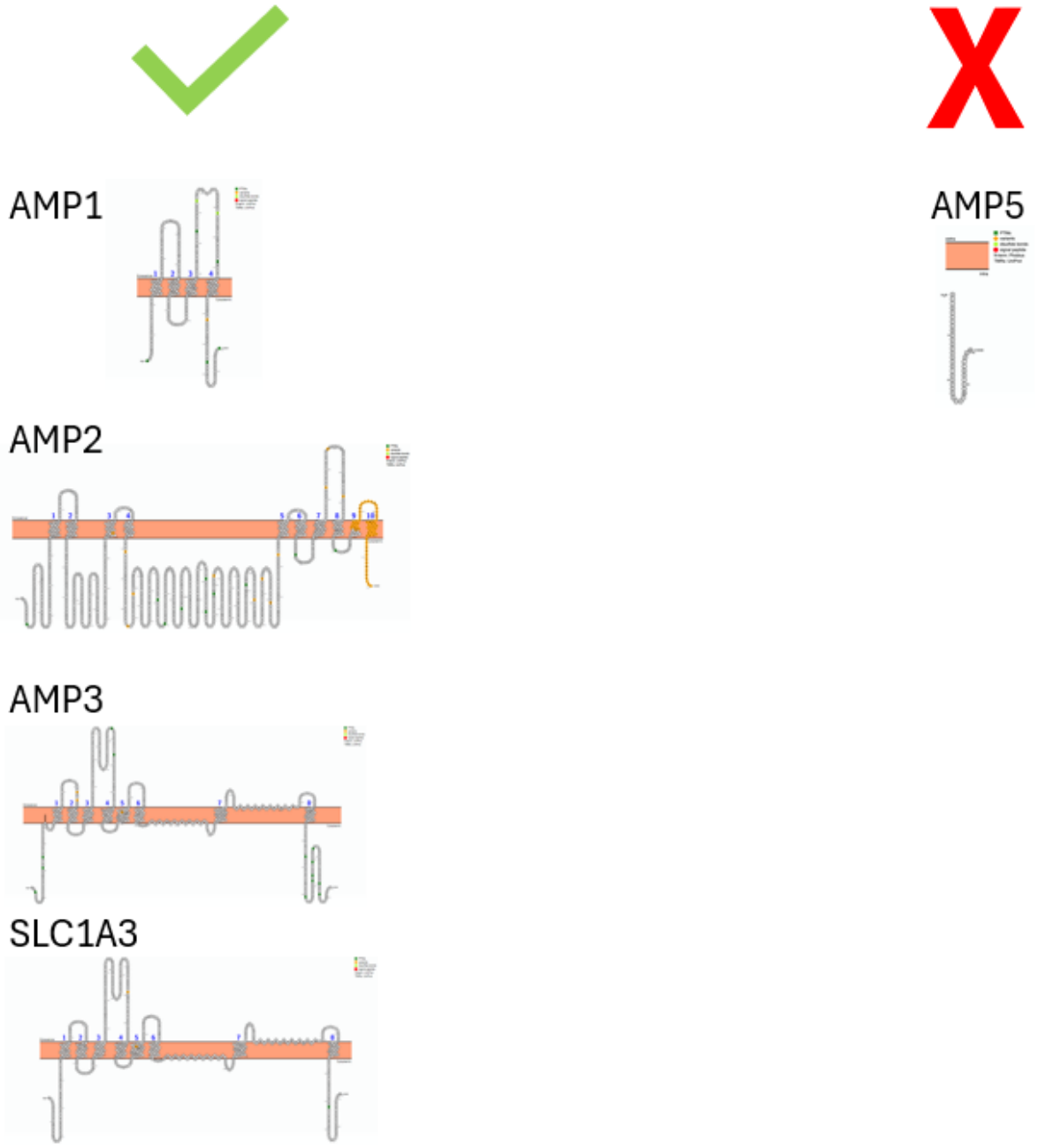

Supplementary Figure 2 | Protter representations of 5 astrocytic membrane candidates

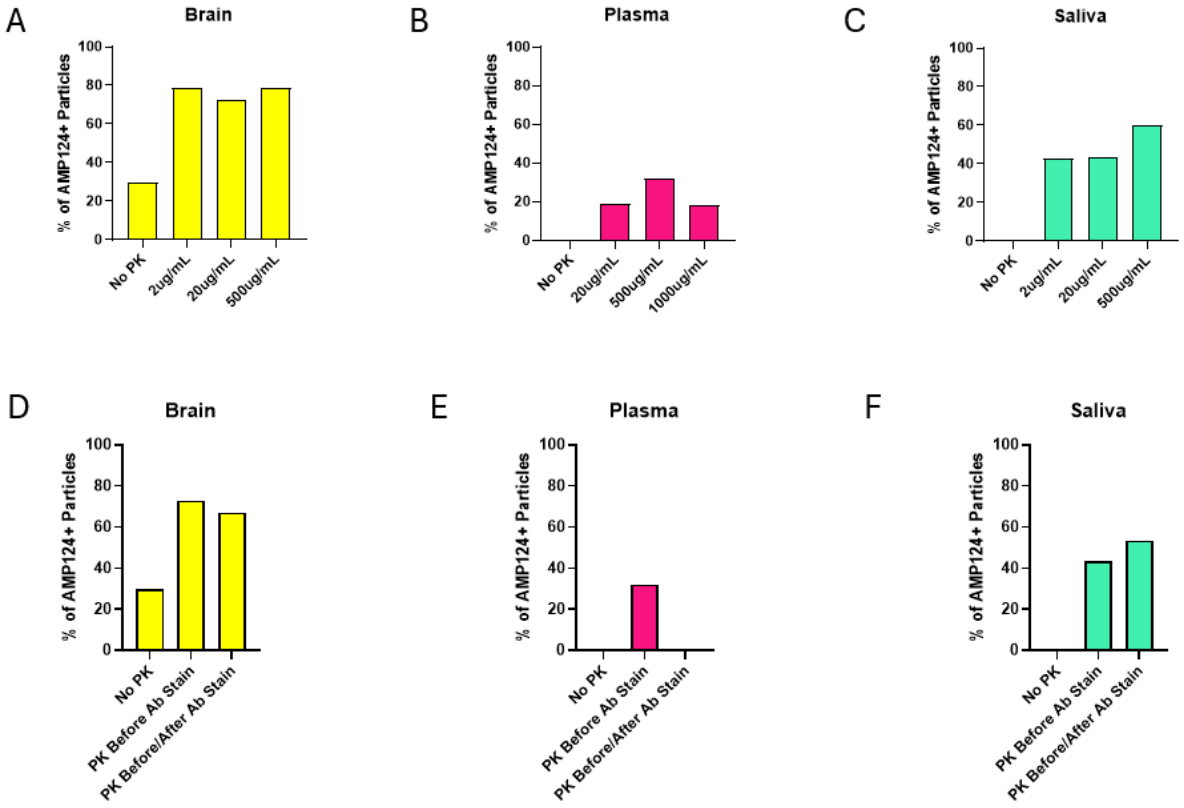

Supplementary Figure 3 | Effect of proteinase K treatments on antibody staining in ISF, plasma, and saliva EVs

A) Bar plot showing the % of AMP124+ EV particles after varying levels of PK treatment in cortex ISF EVs
B) Bar plot showing the % of AMP124+ EV particles after varying levels of PK treatment in plasma EVs
C) Bar plot showing the % of AMP124+ EV particles after varying levels of PK treatment in saliva EVs
D) Bar plot showing the % of AMP124+ EV particles with no PK, one PK treatment before antibody staining, or a PK treatment before antibody staining and a PK treatment after antibody staining in cortex ISF EVs
E) Bar plot showing the % of AMP124+ EV particles with no PK, one PK treatment before antibody staining, or a PK treatment before antibody staining and a PK treatment after antibody staining in plasm EVs
F) Bar plot showing the % of AMP124+ EV particles with no PK, one PK treatment before antibody staining, or a PK treatment before antibody staining and a PK treatment after antibody staining in saliva EVs

ISF = interstitial fluid, EV = extracellular vesicle, PK = Proteinase K

AMP1

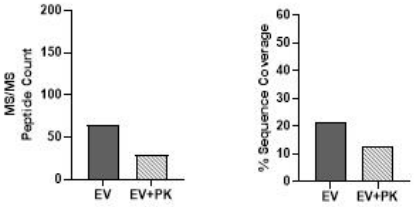

AMP2

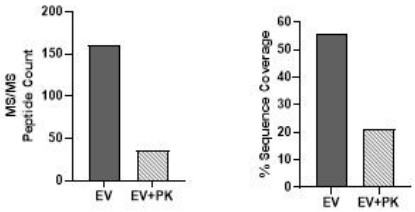

AMP3

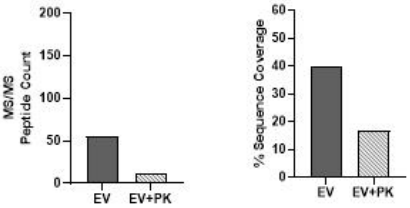

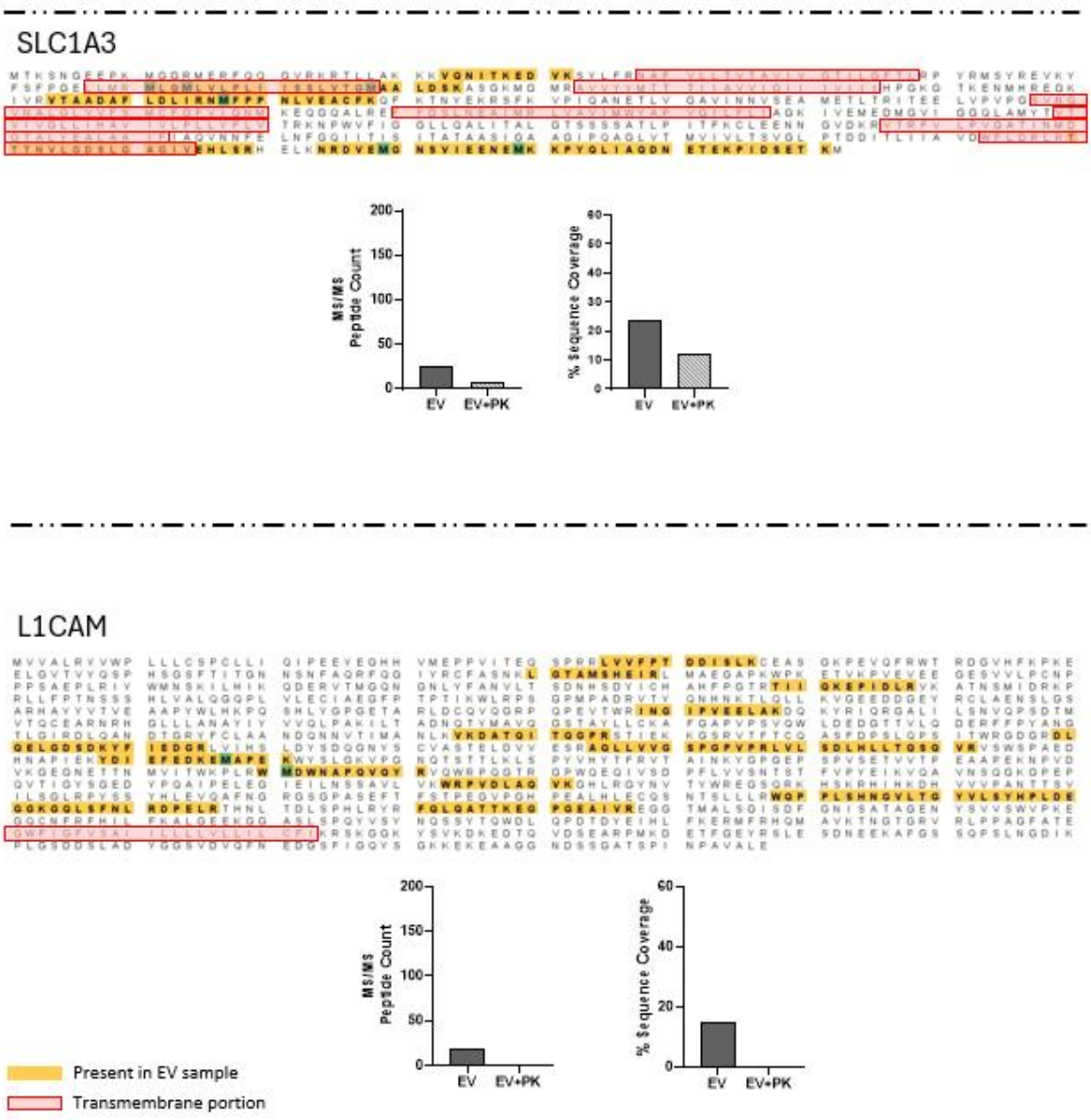

Supplemental Figure 4 | Scaffold Representations of Astrocytic Membrane Proteins and L1CAM Before PK Treatment

Supplementary Figure 4 | Scaffold representations of astrocytic membrane proteins and L1CAM before PK treatment

EV = extracellular vesicle, PK = Proteinase K

Supplementary Table 1 | All EV predicted membrane proteins ranked by abundance

Rank	Elevated in Brain	Brain Cell Specificity
1	Elevated in Brain	Astrocytic
2	Elevated in Brain	Neuronal
3		Neuronal
4	Elevated in Brain	Neuronal
5	Elevated in Brain	Astrocytic
6	Elevated in Brain	Neuronal
7	Elevated in Brain	Neuronal
8	Elevated in Brain	
9	Elevated in Brain	Neuronal
10	Elevated in Brain	
11	Elevated in Brain	Astrocytic
12	Elevated in Brain	
13	Elevated in Brain	
14		
15		Oligodendrocytic
16		
17	Elevated in Brain	Astrocytic
18	Elevated in Brain	
19		
20	Elevated in Brain	Astrocytic
21		
22	Elevated in Brain	Oligodendrocytic
23	Elevated in Brain	Astrocytic
24	Elevated in Brain	
25	Elevated in Brain	Oligodendrocytic
26	Elevated in Brain	
27		Oligodendrocytic
28	Elevated in Brain	
29	Elevated in Brain	Astrocytic
30		Endothelial
31		
32	Elevated in Brain	Neuronal
33		
34	Elevated in Brain	Neuronal
35	Elevated in Brain	
36		Endothelial
37	Elevated in Brain	Astrocytic
38	Elevated in Brain	
39		

40	Elevated in Brain	
41		Neuronal
42	Elevated in Brain	
43		Endothelial
44	Elevated in Brain	Neuronal
45		Astrocytic
46	Elevated in Brain	Astrocytic
47		
48	Elevated in Brain	
49	Elevated in Brain	Astrocytic
50		Astrocytic
51	Elevated in Brain	
52		Endothelial
53	Elevated in Brain	
54		
55		
56		Astrocytic
57	Elevated in Brain	Neuronal
58		Endothelial
59		Endothelial
60		
61		
62		
63		
64		Neuronal
65	Elevated in Brain	Neuronal
66	Elevated in Brain	Neuronal
67	Elevated in Brain	Astrocytic
68	Elevated in Brain	Astrocytic
69		Oligodendrocytic
70		Astrocytic
71	Elevated in Brain	Neuronal
72		
73	Elevated in Brain	Neuronal
74		
75		
76		
77	Elevated in Brain	Astrocytic
78	Elevated in Brain	
79	Elevated in Brain	Neuronal
80	Elevated in Brain	Neuronal
81		Astrocytic
82		

83	Elevated in Brain	
84		Oligodendrocytic
85		Astrocytic
86	Elevated in Brain	
87		
88	Elevated in Brain	Astrocytic
89	Elevated in Brain	Astrocytic
90		Endothelial
91	Elevated in Brain	
92		
93		Neuronal
94		Endothelial
95		
96		
97		
98		
99		
100	Elevated in Brain	
101		Oligodendrocytic
102		
103	Elevated in Brain	
104		
105	Elevated in Brain	Neuronal
106		
107	Elevated in Brain	Neuronal
108	Elevated in Brain	Oligodendrocytic
109		
110	Elevated in Brain	Neuronal
111	Elevated in Brain	Oligodendrocytic
112		Neuronal
113		Astrocytic
114		
115		
116	Elevated in Brain	Neuronal
117		Neuronal
118		
119		
120		Endothelial
121	Elevated in Brain	Oligodendrocytic
122		Microglial
123	Elevated in Brain	
124		
125	Elevated in Brain	

126	Elevated in Brain	Astrocytic
127		
128		
129		
130	Elevated in Brain	
131		
132		
133		Endothelial
134	Elevated in Brain	Astrocytic
135		Microglial
136	Elevated in Brain	Astrocytic
137		Astrocytic
138	Elevated in Brain	Astrocytic
139	Elevated in Brain	
140		
141		Astrocytic
142		
143		
144		Oligodendrocytic
145		
146		Oligodendrocytic
147		Oligodendrocytic
148	Elevated in Brain	
149		Oligodendrocytic
150		
151		
152	Elevated in Brain	Neuronal
153		Endothelial
154		
155		Oligodendrocytic
156		Astrocytic
157		Microglial
158	Elevated in Brain	
159		Astrocytic
160		
161		
162	Elevated in Brain	
163		
164		
165		
166		
167		
168		

169		
170	Elevated in Brain	
171		Astrocytic
172		
173		Astrocytic
174	Elevated in Brain	
175	Elevated in Brain	Neuronal
176		Oligodendrocytic
177	Elevated in Brain	Neuronal
178	Elevated in Brain	
179	Elevated in Brain	Neuronal
180		
181		Astrocytic
182		
183		
184	Elevated in Brain	Neuronal
185	Elevated in Brain	Astrocytic
186	Elevated in Brain	Oligodendrocytic
187	Elevated in Brain	Neuronal
188		
189		
190	Elevated in Brain	
191		
192		
193		
194		Microglial
195		Astrocytic
196		
197	Elevated in Brain	Neuronal
198		
199		Astrocytic
200	Elevated in Brain	Neuronal
201	Elevated in Brain	
202		Neuronal
203		Astrocytic
204		Microglial
205		
206		Oligodendrocytic
207	Elevated in Brain	
208		Astrocytic
209		
210		
211		Endothelial

212	Elevated in Brain	Neuronal
213		
214		Endothelial
215		Microglial
216	Elevated in Brain	Astrocytic
217		
218		
219		Astrocytic
220	Elevated in Brain	Astrocytic
221		
222	Elevated in Brain	Neuronal
223	Elevated in Brain	Astrocytic
224		Microglial
225	Elevated in Brain	Oligodendrocytic
226		
227		
228		
229	Elevated in Brain	Astrocytic
230		
231		
232		
233		
234		Microglial
235	Elevated in Brain	
236		Microglial
237		
238		
239		
240	Elevated in Brain	
241	Elevated in Brain	Neuronal
242	Elevated in Brain	Astrocytic
243	Elevated in Brain	Microglial
244		Endothelial
245	Elevated in Brain	Astrocytic
246		Astrocytic
247		Microglial
248	Elevated in Brain	Neuronal
249		
250		
251	Elevated in Brain	
252		Endothelial
253		Oligodendrocytic
254		

255		Microglial
256		Endothelial
257	Elevated in Brain	
258	Elevated in Brain	Neuronal
259	Elevated in Brain	Neuronal
260		Astrocytic
261		Astrocytic
262	Elevated in Brain	
263	Elevated in Brain	Neuronal
264		
265	Elevated in Brain	Neuronal
266		
267		
268		
269		Astrocytic
270	Elevated in Brain	Neuronal
271		
272	Elevated in Brain	Neuronal
273		
274		
275	Elevated in Brain	
276		
277		
278		Oligodendrocytic
279		Endothelial
280		
281		
282		Astrocytic
283		Neuronal
284		
285		
286		
287		
288		
289		
290		Endothelial
291		Endothelial
292		Endothelial
293		
294	Elevated in Brain	
295		Astrocytic
296		
297	Elevated in Brain	

298		
299		
300		
301	Elevated in Brain	Neuronal
302		
303		
304		
305	Elevated in Brain	Neuronal
306	Elevated in Brain	Neuronal
307		Endothelial
308		Microglial
309		
310		Oligodendrocytic
311		
312		Microglial
313		
314		Oligodendrocytic
315		Microglial
316		
317		Microglial
318		
319		
320		
321		Microglial
322	Elevated in Brain	
323		
324		
325		Oligodendrocytic
326		
327		
328		
329		
330		
331	Elevated in Brain	Oligodendrocytic
332		Microglial
333		
334		
335		
336		
337		Microglial
338		Microglial
339		Microglial
340	Elevated in Brain	Astrocytic

341		
342		
343		Astrocytic
344		Astrocytic
345		
346		
347		Endothelial
348		
349		Endothelial
350		
351		
352		Endothelial
353		
354		Oligodendrocytic
355		
356		
357		Astrocytic
358		Endothelial
359		Microglial
360		Astrocytic
361		
362		
363		
364		
365		
366	Elevated in Brain	Astrocytic
367	Elevated in Brain	Oligodendrocytic
368		Astrocytic
369		Microglial
370	Elevated in Brain	Astrocytic
371		
372	Elevated in Brain	Astrocytic
373		
374		
375		Astrocytic
376		
377	Elevated in Brain	Oligodendrocytic
378		
379		Astrocytic
380		

General Discussion

The work described in this thesis has the broad aim of improving patient diagnosis and stratification in the context of tauopathies. This aim was split into two smaller projects: the first sought to identify unique proteomic signatures in patient brain derived extracellular vesicles (BD-EVs) which could differentiate between 3R and 4R tauopathies, and the second sought to improve upon the existing strategies of BD-EV isolation in peripheral biofluids using an innovative methodology and novel surface markers of BD-EVs.

The study of EVs in neuroscience is relatively recent compared to the study of EVs in other fields such as oncology and immunology. For this reason, the knowledge surrounding BD-EVs is less advanced than that of EVs in the rest of the body. Investigation of BD-EVs must begin in the brain, however the brain is not an easy organ to sample, thus limiting the scope of studies in this field. The first chapter of this work highlights the importance of exploratory studies which seek to understand the proteomic makeup of BD-EVs within the brain and how that material changes in the presence of pathology. Indeed, we have shown that BD-EVs can reflect the cellular and molecular changes which transpire in the tauopathy brain, and that they can even reflect differences between different tauopathies. The implications of this work are monumental in the effort to distinguish primary tauopathies, which do not exhibit amyloid beta pathology and thus are not suited for existing fluid biomarker measurement.

The natural follow-up question to the findings described in Chapter 1 is how can we isolate these EVs outside of the brain? It is not ethical or practical to take a brain biopsy of every patient who comes to a memory center with a cognitive complaint, so for this research to be clinically relevant, it must be feasible to isolate BD-EVs from peripheral biofluids. This is something many groups have been doing for years, however we have proposed a novel methodology to significantly increase the yield and purity of BD-EVs isolated in blood and saliva. By examining the proteins present at the surface of BD-EVs in the brain, we identified three novel surface markers of astrocyte derived EVs which are also found on circulating EVs in plasma and saliva. Additionally, by digesting the protein corona of EVs before immunocapture, we increased the efficiency of capture from less than 1% to 30-60% of EVs in the periphery.

There are still many unanswered questions in this topic which necessitate further research. We still don't know the exact mechanisms by which EVs cross barriers such as the blood-brain barrier, to what extent they are modified in this process, and therefore how similar peripheral BD-EVs are to BD-EVs from the brain. Finding

answers to these questions would help researchers to fully exploit the potential of BD-EVs, while being more knowledgeable on their limitations as a diagnostic tool.

Perspectives

The study of pathology in the brain has long been a challenge due to its intricate complexity and the ethical and technical difficulties of accessing live brain tissue. BD-EVs present an innovative and non-invasive window into this complexity, potentially revolutionizing our understanding of brain diseases. However, the broader implications of this approach warrant careful consideration.

Bridging the Macro and Micro

BD-EVs offer a unique vantage point by providing molecular and biochemical snapshots of the brain's physiological or pathological state. This approach embodies the reductionist paradigm, attempting to decode the vast complexity of the brain through its constituent parts. By analyzing the cargo of EVs—proteins, lipids, DNA, RNA, etc.—researchers aim to reconstruct the pathological processes occurring within the brain. But can we truly grasp the essence of complex brain disorders by studying these minute particles?

Reductionism has been a powerful tool in science, but the brain's emergent properties, arising from the interaction of billions of neurons and glial cells, may elude such granular analysis. The risk is in oversimplifying the brain's systemic nature, potentially missing the forest for the trees. However, the complementary use of BD-EVs alongside other approaches could provide a more holistic understanding, integrating micro-level data with macro-level phenomena.

Ethical and Epistemological Dimensions

Ethically, using EVs derived from biofluids like blood or cerebrospinal fluid offers a less invasive alternative to traditional brain biopsies, aligning with the principle of minimizing harm. This aligns with the utilitarian perspective of maximizing benefits while reducing suffering, particularly in vulnerable populations such as elderly patients with neurodegenerative diseases.

Epistemologically, brain derived EVs challenge our understanding of brain communication and pathology. Traditionally, brain studies relied on direct tissue examination or imaging. EVs represent a paradigm shift, suggesting that peripheral biofluids can reflect central processes. This raises questions about the fidelity and

specificity of EV-derived data: How accurately do these vesicles represent the dynamic and multifaceted environment of the brain?

Moreover, the interpretation of EV data involves complex bioinformatics and requires robust validation against established biomarkers and clinical outcomes. The philosophical underpinning here involves a balance between empirical rigor and openness to novel methodologies, encouraging a cautious yet innovative scientific attitude.

The Broader Implications

On a broader scale, the study of brain derived EVs touches on philosophical debates about the nature of disease and health. It suggests a more fluid and dynamic model of pathology, where diseases are not merely static entities, but processes reflected in the continuous exchange of molecular information. This perspective could pave the way for more personalized and dynamic therapeutic approaches, adapting to the evolving state of the disease.

Furthermore, this approach exemplifies the interconnectedness of bodily systems, reinforcing a holistic view of health where the brain and body are in constant dialogue. Such a paradigm shift could influence not only neuroscience but also the broader field of medicine, encouraging interdisciplinary research and integrated healthcare models.

Conclusion

The use of brain-derived extracellular vesicles to study brain pathology offers a promising yet philosophically complex approach. It challenges traditional reductionist and direct observation paradigms, advocating for a more nuanced understanding of brain diseases. Ethically favorable and epistemologically innovative, this method holds the potential to transform the current approach to brain health, fostering a more integrated and dynamic view of pathology. As with any scientific advancement, it requires a balanced and critical perspective, ensuring that the promise of EVs is realized without overlooking the intricacies of the brain's vast complexity.

Annex 1

Live-imaging of Mitochondrial System in Cultured Astrocytes

Jeanne Espourteille[1], **Valentin Zufferey**[1], **Jean-Honoré Laurent**[1], **Kevin Richetin**[1]

[1] Department of Psychiatry, Center for Psychiatric Neurosciences, Lausanne University Hospital (CHUV) and University of Lausanne

Corresponding Author

Kevin Richetin kevin.Richetin@chuv.ch

Citation

Espourteille, J., Zufferey, V., Laurent, J.H., Richetin, K. Live-imaging of Mitochondrial System in Cultured Astrocytes. *J. Vis. Exp.* (177), e62957, doi:10.3791/62957 (2021).

Date Published

November 16, 2021

DOI

10.3791/62957

URL

jove.com/video/62957

Abstract

While much attention has been given to mitochondrial alterations at the neuronal level, recent evidence demonstrates that mitochondrial dynamics and function in astrocytes are implicated in cognition. This article describes the method for time-lapse imaging of astrocyte cultures equipped with a mitochondrial biosensor: MitoTimer. MitoTimer is a powerful and unique tool to assess mitochondrial dynamics, mobility, morphology, biogenesis, and redox state. Here, the different procedures for culture, image acquisitions, and subsequent mitochondrial analysis are presented.

Introduction

Astrocytes are critical players in the maintenance of brain homeostasis. They are perhaps most well known to have significant structural roles in the brain, as part of the blood-brain barrier[1] and by supporting neurons and synapses throughout the brain[2]. Astrocyte support of neurons is both structural[3] and metabolic[4,5], with astrocytes promoting neurogenesis and synaptogenesis while also providing key metabolites like lactate to active neurons[4,6,7]. Beyond the role of structural support, astrocytes are active cells that take part in Ca^{2+} signaling and buffering (including spontaneous mitochondrial Ca^{2+} influxes)[8,9], K^+ buffering[10], and can adapt and react to the needs of the brain in times of injury[11,12]. Being such dynamic cells, astrocytes have robust energy requirements, which necessitate an efficient mitochondrial network. These mitochondria also have a crucial role in buffering excessive reactive oxygen species (ROS)[13]. In addition to their individual or local roles of energy generation and ROS buffering, mitochondria function as a network[14]. In this sense, they maintain equilibrium between fissioning and fusioning mitochondria, representing new/reduced mitochondria and older/oxidized mitochondria, respectively[15]. The overall redox state of a cell can be gauged by the redox state of the mitochondrial network. In pathology, this is a critical piece of information that can shed light on which cells may not be functioning optimally.

In recent years, many sensors have been developed to study the dynamics and functions of mitochondria in cells. For example, sensors measuring energy exchange (ATP), redox state ($NADH/NAD^+$, ROS), and enzymatic functionality (cAMP, Ca^{2+}, Zn^{2+}) are currently used in the study of mitochondrial function[16]. Among them, MitoTimer permits to follow the changes in mitochondrial morphology (size, shape, surface area), mobility (speed, displacement), and dynamics (fusioning and fissioning events), as well as the overall mitochondrial turnover rate and redox state. MitoTimer is a mutant red fluorescent protein, drFP583[17], with a mitochondrial signal from subunit VIII of human cytochrome c oxidase[18,19] to visualize newly synthesized mitochondria in green (488 nm) and oxidized mitochondria in red (555 nm). Using the green (488 nm) and red (555 nm) fluorescence ratio permits simultaneous evaluation of individual mitochondria, their morphology analysis, fusion/ fission events, and redox state history[20,21]. This unique property can be used to investigate many scientific questions regarding mitochondria's physiological and pathological roles and is therefore very promising for unveiling the underlying mechanisms of mitochondrial dynamics within many different cell types.

We recently developed a new lentiviral vector (LV-G1MitoTimer-MiR124T, hereafter called LV-G1-MitoTimer) to study mitochondria's dynamic and functions specifically in astrocytes *in vitro* and *in vivo*[22]. LV-G1-MitoTimer uses a truncated version of the glial fibrillary acidic protein (GFAP) promoter gfaABC1D, with a B3 enhancer (gfaABC1D(B3), hereafter called G1) combined with the previously described miR124T neuronal detargeting system[23]. It allows exclusive expression of the mitochondrial biosensor in astrocytes *in vitro* and *in vivo*[22]. Presented here are the different steps to perform a culture of rat hippocampal astrocytes and equip them with the LV-G1-MitoTimer biosensor, as well as the different microscopy steps to follow the behavior of astrocyte mitochondria during several consecutive hours/days.

Protocol

The present protocol has been performed with the approval of an ethical committee (agreement VD3602, Lausanne, Switzerland) and follows European guidelines for the use of animals.

1. Rat hippocampal astrocyte primary culture

1. Sacrifice five rat pups (Wistar IGS Rat) by decapitation at postnatal day 1-2.
2. Remove the brain and keep it in a Petri dish containing 5 mL of fresh astrocyte medium (DMEM with GlutaMAX supplemented with 1% Penicillin/Streptomycin and 10% fresh Horse Serum).
3. Isolate the hippocampus. Dissociate in 5 mL of the astrocytic medium by three passages through a 21 G needle and three passages through a 25 G needle.
4. Transfer the dissociated cells to a 15 mL centrifuge tube and count in a hemocytometer.

5. Plate 20,000-25,000 cells/cm^2 in multiwell dishes (9.4 mm x 10.7 mm x 9.3 mm) and store them at 37 °C under an atmosphere containing 5% CO2 for the rest of the experiment.

6. Replace the medium entirely at 3 days *in vitro* (DIV3).

7. At DIV8, add 0.6 pg of p24 antigen per cell of lentiviral vector coding for mitochondrial biosensor MitoTimer (LV-G1-MitoTimer[22]) diluted in phosphate-buffered saline (PBS + 0.01% BSA).

8. At DIV9, wash with pre-warmed 1x sterile PBS (37 °C) and add fresh astrocyte medium.

9. At DIV11, perform 2 washes with pre-warmed 1x sterile PBS (37 °C) and add fresh astrocyte medium without phenol red.

   NOTE: Choice of the coating depends on the intended assay. As a standard coating for astrocyte primary culture, it is recommended to use 0.2 mg/mL poly-D lysine or 8.7 µg/cm^2 of basement membrane matrix (e.g., Matrigel). To visualize the mitochondrial system of astrocytes, it is essential to work on flattened and stretched cells. In this context, the combination of basement membrane matrix on IBIDI u-slides is the most suitable. It is also crucial not to work with phenol red, which is toxic for the cell under repeated exposure to light.

2. Long-term monitoring of the mitochondrial system.

1. Assess the astrocytic mitochondrial system a minimum of 3-5 days after the lentiviral infections with LV-G1MitoTimer (to allow a sufficient level of fluorescence in the mitochondria).

2. Image the cells with an inverted microscope controlled by the acquisition and analysis software and a module for full automation of acquisition.

   NOTE: Refer to the **Table of Materials** for the details of the software and module used in this study.

3. Ensure that the microscope is equipped with a cage incubator (see **Table of Materials**) to maintain astrocyte culture at 5% CO2 and 37 °C throughout the experiment.

4. Capture fluorescence images using sequential excitation at 490 nm (for green channel) and 550 nm (for red channel) with detection of green (500-540 nm for green channel) and red (550-600 nm for red channel) fluorescence signals.

5. Select 5 astrocytes per well with a mitochondrial network expressing sufficient levels of LV-G1-MitoTimer using a magnification of 40x. Take care to select astrocytes as flat and large as possible and not located in clusters of cells (to work on individual cells).

6. Save the coordinates of the 5 selected cells in an xlm file (map.xlm). This map.xlm allows the user to return to the same cells over time.

7. Acquire image sequences (1 image/s for 60 s) using a magnification of 150x (100x oil immersion objective, 1.5x intermediate magnification) for each coordinates.

8. Repeat image acquisition (1 image/s for 60 s) for the same astrocytes 6 h, 12 h, and 24 h after treatments. NOTE: Use a microscope equipped with a fast and efficient autofocus system. In this context, the hardware solution called Perfect Focus System (PFS) was used. PFS uses near-infrared 870-nm LED and CCD line sensors to combat axial focus fluctuations in real-time during long-term imaging investigations.

3. Analysis of individual mitochondrial morphology and LV-G1-MitoTimer ratio

NOTE: NIS General Analysis 3 (GA3) from Nikon was used to automatize morphometric analysis in this study.

1. For each image sequence (baseline, 6 h, 12 h, 24 h), select the first frame for red and green channels by clicking on **ND Processing > Select Frame**.
2. Merge the red and the green channels by selecting **Conversions > Merge Channel**.
3. To correct image shading, select **Preprocessing > Auto Shading Correction**.
4. Apply the Rolling Ball algorithm by selecting **Preprocessing > Rolling Ball**.
5. To generate binary masks for each mitochondrion, select **Segmentation > Threshold**.
6. Remove any objects truncated by the border by selecting **Binary processing > Touching Border**.
7. To measure the surface area, select **Measurement > Object Area**.
8. To measure the diameter, select **Measurement > Eq Diameter**.
9. To measure the length, select **Measurement > Length**.
10. To measure the width, select **Measurement > Width**.
11. To measure roughness, select **Measurement > Roughness**.
12. To measure circularity, select **Measurement > Circularity**.
13. To measure elongation, select **Measurement > Elongation**.
14. Compose a group (right-click) with the above measurement and rename it as MorphoData.
15. Measure mean green intensity by selecting **Measurement > Mean Intensity**.
16. Measure mean red intensity by selecting **Measurement > Mean Intensity**.
17. To measure the Red/Green ratio, select **Measurement > Ratio**.
18. Compose a group (right-click) with the above measurement and rename it as RatioData.
19. Export the table to a CSV file by selecting **Reference > Table to CSV**.
20. Save the GA3 script of analysis by selecting **Save As**

    NOTE: A non-exhaustive list of the criteria used in this procedure is summarized in **Figure 1**, **Table 1**, and **Table 2**. The analysis GA3 script file is available in supplemental (**Supplemental Coding File 1** and **Figure 2**). The thresholds used were adapted to individualize as many mitochondria as possible

    (excluding large mitochondrial networks where possible). Wherever possible, mitochondrial networks are either individualized manually or excluded from the analyses. Due to intercellular variability, perform these analyses on at least 20-25 cells per condition (with a minimum of 50 mitochondria by cell).

4. Analysis of mitochondrial motility

NOTE: Due to the high complexity of mitochondrial movements, manual motility analysis is preferred. Here, Nikon's NIS Element system was used to manually track mitochondria.

1. Open the tracking module in NIS, select **View > Analysis > Tracking**.

2. Click on **Define New ROI**.

3. With the **Automatic Detection Tool**, select 25-50 mitochondria on the first image of the image sequence.

4. Click on **Track Autodetected ROIs Analyze**.

5. If necessary, delete the incorrect ROI tracks.

6. Export the table to a CSV file.

   NOTE: A non-exhaustive list of the criteria used in this procedure is summarized in **Figure 1** and **Table 3**. A tracking analysis generally gives a path depicting the movements of the center of every tracked object. The different tracking options must be set in the tracking option. Favor the selection of isolated mitochondria that are sufficiently distant from each other to facilitate tracking. Keep only the objects that could consistently be tracked over the whole sequence. Proceed the same way to remove outliers due to bad quality tracking. Consequently, the set of objects analyzed in this section is different from the one analyzed for static morphological analyses and will generally be smaller.

5. Data transformation, normalization, and statistical analysis

NOTE: Mainly due to the high heterogeneity of the mitochondria, data generated often have a non-normal distribution.

1. Manually log-transform the measurements prior to processing.

2. For each analysis and time frame, manually normalize the resulting data by the mean of those obtained in the reference acquisition.

3. In addition, consider a second/double normalization to a control condition, for example, to evaluate the effect of a treatment.

4. Then, perform statistical analysis using a two-way matched ANOVA. Here GraphPad Prism V8 was used.

Representative Results

Primary culture of astrocytes infected with LV-G1MitoTimer exhibited typical mitochondrial networks. Before treatment, astrocytes expressing LV-G1-MitoTimer showed the heterogeneous mitochondrial size and various green/red fluorescence intensities (**Figure 3**, **Figure 4**, and **Video 1**).
The mitochondrial system of astrocyte cultures expressing LV-G1-MitoTimer was monitored before and after incubation with H202 (10 µM). The different mitochondrial features described above were calculated over 12 h (every 3 h) and normalized (cell by cell) to their initial state. At the morphological level (**Figure 3B**), the effects of H2O2 start to be visible at about 6 h. Indeed, the mitochondria were fragmented (decrease of length, surface area, and elongation factor). This fragmentation is even more obvious 12 h after the treatment. Note that the diameters, widths, and sphericity were not reduced. Concerning redox state and turnover (**Figure 3C**), 3 h after H2O2 treatment, the proportion of green mitochondria increased in astrocytes (the consequence of a rapid increase in mitochondrial biogenesis). At 6 h, the green/ red ratio returned to baseline levels, but the number of purely red mitochondria increased significantly from basal levels.
After 12 h, the consequences of the oxidative treatment of H2O2 were visible and resulted in a substantial increase in the ratio and number of red puncta. Concerning the dynamics and mobility (**Figure 3D**), 3 h after the treatment, all the criteria were transiently increased. In the longer term (12 h), the mitochondria moved more slowly and over shorter distances.

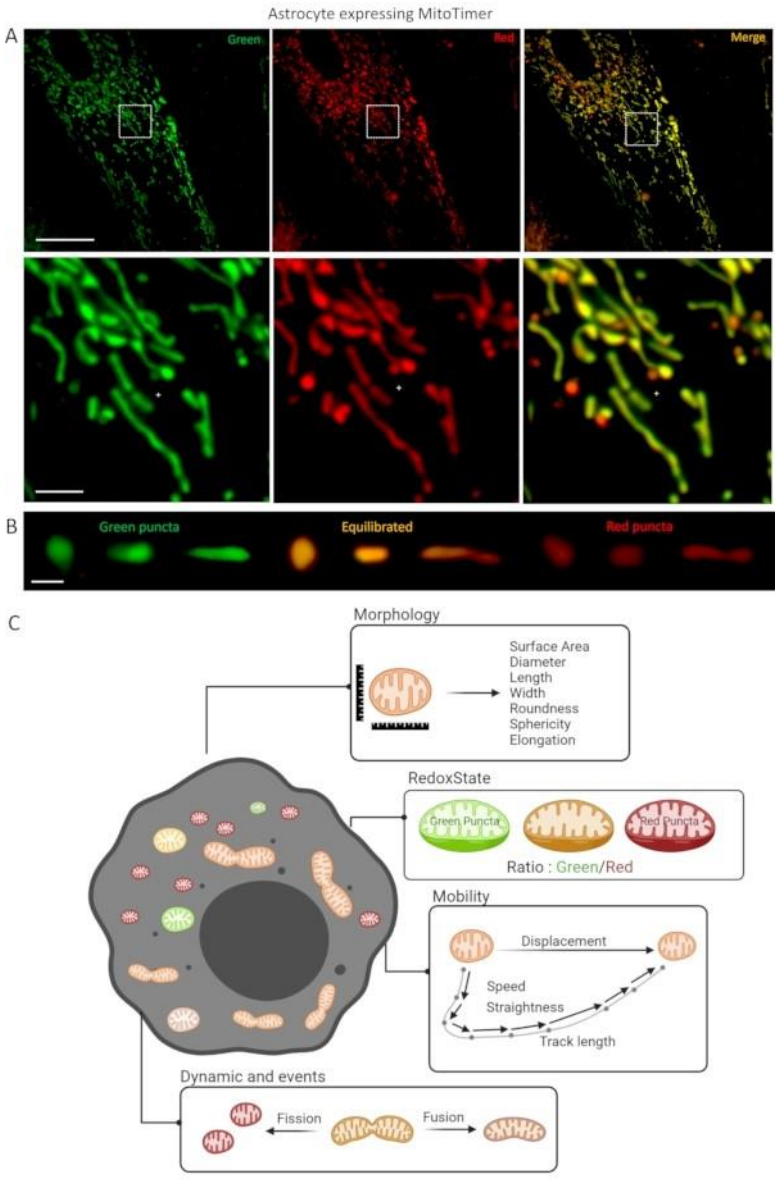

Figure 1: Astrocyte culture expressing LV-G1-MitoTimer biosensor. (**A**) Confocal photographs of astrocytes expressing LV-G1-MitoTimer. (**B**) Selection of confocal photographs of reduced (green) balanced (orange) and oxidized (red) mitochondria with different levels of fragmentation. (**C**) Summary diagram of the different criteria available for analysis in an astrocyte expressing LV-G1-MitoTimer. Scale bar: (**A**) Upper panel: 50 µm, lower panel: 10 µm, (**B**) 1 µm. Please click here to view a larger version of this figure.

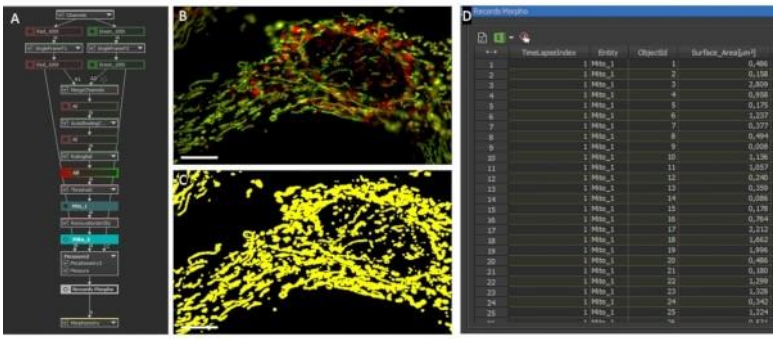

Figure 2: Mitochondrial morphology and ratio analysis. (**A**) GA3 script overview for the analysis of individual mitochondrial morphology and ratio. (**B**) Initial photographs of an astrocyte expressing LV-G1-MitoTimer analyzed with the GA3 script. (**C**) Example of binary masks generated for the mitochondrial system of astrocytes. Scale bar: 10 µm (B-C).

Please click here to view a larger version of this figure.

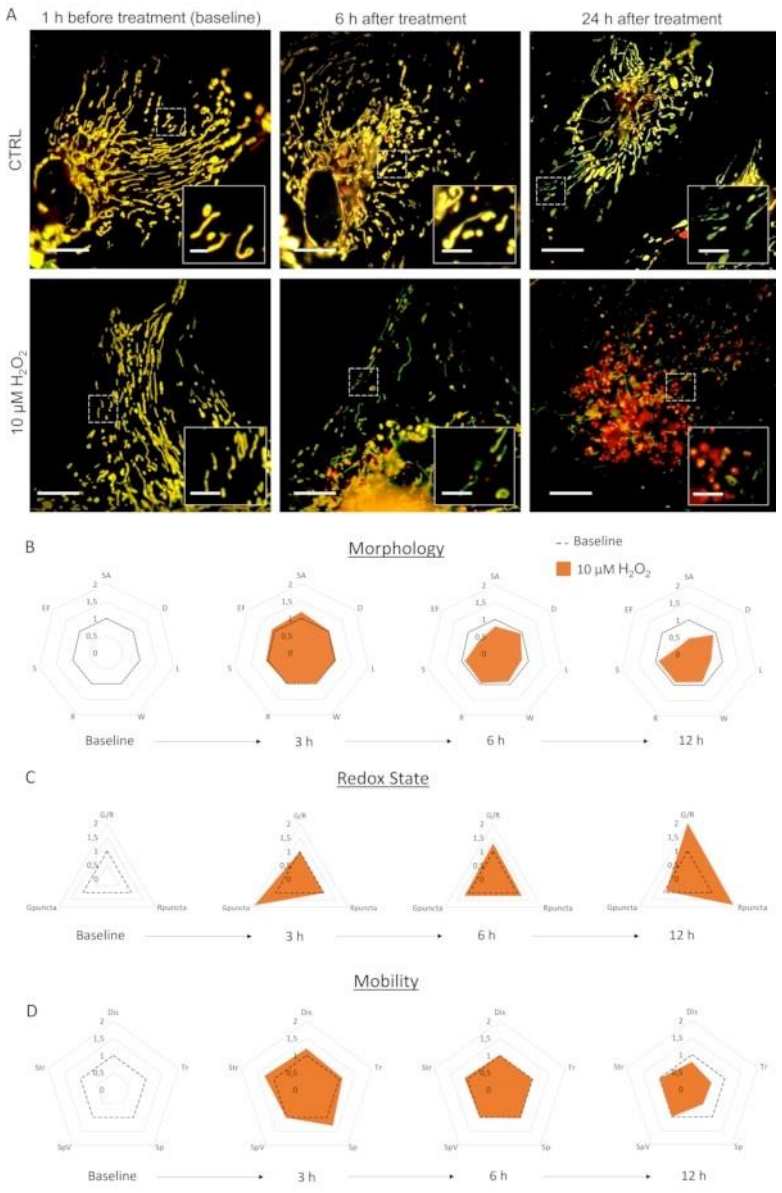

Figure 3: The effects of H2O2 on the mitochondrial system of astrocytes. (**A**) Photographs of astrocytes expressing LV-G1-MitoTimer 1 h before and 6 h, 24 h after treatment with PBS (CTRL) and 10 µM of H2O2. (**B**) Radar charts of mitochondrial morphology, (**C**) redox state and turnover, and (**D**) mobility criteria evaluated on astrocytes during baseline and 3 h, 6 h, and 12 h after H2O2 treatment. SA: Surface area; D: Diameter; L: Length; W: Width; R: Roundness; S: Sphericity; EF: Elongation factor (=L/W); G/R: Individual red/green ratio; Gpuncta: Percentage of green puncta mitochondria; Rpuncta: Percentage of red puncta mitochondria; Dis: Displacement; Tr: Track Length; Sp and SpV: Speed and speed variance; Str: Straightness. Scale bar: 20 µm (A) and 2.5 µm (inset). Please click here to view a larger version of this figure.

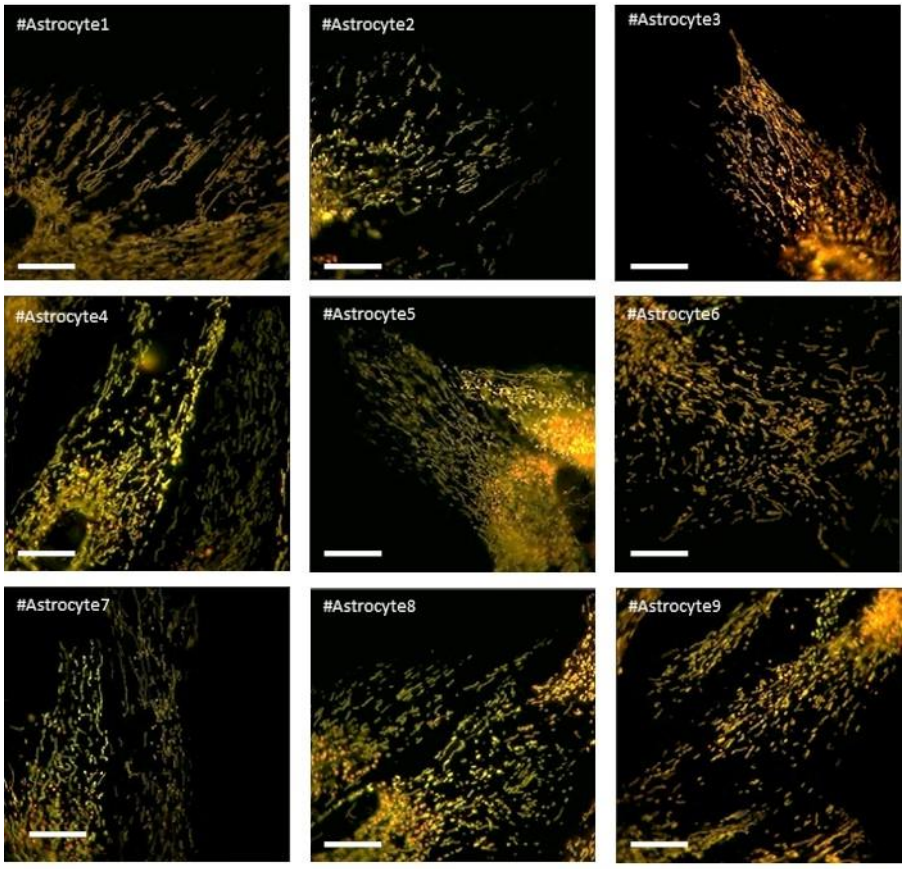

Figure 4: Photographs of astrocytes expressing LV-G1-MitoTimer and showing a homogeneous and balanced mitochondrial network during baseline. Scale bar: 20 µm Please click here to view a larger version of this figure.

Video 1: Effect of H2O2 treatment on the mitochondrial after H2O2 treatment compared to non-treated control cell.

system of cultured astrocytes. Astrocytic mitochondria Please click here to download this File.

before H2O2 treatment (baseline), as well as 6 h and 24 h

Morphology criteria	Range	Remarks
Surface Area (SA)	0.5–4 µm^2	These criteria inform on the fragmented-elongated features of mitochondria. They generally evolve in the same direction. Fragmented mitochondria will have decreased surface area, diameter, length, and elongation factor while roundness, sphericity, and width may be unchanged or increased.
Diameter (D)	0.5–1.5 µm	
Length (L)	0.5–5 µm	
Width (W)	0.5–2 µm	

Roundness (R)	0–1
Sphericity (S)	0–1

Elongation factor (EF = L/W)	1–10	

Table 1: Summary of selected parameters for mitochondrial morphology.

Redox State criteria	Range	Remarks
Individual ratio (G/R)	0–10	The ratio indicates the result of the redox state. It informs about the general state and age of the mitochondria in the cell. It is essential to consider that this ratio is the balance of biogenesis and degradation of mitochondria and the fission/fusion of oxidized mitochondria with reduced mitochondria. Therefore the evaluation of the number of green and red puncta can powerfully help interpret the results. Green puncta mitochondria are determined when the intensity of green is 10 times that of red. Red puncta mitochondria are determined when the intensity of red is 10 times greater than that of green. The redox state of an astrocyte is the average of all the mitochondria ratios of that cell.
Percentage of green puncta mitochondria (G^{puncta})	0%–100%	
Percentage of red puncta mitochondria (R^{puncta})	0%–100%	

Table 2: Summary of selected parameters for mitochondrial redox state.

Mobility criteria	Range	Remarks
Displacement (Dis)	0–10 µm	Together these features inform the general motility dynamics of the network. Stationary mitochondria display short displacement & track length with a low speed. On the other hand, oscillatory particles can be differentiated with a difference between the track length and displacement (resulting in low straightness) and an increased speed compared to static.
Track Length (Tr)	0–10 µm	
Speed and speed variance (Sp and SpV)	0–1.5 µm/s ± 0.2 µm/s	
Straightness (Str = displacement/ track length)	0–1	

Table 3: Summary of selected parameters for mitochondrial mobility.

Supplemental Coding File 1: GA3 script file for analysis of individual mitochondrial morphology.
Please click here to download this File.

Discussion

Here, a novel method to longitudinally follow the dynamics and turnover of the mitochondrial system in a cultured astrocyte is proposed. Unlike a time-lapse approach on a fixed group of cells or one individual cell at a time (most often used in the literature)[24,25], researchers can follow the evolution of the mitochondrial system during several days on the same individual cells. In contrast to single well live imaging where high levels of light exposure are required, and the selection of many individual cells is less feasible, the proposed method takes advantage of this microscope's ability to image several different cells in different areas of a well and to come back to those same cells at various time points to re-image them. Thanks to normalization to a baseline carried out for each measured criterion on each cell of interest, it takes the mitochondrial system's complexity into account and investigates the effect of treatment on each cell relative to its own baseline image. The microscope's ability to autonomously carry out this type of imaging on up to 16 wells at a time (imaging 5 cells per well) allows for the heterogeneity of the mitochondrial system to be properly taken into account during analysis without the experimental variability that comes with imaging various conditions on different days.

The quality of the cultures, the levels of viral infections expressing the LV-G1-MitoTimer biosensor, the type of microscope and objectives, and the selection of suitable cells are critical variables that must remain as consistent as possible in this protocol. The cell densities, the type of vector, and the viral titers can be adapted according to the question. Although previous work shows that LVG1-MitoTimer expression has no deleterious consequences for mitochondrial function and dynamics[21,22,26,27], it is essential to verify that the concentration is not toxic for the cells (for example, checking the total number of cells in control well). As a single focal plane is used, astrocytes should be: (1) as flat as possible, (2) isolated from other labeled cells (to simplify the analysis in case of displacement in the dish), and (3) possessing high fluorescence levels. As cells in culture can be highly variable in morphology, the mitochondrial system can be highly heterogeneous. In this context, analyzing ROIs (and not the whole cell) compensates for some problematic regions, such as the perinuclear regions, and decreases variability. It is essential to do the baseline on relatively similar cells and sample as many cells as possible. Consequently, high content acquisition and analysis microscopes are ideally suited. During this longitudinal monitoring, it is also important not to overexpose the cells to light to avoid biosensor bleaching.

This imaging method is not without its complexities, and throughout the protocol, several notes are included, which take into account troubleshooting done during previous tests with the microscope. For example, the choice of plate coating used depends on the intended assay, but recommendations for the most suitable choices for astrocyte primary cultures have been included. Additionally, image acquisition should be performed on at least 5 cells per condition due to intercellular variability. More specifically, some cells selected at baseline imaging will die, some will move out of the frame of the assigned image acquisition area, and some will change their morphology, making the mitochondria very difficult to individualize in analysis. Imaging many cells from the beginning increase the likelihood of a large enough sample size of cells to analyze at the end of the experiment.
In addition to the more complex aspects of this imaging technique, there are some outright limitations as far as who can benefit from this type of imaging and analysis. In order to take full advantage of the automatization of image acquisition, the microscope used must have an autofocus system that can handle the speed of time intervals between images (i.e., every 3 s in this protocol) and can consistently focus on the cell in question before each image is taken. Additionally, without the JOBS software, which automates the entire image

acquisition process, this method becomes arduous and potentially impossible depending on the number of cells being imaged as it would require manually finding and imaging each cell again at the appropriate time point. Finally, this imaging method is not immune to the issue of photobleaching. For this reason, as with any long-term acquisition method, it is important to choose fluorescent markers that are less susceptible to photobleaching and to tailor image acquisition to avoid this issue as much as possible.

This technique differs from others currently used in a crucial way. Unlike other time-lapse studies, this technique does not require imaging on the same position in the well the entire time, nor does it require manual movement of the plate to image other areas. This allows researchers the ability to image many cells in many conditions in one 24 h timeframe. Consequently, the ability to carry out this imaging and analysis on many cells in each well gives the same population information one would obtain from broadly studying a large group of cells while additionally providing specific measures from each cell imaged. While some specificities to this method may not apply to other image acquisition methods (outlined above), the benefits outweigh the complications with the type of analysis possible after acquisition. This technique allows researchers to see the exact ramifications of various treatments on the mitochondrial system, and consequently, on the cultured astrocytes.

Additionally, this method is highly customizable to many different scientific questions regarding mitochondrial behavior and roles in specific contexts. Here the outlined protocol deals specifically with cultured astrocytes. However, many other cell types can be used, and the treatments that can be tested are limited only by the questions being investigated. This type of imaging has the potential to advance the collective knowledge and understanding of mitochondrial behavior, the underlying mechanisms that lead to mitochondrial dysfunction, and the effects of many pathologies on the innate dynamics present in different types of cells.

Disclosures

The authors declare no competing interests.

Acknowledgments

This study was supported by a Synapsis Foundation fellowship awarded to K.R. and the Lausanne University Hospital (CHUV). The authors thank Nikon for their help, in particular J. Gannevat.

References

1. Ballabh, P., Braun, A., Nedergaard, M. The blood-brain barrier: An overview: Structure, regulation, and clinical implications. *Neurobiology of Disease.* **16** (1), 1-13 (2004).
2. Allen, N.J., Eroglu, C. Cell biology of astrocyte-synapse interactions. *Neuron.* **96** (3), 697-708 (2017).
3. Bernardinelli, Y., Muller, D., Nikonenko, I. Astrocytesynapse structural plasticity. *Neural Plasticity.* **2014**, 232105 (2014).
4. Benarroch, E. E. Neuron-astrocyte interactions: Partnership for normal function and disease in the central nervous system. *Mayo Clinic Proceedings.* **80** (10), 1326-1338 (2005).

5. MacVicar, B. A., Choi, H. B. Astrocytes provide metabolic support for neuronal synaptic function in response to extracellular K+. *Neurochemical Research.* **42** (9), 2588-2594 (2017).

6. Song, H., Stevens, C. F., Gage, F. H. Astroglia induce neurogenesis from adult neural stem cells. *Nature.* **417** (6884), 39-44 (2002).

7. Christopherson, K. S. et al. Thrombospondins are astrocyte-secreted proteins that promote CNS synaptogenesis. *Cell.* **120** (3), 421-433 (2005).

8. Volterra, A., Liaudet, N., Savtchouk, I. Astrocyte Ca2+ signalling: An unexpected complexity. *Nature Reviews Neuroscience.* **15** (5), 327-335 (2014).

9. Huntington, T. E., Srinivasan, R. Astrocytic mitochondria in adult mouse brain slices show spontaneous calcium influx events with unique properties. *Cell Calcium.* **96**, 102383 (2021).

10. Kofuji, P., Newman, E. A. Potassium buffering in the central nervous system. *Neuroscience.* **129** (4), 1045-1056 (2004).

11. Ridet, J. L., Malhotra, S. K., Privat, A., Gage, F. H. Reactive astrocytes: Cellular and molecular cues to biological function. *Trends in Neurosciences.* **20** (12), 570-577(1997).

12. Liddelow, S. A., Barres, B. A. Reactive astrocytes: Production, function, and therapeutic potential. *Immunity.* **46** (6), 957-967 (2017).

13. Young, A., Gill, R., Mailloux, R.J. Protein Sglutathionylation: The linchpin for the transmission of regulatory information on redox buffering capacity in mitochondria. *Chemico-Biological Interactions.* **299**, 151-162 (2019).

14. Lackner, L. L. Shaping the dynamic mitochondrial network. *BMC Biology.* **12**, 35 (2014).

15. Willems, P. H. G. M., Rossignol, R., Dieteren, C. E. J., Murphy, M. P., Koopman, W. J. H. Redox homeostasis and mitochondrial dynamics. *Cell Metabolism.* **22** (2), 207-18 (2015).

16. de Michele, R., Carimi, F., Frommer, W. B. Mitochondrial biosensors. *International Journal of Biochemistry and Cell Biology.* **48**, 39-44 (2014).

17. Terskikh, A. et al. "Fluorescent timer": Protein that changes color with time. *Science.* **290** (5496), 1585-1588 (2000).

18. Rizzuto, R. et al. A gene specifying subunit VIII of human cytochrome c oxidase is localized to chromosome 11 and is expressed in both muscle and non-muscle tissues.
Journal of Biological Chemistry. **264** (18), 10595-10600 (1989).
19. Rizzuto, R., Brini, M., Pizzo, P., Murgia, M., Pozzan, T. Chimeric green fluorescent protein as a tool for visualizing subcellular organelles in living cells. *Current Biology.* **5** (6), 635-642 (1995).
20. Ferree, A. W. et al. MitoTimer probe reveals the impact of autophagy, fusion, and motility on subcellular distribution of young and old mitochondrial protein and on relative mitochondrial protein age. *Autophagy.* **9** (11), 1887-1896
(2013).
21. Hernandez, G. et al. MitoTimer: A novel tool for monitoring mitochondrial turnover. *Autophagy.* **9** (11), 1852-1861 (2013).
22. Richetin, K. et al. Tau accumulation in astrocytes of the dentate gyrus induces neuronal dysfunction and memory deficits in Alzheimer's disease. *Nature Neuroscience.* **23** (12), 1567-1579 (2020).
23. Merienne, N. et al. Gene transfer engineering for astrocyte-specific silencing in the CNS. *Gene Therapy.* **22** (10), 830-839 (2015).
24. Sison, M. et al. 3D Time-lapse imaging and quantification of mitochondrial dynamics. *Scientific Reports.* **7**, 43275 (2017).
25. Miyazono, Y., Hirashima, S., Ishihara, N., Kusukawa, J., Nakamura, K. I., Ohta, K. Uncoupled mitochondria quickly shorten along their long axis to form indented spheroids, instead of rings, in a fission-independent manner. *Scientific Reports.* **8** (1), 350 (2018).
26. Trudeau, K. M., Gottlieb, R. A., Shirihai, O. S. Measurement of mitochondrial turnover and life cycle using MitoTimer. *Methods in Enzymology.* **547**, 21-38 (2014).
27. Stotland, A., Gottlieb, R.A. α-MHC MitoTimer mouse: In vivo mitochondrial turnover model reveals remarkable mitochondrial heterogeneity in the heart. *Journal of Molecular and Cellular Cardiology.* **90**, 53-58 (2016).

Annex 2

Extracellular vesicles: Major actors of heterogeneity in tau spreading among human tauopathies

Elodie Leroux,[1,5] Romain Perbet,[1,5] Raphaëlle Caillierez,[1] Kevin Richetin,[2,3,4] Sarah Lieger,[1] Jeanne Espourteille,[2] Thomas Bouillet,[1] Séverine Bégard,[1] Clément Danis,[1] Anne Loyens,[1] Nicolas Toni,[2] Nicole Déglon,[3,4] Vincent Deramecourt,[1] Susanna Schraen-Maschke,[1] Luc Buée,[1] and Morvane Colin[1]

[1]Université de Lille, INSERM, CHU-Lille, Lille Neuroscience & Cognition, 59000 Lille, France; [2]Department of Psychiatry, Center for Psychiatric Neurosciences, Lausanne University Hospital (CHUV) and University of Lausanne, 1011 Lausanne, Switzerland; [3]Lausanne University Hospital (CHUV) and University of Lausanne, Neuroscience Research Center (CRN), Laboratory of Cellular and Molecular Neurotherapies, 1011 Lausanne, Switzerland; [4]Lausanne University Hospital (CHUV) and University of Lausanne, Department of Clinical Neuroscience (DNC), Laboratory of Cellular and Molecular Neurotherapies, 1011 Lausanne, Switzerland

Tauopathies are neurodegenerative diseases characterized by tau inclusions in brain cells. Seed-competent tau species have been suggested to spread from cell to cell in a stereotypical manner, indicating that this may involve a prion-like mechanism. Although the intercellular mechanisms of transfer are unclear, extracellular vesicles (EVs) could be potential shuttles. We assessed this in humans by preparing vesicles from fluids (brain-derived enriched EVs [BD-EVs]). These latter were isolated from different brain regions in various tauopathies, and their seeding potential was assessed *in vitro* and *in vivo*. We observed considerable heterogeneity among tauopathies and brain regions. The most striking evidence was coming mainly from Alzheimer's disease where the BD-EVs clearly contain pathological species that can induce tau lesions *in vivo*. The results support the hypothesis that BD-EVs participate in the prion-like propagation of tau pathology among tauopathies, and there may be implications for diagnostic and therapeutic strategies.

INTRODUCTION

Tau, a microtubule-associated protein,[1] aggregates into filaments in Alzheimer's disease (AD) and in other related and heterogeneous diseases called tauopathies, which are characterized by the intracellular accumulation of hyperphosphorylated tau.[2] An alternative splicing mechanism gives rise to six major isoforms of tau that coexist in the human brain, which either have three or four repeated sequences of the microtubule-binding region (3R-tau and 4R-tau).[3] In AD, tau protein principally aggregates into paired helical filaments (3R-tau and 4R-tau) within the neurons, while in progressive supranuclear palsy (PSP), tau aggregates consist of straight filaments (4R-tau) and are found in both the neurons and the glia. In Pick's disease (PiD), specific neuronal tau inclusions are seen, known as Pick bodies, in which 3R-tau aggregates to form a spherical shape within the neuronal cell body. These different tauopathy filaments are beginning to be better described and are different among tauopathies.[4–7]

In AD, the most common tauopathy, the progression of neurodegeneration in the brain correlates very well with the clinical signs of the disease at each stage. It follows a sequential, hierarchical progression of brain involvement in a pattern that is similar for all patients: the hippocampal formation, the polymodal association areas, the unimodal association regions, and in the final stages of the disease, the entire cerebral cortex.[8,9] This stereotypical hierarchy of neurodegeneration is known in the literature as the Braak stages.[8] Specific hierarchical pathways have also been described for PSP,[10,11] argyrophilic grain disease,[12] and PiD.[13] These patterns of progression have been considered as steps in the propagation of neurodegeneration and have led to the hypothesis of a prion-like tau propagation.[3] In this hypothesis, an abnormal tau protein conformation would lead to the prion-like transconformation of normal tau proteins into abnormal ones. This would be followed by the secretion of pathological seeds, which would then be internalized by healthy neurons, thus transmitting the pathology.

While tau was first identified as a protein implicated in the assembly and stabilization of microtubules,[1] it is now described as a pleiotropic protein with various cellular locations.[14] It is known that the protein can be secreted by unconventional pathways, mostly in a free form,[15–25] and it has also been found in extracellular vesicles (EVs).[26] EVs have two main cellular origins: (1) EVs known as exosomes are generated from multivesicular bodies, containing

Received 15 March 2021; accepted 20 September 2021;
https://doi.org/10.1016/j.ymthe.2021.09.020.

[5]These authors contributed equally

Correspondence: Morvane Colin, Université de Lille, INSERM, CHU-Lille, Lille Neuroscience & Cognition, Bâtiment Biserte, rue Polonovski, 59045 Lille Cedex, France.
E-mail: morvane.colin@inserm.fr
Correspondence: Luc Buée, PhD, Université de Lille, INSERM, CHU-Lille, Lille Neuroscience & Cognition, Bâtiment Biserte, rue Polonovski, 59045 Lille Cedex, France.
E-mail: luc.buee@inserm.fr

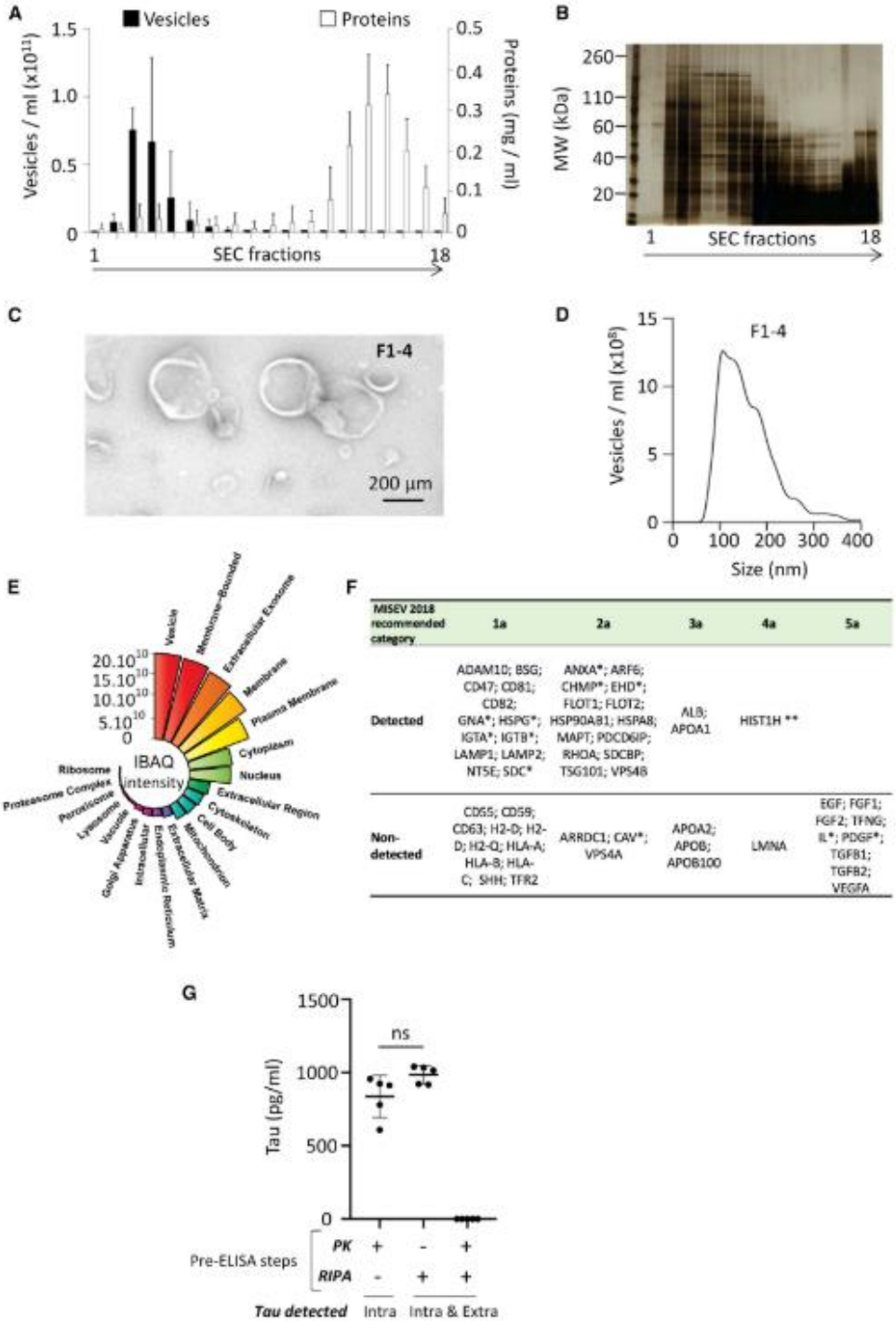

MISEV 2018 recommended category	1a	2a	3a	4a	5a
Detected	ADAM10; BSG; CD47; CD81; CD82; GNA*; HSPG*; IGTA*; IGTB*; LAMP1; LAMP2; NT5E; SDC*	ANXA*; ARF6; CHMP*; EHD*; FLOT1; FLOT2; HSP90AB1; HSPA8; MAPT; PDCD6IP; RHOA; SDCBP; TSG101; VPS4B	ALB; APOA1	HIST1H **	
Non-detected	CD55; CD59; CD63; H2-D; H2-D; H2-Q; HLA-A; HLA-B; HLA-C; SHH; TFR2	ARRDC1; CAV*; VPS4A	APOA2; APOB; APOB100	LMNA	EGF; FGF1; FGF2; TFNG; IL*; PDGF*; TGFB1; TGFB2; VEGFA

(legend on next page)

intraluminal vesicles, that are secreted into the extracellular fluid; and (2) EVs known as ectosomes originate from direct plasma membrane budding.[27] These vesicles have the capacity to transfer many biologically active molecules between cells, and they are known to be dysregulated in many disorders.[28] While the secretion of tau in EVs has been validated using many cell and animal models,[29] there are few data concerning the transfer of pathological tau species or seeds between cells[30] to induce a seeding process in humans.[31] According to the hypothesis of prion-like propagation, once inside the recipient cell, the seeds present in EVs seem to be released from the endolysosome and lead to the recruitment and misfolding of normal endogenous proteins.[32]

While tau aggregation is a common feature of tauopathies, a huge heterogeneity exists between and within these pathologies. Recent data suggest, for instance, that pathological tau seeds in human brains differ between tauopathies,[33] and also within a particular tauopathy, as has been shown for AD.[34] Additionally, the affected brain pathways differ between AD and other tauopathies, and some cell populations are more vulnerable than others.[8,11–13] It is thus essential to understand the underlying reasons for this heterogeneity before designing a specific therapeutic approach.

In this work, we focused our attention on EVs because they have a certain selectivity in terms of the target cell due to the presence of numerous ligands and receptors on their surface.[27] They therefore represent a unique intercellular delivery vehicle for transferring pathological species from one specific neuronal population to another, and they could explain the differing cell vulnerability seen in tauopathies. The work presented herein aims to compare the transmission of tau pathology via EVs that are present within brain-derived fluids (BD-fluids) of patients with various tauopathies. Although EVs isolated from the cerebrospinal fluid,[35–37] and plasma,[38–43] contain tau, the interstitial fluid (ISF) more accurately represents the environment around brain cells. This work therefore focuses on brain-derived enriched EVs (BD-EVs) in different tauopathies (AD, PSP, and certain forms of non-hereditary frontotemporal lobar degeneration with Pick bodies [formerly known as PiD]) as well as in non-demented controls. The seeding ability from BD-EVs purified from both tau transgenic mice and patients with various tauopathies is shown *in vitro*. In addition, AD BD-EVs are able to transmit tau pathology *in vivo* in a prion-like process. These results highlight the importance of defining how the pathology propagates through the brain in different tauopathies in order to design specific and tailored therapies as well as assessment tools for the evaluation of clinical trials.

RESULTS

In the present work, we isolated vesicles from the post-mortem BD-fluid of patients with various tauopathies, and we evaluated whether they contain species that are able to seed and spread the tau pathology in the brain.

EVs are present in the BD-fluid of a transgenic mouse model of tauopathy

To address this issue, we first isolated and characterized murine BD-EVs from a transgenic mouse model of tauopathy, the THY-tau30, that expresses human 1N4R tau protein with two pathogenic mutations (P301S and G272V) under the control of the neuron-specific Thy-1.2 promoter.[44,45] We prepared murine BD-fluids according to the protocol described by Polanco et al.[46] We then purified and characterized vesicles from the murine BD-fluid using size-exclusion chromatography (SEC). As it is critical to remove any aggregated or macroprotein contaminants associated with the BD-EVs, we purified them using SEC rather than classical ultracentrifugation procedures.[47] The concentration and distribution of the vesicles were analyzed by a nanoparticle tracking analysis (NTA) system, and the global protein content and its distribution were determined using UV detection or silver gel staining. SEC allowed us to efficiently enrich vesicles (fractions 1–4 [F1–4]) in our preparations from the protein contaminants, as previously described, while guaranteeing their morphological integrity (Figures 1A–1C). A size distribution of the BD-EV fractions revealed the presence of vesicles ranging from 50 to 400 nm (Figure 1D). Then, we used matrix-assisted laser desorption ionization-time of flight (MALDI-TOF) liquid chromatography-tandem mass spectrometry (LC-MS/MS) and quantitative analysis (intensity-based absolute quantification [IBAQ]) to evaluate F1–4 proteomic content. We identified a total of 2,064 proteins, of which 1,635 (79%) are referenced in the Vesiclepedia database. IBAQ scores combined with Gene Ontology cellular component (GOCC) annotation revealed that GOCC terms associated with EVs represent 76% of total IBAQ scores for the 20 selected terms (Figure 1E). Among proteins recommended by the Minimal Information for Studies of Extracellular Vesicles 2018 (MISEV2018),[48] we identified a majority of categories 1a (non-tissue-specific transmembrane or glycosylphosphatidylinositol [GPI]-anchored proteins), 2a (cytosolic proteins recovered in EVs), and 4a (transmembrane, lipid-bound, and soluble proteins associated to other intracellular compartments

Figure 1. Murine BD-EV characterization

Vesicles from murine BD-fluid were isolated using SEC to separate vesicles from free-floating proteins. They were separated by Sepharose resin columns in PBS and 500 µL per fraction was collected. (A and B) BD-EV concentration was quantified per fraction using NTA and expressed as vesicles/mL (A, filled columns); the amount of total protein was determined using either UV spectrophotometry (A, open columns) or a silver gel coloration (B). (C) Vesicle morphology was studied using electron microscopy in pooled fractions 1–4 (F1–4). The scale bar is indicated on the figure. (D) The size distribution of vesicles was determined using NTA in pooled F1–4. (E) Circular barplot showing IBAQ intensity scores obtained for 20 selected GOCC terms after quantitative proteomic analysis of F1–4. (F) Table listing human gene names corresponding to proteins recommended by MISEV2018 detected in F1–4 after MS-based proteomic analysis. An asterisk is used for families of multiple proteins; for example, for integrins, ITGA* indicates any integrin alpha chain. (G) The intravesicular tau (+PK−RIPA, with RIPA for ELISA tau detection) or the intra tau plus the extravesicular tau (−PK+RIPA) was quantified using ELISA from murine BD-EVs (3-month-old THY-tau30). A positive control showing the global lysis of tau is also shown (+PK+RIPA). ns, not significant. For (A) and (D), means of three independent experiments are shown; for (B) and (C), illustrative data are representative of at least three independent experiments.

than plasma membrane/endosomes) (Figure 1F). Among them are found the cytosolic vesicular markers HSP90 and tau protein (MAPT), which have been validated using either western blot (Figure S1A) or ELISA assays (Figure 1G). In addition, using a proteinase K (PK) digestion assay, we showed that tau is found inside BD-EVs and not associated to their outer leaflet. Indeed, the extravesicular proteolysis (PK^+, radioimmunoprecipitation assay buffer $[RIPA]^-$) does not affect intravesicular tau concentration, thus confirming tau as an intravesicular component (Figure 1G). This full characterization including NTA, silver gel staining, electron microscopy, proteomics, and western blot indicates that F1–4 contained vesicles and are enriched in EVs. This pool was considered as the BD-EVs fraction in the following experiments.

BD-EVs from a transgenic mouse model of tauopathy contain tau seeds

To determine the role of EVs in tau pathology spreading, the tau seeding content of BD-EVs prepared from 1-, 3-, and 6-month-old THY-tau30 mice (a transgenic mouse model with progressive tau lesions) was evaluated.[44,45] As controls, we also isolated BD-EVs from wild-type littermates and transgenic APP/PS1 mice (that develop amyloid deposition) that do not exhibit tau aggregation.[49] Tau lesions were examined in the brains of these animals using two well-characterized anti-tau antibodies (Abs): MC1[50] (tau conformational-dependent Ab) and AT100[51] (human phospho-dependent Ab that allowed the detection of insoluble/aggregated tau). MC1 (Figure S2a–g) and AT100 (Figure S2h–n) immunoreactivities were progressively detected in the hippocampal neurons of the CA1 layer of THY-tau30 mice from 1 to 6 months. Whereas few to no MC1 (Figure S2e) and AT-100 (Figure S2l) immunoreactivities were seen at 1 month of age, respectively, and MC1 immuno-positive neurites were easily detectable at 3 months with a few positive cell bodies (Figure S2f). A very slight AT100 immunostaining was also seen in 3-month-old mice in the subiculum (Figure S2m) when a strong immunoreactivity (in soma and neurites) was shown in 6-month-old animals by both MC1 and AT100 Abs (Figures S2g and n, respectively). No AT100 and MC1 immunoreactivities were observed in the wild-type littermates (Figures S2b–d and i–k) or in the transgenic APP/PS1 controls (Figures S2a and h). We then isolated vesicles of these murine BD-fluids and evaluated their ability to induce a nucleation process using a biosensor assay.[52] This involved a highly sensitive and quantitative assay using a novel fluorescence resonance energy transfer (FRET)-based biosensor cell line that specifically reports tau seeding activity. These cells express soluble forms of repeat domain (RD)-P301Stau-CFP and RD-P301Stau-yellow fluorescent protein (YFP). In the presence of seeds such as recombinant tau fibers, an oligomerization process allows energy transfer between CFP and YFP that is detectable by flow cytometry. BD-EVs were introduced inside the biosensor cells using Lipofectamine and the seeding activity was quantified. BD-EVs of THY-tau30 mice, unlike those obtained from the control lines (littermate of THY-tau30 and APP/PS1), contained seed-competent species (Figure 2A). In fact, the FRET signal was observed in an age-dependent manner only with THY-tau30 samples. The seeding effect was indeed related to BD-EVs since their removal by ultracentrifugation in F1–4 abolished the FRET signal (compare ultracentrifugation supernatant [no vesicle] to pellet [BD-EV fraction]) (Figure 2B). In addition, tau was mainly found within vesicles as demonstrated by tau immunodepletion after BD-EV sonication (Figure 2C). The sonication procedure was applied to ensure release of intravesicular tau and then facilitate its immunodepletion. Indeed, when intravesicular tau was immunodepleted, a 70% decrease in the FRET signal was observed (Figure 2D).

Taken together, these data strongly support the hypothesis that the progressive appearance of tau pathology in mice leads to the release of vesicles in the BD-fluid that contain seed-competent tau species.

The seeding capacity of BD-EVs is heterogeneous among human tauopathies

We showed that the presence of tau seeds inside BD-EVs is related to the progression of tau pathology in the case of mice. Given the heterogeneity among tauopathies, we questioned whether the seeding potential of BD-EVs would differ between these neurodegenerative diseases. Post-mortem brain samples of human non-demented controls (n = 5), AD (n = 10), PSP (n = 10), and PiD (n = 5) patients were obtained (Table 1) in order to isolate BD-EVs, as described above (Figure 1). Three brain regions (the prefrontal cortex, the occipital cortex, and the cerebellum) differentially affected by the pathology were dissected, and tau lesions were quantified by immunohistochemistry (IHC) using AT8, a phospho-dependent anti-tau Ab (Figures 3A and 3B). As expected, tau pathology is higher in AD cases. After SEC purification, the BD-EVs shared the same characteristics (size, morphology, content) as did those isolated from the murine brain (Figure S3). Additionally, the presence of a specific transmembrane tetraspanin associated with the vesicles was validated using immunogold electron microscopy (CD63; Figure S1B).

In contrast to the mice, where the whole brain was analyzed, only specific areas of the human brain were dissected for BD-fluid isolation. To avoid any bias, the results were systematically normalized according to the weight of the brain extracts used to prepare the BD-fluid. Our data showed that the vesicle concentrations (Figure 4A) and the global tau content (Figure 4B) did not differ among the tauopathies. Interestingly, BD-EVs from the brains of the controls contained global tau at a similar level than those from patients with tauopathies. This confirms that tau is physiologically secreted in EVs and gives new insight into the mode of tau secretion in human brain.

To determine whether the tau protein present in BD-EVs can induce a nucleation process and whether this is similar among tauopathies, BD-EVs were applied to biosensor cells, as before. The vesicular contents from the prefrontal and occipital regions of the AD BD-fluid induced a significant FRET signal compared to the non-demented controls. For BD-EVs from the PSP and PiD patients, a weak FRET signal was observed (Figure 4C), which was consistent with neuropathology (Figure 3). It is relevant to note that among the PiD samples, one had BD-EVs displaying a high FRET signal. This patient exhibited, in addition to Pick bodies, neurofibrillary tangles (NFTs) as seen in AD patients (Table 1), which could potentially account for this finding. Whereas

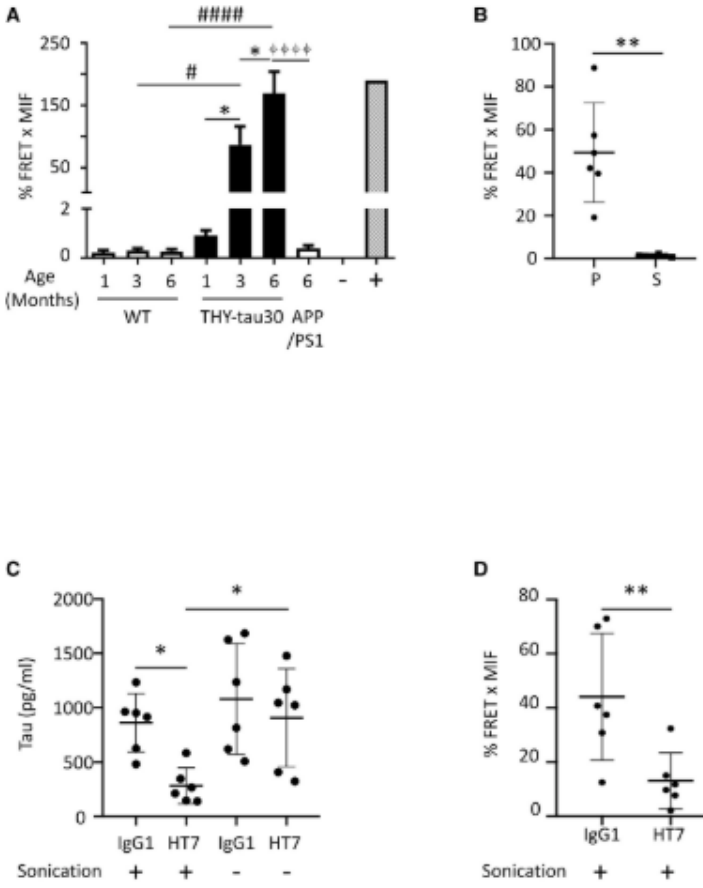

Figure 2. BD-EVs of a transgenic mouse model of tauopathy contain tau seeds

(A) BD-EVs of TgAPP/PS1 mice (6 months old, n = 6), wild-type littermate mice (1 [n = 8], 3 [n = 6], and 6 [n = 8] months old), and THY-tau30 mice (1 [n = 7], 3 [n = 8], and 6 [n = 8] months old) were applied to the HEK-tau biosensor cells, and the FRET signal was quantified using flow cytometry. 2 μM sonicated K18 fibrils were used as a positive control (+) and PBS was used as a negative control (−). (B) BD-EVs isolated from 3-month-old THY-tau30 mice (F1–4) were further ultracentrifuged to deplete vesicles. Pellet-containing vesicles (P) and supernatant (S) were applied to the biosensor assay. (C) Tau ELISA after tau immunodepletion (with or without sonication) from BD-EVs isolated from 3-month-old THY-tau30 mice. HT7 was used to immunodeplete tau, whereas IgG1 was used as a negative control of immunodepletion. (D) After tau immunodepletion of sonicated BD-EVs, fractions were applied to the biosensor assay. For (A), (B), and (D), results are expressed as the percentage of the FRET signal × MFI (% FRET × MFI). $^{*}p < 0.05$, $^{**}p < 0.01$; $^{\#}p < 0.05$, $^{\#\#\#\#}p < 0.0001$; $^{\phi\phi\phi\phi}p < 0.0001$.

the FRET signal is related to the tau lesions in most cases (compare Figures 3B and 4C), as shown for the mice, the FRET signal for the AD cerebellum was significantly higher than that in the controls, even though both were devoid of tau lesions. This FRET signal did not reflect a passive release of intracellular vesicles due to cell death, as there was no correlation between the post-mortem delay and the FRET signal (Figure 4D). Taken together, our results demonstrate that although the global level of tau is similar in BD-EVs, the seeding/nucleation competency is clearly different according to the tauopathy considered, with a particularly high activity found in AD, in accordance with previous studies.[31]

BD-EVs are able to transmit tau pathology *in vivo*

To validate the seeding capacity of BD-EVs and to determine whether these vesicles are able to transmit tau pathology *in vivo*, we adapted our *in vivo* model of seeding.[53] This model is based on the intracerebral injection of material derived from AD brains into the hippocampi of 1-month-old THY-tau30 mice. At this age, the endogenous tau pathology is very weak,[44] thus allowing us to evaluate the seeding activity associated with the injected, human-derived material.

Four prefrontal cortex BD-fluid samples were pooled for each group: AD, PSP, PiD, and control. The BD-EVs were tested using the FRET assay (Figure 5A) before being injected into the animals (6×10^9 vesicles per hippocampus). A lower signal was generated for the PSP and PiD groups compared to the AD group, thus confirming what was previously shown *in vitro* (Figure 4C). These intact BD-EVs were then bilaterally injected in THY-tau30 mice and control littermates. Their respective ability to seed endogenous tau was monitored by IHC using MC1 (tau conformational-dependent Ab) or AT100 (human phospho-dependent Ab that allowed the detection of insoluble/aggregated tau) (Figure 5B). When the BD-EVs were injected into the wild-type mice, no MC1 or AT100 immunoreactivity was observed. No seeding occurred, and the tau species contained within the vesicles were not detected. In contrast, tau seeding was seen when BD-EVs from AD patients were injected in the THY-tau30 mice. MC1 and AT100 immunoreactivities were quantified. In contrast, injected BD-EVs from PSP and PiD did not induce any higher MC1 or AT100 immunoreactivity than did BD-EVs purified from human control brains (Figures 5C and 5D, respectively). This lower seeding capacity of BD-EVs from PSP and PiD than those from AD confirmed our *in vitro* data (Figure 4).

Altogether, our data show that BD-EVs containing tau seeds are capable of mediating the misfolding and phosphorylation of tau.

Table 1. Demographic, biological, and clinical characteristics of the human brain sample donors

Sex	Death (years)	PMD (h)	Diagnosis	Tau lesions	Braak	Thal stages	Cause of death
[a]M	78	19	Control	none	0	0	invasive aspergillosis
[a]F	82	NA	Control	none	1	1	pericarditis
[a]M	23	24	Control	none	0	0	myocarditis
[a]M	59	13	Control	none	0	0	Septic shock
M	41	11	Control	none	0	0	suffocation
M	70	30	AD	NFT	VI	4	
[b]F	63	15	AD	NFT	VI	4	
F	60	24	AD	NFT	VI	5	
F	82	84	AD	NFT	VI	5	
F	87	24	AD	NFT	VI	5	
[b]F	71	4	AD	NFT	VI	4	
M	64	20	AD	NFT	VI	4	
[b]M	66	27	AD	NFT	VI	5	
F	66	16	AD	NFT	VI	4	
[b]M	69	6	AD	NFT	VI	4	
[c]M	74	9	PSP	NFT and GFT	NA	1	
[c]M	90	36	PSP	NFT and GFT	NA	2	
M	88	3	PSP	NFT and GFT	NA	4	
[c]M	69	17	PSP	NFT and GFT	NA	0	
[c]F	79	4	PSP	NFT and GFT	NA	0	
M	65	18	PSP	NFT and GFT	NA	0	
M	82	4	PSP	NFT and GFT	NA	0	
M	64	18	PSP	NFT and GFT	NA	0	
F	77	9	PSP	NFT and GFT	NA	3	
M	57	20	PSP	NFT and GFT	NA	1	
[d]M	57	22	PiD	Pick bodies	NA	0	
[d]M	71	21	PiD	Pick bodies	NA	3	
[d]F	78	11	PiD	Pick bodies&NFT	NA	0	
[d]M	68	15	PiD	Pick bodies	NA	0	
M	68	8	PiD	Pick bodies	NA	0	

Demographic, biological, and clinical characteristics of the human brain sample donors- Brain samples used for BD-fluid isolation are listed (n = 5 non-demented controls, n = 10 AD, n = 10 PSP, and n = 5 PiD). PMD, post-mortem-delay.

[a]Non-demented controls.

[b]AD patients.

[c]PSP patients.

[d]PiD patients selected for the intracranial delivery of the BD-EVs in mice.

The data then strongly suggest the ability of the vesicular content to recruit and convert endogenous tau into an abnormal conformational form that differs among tauopathies, consistent with neuropathology, thus suggesting the existence of specific species inside the BD-EVs according to the particular tauopathy.

DISCUSSION

In this study, we investigated the role of BD-EVs in the heterogeneity and cell vulnerability of tauopathies. EVs possess ligands and/or receptors that are compatible with a specific cell type, and this could explain the neuronal selectivity and the hierarchy of neurodegeneration within tauopathies. To date, most studies have investigated the role of EVs in cell or animal models,[26,32,46,54,55] but few data are available for humans, especially when considering the ISF that is in direct contact with the brain cells and that is likely to be part of the prion-like process. The presence of EVs capable of transferring material between cells (Figures 5 and S4)[31,56] can help to explain the progression of the pathology in tauopathies. A very recent and elegant study carried out by Ruan et al.[31] showed for the first time that AD brain-derived EVs spread tau pathology with defined interneurons as their

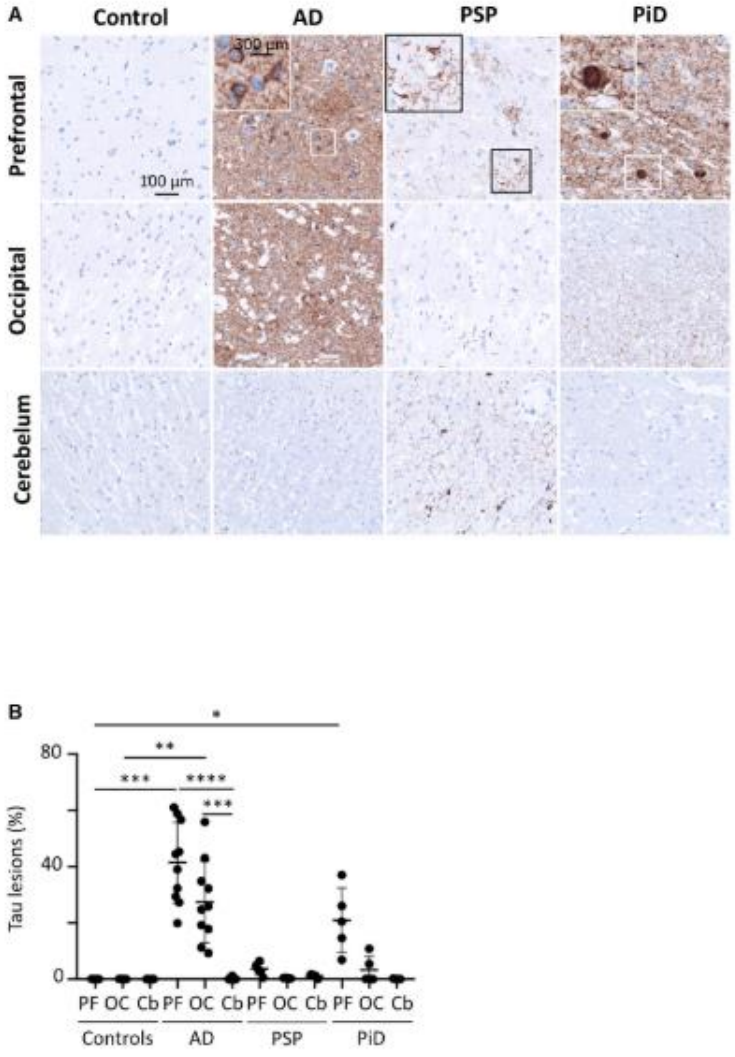

Figure 3. Tau lesions in human brain tauopathies

Prefrontal (PF), occipital (OC), and cerebellum (Cb) brain regions were dissected post-mortem from non-demented controls (n = 5) and patients with PSP (n = 5), PiD (n = 5), and AD (n = 10). (A) IHC of tau lesions using the AT8 antibody in mirror zones. Scale bars are indicated on the figure. (B) Human brain sections were blindly quantified using QuPath 0.2.1 software. Results are expressed as a percentage of tau lesions ([AT8-positive pixels/total pixels] × 100). *$p < 0.05$, **$p < 0.01$, ***$p < 0.001$, ****$p < 0.0001$.

target. Here, we go further into this mechanism by determining the contribution of vesicles to the heterogeneity of tauopathies by isolating and comparing BD-EVs from AD, PSP, and PiD, and from various brain regions differentially affected by the tau pathology.

Using our mouse models, we were able to (1) control the quality of BD-EV preparations, (2) demonstrate the role of BD-EVs-tau in the seeding process, and, most importantly, (3) highlight a link between BD-EV seeding capacity and the severity of the tau pathology. We confirmed these results in humans using brain regions that are differentially affected by the pathology (the prefrontal cortex, the occipital cortex, and the cerebellum), and the BD-EV seeding capacity was particularly striking in the case of AD. Specifically, BD-EVs from AD patients clearly contained seed-competent tau species (shown in the FRET assay), whereas such tau species were lower in the PSP and PiD materials. In general, tau pathology is much weaker in PSP and PiD than in AD, and this may contribute to the low seeding capacity of vesicles in these pathologies. However, other explanations are also possible: (1) although not unanimous, the prion-like propagation hypothesis may not be appropriate for PSP and PiD;[3] (2) a prion-like propagation may also exist for PSP and PiD, but EVs may not be the preferred shuttle, contrary to AD; and (3) the FRET assay used to measure seeding in PSP and PiD was less effective than in AD. In line with this latter possibility, previous studies found that PSP materials gave heterogeneous FRET signals.[33,57] Although a FRET signal was previously reported in PiD,[33] we did not observe a strong signal for most of the PiD cases in the present work. In fact, the only PiD patient showing a FRET signal also displayed NFTs, and this was the oldest PiD patient. We previously published that PiD patients displaying Pick bodies with additional NFTs have aging/AD-like materials, namely a pathological tau triplet revealed by immunoblotting.[58,59] The presence of such AD-like materials in this PiD patient could explain the high FRET signal as observed in the AD group.

Overall, our results suggest that the species shuttled by BD-EVs are very heterogeneous among tauopathies. What do we know about tauopathies? In PiD, there is an accumulation of 3R-tau in Pick bodies, and it is currently classified as frontotemporal lobar degeneration (FTLD)-tau.[60] Nevertheless, it is difficult to differentiate PiD and FTLD-tau with MAPT mutations (formerly FTDP-17). Both disorders have Pick bodies, but it has been shown that the Pick bodies are pS262-negative in PiD[61,62] and immunoreactive in FTLD-tau with

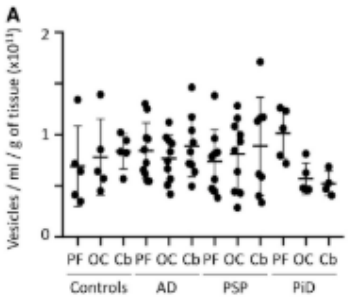

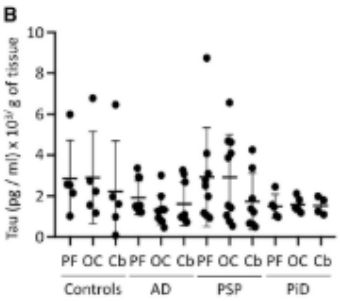

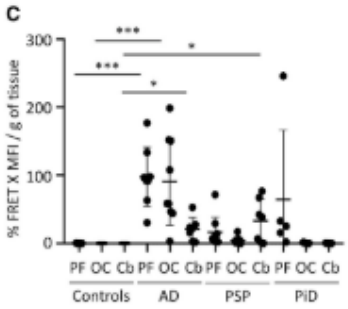

D

PMD versus.	PF-AD	OC-AD	Cb AD
Spearman (r)	- 0.6587	-0.6307	0.1
P value (two-tailed)	0.0839	0.1413	0.9500
P value summary	NS	NS	NS

Figure 4. Seed-competent species are found in BD-EVs in human tauopathies

BD-fluid was purified from the different brain regions and vesicles were isolated from 500 μL of BD-fluid. (A) BD-EV concentration was analyzed using NTA and expressed as vesicles/g/mL of tissue used to prepare the BD-fluid, and (B) global tau content was determined by ELISA (INNOTEST hTAU Ag, Fujirebio). Results are expressed as tau (pg/mL)/g of tissue. (C) BD-EVs were applied to the HEK-tau biosensor cells, and the FRET signal was quantified using flow cytometry. Results are expressed as % FRET × MFI/g of tissue. (D) Non-parametric Spearman correlation between the post-mortem delay (PMD) and the FRET signal generated by BD-EVs from the AD PF, AD OC, and AD Cb regions. *p < 0.05, ***p < 0.001.

MAPT mutations.[63,64] In any case, this lesion would appear to be particularly harmful because PiD often affects people who are relatively young (around 50 years of age), and it is characterized by very severe frontotemporal atrophy that is associated with neuronal death. Pick bodies are mostly found in layers II and VI of the frontotemporal isocortex and in the granular cell layer of the dentate gyrus.[59,65] These cells mainly express 3R-tau isoforms. It can therefore be postulated that these 3R-positive cells are fragile,[66] or else that the 3R-tau isoforms are more harmful than propagative.[67–69] In PSP, 4R-tau isoforms mostly aggregate to cause neurofibrillary degeneration. It is possible that the 4R-tau variants are secreted and captured by the glia. In line with this, both PSP and corticobasal degeneration are also characterized by gliofibrillary lesions.[60,70,71] Finally, in AD, all six tau isoforms aggregate, and neurofibrillary degeneration progresses in a hierarchical pathway from limbic, polymodal association, and unimodal association regions to the entire cerebral cortex. These observations suggest that tau seeds circulate in the ISF of AD brains. Our data support this hypothesis since tau seeds were identified in circulating EVs in all brain areas studied, even those devoid of tau lesions, such as the cerebellum. Depending on the brain area, EV receptor/ligand-bearing cells may or may not be present, which explains why some regions are affected by pathology while others are not. The combination of tau seeds in EVs and their ligand/receptor composition may therefore explain the neuronal selectivity/vulnerability and hierarchical pathway of neurodegeneration among tauopathies.

The molecular species involved in the pathological cycle of cell-to-cell transmission remain unknown, even though a great deal of work has been done to examine the roles of phosphorylation, truncation, oligomers, and high molecular weight species, among others.[29] Nevertheless, our work highlights the diversity of tau species inside BD-EVs among tauopathies, and it reinforces the hypothesis of prion-like propagation. It supports a transcellular transmission mechanism with a specificity that could explain the hierarchical and stereotypical propagation compatible with the Braak stages in AD.

Taken together, our data strongly support the existence of various tau species or co-factors inside BD-EVs among tauopathies, and their identification is now necessary in order to be able to determine the mechanism of tau pathology progression in these different diseases. The study raises a number of questions about therapeutic strategies, such as immunotherapy, that target free extracellular tau. Deciphering the nature of the pathological seeds found in the vesicles isolated from human brains, as well as the characteristics of the cargos/shuttles, will help in the design of specific tools aiming to block tau spreading.

MATERIALS AND METHODS

Abs

The following Abs were used for IHC, biochemical assays, and electron microscopy at the dilutions indicated below. The monoclonal Ab (mAb) AT8 recognizes the phosphoserine 202, phosphoserine 208, and phosphothreonine 205 residues of tau (MN1020; Thermo Scientific, Illkirch, France; 1:500 for IHC).[72] The mAb MC1 (a generous gift from Dr. Peter Davis; 1:1,000 for IHC) recognizes conformational changes, and its reactivity depends on both the N terminus (amino acids 7–9) and an amino acid sequence of tau (amino acids 313–322) in the third microtubule-binding domain.[50,73] The mAb AT100 (MN1060; Thermo Scientific, Illkirch, France; 1:500 for IHC)

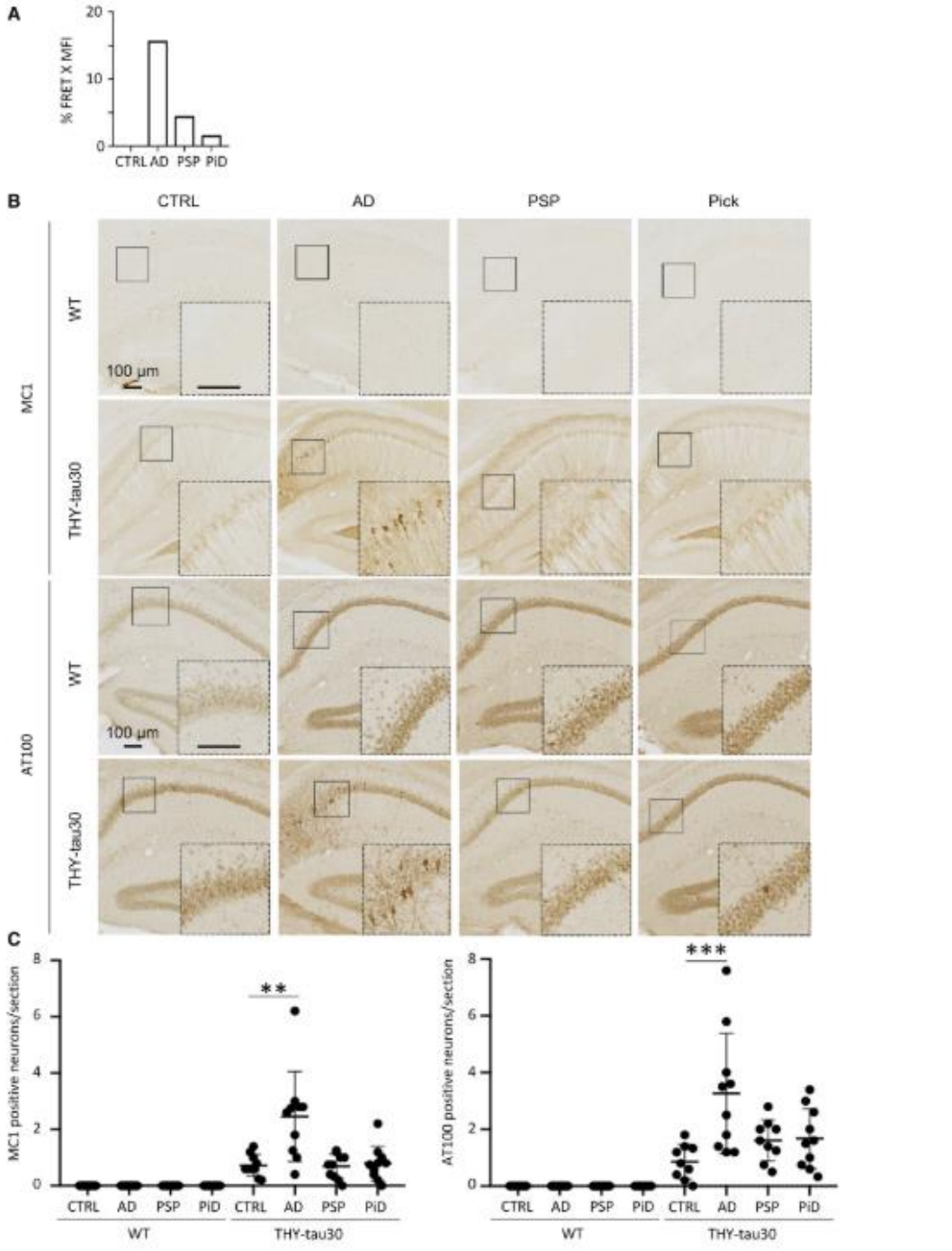

(legend on next page)

recognizes phosphothreonine 212 and phosphoserine 214 and allowed the detection of insoluble/aggregated tau.[51,74–76] The mAb HT7 (MN100; Thermo Scientific, Illkirch, France; used in the INNOTEST hTAU, as recommended by the manufacturer, Fujirebio) recognizes human tau (amino acids 159–163). Anti-heat shock protein (HSP) 90α/β (F-8; sc-13119; 1:100 for western blotting) is a mouse monoclonal antibody raised against amino acids 610-723 of HSP 90α/β of human origin. It is is recommended for detection of HSP 90α and HSP 90β of mouse, rat and human origin. Anti-CD63 is a mouse mAb (Novus Biologicals H5C6; nbp2-42225; 1:50 for electron microscopy), anti-NeuN is a rabbit mAb (Chemicon MAB377; 1:1000), and anti-V5 is a mouse mAb (Millipore AB3792; 1:500).

Animals and human samples

The study was performed in accordance with the ethical standards laid down in the 1964 Declaration of Helsinki and its later amendments. The experimental research was performed with the approval of an Ethics Committee (agreement APAFIS#2264-2015101320 441671 from CEEA75, Lille, France) and follows European guidelines for the use of animals. The animals (males and females) were housed in a temperature-controlled room (20°C–22°C) and maintained on a 12-h day/12-h night cycle with food and water provided *ad libitum* in a specific, pathogen-free animal facility (with five mice per cage or four rats per cage). Animals were randomly allocated to the different experimental groups. THY-tau30 mice were used that express human 1N4R tau protein with two pathogenic mutations (P301S and G272V) under the control of the neuron-specific Thy-1.2 promoter.[44,45]

Non-demented human control (n = 5), AD (n = 10), PSP (n = 10), and PiD (n = 5) brain extracts were obtained from the Lille Neurobank (fulfilling French legal requirements concerning biological resources and declared to the competent authority under the number DC-2008-642) with donor consent, data protection, and Ethics Committee approval. Samples were managed by the CRB/CIC1403 Biobank, BB-0033-00030. The demographic data are listed in Table 1.

Cell culture

The TauRDP301SFRET biosensor cells (ATCC CRL-3275), HEK293T cells, and HeLa cells were cultivated in Dulbecco's modified Eagle's medium with 10% fetal bovine serum, 1% GlutaMAX, and without HEPES. The cells were maintained in a humidified incubator with 5% CO_2. All cell lines were passaged twice a week. Rat primary cortical neurons were prepared from 17-day-old Wistar rat embryos, as previously described.[77] Ten days later, cells were infected with lentiviral vectors (LVs) encoding human 1N4R wild-type tau, as previously described.[78]

Brain-derived fluid isolation

BD-fluids were isolated as previously described.[46] For the frozen human brains, specific regions were removed (prefrontal cortex, occipital cortex, and cerebellum). 85 samples were used with a mean of 1.5 ± 0.07 g of tissue. Some brain areas were no longer available, that is, cerebellum (one AD, one PiD, and two PSP) and prefrontal cortex (one PSP). To avoid any bias in our results, normalization according to the weight of the brain extracts was systematically done.

For the mice, immediately after death, the whole brain (without the olfactory bulb and cerebellum) was recovered and frozen. The tissues were incubated on ice in 5 mL of Hibernate-A (50 mM NaF, 200 nM Na_3VO_4, 10 nM protease inhibitor [E64 from Sigma and protease inhibitor cocktail from Roche]). The tissues were gently mixed in a Potter homogenizer, and 2 mL of 20 U/mL papain (LS003119, Worthington Biochemical) in Hibernate-A was added to the homogenate for 20 min at 37°C with agitation. 15 mL of cold Hibernate-A buffer was then added and mixed by pipetting to stop the enzymatic activity. Successive centrifugations were applied at 4°C (300, 2,000, and 10,000 × *g*) to remove cells, membranes, and debris, respectively. The final supernatant was kept at −80°C before the BD-EV isolation procedures were applied.

BD-EV isolation

The procedures to isolate the BD-EVs from the murine or human BD-fluid were carried out in accordance with the MISEV guidelines that were established and updated in 2018 by the International Society for Extracellular Vesicles.[48] We applied various controls to validate the enrichment and the content of the BD-EVs, as recommended in these guidelines. However, the procedure described above to recover BD-fluids may lead to cell lysis. The presence of intraluminal vesicles in our preparations cannot be exclude. Because our fractions might be contaminated by ILVs, we refer them as BD-EVs. 500 µL of BD-fluid was loaded on the top of a SEC column (10-mL column, CL2B Sepharose, pore size 75 nm, Millipore).[79] This allowed us to recover a mean of 7.94×10^{10} ($\pm 3.36 \times 10^{9}$ vesicles/g of tissue in F1–4 (n = 85 samples). Isolation was carried out in phosphate-buffered saline (PBS) with a flow of 36–48 s/mL. The first 3 mL was eliminated and the following 20 fractions were recovered (with 500 µL per fraction). NTAs were performed on individual fractions diluted in PBS with a NanoSight NS300 (Malvern Panalytical). To generate statistical data, five videos of 90 s were recorded and analyzed using NTA software (camera level, 15; detection threshold, 4). When indicated, a further ultracentrifugation (100,000 × *g*, 50 min at 4°C, TLA110 rotor) was done.

Figure 5. AD BD-EVs efficiently seed host human mutated tau in young THY-tau30 mice

(A) Four AD, four PiD, four PSP, and four non-demented control BD-fluids were purified (Table 1), and isolated vesicles were pooled. 2 µL (6×10^9 vesicles) was applied to the HEK-tau biosensor cells, and the FRET signal was quantified using flow cytometry. Results are expressed as % FRET × MFI. (B) BD-EVs (6×10^9) were bilaterally injected into the hippocampi of 1-month-old THY-tau30 or wild-type mice littermates (n = 5). Mice were sacrificed 4 weeks post-injection and the tau pathology was analyzed by DAB immunostaining with the MC1 (upper) or AT100 (lower) antibodies. Sections from the hippocampus (injection site) are shown. Scale bars are indicated on the figure. (C) The numbers of MC1 (left) or AT100 (right) immunoreactive neurons per brain section were quantified (bregma −2.3 to −2.8 mm), and the data are presented as mean ± SD. $^{**}p < 0.01$, $^{***}p < 0.001$.

Electron microscopy

F1–4 from the SEC were pooled and concentrated to a final volume of 50 µL using Amicon Ultra 3K (Merck Millipore). Samples (5 µL) were deposited on a carbon film-supported grid (400 mesh) and incubated at room temperature (RT) for 20 min. For immunogold labeling, fixation in 2% paraformaldehyde (PFA; 0.1 M PO_4 buffer, pH 7.4) was performed for 20 min. Grids were rinsed for 2–3 min in PBS-glycine (50 mM) at RT. They were then soaked in a mixture containing 1% PBS-bovine serum albumin (BSA) and 1% normal goat serum for 1 h at RT before incubation with the primary Ab (1:50) in a mixture of 1% PBS-BSA and 1% normal goat serum, followed by rinsing in 0.1% PBS-BSA. Grids were then incubated for 1 h at RT with the appropriate goat anti-mouse secondary Ab (1:20, 12-nm colloidal gold) and finally washed in PBS. For immunogold labeling and morphological analyses, the grids were fixed in PBS-glutaraldehyde (1%) for 5 min at RT and then rinsed in distilled water. They were incubated for 5 min in 1% uranyl acetate and for 10 min on ice in a mixture containing 1% uranyl acetate/2% methylcellulose. Dry grids were observed under a transmission electron microscope (Zeiss EM900).

LC-MS/MS analysis

(1) Protein digestion: F1-4 fractions were digested according to a modified version of the iST method[80] (named miST method). Briefly, 50 µl solution in PBS were supplemented with in 50 µl miST lysis buffer (1% Sodium deoxycholate, 100 mM Tris pH 8.6, 10 mM DTT) and heated at 95°C for 5 min. Samples were then diluted 1:1 (v:v) with water and reduced disulfides were alkylated by adding $^1/_4$ vol of 160 mM chloroacetamide (final 32 mM) and incubating at 25°C for 45 min in the dark. Samples were adjusted to 3 mM EDTA and digested with 0.5 µg Trypsin/LysC mix (Promega #V5073) for 1h at 37°C, followed by a second 1h digestion with a second and identical aliquot of proteases. To remove sodium deoxycholate and desalt peptides, two sample volumes of isopropanol containing 1% TFA were added to the digests, and the samples were desalted on a strong cation exchange (SCX) plate (Oasis MCX; Waters Corp., Milford, MA) by centrifugation. After washing with isopropanol/1% TFA, peptides were eluted in 250 µl of 80% MeCN, 19% water, 1% (v/v) ammonia; **(2) Liquid chromatography-tandem mass spectrometry:** Eluates after SCX desalting were frozen, dried, and resuspended in variable volumes of 0.05% trifluoruacetic acid, 2% acetonitrile to equilibrate concentrations. Approximately 1 µg of each sample was injected on column for nanoLC-MS analysis; **(3) MS and MS data analysis:** dependent LC-MS/MS analysis of TMT sample was carried out on a Fusion Tribrid Orbitrap mass spectrometer (Thermo Fisher Scientific) interfaced through a nano-electrospray ion source to an Ultimate 3000 RSLCnano HPLC system (Dionex). Peptides were separated on a reversed-phase custom packed 40 cm C18 column (75 µm ID, 100Å, Reprosil Pur 1.9 µm particles, Dr. Maisch, Germany) with a 4-76% acetonitrile gradient in 0.1% formic acid (total time 140 min). Full MS survey scans were performed at 120'000 resolution. A data-dependent acquisition method controlled by Xcalibur 4.2 software (Thermo Fisher Scientific) was used that optimized the number of precursors selected ("top speed") of charge 2+ to 5+ while maintaining a fixed scan cycle of 1.5s. The precursor isolation window used was 0.7 Th. Full survey scans were performed at a 120'000 resolution, and a top speed precursor selection strategy was applied to maximize acquisition of peptide tandem MS spectra with a maximum cycle time of 0.6s. HCD fragmentation mode was used at a normalized collision energy of 32%, with a precursor isolation window of 1.6 m/z, and MS/MS spectra were acquired in the ion trap. Peptides selected for MS/MS were excluded from further fragmentation during 60s.

Tandem MS data were processed by the MaxQuant software (version 1.6.3.4)[81] incorporating the Andromeda search engine[82]. The UniProt reference proteome (RefProt) databases for Homo sapiens and mouse were used, supplemented with sequences of common contaminants. Trypsin (cleavage at K, R) was used as the enzyme definition, allowing 2 missed cleavages. Carbamidomethylation of cysteine was specified as a fixed modification. N-terminal acetylation of protein and oxidation of methionine were specified as variable modifications. All identifications were filtered at 1% FDR at both the peptide and protein levels with default MaxQuant parameters[83]. MaxQuant data were further processed with Perseus software[84], R statistical software and Microsoft Excel. We considered proteins as present in sample when unique + Razor Peptide Score >2 and an MS/MS Count >2. IBAQ values were calculated based on the summed intensities of all unique peptides for a protein divided by the number of theoretical tryptic peptides between 6 and 30 amino acids in length[85].

Western blotting and silver gel staining

Western blotting was performed as previously described.[86] Briefly, boiled samples (10 min, 100°C) were loaded onto a 4%–12% Bis-Tris NuPAGE Novex gel (Invitrogen), followed by transfer onto a 0.45-µm membrane using the Novex system from Life Technologies (XCell II blot module). The membrane was then incubated with blocking solution for 1 h at RT before incubation with the appropriate primary Ab overnight at 4°C. The membrane was then incubated for 1 h with the appropriate secondary Ab (horseradish peroxidase [HRP]-conjugated Ab, 1:50,000). The signal was visualized using enhanced chemiluminescence western blotting detection reagents (GE Healthcare). For silver gel staining, the same procedure was followed without the transfer onto a membrane. The gel was fixed overnight after migration in a mixture containing 40% ethanol and 10% acetic acid. Proteins were revealed by silver staining using the PlusOne silver staining kit and following the manufacturer's procedures (GE Healthcare).

Tau immunodepletion

BD-EV fractions were isolated from the BD-fluid of 3-month-old THY-tau30 mice. Immunodepletion of tau from F1–4 was performed using a Magna chromatin immunoprecipitation (ChIP) protein A+G magnetic beads (#16-663, Sigma-Aldrich). After 30 min in a water bath sonicator, F1–4 were incubated overnight with 2 µg of anti-tau Ab (HT7, #MN1000, Thermo Scientific) or control mouse monoclonal IgG1 Ab (GST [B-14]), Santa Cruz) with rotation at 4°C.

20 µL of magnetic beads was incubated with the complex Ab-antigen for 2 h with rotation at 4°C. A magnetic beads-Ab-antigen complex was isolated using a magnetic holder and the supernatant was collected.

PK treatment

A PK assay was done as previously described.[31,56] BD-EVs (lysis or not with radioimmunoprecipitation assay [RIPA] buffer) were incubated with 10 µg/mL PK for 30 min at 37°C to remove extravesicular proteins. The PK activity was then inhibited by adding 5 mM phenylmethylsulfonyl fluoride (PMSF) for 10 min at room temperature.

Recombinant K18 fibrils

The tau K18 recombinant protein and heparin were mixed to a ratio of 4:1 in aggregation buffer (HEPES at 10 mM, pH 6.9; NaCl at 1,000 mM) with a final protein concentration of 8 µM and incubated for 36–48 h at 37°C without shaking. The aggregation was confirmed at the end of the experiment by adding 50 µM thioflavin T to a 100 µL aliquot and comparing this to a negative control without the addition of heparin. The thioflavin T emission was detected at 490 nm after excitation at 440 nm using a PHERAstar (BMG Labtech, Ortenberg, Germany).

FRET assay

Cells were plated into a 12-well plate (150,000 cells per well) 24 h before treatment. Sonicated K18 fibrils (2 µM) were used as a positive control and PBS was the negative control. BD-EV fractions were pooled (F1–4) and concentrated in Amicon 3K columns to generate a final volume of 50 µL. The transfection mixture (50 µL of EVs + 50 µL of Opti-MEM plus 10 µL of Lipofectamine 2000 + 90 µL of Opti-MEM) was incubated for 20 min at RT and added to the cells. After 72 h, the cells were removed by scraping, and cell death was evaluated by adding Zombie NIR for 30 min at RT (as recommended by the manufacturer of the Zombie NIR fixable viability kit; BioLegend, 1:200). After one rinse in PBS, cells were fixed in 2% PFA for 10 min at RT and finally suspended in PBS for cytometry analyses using the flow cytometer Aria SORP (BD Biosciences; acquisition software FACSDiva v7.0, BD Biosciences) with the following excitation/emission wavelengths: excitation 405 nm, CFP emission 466 ± 40 nm and FRET YFP 529 ± 30 nm; excitation 488 nm, YFP emission 529 ± 30 nm. The FRET data were quantified using the Kaluza analysis software v2. Results are expressed as the percentage of FRET-positive cells × MFI (median fluorescence intensity). For the human brain samples, this value was normalized according to the weight of the tissue used to prepare the BD-fluid (percentage of FRET-positive cells × MFI/g of tissue).

Stereotaxic injections

Four BD-fluids (500 µL) were pooled for each of the AD, PSP, PiD, and control groups (Table 1), and the vesicles were isolated and concentrated to a final volume of 150 µL, as described above. For each of these, 2 µL (6×10^9 vesicles) was bilaterally injected into the hippocampi of 1-month-old anesthetized (100 mg/kg ketamine, 20 mg/kg xylazine) THY-tau30 mice and littermates (n = 5 per group; weight = 15–20 g), as done previously (anterior-posterior, −2.5 mm; medial-lateral, ±1 mm; dorsal-ventral, −1.8 mm to bregma).[53] The standard injection procedure involved the delivery of BD-EVs into THY-tau30 mice using a 10 µL Hamilton glass syringe with a fixed needle. After injection at a rate of 0.25 µL per minute, the needle was left in place for 5 min before removal to prevent any leakage of the injected material. For the experiments performed in rats (Figure S4), 3-month-old animals were anesthetized by intraperitoneal injection of a mixture of 100 mg/kg ketamine (Ketasol, Graeub, Bern, Switzerland) and 10 mg/kg xylazine (Rompun, Bayer Health Care, Uznach, Switzerland). The animals were bilaterally injected with 3 µL of BD-EVs into the dorsal dentate gyrus (anterior-posterior, −3 mm; medial-lateral, ±2.5 mm; dorsal-ventral, −3.4 mm to bregma). The vesicles were injected at a rate of 0.2 µL/min, and the needle was left in place for 5 min. In contrast to the FRET assay, in all *in vivo* experiments, intact BD-EVs were stereotactically injected without any Lipofectamine.

Tissue processing, IHC, and immunofluorescence

For the human brains, the different cerebral regions (the prefrontal cortex, the occipital cortex, and the cerebellum) were dissected, and the tau lesion quantification was performed using the mirror zones. For the mice, the whole brains were dissected and the tau lesions were quantified using dedicated mice. For the human brain sections, automated IHC was performed using 4-µm-thick formalin-fixed, paraffin-embedded (FFPE) tissue on a BenchMark Ultra (Roche Tissue Diagnostics) with the UltraView diaminobenzidine (DAB) IHC detection kit (Ventana) and the primary Ab AT8 (1:500). For the THY-tau30 and littermate mice, at 4 weeks post-injection they were deeply anesthetized and transcardially perfused with ice-cold 0.9% saline solution and subsequently with 4% PFA for 10 min. The brains were immediately removed, fixed overnight in 4% PFA, washed in PBS, placed in 20% sucrose for 24 h, and frozen until further use. Free-floating coronal sections (40 µm thick) were obtained using a cryostat microtome. For IHC, the brain sections were washed in PBS-0.2% Triton X-100, treated for 30 min at RT with 0.3% H_2O_2, and then washed three times. Non-specific binding was blocked using Mouse on Mouse reagent (1:100 in PBS, Vector Laboratories) for 60 min at RT. After three rinses in PBS-0.2% Triton X-100, the sections were incubated with the primary Ab MC1 (1:1,000) or AT100 (1:500) in PBS-0.2% Triton X-100 (1:1,000) overnight at 4°C. After three rinses in PBS-0.2% Triton X-100, labeling was amplified by incubation with anti-mouse biotinylated IgG (1:400 in PBS-0.2% Triton X-100, Vector Laboratories) for 60 min at RT. This was followed by a 120-min application of the avidin-biotin-HRP complex (ABC kit, 1:400 in PBS, Vector Laboratories) prior to the addition of diaminobenzidine tetrahydrochloride (Vector Laboratories) in Tris-HCl 0.2 mol/L (pH 7.6) containing 0.0015% H_2O_2 for visualization. Brain sections were then mounted, air-dried, dehydrated by passage through a graded series of alcohol (30%, 70%, 95%, 100%) and toluene baths, and finally mounted with VectaMount (Vector Laboratories). For the rats, 3 weeks after the BD-EV injections, they were deeply anesthetized and

transcardially perfused with 4% PFA. A series of one-in-six 30-μm-thick coronal sections were prepared and incubated at 4°C for 24 h in PBS containing 0.3% Triton X-100 with the following primary Abs: rabbit anti-NeuN and mouse anti-V5. After several rinses with PBS, the sections were incubated for 90 min at RT in a PBS solution containing a mixture of the appropriate secondary Abs: Alexa Fluor 488 and Alexa Fluor 555 mouse secondary Abs (1:500, Life Technologies). All of the sections were counterstained for 10 min with 4′,6-diamidino-2-phenylindole (DAPI; Merck; 1:5,000 dilution) to label the nuclei. IHC against V5/NeuN was followed by a final autofluorescence elimination step. To this end, autofluorescence eliminator reagent (EMD Millipore, 2160) was used, according to the manufacturer's instructions. Samples were mounted in Vectashield. Images were acquired (series of 50–75 multiple optical sections, z = 0.2 μm) with a Zeiss LSM 880 Quasar confocal system (×63 + ×4 numerical zoom) equipped with Airyscan.

Tau lesion quantification

For blinded quantification of MC1 and AT100 immunoreactivity, the CA1 region of the hippocampus was chosen as the quantification zone. We selected and quantified five brain sections covering the entire hippocampus (bregmas −2.30 to −2.8) and manually counted the number of MC1- or AT100-positive somas per brain section. Results are presented as the number of neurofibrillary tangles per brain section. Human brain sections were blindly quantified using QuPath 0.2.1 software for the full mirror image of the paraffin-embedded sections. Thresholds were established using a dedicated artificial intelligence algorithm (Artificial Neuronal Network; ANN_MLP) with identified objects on a set of slides, and these segmentation thresholds remained constant throughout the analyses. Results are expressed as a percentage of tau lesions ([AT8-positive pixels/total pixels] × 100).

Statistical analyses

Statistics and plots were generated using GraphPad Prism 8 software (version 8.0.0). The normality of the distributions was assessed graphically and using the Shapiro-Wilk test. In the case of a non-Gaussian distribution, the Mann-Whitney U test was used for one-to-one comparisons, and one-way non-parametric ANOVAs (Kruskal-Wallis) with a post hoc test were used for multiple comparisons. In the case of a Gaussian distribution, one-way ANOVAs with a post hoc test were used for multiple comparisons. Data are reported as the mean ± standard deviation (SD). Correlation analyses were performed using a non-parametric Spearman correlation test. The statistical tests adopted a two-tailed α level of 0.05.

SUPPLEMENTAL INFORMATION

Supplemental information can be found online at https://doi.org/10.1016/j.ymthe.2021.09.020.

ACKNOWLEDGMENTS

This work was supported by grants from the program Investissement d'Avenir LabEx (investing in the future laboratory excellence) DISTALZ (Development of Innovative Strategies for a Transdisciplinary Approach to Alzheimer's Disease), France Alzheimer, FONDATION ALZHEIMER (project EcTAUsome cohort), Fondation pour la Recherche Médicale, ANR grants (GRAND, TONIC), and by the PSP France Association. Our laboratories are also supported by LiCEND (Lille Centre of Excellence in Neurodegenerative Disorders), CNRS, Inserm, Métropole Européenne de Lille, University of Lille, I-SITE ULNE, Région Hauts de France, and FEDER. We are grateful to the Lille Neurobank and Prof. Claude-Alain Maurage for the access to the human brain samples. This study was also supported by a Synapsis Foundation fellowship awarded to K.R. and the Lausanne University Hospital (CHUV). The authors thank the Protein Analysis Facility of the University of Lausanne for technical support, in particular Dr. M. Quadroni. We also thank L. Culebras for help for circular graphical representation. We are grateful to the UMS-2014 US41 PLBS for access to the confocal microscopy and flow cytometry core facility platform at the HU site of the BioImaging Center Lille for help and for access to the cytometer. We thank Peter Davies for providing the MC1 antibody.

AUTHOR CONTRIBUTIONS

M.C. and L.B. designed and conceptualized the study, wrote the original draft, and then reviewed the manuscript. E.L, K.R., N.D., and N.T. helped with the manuscript editing; and E.L., R.P., R.C., S.L., T.B., S.B., V.D., A.L., S.S.-M., C.D., J.E., and K.R. performed the experiments.

DECLARATION OF INTERESTS

The authors declare no competing interests.

REFERENCES

1. Weingarten, M.D., Lockwood, A.H., Hwo, S.Y., and Kirschner, M.W. (1975). A protein factor essential for microtubule assembly. Proc. Natl. Acad. Sci. USA *72*, 1858–1862.

2. Spillantini, M.G., and Goedert, M. (2013). Tau pathology and neurodegeneration. Lancet Neurol. *12*, 609–622.

3. Colin, M., Dujardin, S., Schraen-Maschke, S., Meno-Tetang, G., Duyckaerts, C., Courade, J.P., and Buée, L. (2020). From the prion-like propagation hypothesis to therapeutic strategies of anti-tau immunotherapy. Acta Neuropathol. *139*, 3–25.

4. Falcon, B., Zhang, W., Schweighauser, M., Murzin, A.G., Vidal, R., Garringer, H.J., Ghetti, B., Scheres, S.H.W., and Goedert, M. (2018). Tau filaments from multiple cases of sporadic and inherited Alzheimer's disease adopt a common fold. Acta Neuropathol. *136*, 699–708.

5. Falcon, B., Zivanov, J., Zhang, W., Murzin, A.G., Garringer, H.J., Vidal, R., Crowther, R.A., Newell, K.L., Ghetti, B., Goedert, M., and Scheres, S.H.W. (2019). Novel tau filament fold in chronic traumatic encephalopathy encloses hydrophobic molecules. Nature *568*, 420–423.

6. Fitzpatrick, A.W.P., Falcon, B., He, S., Murzin, A.G., Murshudov, G., Garringer, H.J., Crowther, R.A., Ghetti, B., Goedert, M., and Scheres, S.H.W. (2017). Cryo-EM structures of tau filaments from Alzheimer's disease. Nature *547*, 185–190.

7. Duyckaerts, C., Bennecib, M., Grignon, Y., Uchihara, T., He, Y., Piette, F., and Hauw, J.J. (1997). Modeling the relation between neurofibrillary tangles and intellectual status. Neurobiol. Aging *18*, 267–273.

8. Braak, H., and Braak, E. (1991). Neuropathological stageing of Alzheimer-related changes. Acta Neuropathol. *82*, 239–259.

9. Delacourte, A., David, J.P., Sergeant, N., Buée, L., Wattez, A., Vermersch, P., Ghozali, F., Fallet-Bianco, C., Pasquier, F., Lebert, F., et al. (1999). The biochemical pathway of

neurofibrillary degeneration in aging and Alzheimer's disease. Neurology *52*, 1158–1165.

10. Verny, M., Duyckaerts, C., Agid, Y., and Hauw, J.J. (1996). The significance of cortical pathology in progressive supranuclear palsy. Clinico-pathological data in 10 cases. Brain *119*, 1123–1136.

11. Williams, D.R., Holton, J.L., Strand, C., Pittman, A., de Silva, R., Lees, A.J., and Revesz, T. (2007). Pathological tau burden and distribution distinguishes progressive supranuclear palsy-parkinsonism from Richardson's syndrome. Brain *130*, 1566–1576.

12. Saito, Y., Ruberu, N.N., Sawabe, M., Arai, T., Tanaka, N., Kakuta, Y., Yamanouchi, H., and Murayama, S. (2004). Staging of argyrophilic grains: An age-associated tauopathy. J. Neuropathol. Exp. Neurol. *63*, 911–918.

13. Irwin, D.J., Brettschneider, J., McMillan, C.T., Cooper, F., Olm, C., Arnold, S.E., Van Deerlin, V.M., Seeley, W.W., Miller, B.L., Lee, E.B., et al. (2016). Deep clinical and neuropathological phenotyping of Pick disease. Ann. Neurol. *79*, 272–287.

14. Sotiropoulos, I., Galas, M.C., Silva, J.M., Skoulakis, E., Wegmann, S., Maina, M.B., Blum, D., Sayas, C.L., Mandelkow, E.M., Mandelkow, E., et al. (2017). Atypical, non-standard functions of the microtubule associated Tau protein. Acta Neuropathol. Commun. *5*, 91.

15. Fontaine, S.N., Zheng, D., Sabbagh, J.J., Martin, M.D., Chaput, D., Darling, A., Trotter, J.H., Stothert, A.R., Nordhues, B.A., Lussier, A., et al. (2016). DnaJ/Hsc70 chaperone complexes control the extracellular release of neurodegenerative-associated proteins. EMBO J. *35*, 1537–1549.

16. Kang, S., Son, S.M., Baik, S.H., Yang, J., and Mook-Jung, I. (2019). Autophagy-mediated secretory pathway is responsible for both normal and pathological tau in neurons. J. Alzheimers Dis. *70*, 667–680.

17. Katsinelos, T., Zeitler, M., Dimou, E., Karakatsani, A., Müller, H.M., Nachman, E., Steringer, J.P., Ruiz de Almodovar, C., Nickel, W., and Jahn, T.R. (2018). Unconventional secretion mediates the trans-cellular spreading of tau. Cell Rep. *23*, 2039–2055.

18. Lee, J., and Ye, Y. (2018). The roles of endo-lysosomes in unconventional protein secretion. Cells *7*, 198.

19. Merezhko, M., Brunello, C.A., Yan, X., Vihinen, H., Jokitalo, E., Uronen, R.L., and Huttunen, H.J. (2018). Secretion of tau via an unconventional non-vesicular mechanism. cell rep. *25*, 2027–2035.e4.

20. Mohamed, N.V., Desjardins, A., and Leclerc, N. (2017). Tau secretion is correlated to an increase of Golgi dynamics. PLoS ONE *12*, e0178288.

21. Pooler, A.M., Phillips, E.C., Lau, D.H., Noble, W., and Hanger, D.P. (2013). Physiological release of endogenous tau is stimulated by neuronal activity. EMBO Rep. *14*, 389–394.

22. Rodriguez, L., Mohamed, N.V., Desjardins, A., Lippé, R., Fon, E.A., and Leclerc, N. (2017). Rab7A regulates tau secretion. J. Neurochem. *141*, 592–605.

23. Sato, C., Barthélemy, N.R., Mawuenyega, K.G., Patterson, B.W., Gordon, B.A., Jockel-Balsarotti, J., Sullivan, M., Crisp, M.J., Kasten, T., Kirmess, K.M., et al. (2018). Tau kinetics in neurons and the human central nervous system. Neuron *97*, 1284–1298.e7.

24. Sayas, C.L., Medina, M., Cuadros, R., Ollá, I., Garcia, E., Pérez, M., Ferrer, I., Hernández, F., and Avila, J. (2019). Role of tau N-terminal motif in the secretion of human tau by End Binding proteins. PLoS ONE *14*, e0210864.

25. Tang, Z., Ioja, E., Bereczki, E., Hultenby, K., Li, C., Guan, Z., Winblad, B., and Pei, J.J. (2015). mTor mediates tau localization and secretion: Implication for Alzheimer's disease. Biochim. Biophys. Acta *1853*, 1646–1657.

26. Pérez, M., Avila, J., and Hernández, F. (2019). Propagation of tau via extracellular vesicles. Front. Neurosci. *13*, 698.

27. van Niel, G., D'Angelo, G., and Raposo, G. (2018). Shedding light on the cell biology of extracellular vesicles. Nat. Rev. Mol. Cell Biol. *19*, 213–228.

28. Maas, S.L.N., Breakefield, X.O., and Weaver, A.M. (2017). Extracellular vesicles: Unique intercellular delivery vehicles. Trends Cell Biol. *27*, 172–188.

29. Pernègre, C., Duquette, A., and Leclerc, N. (2019). Tau secretion: Good and bad for neurons. Front. Neurosci. *13*, 649.

30. Wang, Y.P., Biernat, J., Pickhardt, M., Mandelkow, E., and Mandelkow, E.M. (2007). Stepwise proteolysis liberates tau fragments that nucleate the Alzheimer-like aggregation of full-length tau in a neuronal cell model. Proc. Natl. Acad. Sci. USA *104*, 10252–10257.

31. Ruan, Z., Pathak, D., Venkatesan Kalavai, S., Yoshii-Kitahara, A., Muraoka, S., Bhatt, N., Takamatsu-Yukawa, K., Hu, J., Wang, Y., Hersh, S., et al. (2021). Alzheimer's disease brain-derived extracellular vesicles spread tau pathology in interneurons. Brain *144*, 288–309.

32. Polanco, J.C., Hand, G.R., Briner, A., Li, C., and Götz, J. (2021). Exosomes induce endolysosomal permeabilization as a gateway by which exosomal tau seeds escape into the cytosol. Acta Neuropathol. *141*, 235–256.

33. Sanders, D.W., Kaufman, S.K., DeVos, S.L., Sharma, A.M., Mirbaha, H., Li, A., Barker, S.J., Foley, A.C., Thorpe, J.R., Serpell, L.C., et al. (2014). Distinct tau prion strains propagate in cells and mice and define different tauopathies. Neuron *82*, 1271–1288.

34. Dujardin, S., Commins, C., Lathuiliere, A., Beerepoot, P., Fernandes, A.R., Kamath, T.V., De Los Santos, M.B., Klickstein, N., Corjuc, D.L., Corjuc, B.T., et al. (2020). Tau molecular diversity contributes to clinical heterogeneity in Alzheimer's disease. Nat. Med. *26*, 1256–1263.

35. Saman, S., Kim, W., Raya, M., Visnick, Y., Miro, S., Saman, S., Jackson, B., McKee, A.C., Alvarez, V.E., Lee, N.C., and Hall, G.F. (2012). Exosome-associated tau is secreted in tauopathy models and is selectively phosphorylated in cerebrospinal fluid in early Alzheimer disease. J. Biol. Chem. *287*, 3842–3849.

36. Spitzer, P., Mulzer, L.M., Oberstein, T.J., Munoz, L.E., Lewczuk, P., Kornhuber, J., Herrmann, M., and Maler, J.M. (2019). Microvesicles from cerebrospinal fluid of patients with Alzheimer's disease display reduced concentrations of tau and APP protein. Sci. Rep. *9*, 7089.

37. Muraoka, S., DeLeo, A.M., Sethi, M.K., Yukawa-Takamatsu, K., Yang, Z., Ko, J., Hogan, J.D., Ruan, Z., You, Y., Wang, Y., et al. (2020). Proteomic and biological profiling of extracellular vesicles from Alzheimer's disease human brain tissues. Alzheimers Dement. *16*, 896–907.

38. Fiandaca, M.S., Kapogiannis, D., Mapstone, M., Boxer, A., Eitan, E., Schwartz, J.B., Abner, E.L., Petersen, R.C., Federoff, H.J., Miller, B.L., and Goetzl, E.J. (2015). Identification of preclinical Alzheimer's disease by a profile of pathogenic proteins in neurally derived blood exosomes: A case-control study. Alzheimers Dement. *11*, 600–607.e1.

39. Guix, F.X., Corbett, G.T., Cha, D.J., Mustapic, M., Liu, W., Mengel, D., Chen, Z., Aikawa, E., Young-Pearse, T., Kapogiannis, D., et al. (2018). Detection of aggregation-competent tau in neuron-derived extracellular vesicles. Int. J. Mol. Sci. *19*, 663.

40. Jia, L., Qiu, Q., Zhang, H., Chu, L., Du, Y., Zhang, J., Zhou, C., Liang, F., Shi, S., Wang, S., et al. (2019). Concordance between the assessment of Aβ42, T-tau, and P-T181-tau in peripheral blood neuronal-derived exosomes and cerebrospinal fluid. Alzheimers Dement. *15*, 1071–1080.

41. Mustapic, M., Eitan, E., Werner, J.K., Jr., Berkowitz, S.T., Lazaropoulos, M.P., Tran, J., Goetzl, E.J., and Kapogiannis, D. (2017). Plasma extracellular vesicles enriched for neuronal origin: A potential window into brain pathologic processes. Front. Neurosci. *11*, 278.

42. Perrotte, M., Haddad, M., Le Page, A., Frost, E.H., Fulöp, T., and Ramassamy, C. (2020). Profile of pathogenic proteins in total circulating extracellular vesicles in mild cognitive impairment and during the progression of Alzheimer's disease. Neurobiol. Aging *86*, 102–111.

43. Winston, C.N., Goetzl, E.J., Akers, J.C., Carter, B.S., Rockenstein, E.M., Galasko, D., Masliah, E., and Rissman, R.A. (2016). Prediction of conversion from mild cognitive impairment to dementia with neuronally derived blood exosome protein profile. Alzheimers Dement. (Amst.) *3*, 63–72.

44. Leroy, K., Bretteville, A., Schindowski, K., Gilissen, E., Authelet, M., De Decker, R., Yilmaz, Z., Buée, L., and Brion, J.P. (2007). Early axonopathy preceding neurofibrillary tangles in mutant tau transgenic mice. Am. J. Pathol. *171*, 976–992.

45. Schindowski, K., Bretteville, A., Leroy, K., Bégard, S., Brion, J.P., Hamdane, M., and Buée, L. (2006). Alzheimer's disease-like tau neuropathology leads to memory deficits and loss of functional synapses in a novel mutated tau transgenic mouse without any motor deficits. Am. J. Pathol. *169*, 599–616.

46. Polanco, J.C., Scicluna, B.J., Hill, A.F., and Götz, J. (2016). Extracellular vesicles isolated from the brains of rTg4510 mice seed tau protein aggregation in a threshold-dependent manner. J. Biol. Chem. *291*, 12445–12466.

47. Böing, A.N., van der Pol, E., Grootemaat, A.E., Coumans, F.A., Sturk, A., and Nieuwland, R. (2014). Single-step isolation of extracellular vesicles by size-exclusion chromatography. J. Extracell. Vesicles *3*, 1.

48. Théry, C., Witwer, K.W., Aikawa, E., Alcaraz, M.J., Anderson, J.D., Andriantsitohaina, R., Antoniou, A., Arab, T., Archer, F., Atkin-Smith, G.K., et al. (2018). Minimal information for studies of extracellular vesicles 2018 (MISEV2018): A position statement of the International Society for Extracellular Vesicles and update of the MISEV2014 guidelines. J. Extracell. Vesicles *7*, 1535750.

49. Jankowsky, J.L., Slunt, H.H., Ratovitski, T., Jenkins, N.A., Copeland, N.G., and Borchelt, D.R. (2001). Co-expression of multiple transgenes in mouse CNS: A comparison of strategies. Biomol. Eng. *17*, 157–165.

50. Jeganathan, S., Hascher, A., Chinnathambi, S., Biernat, J., Mandelkow, E.M., and Mandelkow, E. (2008). Proline-directed pseudo-phosphorylation at AT8 and PHF1 epitopes induces a compaction of the paperclip folding of Tau and generates a pathological (MC-1) conformation. J. Biol. Chem. *283*, 32066–32076.

51. Allen, B., Ingram, E., Takao, M., Smith, M.J., Jakes, R., Virdee, K., Yoshida, H., Holzer, M., Craxton, M., Emson, P.C., et al. (2002). Abundant tau filaments and nonapoptotic neurodegeneration in transgenic mice expressing human P301S tau protein. J. Neurosci. *22*, 9340–9351.

52. Holmes, B.B., Furman, J.L., Mahan, T.E., Yamasaki, T.R., Mirbaha, H., Eades, W.C., Belaygorod, L., Cairns, N.J., Holtzman, D.M., and Diamond, M.I. (2014). Proteopathic tau seeding predicts tauopathy in vivo. Proc. Natl. Acad. Sci. USA *111*, E4376–E4385.

53. Albert, M., Mairet-Coello, G., Danis, C., Lieger, S., Caillierez, R., Carrier, S., Skrobala, E., Landrieu, I., Michel, A., Schmitt, M., et al. (2019). Prevention of tau seeding and propagation by immunotherapy with a central tau epitope antibody. Brain *142*, 1736–1750.

54. Polanco, J.C., Li, C., Durisic, N., Sullivan, R., and Götz, J. (2018). Exosomes taken up by neurons hijack the endosomal pathway to spread to interconnected neurons. Acta Neuropathol. Commun. *6*, 10.

55. Winston, C.N., Aulston, B., Rockenstein, E.M., Adame, A., Prikhodko, O., Dave, K.N., Mishra, P., Rissman, R.A., and Yuan, S.H. (2019). Neuronal exosome-derived human tau is toxic to recipient mouse neurons in vivo. J. Alzheimers Dis. *67*, 541–553.

56. Wang, Y., Balaji, V., Kaniyappan, S., Krüger, L., Irsen, S., Tepper, K., Chandupatla, R., Maetzler, W., Schneider, A., Mandelkow, E., and Mandelkow, E.M. (2017). The release and trans-synaptic transmission of Tau via exosomes. Mol. Neurodegener. *12*, 5.

57. Kaufman, S.K., Sanders, D.W., Thomas, T.L., Ruchinskas, A.J., Vaquer-Alicea, J., Sharma, A.M., Miller, T.M., and Diamond, M.I. (2016). Tau prion strains dictate patterns of cell pathology, progression rate, and regional vulnerability in vivo. Neuron *92*, 796–812.

58. Buée Scherrer, V., Hof, P.R., Buée, L., Leveugle, B., Vermersch, P., Perl, D.P., Olanow, C.W., and Delacourte, A. (1996). Hyperphosphorylated tau proteins differentiate corticobasal degeneration and Pick's disease. Acta Neuropathol. *91*, 351–359.

59. Hof, P.R., Bouras, C., Perl, D.P., and Morrison, J.H. (1994). Quantitative neuropathologic analysis of Pick's disease cases: Cortical distribution of Pick bodies and coexistence with Alzheimer's disease. Acta Neuropathol. *87*, 115–124.

60. Forrest, S.L., Kril, J.J., Stevens, C.H., Kwok, J.B., Hallupp, M., Kim, W.S., Huang, Y., McGinley, C.V., Werka, H., Kiernan, M.C., et al. (2018). Retiring the term FTDP-17 as *MAPT* mutations are genetic forms of sporadic frontotemporal tauopathies. Brain *141*, 521–534.

61. Delacourte, A., Sergeant, N., Wattez, A., Gauvreau, D., and Robitaille, Y. (1998). Vulnerable neuronal subsets in Alzheimer's and Pick's disease are distinguished by their tau isoform distribution and phosphorylation. Ann. Neurol. *43*, 193–204.

62. Mailliot, C., Sergeant, N., Bussière, T., Caillet-Boudin, M.L., Delacourte, A., and Buée, L. (1998). Phosphorylation of specific sets of tau isoforms reflects different neurofibrillary degeneration processes. FEBS Lett. *433*, 201–204.

63. Chaunu, M.P., Deramecourt, V., Buée-Scherrer, V., Le Ber, I., Brice, A., Ehrle, N., El Hachimi, K., Pluot, M., Maurage, C.A., Bakchine, S., and Buée, L. (2013). Juvenile frontotemporal dementia with parkinsonism associated with tau mutation G389R. J. Alzheimers Dis. *37*, 769–776.

64. Deramecourt, V., Lebert, F., Maurage, C.A., Fernandez-Gomez, F.J., Dujardin, S., Colin, M., Sergeant, N., Buée-Scherrer, V., Clot, F., Ber, I.L., et al. (2012). Clinical, neuropathological, and biochemical characterization of the novel tau mutation P332S. J. Alzheimers Dis. *31*, 741–749.

65. Buée, L., Bussière, T., Buée-Scherrer, V., Delacourte, A., and Hof, P.R. (2000). Tau protein isoforms, phosphorylation and role in neurodegenerative disorders. Brain Res. Brain Res. Rev. *33*, 95–130.

66. Richetin, K., Steullet, P., Pachoud, M., Perbet, R., Parietti, E., Maheswaran, M., Eddarkaoui, S., Bégard, S., Pythoud, C., Rey, M., et al. (2020). Tau accumulation in astrocytes of the dentate gyrus induces neuronal dysfunction and memory deficits in Alzheimer's disease. Nat. Neurosci. *23*, 1567–1579.

67. Dujardin, S., Bégard, S., Caillierez, R., Lachaud, C., Carrier, S., Lieger, S., Gonzalez, J.A., Deramecourt, V., Déglon, N., Maurage, C.A., et al. (2018). Different tau species lead to heterogeneous tau pathology propagation and misfolding. Acta Neuropathol. Commun. *6*, 132.

68. Sealey, M.A., Vourkou, E., Cowan, C.M., Bossing, T., Quraishe, S., Grammenoudi, S., Skoulakis, E.M.C., and Mudher, A. (2017). Distinct phenotypes of three-repeat and four-repeat human tau in a transgenic model of tauopathy. Neurobiol. Dis. *105*, 74–83.

69. Xu, C., Guo, J., Li, L., Wang, X., Zhou, Q., Sun, D., Zhang, S., Li, S., Ye, J., Liu, Y., et al. (2020). Co-expression of three wild-type 3R-tau isoforms induces memory deficit via oxidation-related DNA damage and cell death: A promising model for tauopathies. J. Alzheimers Dis. *73*, 1105–1123.

70. Rösler, M., Retz, W., Retz-Junginger, P., and Dennler, H.J. (1998). Effects of two-year treatment with the cholinesterase inhibitor rivastigmine on behavioural symptoms in Alzheimer's disease. Behav. Neurol. *11*, 211–216.

71. Jadhav, S., Avila, J., Schöll, M., Kovacs, G.G., Kövari, E., Skrabana, R., Evans, L.D., Kontsekova, E., Malawska, B., de Silva, R., et al. (2019). A walk through tau therapeutic strategies. Acta Neuropathol. Commun. *7*, 22.

72. Malia, T.J., Teplyakov, A., Ernst, R., Wu, S.J., Lacy, E.R., Liu, X., Vandermeeren, M., Mercken, M., Luo, J., Sweet, R.W., and Gilliland, G.L. (2016). Epitope mapping and structural basis for the recognition of phosphorylated tau by the anti-tau antibody AT8. Proteins *84*, 427–434.

73. Jicha, G.A., Bowser, R., Kazam, I.G., and Davies, P. (1997). Alz-50 and MC-1, a new monoclonal antibody raised to paired helical filaments, recognize conformational epitopes on recombinant tau. J. Neurosci. Res. *48*, 128–132.

74. Hoffmann, R., Lee, V.M., Leight, S., Varga, I., and Otvos, L., Jr. (1997). Unique Alzheimer's disease paired helical filament specific epitopes involve double phosphorylation at specific sites. Biochemistry *36*, 8114–8124.

75. Zheng-Fischhöfer, Q., Biernat, J., Mandelkow, E.M., Illenberger, S., Godemann, R., and Mandelkow, E. (1998). Sequential phosphorylation of Tau by glycogen synthase kinase-3beta and protein kinase A at Thr212 and Ser214 generates the Alzheimer-specific epitope of antibody AT100 and requires a paired-helical-filament-like conformation. Eur. J. Biochem. *252*, 542–552.

76. Yoshida, H., and Goedert, M. (2006). Sequential phosphorylation of tau protein by cAMP-dependent protein kinase and SAPK4/p38δ or JNK2 in the presence of heparin generates the AT100 epitope. J. Neurochem. *99*, 154–164.

77. Galas, M.C., Dourlen, P., Bégard, S., Ando, K., Blum, D., Hamdane, M., and Buée, L. (2006). The peptidylprolyl *cis/trans*-isomerase Pin1 modulates stress-induced dephosphorylation of Tau in neurons. Implication in a pathological mechanism related to Alzheimer disease. J. Biol. Chem. *281*, 19296–19304.

78. Dujardin, S., Bégard, S., Caillierez, R., Lachaud, C., Delattre, L., Carrier, S., Loyens, A., Galas, M.C., Bousset, L., Melki, R., et al. (2014). Ectosomes: A new mechanism for non-exosomal secretion of tau protein. PLoS ONE *9*, e100760.

79. Hagel, L., Östberg, M., and Andersson, T. (1996). Apparent pore size distributions of chromatography media. J. Chromatogr. A *743*, 33–42.

80. Kulak, N.A., Pichler, G., Paron, I., Nagaraj, N., and Mann, M. (2014). Minimal, encapsulated proteomic-sample processing applied to copy-number estimation in eukaryotic cells. Nat. Methods *11*, 319–324.

81. Cox, J., and Mann, M. (2008). MaxQuant enables high peptide identification rates, individualized p.p.b.-range mass accuracies and proteome-wide protein quantification. Nat. Biotechnol. *26*, 1367–1372.

82. Cox, J., Neuhauser, N., Michalski, A., Scheltema, R.A., Olsen, J.V., and Mann, M. (2011). Andromeda: A peptide search engine integrated into the MaxQuant environment. J. Proteome Res. *10*, 1794–1805.

83. Baietti, M.F., Zhang, Z., Mortier, E., Melchior, A., Degeest, G., Geeraerts, A., Ivarsson, Y., Depoortere, F., Coomans, C., Vermeiren, E., et al. (2012). Syndecan-syntenin-ALIX regulates the biogenesis of exosomes. Nat. Cell Biol. *14*, 677–685.

84. Tyanova, S., Temu, T., Sinitcyn, P., Carlson, A., Hein, M.Y., Geiger, T., Mann, M., and Cox, J. (2016). The Perseus computational platform for comprehensive analysis of (prote)omics data. Nat. Methods *13*, 731–740.

85. Schwanhäusser, B., Busse, D., Li, N., Dittmar, G., Schuchhardt, J., Wolf, J., Chen, W., and Selbach, M. (2011). Global quantification of mammalian gene expression control. Nature *473*, 337–342.

86. d'Orange, M., Aurégan, G., Cheramy, D., Gaudin-Guérif, M., Lieger, S., Guillermier, M., Stimmer, L., Joséphine, C., Hérard, A.S., Gaillard, M.C., et al. (2018). Potentiating tangle formation reduces acute toxicity of soluble tau species in the rat. Brain *141*, 535–549.

Annex 3

cells

MDPI

Article

Tau Transfer via Extracellular Vesicles Disturbs the Astrocytic Mitochondrial System

Romain Perbet [1], Valentin Zufferey [2], Elodie Leroux [1], Enea Parietti [2], Jeanne Espourteille [2], Lucas Culebras [2], Sylvain Perriot [3], Renaud Du Pasquier [3], Séverine Bégard [1], Vincent Deramecourt [1], Nicole Déglon [4], Nicolas Toni [2], Luc Buée [1], Morvane Colin [1,*,†] and Kevin Richetin [2,*,†]

[1] Univ. Lille, Inserm, CHU Lille, LilNCog—Lille Neuroscience & Cognition, 59000 Lille, France; vincent.deramecourt@chu-lille.fr (V.D.)
[2] Department of Psychiatry, Center for Psychiatric Neurosciences, Lausanne University Hospital (CHUV) and University of Lausanne, 1011 Lausanne, Switzerland
[3] Laboratory of Neuroimmunology, Neuroscience Research Centre, Department of Clinical Neurosciences, CHUV, 1011 Lausanne, Switzerland
[4] Lausanne University Hospital (CHUV) and University of Lausanne, Neuroscience Research Center (CRN), Laboratory of Neurotherapies and Neuromodulation, 1011 Lausanne, Switzerland
* Correspondence: morvane.colin@inserm.fr (M.C.); kevin.richetin@chuv.ch (K.R.)
† These authors contributed equally to this work.

Abstract: Tauopathies are neurodegenerative disorders involving the accumulation of tau isoforms in cell subpopulations such as astrocytes. The origins of the 3R and 4R isoforms of tau that accumulate in astrocytes remain unclear. Extracellular vesicles (EVs) were isolated from primary neurons overexpressing 1N3R or 1N4R tau or from human brain extracts (progressive supranuclear palsy or Pick disease patients or controls) and characterized (electron microscopy, nanoparticle tracking analysis (NTA), proteomics). After the isolated EVs were added to primary astrocytes or human iPSC-derived astrocytes, tau transfer and mitochondrial system function were evaluated (ELISA, immunofluorescence, MitoTracker staining). We demonstrated that neurons in which 3R or 4R tau accumulated had the capacity to transfer tau to astrocytes and that EVs were essential for the propagation of both isoforms of tau. Treatment with tau-containing EVs disrupted the astrocytic mitochondrial system, altering mitochondrial morphology, dynamics, and redox state. Although similar levels of 3R and 4R tau were transferred, 3R tau-containing EVs were significantly more damaging to astrocytes than 4R tau-containing EVs. Moreover, EVs isolated from the brain fluid of patients with different tauopathies affected mitochondrial function in astrocytes derived from human iPSCs. Our data indicate that tau pathology spreads to surrounding astrocytes via EVs-mediated transfer and modifies their function.

Keywords: tauopathies; tau spreading; extracellular vesicles; astrocytes; mitochondria

Citation: Perbet, R.; Zufferey, V.; Leroux, E.; Parietti, E.; Espourteille, J.; Culebras, L.; Perriot, S.; Du Pasquier, R.; Bégard, S.; Deramecourt, V.; et al. Tau Transfer via Extracellular Vesicles Disturbs the Astrocytic Mitochondrial System. *Cells* **2023**, *12*, 985. https://doi.org/10.3390/cells12070985

Academic Editors: Anna Wilkaniec and Agata Adamczyk

Received: 15 February 2023
Revised: 8 March 2023
Accepted: 18 March 2023
Published: 23 March 2023

1. Introduction

Tauopathies are a group of more than 20 diseases that include Alzheimer's disease (AD), progressive supranuclear palsy (PSP), Pick disease (PiD), frontotemporal lobar degeneration and primary age-related tauopathy.

Although all tauopathies are associated with the accumulation of tau (predominantly in neurons), there are notable differences among them in terms of (1) the affected region, (2) the presence or absence of tau inclusions in glia, and (3) the tau isoform (3R/4R) that constitutes the observed inclusions/aggregates. Indeed, as a result of alternative splicing, six major isoforms of tau coexist in the human brain, each with a microtubule-binding region consisting of three (3R tau isoforms) or four (4R tau isoforms) repeated sequences [1,2]. In the healthy human brain, the 3R and 4R tau isoforms are present at equally low levels in glial cells [3–5]. However, analysis of patients' brains has revealed

that some tauopathies are exclusively associated with 3R or 4R tau inclusions, whereas others are associated with mixed tau inclusions [6]. Additionally, many studies have shown the presence of tau inclusions in glial cells, including astrocytes, oligodendrocytes, and microglia [7–10].

Furthermore, there is evidence of prion-like propagation of tau pathology, especially in AD [11]. This process involves neurons and affects glial cells [12]. While the origin of tau in these cells is not yet well defined, astrocytes are a particularly interesting possibility due to their function in the tripartite synapse [13]. Tau uptake and its role in the spread of tau pathology through astrocytes have become the focus of increasing attention [14]. De Gérando and collaborators showed that astrocytic tau pathology can emerge secondary to neuronal pathology [15]. It also appears that astrocytes can internalize tau fibrils, which are subsequently degraded by lysosomes, potentially contributing to reduced spread of tau [16]. The details of these tau species and how they are shuttled from neurons to astrocytes remain currently unknown.

Considering the importance of (1) tau propagation in interconnected regions and (2) the role of astrocytes in synaptic function, it is important to study the role of astrocytes in tau propagation and the underlying mechanisms involved. A few studies have investigated tau transfer between neurons and astrocytes in cell and animal models [15,16], but the cellular mechanisms underlying this exchange of material have not been explored, and no data from human samples are available. Cells exchange material with their neighbors in various ways, and these intercellular communications are fundamental to maintaining tissue homeostasis, which is often dysregulated in patients with disease. Extracellular vesicles (EVs) have emerged as critical cell-to-cell communication regulators under physiological conditions and in disorders such as neurodegenerative diseases [17,18]. They are secreted by cells through unconventional protein secretion [19] and shuttle many components, such as nucleic acids, lipids, active metabolites, and cytosolic and cell surface proteins [20]. Due to their membrane composition, they can act as unique intercellular delivery vehicles for the transfer of pathological species between cells, thereby allowing the propagation of tau pathology.

We and others recently demonstrated that EVs isolated from AD brain-derived fluids (BDFs) play a role in the spread of human tau [21,22]. Although tau has been detected in exosomes isolated from primary astrocyte cultures [23], their involvement in tau propagation is still debated. Other researchers using in animal models have suggested that tau is mainly found in exosomes derived from microglia [9]. Whether tau accumulation in astrocytes is beneficial or deleterious to the astrocytes remains also to be confirmed. We recently observed complex topographic patterns of tau isoforms and accumulation of amyloid-β in the hippocampi of AD patients. We showed that the accumulation of 3R tau (but not phospho-4R tau) in astrocytes is exacerbated by amyloid-β accumulation and impairs mitochondrial function and ATP production, thus inducing a reduction in the number of inhibitory neurons in the hippocampus, which is associated with memory decline [24]. However, the mechanism of 3R and 4R tau accumulation and their origin in hippocampal astrocytes remain poorly understood. We considered whether EV-mediated transfer of 3R/4R tau might underlie tau accumulation in astrocytes and consequent astrocyte dysfunction. In the present work, we demonstrate that (1) 3R and 4R tau are transferred from neurons to astrocytes; (2) neuronal tau is mainly secreted in the free form, while tau isoforms are shuttled from neurons to astrocytes mainly through EVs (large EVs); and (3) EV-mediated tau accumulation, especially 3R tau accumulation, in astrocytes alters mitochondrial function.

2. Materials and Methods

2.1. Human Samples

Prefrontal brain extracts from non-demented control subjects (n = 5), PSP (n = 5), and PiD (n = 5) patients were obtained from the Lille Neurobank (fulfilling French legal requirements concerning biological resources and declared to the competent authority

under number DC-2008-642); donor consent and ethics committee approval were obtained, and the data were protected. The samples were managed by the CRB/CIC1403 Biobank, BB-0033-00030. The demographic data are listed in Table 1.

Table 1. Demographic, biological, and clinical characteristics of the brain sample donors. The characteristics of the donors who provided brain samples used for BDF isolation are listed (n = 5 non-demented control subjects, n = 5 PSP patients, and n = 5 PiD patients). PMD, postmortem delay; NFTs, neurofibrillary tangles; GFTs, glial fibrillary tangles; NA, not applicable. Braak and Thal stages are the two hallmarks of Alzheimer's disease. These stages are used here to categorize NFT or amyloid β peptide (Aβ) deposition, respectively, and are classified in stages I to VI for NFT [25] and 1 to 5 for Aβ deposits [26]).

Diagnosis	Gender	Death (y)	PMD (h)	Tau Lesions	Braak	Thal	Cause of Death
Control	M	78	19	None	0	0	Invasive aspergillosis
	F	82	NA	None	I	1	Pericarditis
	M	23	24	None	0	0	Myocarditis
	M	59	13	None	0	0	Septic shock
	M	41	11	None	0	0	Suffocation
PSP	M	74	9	NFT and GFT	0	1	
	M	90	36	NFT and GFT	0	2	
	M	88	3	NFT and GFT	0	4	
	M	69	17	NFT and GFT	0	0	
	F	79	4	NFT and GFT	0	0	
PiD	M	57	22	Pick bodies	NA	0	
	M	71	21	Pick bodies	NA	3	
	F	78	11	Pick bodies and NFT	NA	0	
	M	68	15	Pick bodies	NA	0	
	M	68	8	Pick bodies	NA	0	

2.2. Rat Primary Neuron and Astrocyte Cultures

Primary hippocampal neurons were prepared from 17-day-old Wistar rat embryos, as previously described [27]. Five days later, the cells were infected with a lentiviral vector (LV) encoding human 1N4R-V5 or 1N3R-V5 (PGK-4R-V5-SIN, PGK-3R-V5-SIN), as previously described [28]. The LVs were produced and validated according to established protocol [29,30].

Primary hippocampal astrocytes were isolated from postnatal day 1 rat pups (Wistar rats from Janvier Laboratory), as previously described [31]. Briefly, the brains were removed aseptically from the skulls, the meninges were excised under a dissecting microscope, and the hippocampus was dissected. The cells were dissociated by passage through needles of decreasing gauge (1.1 × 40; 0.8 × 40; and 0.5 × 16) 4 or 5 times with a 5-mL syringe. The cells were plated at a density of 20,000 cells per cm^2 in 6-well plates in DMEM containing 25 mM glucose and supplemented with 10% fetal calf serum, 44 mM $NaHCO_3$, and 10 mL/L antibiotic/antimycotic solution (pH 7.2) in a final volume of 3 mL/well, and incubated at 37 °C in an atmosphere containing 5% CO_2/95% air. The culture medium was replaced 4–5 days after plating and every 2–3 days thereafter, after gently tapping the plates to remove the less adherent cells (oligodendrocytes and microglia). For the neuron-to-astrocyte tau transfer experiment, 10^5 astrocytes (1 well) were treated with 10 µL of neuron-derived small EVs (ND-SEVs), neuron-derived large EVs (ND-LEVs),

and neuron-derived free protein (ND-FFP) (obtained from 10^6 neurons, 1 well) at 10 days in vitro (D.I.V. 10).

For the microfluidic experiment, astrocytes plated in 6-well plates were detached with trypsin at D.I.V. 10 and plated in the axonal compartment. To monitor the effects of tau accumulation in astrocytes on astrocytic mitochondria, cells were infected with an LV-encoding MitoTimer (LV-G1-MitoTimer-miR124T) at D.I.V. 7–8, as previously described [28].

2.3. Human iPSC-Derived Astrocyte Culture

Human iPSCs were differentiated into astrocytes, as previously described in detail [32]. Briefly, human iPSCs were plated onto poly-L-ornithine/laminin (PO/L)-coated plates and cultured in neural induction medium (DMEM/F-12 supplemented with N2 supplement (1×), B27 supplement without vitamin A (1×), noggin (500 ng/mL), SB431542 (20 µM), and FGF2 (4 ng/mL)) to allow the formation of embryoid bodies. The medium was changed every other day for 12 days. After 12 days, neural precursor cells (NPCs) were passaged and grown for at least 3 weeks in single-cell culture in NPC expansion medium (DMEM/F-12 supplemented with N2 supplement (1×), B27 supplement without vitamin A (1×), FGF2 (10 ng/mL), and EGF (10 ng/mL)). Then, the medium was replaced with astrocyte induction medium (DMEM/F-12 supplemented with N2 supplement (1×), B27 supplement without vitamin A (1×), LIF (10 ng/mL), and EGF (10 ng/mL)). The medium was changed every other day, and the cells were passaged when they reached confluence. After 2 weeks, the medium was replaced with astrocyte medium (DMEM/F-12 supplemented with B27 supplement without vitamin A) supplemented with CNTF (20 ng/mL). After culture for 4 weeks in this medium, the cells displayed the cellular characteristics of mature human astrocytes [33]. Then, the astrocytes were infected with an LV-encoding MitoTimer (LV-G1-MitoTimer-miR124T). Four days later, the astrocytes were treated with 10 µL of BDF-LEVs (10^6 EVs per astrocyte), and mitochondrial system function and dynamics were evaluated. The dose of EVs was selected based on a cell toxicity experiment (the number of DAPI-stained cells remaining 24 h after treatment was counted and normalized with the control); in this experiment, no toxicity was observed at this dose (Figure S1). These experiments were performed according to a protocol approved by our institutional review committee (approval n° CER-VD 2018-01622).

2.4. Microfluidic System and Immunofluorescence

Glass coverslips were coated overnight at 4 °C with 0.5 mg/mL poly-D-lysine. Microfluidic chambers (AXIS™, Temecula, CA, USA) were subsequently placed on the coated glass coverslips and attached to the glass. All chambers had microgrooves 450 µm in length and 10 µm in width. Rat primary embryonic neurons were cultured as described above, and approximately 30,000 cells were plated in the two wells of the somatodendritic compartment. The cultures were maintained at 37 °C for 7 days to allow differentiation, with a volume gradient from the somatodendritic compartment to the astrocytic compartment to assist with axonal guidance. At D.I.V. 7, Tau-V5-LV (200 ng of LV per well) was added to the somatodendritic compartment after first reversing the volume gradient between the compartments to counteract viral diffusion. The quality controls for compartment isolation were as previously described by Dujardin and collaborators [28]. Primary astrocytes were then plated in the axonal compartment in neurobasal medium and maintained at 37 °C for 5 days. V5 immunolabeling was performed to evaluate tau transfer from neurons to astrocytes. The cells in the compartments (somatodendritic and axonal) were washed once with phosphate-buffered saline (PBS) and fixed with 4% paraformaldehyde (PFA) for 20 min. After removing the fixative, the cells were washed three more times with 50 mM NH4Cl and permeabilized with Triton X-100 (0.1%, 10 min at room temperature). Subsequently, the slides were incubated with primary antibodies at 4 °C overnight, and labeling was performed by incubation with the appropriate Alexa Fluor conjugated secondary antibodies (1:400) for 45 min at room temperature. The cells were mounted with Vectashield medium containing DAPI.

2.5. EVs Isolation from Primary Cultures

Neuron media (10×10^6; 10 wells) were collected and placed on ice 10 days after LV infection. Protease inhibitors were added before centrifugation for 10 min at 2000× *g* and 4 °C. The supernatant was centrifuged for 50 min at 20,000× *g*, and the pellet, which contained ND-LEVs, was collected. The supernatant was then centrifuged for 50 min at 100,000× *g* to obtain ND-SEVs (pellet) and FFP (supernatant). ND-LEVs and ND-SEVs were suspended in 100 µL 100 µL of 4% PFA (diluted in phosphate buffer (0.08 M Na_2HPO_4 and 0.02 M NaH_2PO_4)) for electron microscopy analyses or 100 µL of phosphate buffer (0.08 M Na_2HPO_4 and 0.02 M NaH_2PO_4) for astrocyte treatment. The FFP was concentrated to a volume of 100 µL using an Amicon device (3 kDa).

2.6. EV Isolation from Human Prefrontal Cortex Tissue

BDF-EVs were isolated from human prefrontal cortex tissue as previously described [22,34]. The fluid was a suspension obtained by gentle papain digestion of brain extract and not a directly collected fluid sample. Briefly, the tissue was incubated on ice in 5 mL of Hibernate-A. It was gently mixed in a Potter homogenizer, and 2 mL of 20 units/mL papain in Hibernate-A was added to the homogenate for 20 min at 37 °C with agitation. Then, 15 mL of cold Hibernate-A buffer (50 mM NaF, 200 nM Na_3VO_4, 10 nM protease inhibitor) was added, and the sample was mixed by pipetting to stop the enzymatic activity. Successive centrifugation was performed at 4 °C (300, 2000, and 10,000× *g*) to remove cells, membranes, and debris, respectively. The final supernatant was kept at −80 °C until EV isolation was performed. BDF-LEVs and BDF-SEVs were pooled from 5 patients per group. Isolation of EVs from cell medium or human BDF was carried out using differential ultracentrifugation as previously described [35] to obtain LEV-, SEV- and FFP-enriched fractions. The final pellets were suspended in a final volume of 400 µL and kept at −80 °C.

2.7. Nanoparticle Tracking Analysis (NTA)

The size, number, and distribution of particles were determined using NTA (Nanosight NS300, Malvern, Cambridge, United Kingdom) as described previously [22]. To generate statistical data, five 90-s videos were recorded and analyzed using NTA software (camera level: 15; detection threshold: 4).

2.8. Electron Microscopy [22,35]

Samples (5 µL) were deposited on a carbon film-supported grid (400 mesh) and incubated at room temperature (RT) for 20 min. The grids were fixed in PBS-glutaraldehyde (1%) for 5 min at RT and then rinsed in distilled water. They were incubated for 5 min in 1% uranyl acetate and then for 10 min on ice in a mixture of 1% uranyl acetate/2% methylcellulose. Dry grids were observed under a transmission electron microscope (Zeiss EM900). When indicated, immunolabeling was performed. The grids were rinsed once in PBS and incubated twice (3 min at RT) in PBS-50 mM glycine before incubation in PBS-1% bovine serum albumin (BSA) for 10 min at RT. A primary antibody diluted in PBS-1% BSA was applied for 1 h at RT and detected using an appropriate secondary antibody diluted in PBS-1% BSA (18 nm gold colloidal goat anti-mouse). After rinsing in PBS, the grids were processed as described above.

2.9. Antibodies

The following antibodies were used for immunohistofluorescence and immunohistochemistry at the indicated dilutions: a polyclonal rabbit antibody against the C-terminus of Tau (C-Ter), which recognizes the last 15 AA of the protein (C-Ter, raised in house, 1:1000 for electronic microscopy) [36]; a mouse monoclonal antibody against V5 (1:10,000) that recognizes the V5 epitope of tagged tau [24,28]; and a polyclonal rabbit antibody that recognizes glial fibrillary acidic protein (GFAP) (1:10,000).

2.10. ELISA

Fractions were obtained after ultracentrifugation of culture medium or BDF as described above, and 10 µL were added to astrocytes. Tau levels were then determined using INNOTEST hTau Ag (Fujirebio/Innogenetics, Gent, Belgium), which is a sandwich ELISA microplate assay for the quantitative determination of human tau antigen levels in fluids, according to the manufacturer's instructions. The capture antibody was an AT120 antibody, and biotinylated HT7 and BT2 antibodies were used as detection antibodies [37]. For cell samples, we customized the INNOTEST hTau Ag ELISA kit to quantify Tau-V5 levels. The original INNOTEST kit plate was replaced with a 96-well MicroWell™ MaxiSorp™ flat bottom plate coated with V5 antibody (Invitrogen P/N-0705; 1:10,000) in carbonate buffer ($NaHCO_3$ 0.1 mM, Na_2CO_3 0.1 mM; pH = 9.6) overnight at 4 °C. The other steps were performed according to the manufacturer's instructions. Tau uptake by astrocytes was evaluated 24 h after incubation of astrocytes with ND-FFP and ND-LEV fractions from control neurons (NI) or neurons overexpressing 1N3R or 1N4R Tau-V5. Tau uptake efficiency was calculated with the following equation: % of tau uptake= [Quantity of tau in astrocytes x 100]/[Quantity of tau added to astrocytes].

2.11. Quantification of Tau-V5 Levels in Primary Culture

The optical density (OD) of Tau-V5 was measured in 5 regions of interest (ROI) in each compartment (somatodendritic compartment, microgrooves, and axonal compartment). The optical density in each region of interest was evaluated using Zen 2 image analysis software (blue edition). Each OD value was normalized by subtracting the OD in an ROI in which no Tau-V5 signal was present (NI). The OD of Tau-V5 in astrocytes was measured from confocal scanning images taken with a Zeiss LSM 710 Quasar microscope equipped with a 40× oil immersion objective at a z-axis resolution of 0.9 µm. We used Imaris software to measure the intensity of Tau-V5 in the reconstructed GFAP+ region of the axonal compartment.

2.12. Analysis of Mitochondrial Redox State, Morphology and Dynamics by MitoTimer

We recently developed a new lentiviral vector (LV-G1-MitoTimer-MiR124T, hereafter called LV-G1-MitoTimer) to study the dynamics and functions of mitochondria, specifically in astrocytes in vitro and in vivo. LV-G1-MitoTimer uses a truncated version of the glial fibrillary acidic protein (GFAP) promoter gfaABC1D, with a B3 enhancer (gfaABC1D(B3), hereafter called G1) combined with the previously described miR124T neuronal detargeting system. It allows exclusive expression of the mitochondrial biosensor in astrocytes in vitro and in vivo. MitoTimer is a mutant red fluorescent protein, drFP58317, with a mitochondrial signal from subunit VIII of human cytochrome c oxidase, capable of visualizing newly synthesized mitochondria in green (488 nm) and oxidized mitochondria in red (555 nm). The green (488 nm) and red (555 nm) fluorescence ratio enables simultaneous evaluation of individual mitochondria, their morphology analysis, fusion/fission events, and redox state history. This unique property can be applied to investigate many scientific questions regarding mitochondria's physiological and pathological roles, and is therefore very promising for unveiling the underlying mechanisms of mitochondrial dynamics within many different cell types [38,39]. Briefly, using an inverted microscope (Nikon Eclipse Ti-2, Melville, NY, USA) (150× magnification, 100× oil immersion objective, 1.5× intermediate magnification) and the Perfect Focus System (PFS), 16 bit image sequences (1 frame/s for 60 s) were taken at baseline (BL) and 6 h and 24 h after treatment with EVs. Sequential excitation at 490 nm (for the green channel) and 550 nm (for the red channel) and detection of green (500–540 nm) and red (550–600 nm) signals were carried out. Then, using GA3 software, we selected the first frame of each image sequence in the red and green channels to generate binary masks for each mitochondrion. The resulting segmentations were filtered by intensity and size to remove poor-quality objects, and by position within the region of interest (ROI) to remove objects truncated by the ROI boundary. We extracted statistics of individual mitochondria (masks) such as elongation factor (length to width)

and mitochondrial length, as well as the ratio of the average red (555 nm) to green (488 nm) intensity corresponding to the redoxstate ratio. We performed these analyses for at least 20–25 cells per condition (a minimum of fifty mitochondria per cell). Then, we considered mitochondria that could be tracked along the entire sequence length to analyze the mitochondrial dynamics. We extracted the following parameters for each reconstructed track: the total displacement (displacement) corresponding to the distance (um) between the track's beginning and end and the average speed (speed) in um/s. Analysis of the fusion and fission events was performed manually on identical images with the successive counts of objects normalized to the average number of mitochondria per image constructed from the previous images. This resulted in the estimation of the event rate per particle. The event rate can provide information on the activity of fusion and fission events, among the most critical mechanisms of mitochondrial dynamics. In addition, we calculated the number of branches for each reconstructed mitochondria, indicating the tendency of mitochondria to assemble and form complex structures observed in astrocytes. Nikon's NIS Element system was employed to manually track 25–50 mitochondria per cell. Finally, after log transformation, the change in score [39] relative to the BL was calculated and normalized to that of the control group (ND-LEVs-CFP for primary cultures and BDF-LEVs from human controls) [38].

2.13. Sample Sizes, Calculations and Statistical Analysis

Human samples were classified based on neurological and neuropathological examination. The order of culture and procedures was randomized for each experiment. Investigators were blinded to group allocation when processing the tissue and performing cell counts and during confocal image acquisition. Values are presented as the mean ± s.e.m.; N corresponds to the number of independent experiments, and n corresponds to the overall number of values. Statistical analyses of raw data were performed with GraphPad Prism software v8.0. The normality of the data was verified using the Shapiro-Wilk test. Differences between two experimental groups were analyzed using Student's *t* test (parametric test) or the Mann–Whitney test (nonparametric test). Statistical analyses of differences among more than two experimental groups were performed using one-way ANOVA followed by Dunn's post hoc analyses for multiple comparisons (parametric test) or the Kruskal–Wallis test (nonparametric test). For MitoTimer score change analysis, as previously described [38], we used two-way ANOVA followed by Tukey's post hoc analysis with time as the independent variable to compare the differences in mitochondrial function between the 3R and 4R tau groups. In addition, we used the Wilcoxon signed-rank test to compare each parameter measured at 6 h and 24 h with the baseline values for each astrocyte.

3. Results

3.1. 3R and 4R Tau Transfer from Neurons to Astrocytes

To study the origin of the accumulated 3R and 4R tau in astrocytes, we overexpressed human wild-type 1N3R and 1N4R tau (fused to a V5 tag) in primary hippocampal neuron cultures in a microfluidic system. Due to axonal growth in the microgrooves, the hippocampal neurons in the somatodendritic compartment (SD) were connected to a second chamber (axonal compartment, AX) containing primary astrocytes. 1N3R or 1N4R tau was overexpressed in the somatodendritic compartment using LVs (Figure 1A). Five days later (D.I.V. 12), immunochemistry for V5 revealed accumulation of 1N3R and 1N4R tau in the somatodendritic (containing soma and dendrites) compartment and axons in the microgrooves (Figure 1B). Both isoforms were overexpressed in neurons at similar levels (Figure 1C). Interestingly, we observed that a large population of astrocytes in the axonal compartment (identified by GFAP immunochemistry) exhibited Tau-V5 puncta in the cytoplasm (Figure 1B,D). Quantification of 1N3R and 1N4R tau inclusions in astrocytes through measurement of the V5 intensity in GFAP+ astrocytes indicated that both isoforms could be transferred from hippocampal neurons to astrocytes in similar degrees (Figure 1E).

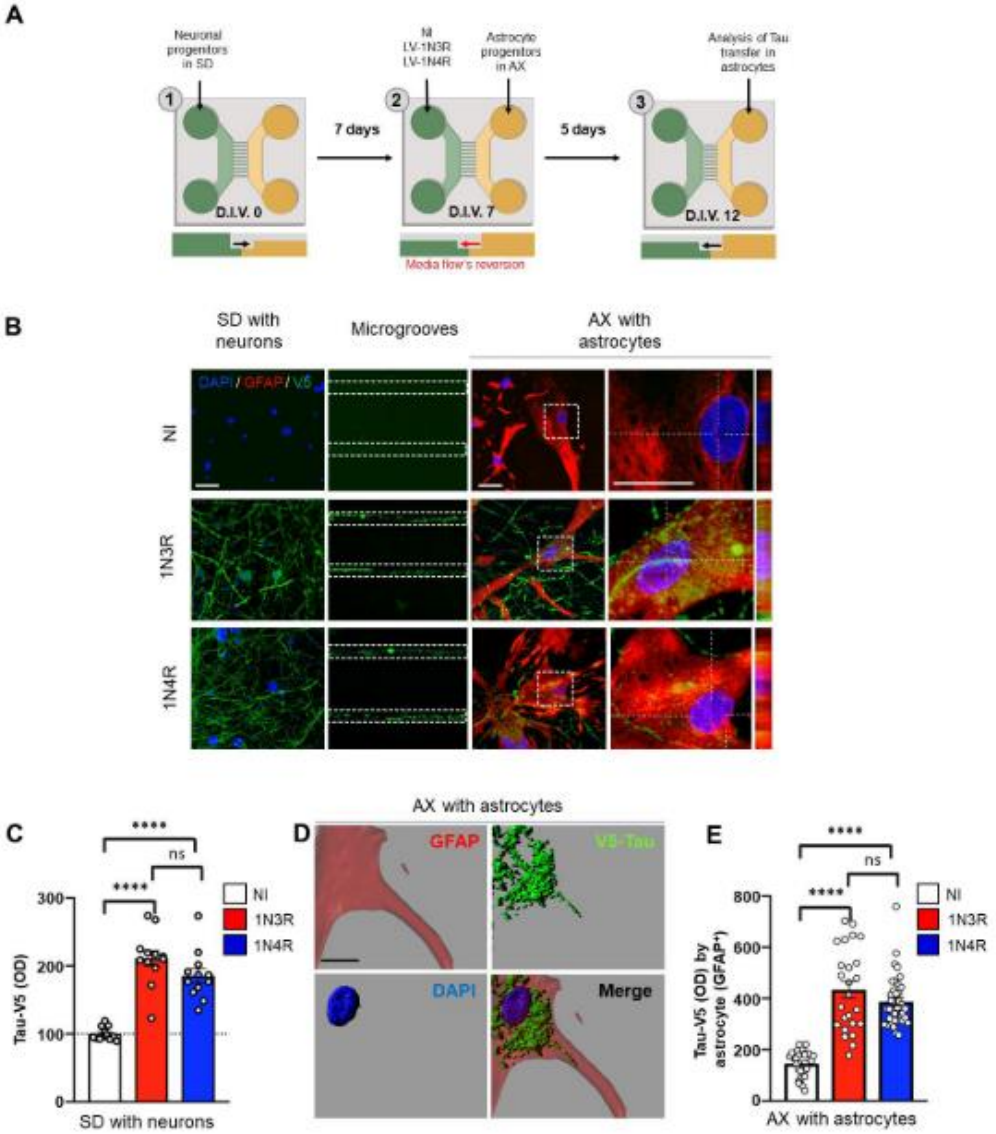

Figure 1. Tau is shuttled from neurons to astrocytes. (**A**) Schematic of the microfluidic system used to investigate tau transfer from hippocampal neurons to astrocytes. (**B**) Confocal micrographs showing 1N3R or 1N4R tau (V5+) and astrocytes (GFAP+) in the somatodendritic and axonal compartments and microgrooves. (**C**) Histogram showing the Tau-V5 optical density in the somatodendritic compartment. (**D**) 3D reconstruction of confocal micrographs showing tau (V5+) in an astrocyte (GFAP+) in the axonal compartment. (**E**) Histogram showing the number of Tau-V5 inclusions detected per astrocyte. The scale bars are 20 µm (**B**) and 5 µm (**D**). SD = somatodendritic compartment, AX = axonal compartment, LV = lentiviral vector, NI = noninfected. For (**C**,**E**), N = cultures/microfluidic chambers/cells: NI: 1/3/32, 1N3R: 1/3/25, 1N4R: 4/3/39. Ordinary one-way ANOVA with Sidak's multiple comparison test. (^{ns} $p > 0.05$, **** $p < 0.0001$).

3.2. Neuronal Tau Is Mainly Secreted in the Free Form

Transfer of tau to adjacent cells requires secretion by the donor cell. First, we assessed which form(s) of tau is (are) secreted by primary neurons. Culture media from primary neurons overexpressing 1N3R or 1N4R tau at similar levels (Figure 2A,B) were collected and fractioned to separate EVs from free proteins. EVs present in extracellular media are a heterogeneous population in which different biogenesis pathways are active. EVs include (1) exosomes (small vesicles, size < 150 nm), which are generated from multivesicular bodies containing intraluminal vesicles that are secreted into the extracellular fluid, and (2) ectosomes (large vesicles, size > 150 nm) that originate directly from budding at the plasma membrane [20]. To further investigate the EV subtypes that might be involved in tau transfer to astrocytes, we separated small from large vesicles as previously reported [35]. Fractions containing ND-LEVs, ND-SEVs, and ND-FFP were then collected and characterized. Electron microscopy (Figure 2C) and NTA (Figure 2D,E) confirmed that ND-SEVs and ND-LEVs with intact structures were present in our fractions. Totals of 26.3 ± 5.8% and 35 ± 18.7% ND-SEVs of size > 150 nm and 73.6 ± 5.8% and 65 ± 18.7% ND-SEVs of size between 10 and 150 nm were isolated from cells overexpressing 1N3R and 1N4R tau, respectively (Figure 2D). Totals of 71.3 ± 9.2% and 63.6 ± 13.8% ND-LEVs of size > 150 nm and 28.6 ± 9.2% and 36.3 ± 13.8% ND-LEVs of size between 10 and 150 nm were isolated from cells overexpressing 1N3R and 1N4R tau, respectively (Figure 2E). It should be noted that size repartition was not altered by the expression of different tau isoforms in neurons (Figure 2D,E nonsignificant difference between the 1N3R and 1N4R groups). The presence of tau in these fractions was detected by electron microscopy (Figure 2F), and tau levels were quantified by ELISA (Figure 2G). While a large majority (93% ± 0.2 and 93.3 ± 0.2 for 1N3R and 1N4R tau, respectively) of tau protein was found in the free form (ND-FFP), only 4.7% ± 0.3 of 1N3R tau and 4.5% ± 0.2 of 1N4R tau was found in the ND-LEV fractions (Figure 2G).

3.3. Tau Isoforms Are Shuttled from Neurons to Astrocytes Mainly by EVs

The three fractions were applied to rat hippocampal astrocyte cultures, and tau transfer was evaluated at 24 h (homemade ELISA Tau-V5 and immunofluorescence) (Figure 3A). The presence of 1N3R and 1N4R tau in astrocytes after ND-LEV treatment was detected by immunofluorescence with antibodies against the V5 epitope and GFAP (Figure 3B), and 1N3R and 1N4R tau levels in astrocytes were quantified by ELISA (Figure 3C). Although the vast majority of tau secreted by neurons was in the free form (Figure 2G), only the human 3R isoform was detected after treatment of astrocytes with ND-FFP. In contrast, among EVs, only ND-LEVs had the ability to deliver both human 1N3R and 1N4R tau to astrocytes (Figure 3C). We then considered whether tau in ND-LEVs is transferred from neurons to astrocytes more efficiently than in ND-FFP. We normalized the [Tau-V5] in astrocytes to the [Tau-V5] in the fractions applied to astrocytes and secreted by neurons (ND-FFP and ND-LEVs). The percentage of tau taken up by astrocytes was significantly different between the ND-FFP and ND-LEV groups, and tau accumulation was not significantly affected by the tau isoform (Figure 3D). Altogether, these results highlight the major role of LEVs in tau transfer between neurons and astrocytes.

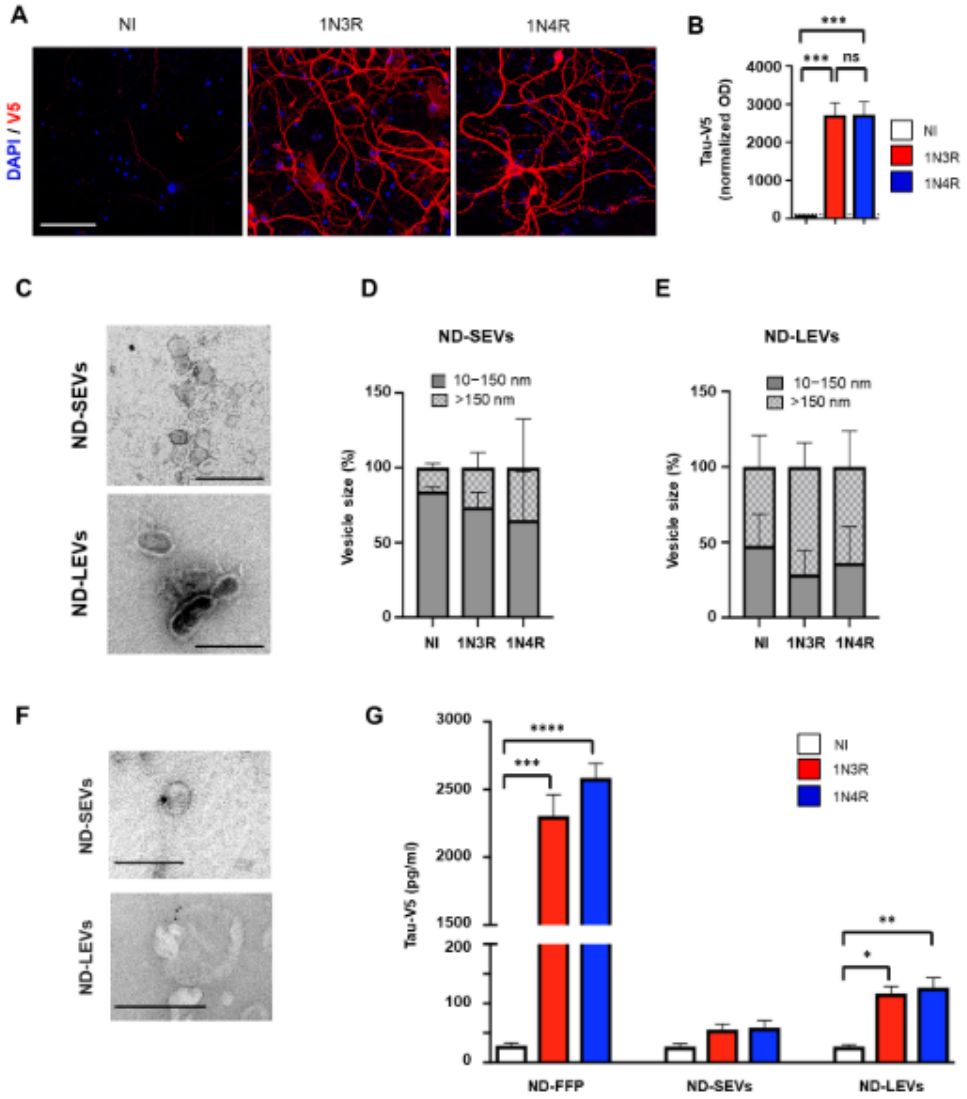

Figure 2. Neuronal tau is mainly secreted in a free form. (**A**) Confocal micrographs showing tau (V5+) in rat hippocampal neurons infected by LVs overexpressing 1N3R or 1N4R tau; NI = noninfected. (**B**) Histogram showing Tau-V5 accumulation (optical density normalized to that in the NI condition) in rat hippocampal neurons overexpressing 1N3R or 1N4R tau. (**C**) Electron microscopy images of ND-SEVs and ND-LEVs isolated from cultured neurons. The scale bar is 250 nm. (**D**) Histogram showing the percentage of ND-SEVs with a size between 100–150 nm and greater than 150 nm. (**E**) Histogram showing the percentage of ND-LEVs with a size between 100–150 nm and greater than 150 nm. (**F**) Electron microscopy and immunogold labeling (Cter-tau) of ND-SEVs and ND-LEVs isolated from the supernatant of neurons overexpressing 1N4R tau. The scale bar is 100 nm for ND-SEVs and 250 nm for ND-LEVs. (**G**) Histogram showing Tau-V5 concentration in the ND-FFP, ND-SEV, and ND-LEV fractions from control rat hippocampal neurons (NI) and those overexpressing 1N3R or 1N4R tau. For (**B**,**G**), $n = 4$ cultures per condition; ordinary one-way ANOVA with Sidak's multiple comparison test and the nonparametric Kruskal–Wallis test, in (**B**) and (**G**), respectively. (^{ns} $p > 0.05$, * $p < 0.05$, ** $p < 0.01$, *** $p < 0.001$, **** $p < 0.0001$).

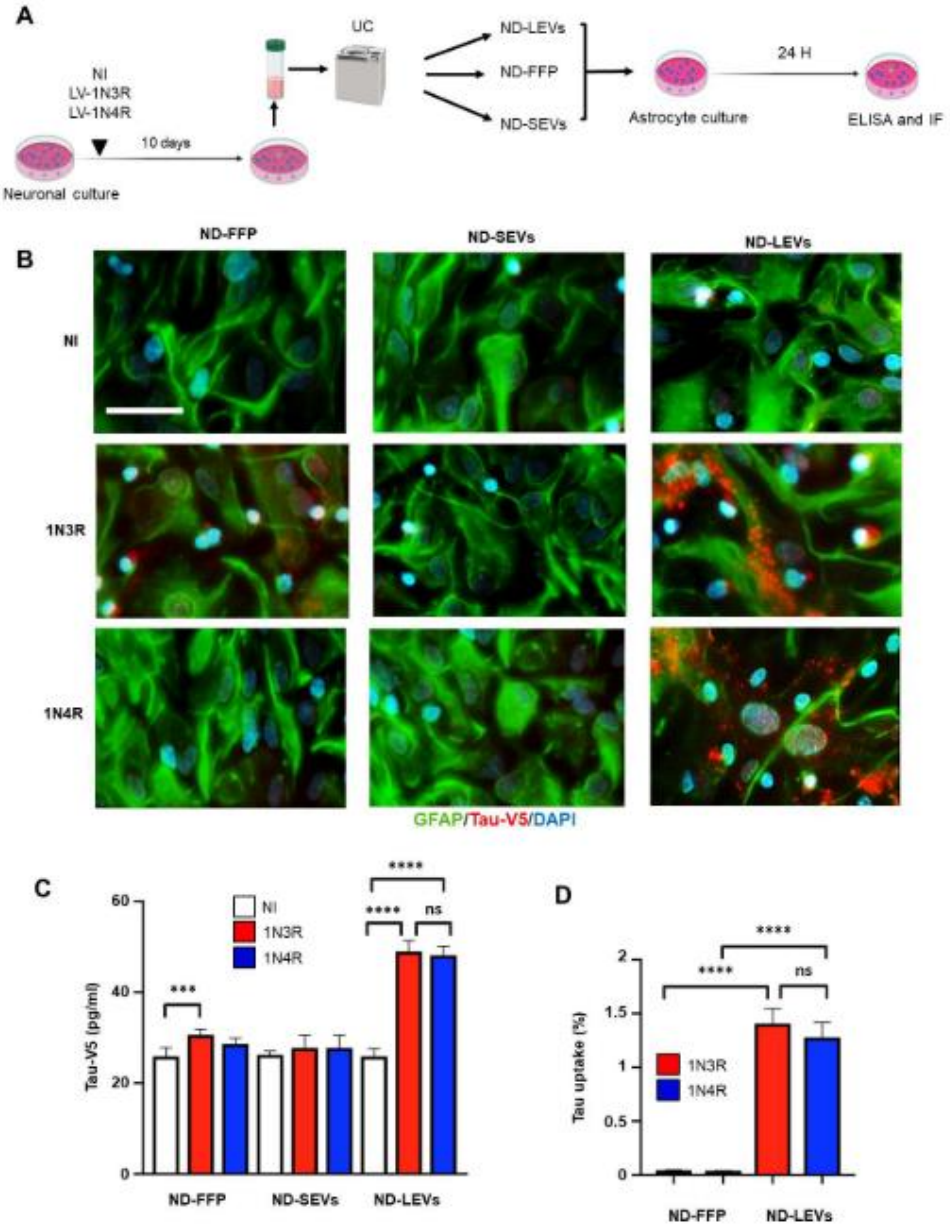

Figure 3. Tau is shuttled from neurons to astrocytes via LEVs. (**A**) Schematic representation of the protocol employed to isolate ND-EVs from neurons infected by LVs overexpressing 1N3R or 1N4R tau. ND-EVs from NI cultures were used as controls. (**B**) Example of confocal images showing the transfer of ND-FFP, or tau in ND-SEVs and ND-LEVs from neurons overexpressing 1N3R or 1N4R tau. The scale bar is 25 µm. (**C**) Histogram showing the Tau-V5 concentration in astrocytes 24 h after incubation with the ND-FFP, ND-SEV, and ND-LEV fractions from control rat hippocampal neurons (NI) and those overexpressing 1N3R or 1N4R tau. (**D**) Histogram showing the tau uptake efficiency 24 h after incubation with the ND-FFP and ND-LEV fractions from control rat hippocampal neurons (NI) and those overexpressing 1N3R or 1N4R tau. For (**C**) and (**D**), $n = 4$ cultures per condition; ordinary one-way ANOVA with Sidak's multiple comparison test. (^{ns} $p > 0.05$, *** $p < 0.001$, **** $p < 0.0001$).

3.4. 3R and 4R Tau-Accumulating LEVs Treatments Induce Differential Mitochondrial Consequences in Astrocytes

We previously demonstrated that the accumulation of different human tau isoforms in astrocytes differentially affects the astrocytic mitochondrial system [24]. The effect of ND-LEVs derived from neurons accumulating 3R or 4R tau was assessed by following a MitoTimer biosensor with high-content live microscopy (Figure 4A). This multiparametric approach can reveal changes in individual mitochondria over several hours/days [38]. Mitochondrial features (including the redox state, morphology, and dynamic changes) were measured before (BL) ND-LEV^{CFP}, ND-LEV^{3R}, or ND-LEV^{4R} treatment and at 6 h and 24 h after treatment. For each astrocyte- and each mitochondria-related criterion, the change score was calculated relative to the BL value and normalized to that of the control group (ND-LEVs^{CFP}).

Six hours after ND-LEV^{3R} or ND-LEV^{4R} treatments, we observed that the number of mitochondrial events (fusion/fission) significantly increased compared with the control condition ND-LEVs^{CFP} (Figure 4B). However, only ND-LEVs^{4R} increased the morphological complexity by significantly increasing the number of branches of mitochondria (Figure 4B). At 6H, multiple *t*-tests between treatments indicated that the mitochondrial branch criteria distinguish between the two types of ND-LEV^{3R} or ND-LEV^{4R} treatments (Figure 4B). Twenty-four hours after ND-LEV^{3R} or ND-LEV^{4R} treatments, we observed that ND-LEVs^{3R} significantly increased the redox state of mitochondria and reduced the number of events and the elongation of astrocyte mitochondria (Figure 4C). Conversely, ND-LEVs^{4R} reduced the redox state and tended toward more branched mitochondria. Multiple *t* tests between treatments revealed that the mitochondrial redox state and elongation significantly differed between ND-LEV^{3R} and ND-LEV^{4R} treatments (Figure 4C). These data suggest that the mitochondrial system of astrocytes is rapidly sensitive (6h) to the pathological content of LEVs, and the effect may be damaging in the longer term (24H).

Then, we evaluated changes in mitochondrial parameters (24 h) in human iPSC-derived astrocytes (expressing the biosensor MitoTimer) treated with BDF-LEVs isolated from a pool of patients diagnosed with 3R-tau (PiD) or 4R-tau (PSP) tauopathy, and non-demented control subjects (C) (Figures 5A and S2A). The size, concentration, and protein content of BDF-LEVs were initially measured using NTA and chromatography–tandem mass spectrometry (LC–MS/MS) (Figure S2A–C). Regarding redox state, astrocytes treated with BDF-LEVs^{PID} exhibited significantly increased mitochondrial oxidation, whereas mitochondrial oxidation was significantly reduced in astrocytes treated with BDF-LEVs^{PSP} (Figure 5B,C). Moreover, BDF-LEVs^{PID} significantly reduced mitochondrial elongation, whereas the mitochondria of astrocytes treated with BDF-LEVs^{PSP} appeared significantly more elongated and widely distributed in the cell (Figure 5B,D). Altogether, these results revealed that EVs from cells with 3R tau accumulation had deleterious effects on mitochondrial redox state and morphology, while EVs from cells with 4R tau accumulation induced filamentation and had less severe functional effects on the astrocytic mitochondrial system.

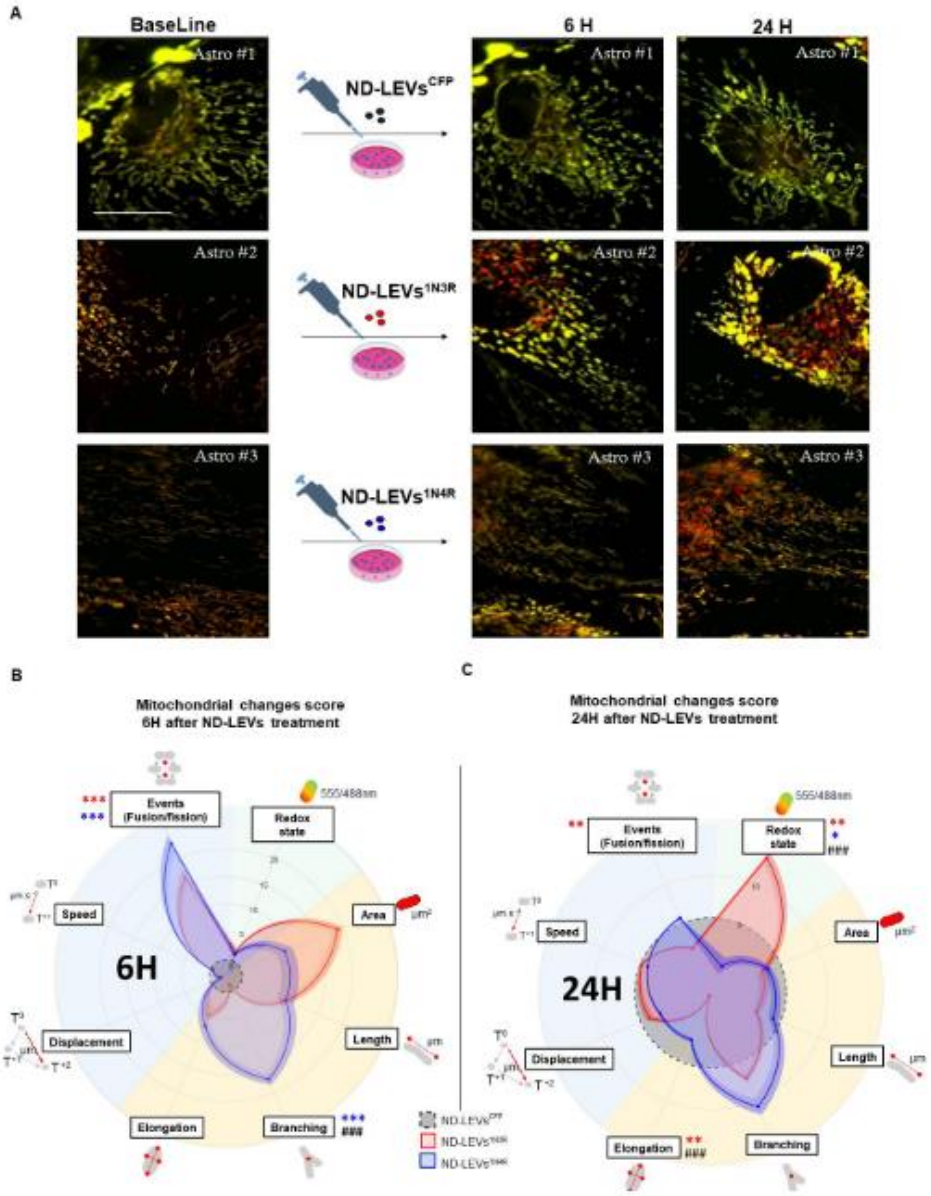

Figure 4. Tau isoform-containing LEVs induce mitochondrial dysfunction in primary rat astrocytes. (**A**) Micrographs of the mitochondria labeled with the biosensor MitoTimer before (BL) and after (6 h and 24 h) treatment with ND-LEVs^{CFP}, ND-LEVs^{1N3R}, and ND-LEVs^{1N4R}. (**B**,**C**) Radar charts showing MitoTimer ratio 555/488nm, morphology (surface area, length, number of branches, factor of elongation,), mobility (displacement and speed), and number of event changes (fusion/fission), normalized to BL values and the value of the ND-LEV^{CFP} group, in astrocytes treated with ND-LEVs^{1N3R} and ND-LEVs^{1N4R}. Two-way matched ANOVA followed by post hoc analysis (Tukey's test) was applied to compare the effect of each treatment with that of ND-LEVs^{CFP} (* $p < 0.05$, ** $p < 0.01$ and *** $p < 0.001$). A multiple t test was performed on each criterion between ND-LEVs^{1N3R} and ND-LEVs^{1N4R} to evaluate the difference in effect between the 3R and 4R isoforms ### $p < 0.001$).

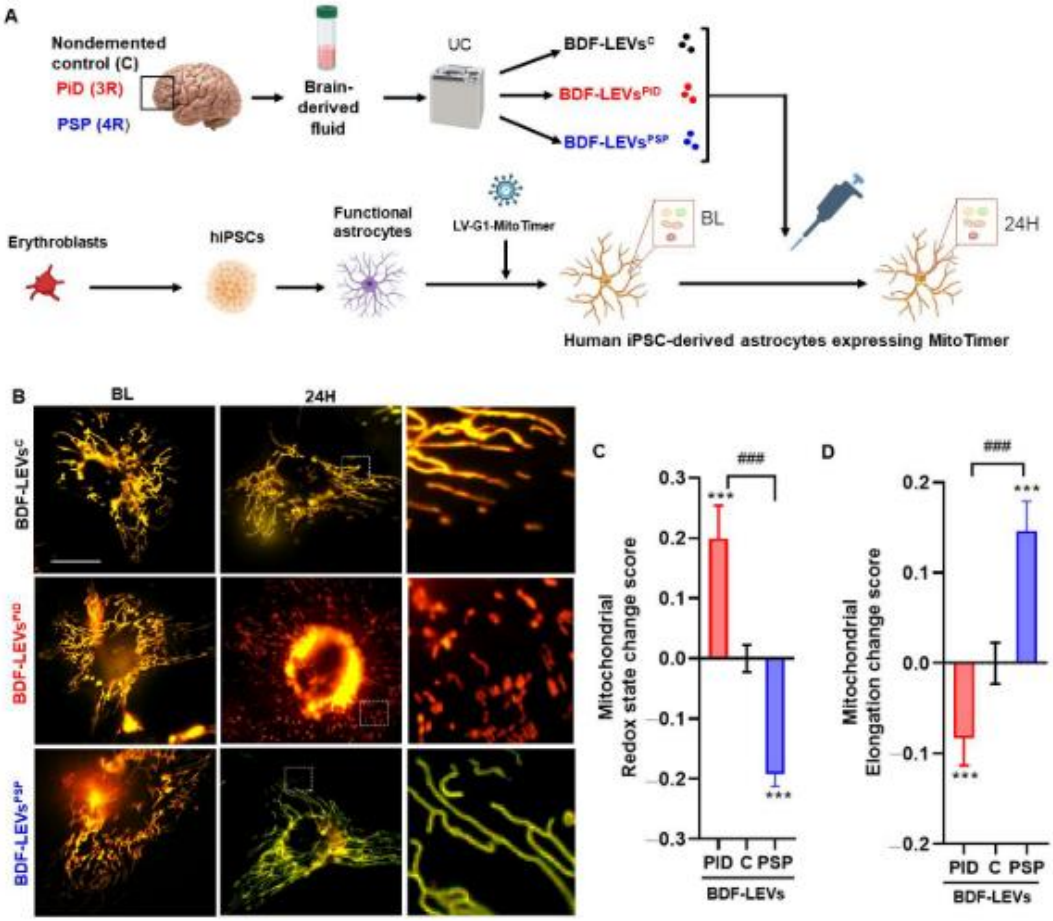

Figure 5. LEVs from 3R and 4R tauopathies induce differential mitochondrial dysfunction in iPSC-derived astrocytes. (**A**) Schematic representation of the protocols used to isolate BDF-EVs from patients diagnosed with PiD or PSP and non-demented control subjects (**C**) and to treat iPSC-derived astrocytes. (**B**) Micrographs of the mitochondrial system in human iPSC-derived astrocytes expressing the biosensor MitoTimer before (BL) and after (6 h and 24 h) treatment with BDF-LEVs^{PiD} and BDF-LEVs^{PSP}. (**C**) Histogram showing mitochondrial redox state changes in iPSC-derived astrocytes 24 h after BDF-LEVs treatment. (**D**) Histogram showing mitochondrial elongation in iPSC-derived astrocytes 24 h after BDF-LEVs treatment. N = cultures/cells/mitochondria; ND-LEVs^{CFP}: 3/21/801, ND-LEVs^{1N3R}: 3/15/958, ND-LEVs^{1N4R}: 4/14/789, BFD-LEVs^{C}: 3/19/3883, BFD-LEVs^{PiD}: 3/21/749, BFD-LEVs^{PSP}: 4/17/2555. Two-way matched ANOVA followed by post hoc analyses (Tukey's test) were used to compare the effects of treatments with those of the other treatments (### $p < 0.001$) and with the nondemented control group (*** $p < 0.001$). Scale bars are 30 μm.

4. Discussion

This study investigates the involvement of glial cells and EVs in the spread of tau. To date, most studies addressing the spreading process have focused on neurons. These cells are indeed the most affected cells in tauopathies, especially in AD, the main feature of which is the aggregation of tau protein (3R and 4R tau) into paired helical filaments within neurons. Nevertheless, tau inclusions are also found in glial cells, including astrocytes,

in other primary tauopathies. Astrocytes are the principal glial cells in the brain and play a supporting role in supplying energy and nutrition to neurons. Evidence shows that astroglial atrophy occurs in early stages of neurodegeneration, potentially leading to disruption in synaptic connectivity [40]. Astrocytes form a direct link between pre- and postsynaptic neurons and may therefore be involved in the propagation of tau between interconnected brain regions. Moreover, tau in astrocytes involved in tripartite synapses can impair synaptic function, as has been described in the brains of AD patients [41].

Here, we evaluated whether tau protein is shuttled from neurons to astrocytes via EVs, seeking a potential explanation for the accumulation of tau in astrocytes in the AD brain [24]. We first investigated the related cellular mechanisms in primary neurons overexpressing either 3R or 4R tau. EVs from murine primary neurons expressing human 3R or 4R tau were isolated and applied to murine primary astrocytes. Whereas tau is mainly secreted in a free form, EVs transfer both the two isoforms to astrocytes in equal quantities. In agreement with the work of Mate de Gerando and colleagues [15], we confirmed that tau is transferred from neurons to astrocytes. Narasimham and collaborators also demonstrated that while oligodendroglial tau pathology propagated across the mouse brain in the absence of neuronal tau pathology, astrocytic tau pathology did not. This suggests that pathological forms present in astrocytes are derived from neurons, and supports the existence of tau spreading between neurons and astrocytes [42].

Most importantly, through a direct comparison of free and EVs-associated tau, we validated the high potential of EVs to shuttle tau between neurons and astrocytes. This comparison also highlights the importance of brain-derived EVs in spreading tau pathology in Alzheimer's disease [21,22]. Contrary to our findings, some other studies have reported that free tau is taken up in astrocytes. They applied full-length recombinant proteins (2N4R isoform) [5] or preformed fibrils of human tau with P301L mutation not found in primary tauopathies such as PSP or Pick's disease (K18-P301L) [16]. In our experimental design, we applied neuronal tau secretome. We speculate that this secretome is closer to pathology, as many studies now validated the presence of tau peptides in biological fluids and not exclusively the full-length tau.

We then studied the effects on astrocytes of EV-mediated 3R or 4R tau transfer. Our data demonstrated that the transfer of EVs from neurons with 3R or 4R tau accumulation induced precise changes in the astrocytic mitochondrial system. Indeed, EVs originating from neurons with 3R tau accumulation rapidly showed features of mitochondrial dysfunction/damage (a transient increase in the number of events that result in fragmentation, and a substantial rise in the mitochondrial redox state). In contrast, astrocytes treated with EVs originating from neurons with 4R tau accumulation show features of transient adaptation/compensation of the mitochondrial system (transient ramification, a reduction in the redox state and/or an increase in mitochondrial turnover) [43,44]. Similar results were obtained after overexpression of 3R and 4R tau in astrocytes [24], whereas opposite effects were observed in neurons [45].

Numerous studies have already shown that the accumulation of abnormal tau protein impairs mitochondrial function, which leads to cell degeneration. These alterations in function include aspects of mitochondrial transport, dynamics, bioenergetics, and mitophagy [46].

Because tau is a microtubule-binding protein, mitochondrial disturbances due to abnormal tau had long been attributed to changes in the organization of the cytoskeletal network [47]. However, several recent studies have demonstrated that abnormal tau has a direct effect on mitochondria via binding. Indeed, it has been shown that abnormal tau can alter MFN2 levels and trigger the mislocalization and clustering of DRP1, triggering the elongation of mitochondria [48]. Abnormal tau can also directly interfere with the Parkin protein, inhibit mitophagy [49], and significantly reduce the activity of complex I, voltage-dependent anion channels (VDACs), and respiratory complex V subunits [50]. Abnormal tau protein may also impact ER-mitochondrial coupling, which could affect all mitochondrial functions [51]. The large majority of related studies have used neurons and

Our studies demonstrated that 3R and 4R tau are transferred from neurons to astrocytes with the same efficiency. We can hypothesize that 3R and 4R tau act on astrocytic mitochondria through different molecular mechanisms. First, whether three or four microtubule-binding domains are present slightly influences the binding affinity of tau to microtubules. Indeed, 4R tau binds to microtubules with a three-fold higher affinity than 3R tau [52]. We can also assume, as demonstrated in neurons, that tau protein may bind differently to filamentous actin to induce the formation of aligned bundles of actin filaments, therefore modifying the organization of the cytoskeletal network [47]. Second, because it is more soluble and has stronger kinesin inhibitory activity than 4R tau, 3R tau may induce strong steric inhibition of the binding of mitochondria to microtubules, leading to their immobilization [53]. Furthermore, the presence of a single cysteine (C322) in 3R tau allows the formation of intermolecular bridges, whereas the presence of two cysteines (C291, C322) in 4R tau leads mainly to the formation of intramolecular bridges [54]. These differences in the ability to form inter- or intradisulfide bridges may explain why 3R tau more readily aggregates to form oligomers and polymers than 4R tau. If these differences in properties are maintained in EVs, they could explain the differential effects of 3R and 4R tau on mitochondria observed in our study. Indeed, EVs carrying 3R tau may contain more tau peptides that are directly toxic to mitochondria [21,22,46] than EVs containing 4R tau. To extrapolate this effect to the human condition, we next isolated EVs from the brain fluids of patients with a 3R tau-related primary tauopathy (PiD) and a 4R tau-related primary tauopathy (PSP). Recently, we and others showed that EVs isolated from tauopathy patient-derived brain fluids contain tau seeds that might be involved in tau spreading [21]. Application of these EVs to iPSC-derived astrocytes validated their deleterious effect on mitochondria and showed that EVs from pure 3R tau-related tauopathy samples are the most aggressive, confirming our data from murine primary cultures. Altogether, our data are consistent with our previous study showing that 3R and 4R tau overexpression in astrocytes differentially alters the mitochondrial localization, trafficking, and function of these tau isoforms, suggesting that astrocytes may play a more substantial role than expected in AD [24] and other pure tauopathies. However, it is very important to mention that the observed effects on mitochondria may be more complex than the effect of tau alone. Indeed, EVs carry many other proteins (or protein peptides) and mRNAs that could impact the astrocytic mitochondrial system. Recent evidence suggests that the transfer of mitochondrial content by EVs modifies metabolic and inflammatory responses in recipient cells [55]. Alone or in combination, these effects are consistent with our observations of altered mitochondrial transport and dynamics after EV-mediated 3R tau transfer.

Here, we found that human-derived EVs play a role in astrocytic dysregulation. We also described a new potential pathway for the spread of tau between interconnected regions surrounding the synaptic cleft. We showed that EVs play a significant role in propagating 3R and 4R tau to astrocytes. Treatment with accumulated tau-containing EVs originating from neurons with 3R tau accumulation disturbed the astrocytic mitochondrial system and had very damaging effects. These data are in accordance with the severity of Pick disease. Indeed, in contrast to PSP, Pick disease is much more aggressive and damaging, involving huge cortical atrophy [56]. The current study raises many questions about strategies for clearing free extracellular tau. However, targeting pathological EVs is very challenging, and further studies are required to characterize EV cargos/transport, as recently described [57–59]. This will help not only in differentiating tauopathies but also in designing specific tools to block tau spreading.

5. Conclusions

In this study, we have discovered new mechanisms that explain how pathology spreads from neurons to surrounding astrocytes and alters their functioning. We utilized several innovative materials and technologies, including viral vectors encoding human

tau isoforms, IPSC-derived astrocytes, human brain samples, microfluidic chambers, and live high-resolution imaging of mitochondrial biosensors. Our findings shed light on how astrocytes uptake tau and the functional consequences of this process. Specifically, we demonstrate that human tau 3R and 4R are equally transferred from neurons to astrocytes, that tau isoforms are mainly transported via LEVs from neurons to astrocytes, and that exposure to LEVs with tau 3R pathology has devastating effects on the mitochondrial system of recipient astrocytes.

Supplementary Materials: The following supporting information can be downloaded at: https://www.mdpi.com/article/10.3390/cells12070985/s1, Figure S1. BFD-LEVs cell toxicity assay. Histogram showing the number of astrocytes still present in the well (counting of DAPI+ cells) 24 h after treatment with BDF-LEVs isolated from non-demented control subjects (C), PiD patients and PSP patients. BDF-LEVs were administered at doses of 10^5, 10^6 and 10^7 BDF-EVs/astrocyte. N = 5–7 cultures per condition; ordinary one-way ANOVA with Sidak's multiple comparison test. Figure S2. BFD-LEVs characterization and quality control. (A) Table showing the number of vesicles per ml, the level of hTau per vesicle and the level of hTau per vesicle normalized to tissue weight for each pooled sample (C, PiD and PSP). (B) Histogram of the size distribution of BFD-LEVs (between 10 and 150 nm or larger than 150 nm). (C) Heatmap depicting the relative abundances of proteins in different GOCC categories characterized as noncontaminant or potential contaminant in BFD-LEVs. (D) Histogram depicting the relative abundances of proteins in different MISEV18 categories characterized as EVs-associated or non-EVs-associated.

Author Contributions: Study design and conceptualization: K.R., M.C. and L.B. Writing, review, and editing: K.R., M.C. and L.B. Support for manuscript editing: R.P., E.L., N.D. and N.T. Experimentation: R.P., J.E., E.L., E.P., V.Z., L.C., S.P., R.D.P., S.B. and V.D. Funding acquisition: K.R., N.T, M.C. and L.B. Supervision: K.R. and M.C. All authors have read and agreed to the published version of the manuscript.

Funding: This research was funded by grants from the Investissement d'Avenir LabEx (Investing in the Future Laboratory Excellence) program, DISTALZ (Development of Innovative Strategies for a Transdisciplinary Approach to Alzheimer's disease), Fondation France Alzheimer (project: EV-Tau and spreading), Fondation Alzheimer (project Ectausome), Fondation pour la Recherche Médicale, ANR grants (GRAND, TONIC, TAUSEED), and the PSP France Association. Our laboratories were also supported by LiCEND (Lille Centre of Excellence in Neurodegenerative Disorders), CNRS, Inserm, Métropole Européenne de Lille, the University of Lille, I-SITE ULNE, Région Hauts de France, and FEDER.

Institutional Review Board Statement: For human- or murine-derived primary cultures, experiments were performed according to an ethics protocol approved by our institutional review committee (CER-VD 2018-01622, Lausanne, Switzerland and APAFIS#2264-2015101320441671 from CEEA75, Lille, France).

Informed Consent Statement: The study was conducted in accordance with the Declaration of Helsinki. Brain extracts were obtained from the Lille Neurobank (fulfilling French legal requirements concerning biological resources and declared to the competent authority under the number DC-2008-642) with donor consent and ethics committee approval in compliance with data protection regulations.

Data Availability Statement: The data presented in this study are openly available on http://doi.org/10.5281/zenodo.7759063.

Acknowledgments: We are grateful to the Lille Neurobank and Pr Claude-Alain Maurage for access to the human brain samples. This study was also supported by the Synapsis Foundation and the Lausanne University Hospital (CHUV). The authors thank the Protein Analysis Facility of the University of Lausanne, particularly M. Quadroni, for technical support. We are grateful to UMS-2014 US41 PLBS for access to the confocal microscopy at the HU site of the BioImaging Center Lille and for their assistance.

Conflicts of Interest: The authors declare no conflict of interest.

References

1. Buee, L.; Bussiere, T.; Buee-Scherrer, V.; Delacourte, A.; Hof, P.R. Tau protein isoforms, phosphorylation and role in neurodegenerative disorders. *Brain Res. Brain Res. Rev.* **2000**, *33*, 95–130. [CrossRef] [PubMed]
2. Himmler, A.; Drechsel, D.; Kirschner, M.W.; Martin, D.W., Jr. Tau consists of a set of proteins with repeated C-terminal microtubule-binding domains and variable N-terminal domains. *Mol. Cell Biol.* **1989**, *9*, 1381–1388. [PubMed]
3. Muller, R.; Heinrich, M.; Heck, S.; Blohm, D.; Richter-Landsberg, C. Expression of microtubule-associated proteins MAP2 and tau in cultured rat brain oligodendrocytes. *Cell. Tissue Res.* **1997**, *288*, 239–249. [CrossRef]
4. Kahlson, M.A.; Colodner, K.J. Glial Tau Pathology in Tauopathies: Functional Consequences. *J. Exp. Neurosci.* **2015**, *9*, 43–50. [CrossRef] [PubMed]
5. Perea, J.R.; Lopez, E.; Diez-Ballesteros, J.C.; Avila, J.; Hernandez, F.; Bolos, M. Extracellular Monomeric Tau Is Internalized by Astrocytes. *Front. Neurosci.* **2019**, *13*, 442. [CrossRef]
6. Rosler, T.W.; Tayaranian Marvian, A.; Brendel, M.; Nykanen, N.P.; Hollerhage, M.; Schwarz, S.C.; Hopfner, F.; Koeglsperger, T.; Respondek, G.; Schweyer, K.; et al. Four-repeat tauopathies. *Prog. Neurobiol.* **2019**, *180*, 101644. [CrossRef]
7. Ikeda, M.; Shoji, M.; Kawarai, T.; Kawarabayashi, T.; Matsubara, E.; Murakami, T.; Sasaki, A.; Tomidokoro, Y.; Ikarashi, Y.; Kuribara, H.; et al. Accumulation of filamentous tau in the cerebral cortex of human tau R406W transgenic mice. *Am. J. Pathol.* **2005**, *166*, 521–531. [CrossRef] [PubMed]
8. De Calignon, A.; Polydoro, M.; Suarez-Calvet, M.; William, C.; Adamowicz, D.H.; Kopeikina, K.J.; Pitstick, R.; Sahara, N.; Ashe, K.H.; Carlson, G.A.; et al. Propagation of tau pathology in a model of early Alzheimer's disease. *Neuron* **2012**, *73*, 685–697. [CrossRef]
9. Asai, H.; Ikezu, S.; Tsunoda, S.; Medalla, M.; Luebke, J.; Haydar, T.; Wolozin, B.; Butovsky, O.; Kugler, S.; Ikezu, T. Depletion of microglia and inhibition of exosome synthesis halt tau propagation. *Nat. Neurosci.* **2015**, *18*, 1584–1593. [CrossRef]
10. Bolos, M.; Llorens-Martin, M.; Jurado-Arjona, J.; Hernandez, F.; Rabano, A.; Avila, J. Direct Evidence of Internalization of Tau by Microglia In Vitro and In Vivo. *J. Alzheimers Dis.* **2016**, *50*, 77–87. [CrossRef]
11. Colin, M.; Dujardin, S.; Schraen-Maschke, S.; Meno-Tetang, G.; Duyckaerts, C.; Courade, J.P.; Buee, L. From the prion-like propagation hypothesis to therapeutic strategies of anti-tau immunotherapy. *Acta Neuropathol.* **2020**, *139*, 3–25. [CrossRef] [PubMed]
12. Amro, Z.; Yool, A.J.; Collins-Praino, L.E. The potential role of glial cells in driving the prion-like transcellular propagation of tau in tauopathies. *Brain Behav. Immun. Health* **2021**, *14*, 100242. [CrossRef] [PubMed]
13. Liu, X.; Ying, J.; Wang, X.; Zheng, Q.; Zhao, T.; Yoon, S.; Yu, W.; Yang, D.; Fang, Y.; Hua, F. Astrocytes in Neural Circuits: Key Factors in Synaptic Regulation and Potential Targets for Neurodevelopmental Disorders. *Front. Mol. Neurosci.* **2021**, *14*, 729273. [CrossRef]
14. Fleeman, R.M.; Proctor, E.A. Astrocytic Propagation of Tau in the Context of Alzheimer's Disease. *Front. Cell Neurosci.* **2021**, *15*, 645233. [CrossRef] [PubMed]
15. Mate de Gerando, A.; D'Orange, M.; Augustin, E.; Josephine, C.; Auregan, G.; Gaudin-Guerif, M.; Guillermier, M.; Herard, A.S.; Stimmer, L.; Petit, F.; et al. Neuronal tau species transfer to astrocytes and induce their loss according to tau aggregation state. *Brain* **2021**, *144*, 1167–1182. [CrossRef]
16. Martini-Stoica, H.; Cole, A.L.; Swartzlander, D.B.; Chen, F.; Wan, Y.W.; Bajaj, L.; Bader, D.A.; Lee, V.M.Y.; Trojanowski, J.Q.; Liu, Z.; et al. TFEB enhances astroglial uptake of extracellular tau species and reduces tau spreading. *J. Exp. Med.* **2018**, *215*, 2355–2377. [CrossRef]
17. Xiao, Y.; Wang, S.K.; Zhang, Y.; Rostami, A.; Kenkare, A.; Casella, G.; Yuan, Z.Q.; Li, X. Role of extracellular vesicles in neurodegenerative diseases. *Prog. Neurobiol.* **2021**, *201*, 102022. [CrossRef] [PubMed]
18. Leroux, E.; Perbet, R.; Buee, L.; Colin, M. Extracellular vesicles in the central nervous system. *Med. Sci.* **2021**, *37*, 1133–1138. [CrossRef]
19. Rabouille, C. Pathways of Unconventional Protein Secretion. *Trends Cell Biol.* **2017**, *27*, 230–240. [CrossRef]
20. Van Niel, G.; D'Angelo, G.; Raposo, G. Shedding light on the cell biology of extracellular vesicles. *Nat. Rev. Mol. Cell Biol.* **2018**, *19*, 213–228. [CrossRef]
21. Ruan, Z.; Pathak, D.; Venkatesan Kalavai, S.; Yoshii-Kitahara, A.; Muraoka, S.; Bhatt, N.; Takamatsu-Yukawa, K.; Hu, J.; Wang, Y.; Hersh, S.; et al. Alzheimer's disease brain-derived extracellular vesicles spread tau pathology in interneurons. *Brain* **2020**, *144*, 288–309. [CrossRef] [PubMed]
22. Leroux, E.; Perbet, R.; Caillierez, R.; Richetin, K.; Lieger, S.; Espourteille, J.; Bouillet, T.; Begard, S.; Danis, C.; Loyens, A.; et al. Extracellular vesicles: Major actors of heterogeneity in tau spreading among human tauopathies. *Mol. Ther.* **2022**, *30*, 782–797. [CrossRef]
23. Chiarini, A.; Armato, U.; Gardenal, E.; Gui, L.; Dal Pra, I. Amyloid beta-Exposed Human Astrocytes Overproduce Phospho-Tau and Overrelease It within Exosomes, Effects Suppressed by Calcilytic NPS 2143-Further Implications for Alzheimer's Therapy. *Front. Neurosci.* **2017**, *11*, 217. [CrossRef]
24. Richetin, K.; Steullet, P.; Pachoud, M.; Perbet, R.; Parietti, E.; Maheswaran, M.; Eddarkaoui, S.; Begard, S.; Pythoud, C.; Rey, M.; et al. Tau accumulation in astrocytes of the dentate gyrus induces neuronal dysfunction and memory deficits in Alzheimer's disease. *Nat. Neurosci.* **2020**, *23*, 1567–1579. [CrossRef] [PubMed]

25. Braak, H.; Alafuzoff, I.; Arzberger, T.; Kretzschmar, H.; Del Tredici, K. Staging of Alzheimer disease-associated neurofibrillary pathology using paraffin sections and immunocytochemistry. *Acta Neuropathol.* **2006**, *112*, 389–404. [CrossRef]
26. Thal, D.R.; Rub, U.; Orantes, M.; Braak, H. Phases of A beta-deposition in the human brain and its relevance for the development of AD. *Neurology* **2002**, *58*, 1791–1800. [CrossRef]
27. Kaech, S.; Banker, G. Culturing hippocampal neurons. *Nat. Protoc.* **2006**, *1*, 2406–2415. [CrossRef] [PubMed]
28. Dujardin, S.; Lecolle, K.; Caillierez, R.; Begard, S.; Zommer, N.; Lachaud, C.; Carrier, S.; Dufour, N.; Auregan, G.; Winderickx, J.; et al. Neuron-to-neuron wild-type Tau protein transfer through a trans-synaptic mechanism: Relevance to sporadic tauopathies. *Acta Neuropathol. Commun.* **2014**, *2*, 14. [CrossRef]
29. Caillierez, R.; Begard, S.; Lecolle, K.; Deramecourt, V.; Zommer, N.; Dujardin, S.; Loyens, A.; Dufour, N.; Auregan, G.; Winderickx, J.; et al. Lentiviral Delivery of the Human Wild-type Tau Protein Mediates a Slow and Progressive Neurodegenerative Tau Pathology in the Rat Brain. *Mol. Ther.* **2013**, *21*, 1358–1368. [CrossRef] [PubMed]
30. Dujardin, S.; Begard, S.; Caillierez, R.; Lachaud, C.; Carrier, S.; Lieger, S.; Gonzalez, J.A.; Deramecourt, V.; Deglon, N.; Maurage, C.A.; et al. Different tau species lead to heterogeneous tau pathology propagation and misfolding. *Acta Neuropathol. Commun.* **2018**, *6*, 132. [CrossRef]
31. Vega, C.; Pellerin, L.; Dantzer, R.; Magistretti, P.J. Long-term modulation of glucose utilization by IL-1 alpha and TNF-alpha in astrocytes: Na+ pump activity as a potential target via distinct signaling mechanisms. *Glia* **2002**, *39*, 10–18. [CrossRef] [PubMed]
32. Perriot, S.; Canales, M.; Mathias, A.; Du Pasquier, R. Differentiation of functional astrocytes from human-induced pluripotent stem cells in chemically defined media. *STAR Protoc.* **2021**, *2*, 100902. [CrossRef]
33. Perriot, S.; Mathias, A.; Perriard, G.; Canales, M.; Jonkmans, N.; Merienne, N.; Meunier, C.; El Kassar, L.; Perrier, A.L.; Laplaud, D.A.; et al. Human Induced Pluripotent Stem Cell-Derived Astrocytes Are Differentially Activated by Multiple Sclerosis-Associated Cytokines. *Stem Cell Rep.* **2018**, *11*, 1199–1210. [CrossRef] [PubMed]
34. Polanco, J.C.; Scicluna, B.J.; Hill, A.F.; Gotz, J. Extracellular Vesicles Isolated from the Brains of rTg4510 Mice Seed Tau Protein Aggregation in a Threshold-dependent Manner. *J. Biol. Chem.* **2016**, *291*, 12445–12466. [CrossRef]
35. Dujardin, S.; Begard, S.; Caillierez, R.; Lachaud, C.; Delattre, L.; Carrier, S.; Loyens, A.; Galas, M.C.; Bousset, L.; Melki, R.; et al. Ectosomes: A new mechanism for non-exosomal secretion of tau protein. *PLoS ONE* **2014**, *9*, e100760. [CrossRef] [PubMed]
36. Sergeant, N.; Sablonniere, B.; Schraen-Maschke, S.; Ghestem, A.; Maurage, C.A.; Wattez, A.; Vermersch, P.; Delacourte, A. Dysregulation of human brain microtubule-associated tau mRNA maturation in myotonic dystrophy type 1. *Hum. Mol. Genet.* **2001**, *10*, 2143–2155. [CrossRef]
37. Troquier, L.; Caillierez, R.; Burnouf, S.; Fernandez-Gomez, F.J.; Grosjean, M.E.; Zommer, N.; Sergeant, N.; Schraen-Maschke, S.; Blum, D.; Buee, L. Targeting phospho-Ser422 by active Tau Immunotherapy in the THYTau22 mouse model: A suitable therapeutic approach. *Curr. Alzheimer Res.* **2012**, *9*, 397–405.
38. Espourteille, J.; Zufferey, V.; Laurent, J.H.; Richetin, K. Live-imaging of Mitochondrial System in Cultured Astrocytes. *J. Vis. Exp.* **2021**. [CrossRef]
39. Allison, P.D. Change Scores as Dependent Variables in Regression Analysis. *Sociol. Methodol.* **1990**, *20*, 93–114. [CrossRef]
40. Verkhratsky, A.; Olabarria, M.; Noristani, H.N.; Yeh, C.Y.; Rodriguez, J.J. Astrocytes in Alzheimer's disease. *Neurotherapeutics* **2010**, *7*, 399–412. [CrossRef]
41. Wu, M.; Zhang, M.; Yin, X.; Chen, K.; Hu, Z.; Zhou, Q.; Cao, X.; Chen, Z.; Liu, D. The role of pathological tau in synaptic dysfunction in Alzheimer's diseases. *Transl. Neurodegener.* **2021**, *10*, 45. [CrossRef]
42. Narasimhan, S.; Changolkar, L.; Riddle, D.M.; Kats, A.; Stieber, A.; Weitzman, S.A.; Zhang, B.; Li, Z.; Roberson, E.D.; Trojanowski, J.Q.; et al. Human tau pathology transmits glial tau aggregates in the absence of neuronal tau. *J. Exp. Med.* **2020**, *217*, e20190783. [CrossRef] [PubMed]
43. Gollihue, J.L.; Norris, C.M. Astrocyte mitochondria: Central players and potential therapeutic targets for neurodegenerative diseases and injury. *Ageing Res. Rev.* **2020**, *59*, 101039. [CrossRef] [PubMed]
44. Jackson, J.G.; Robinson, M.B. Regulation of mitochondrial dynamics in astrocytes: Mechanisms, consequences, and unknowns. *Glia* **2018**, *66*, 1213–1234. [CrossRef] [PubMed]
45. Stoothoff, W.; Jones, P.B.; Spires-Jones, T.L.; Joyner, D.; Chhabra, E.; Bercury, K.; Fan, Z.; Xie, H.; Bacskai, B.; Edd, J.; et al. Differential effect of three-repeat and four-repeat tau on mitochondrial axonal transport. *J. Neurochem.* **2009**, *111*, 417–427. [CrossRef]
46. Szabo, L.; Eckert, A.; Grimm, A. Insights into Disease-Associated Tau Impact on Mitochondria. *Int. J. Mol. Sci.* **2020**, *21*, 6344. [CrossRef] [PubMed]
47. Fulga, T.A.; Elson-Schwab, I.; Khurana, V.; Steinhilb, M.L.; Spires, T.L.; Hyman, B.T.; Feany, M.B. Abnormal bundling and accumulation of F-actin mediates tau-induced neuronal degeneration in vivo. *Nat. Cell Biol.* **2007**, *9*, 139–148. [CrossRef] [PubMed]
48. DuBoff, B.; Gotz, J.; Feany, M.B. Tau promotes neurodegeneration via DRP1 mislocalization in vivo. *Neuron* **2012**, *75*, 618–632. [CrossRef]
49. Cummins, N.; Tweedie, A.; Zuryn, S.; Bertran-Gonzalez, J.; Gotz, J. Disease-associated tau impairs mitophagy by inhibiting Parkin translocation to mitochondria. *EMBO J.* **2019**, *38*, e99360. [CrossRef]
50. Manczak, M.; Reddy, P.H. Abnormal interaction of VDAC1 with amyloid beta and phosphorylated tau causes mitochondrial dysfunction in Alzheimer's disease. *Hum. Mol. Genet.* **2012**, *21*, 5131–5146. [CrossRef]

51. Cieri, D.; Vicario, M.; Vallese, F.; D'Orsi, B.; Berto, P.; Grinzato, A.; Catoni, C.; De Stefani, D.; Rizzuto, R.; Brini, M.; et al. Tau localizes within mitochondrial sub-compartments and its caspase cleavage affects ER-mitochondria interactions and cellular Ca(2+) handling. *Biochim. Biophys. Acta Mol. Basis Dis.* **2018**, *1864*, 3247–3256. [CrossRef] [PubMed]
52. Bachmann, S.; Bell, M.; Klimek, J.; Zempel, H. Differential Effects of the Six Human TAU Isoforms: Somatic Retention of 2N-TAU and Increased Microtubule Number Induced by 4R-TAU. *Front. Neurosci.* **2021**, *15*, 643115. [CrossRef] [PubMed]
53. Ebneth, A.; Godemann, R.; Stamer, K.; Illenberger, S.; Trinczek, B.; Mandelkow, E. Overexpression of tau protein inhibits kinesin-dependent trafficking of vesicles, mitochondria, and endoplasmic reticulum: Implications for Alzheimer's disease. *J. Cell Biol.* **1998**, *143*, 777–794. [CrossRef]
54. Schweers, O.; Schonbrunn-Hanebeck, E.; Marx, A.; Mandelkow, E. Structural studies of tau protein and Alzheimer paired helical filaments show no evidence for beta-structure. *J. Biol. Chem.* **1994**, *269*, 24290–24297. [CrossRef] [PubMed]
55. Amari, L.; Germain, M. Mitochondrial Extracellular Vesicles—Origins and Roles. *Front. Mol. Neurosci.* **2021**, *14*, 767219. [CrossRef]
56. Davis, R.L.; Robertson, D.M. (Eds.) *Textbook of Neuropathology*, 2nd ed.; Elsevier: Amsterdam, The Netherlands, 1991; pp. 918–921, 934–936.
57. You, Y.; Muraoka, S.; Jedrychowski, M.P.; Hu, J.; McQuade, A.K.; Young-Pearse, T.; Aslebagh, R.; Shaffer, S.A.; Gygi, S.P.; Blurton-Jones, M.; et al. Human neural cell type-specific extracellular vesicle proteome defines disease-related molecules associated with activated astrocytes in Alzheimer's disease brain. *J. Extracell. Vesicles* **2022**, *11*, e12183. [CrossRef]
58. Muraoka, S.; DeLeo, A.M.; Sethi, M.K.; Yukawa-Takamatsu, K.; Yang, Z.; Ko, J.; Hogan, J.D.; Ruan, Z.; You, Y.; Wang, Y.; et al. Proteomic and biological profiling of extracellular vesicles from Alzheimer's disease human brain tissues. *Alzheimers Dement.* **2020**, *16*, 896–907. [CrossRef]
59. Muraoka, S.; Jedrychowski, M.P.; Yanamandra, K.; Ikezu, S.; Gygi, S.P.; Ikezu, T. Proteomic Profiling of Extracellular Vesicles Derived from Cerebrospinal Fluid of Alzheimer's Disease Patients: A Pilot Study. *Cells* **2020**, *9*, 1959. [CrossRef]

Annex 4

Karger OPEN ACCESS
Neurodegenerative Diseases

Neurodegenerative Diseases, DOI: 10.1159/000538623

Received: December 13, 2023

Accepted: March 28, 2024

Published online: March 29, 2024

Circulating Biomarkers for Alzheimer's Disease: Unlocking the diagnostic potential in Low-and Middle-Income Countries, focusing on Africa

Nwamekang Belinga L, Espourteille J, Wepnyu Njamnshi Y, Zafack Zeukang A, Rouaud O, Kongnyu Njamnshi A, Allali G, Richetin K

ISSN: 1660-2854 (Print), eISSN: 1660-2862 (Online)

https://www.karger.com/NDD

Neurodegenerative Diseases

Circulating Biomarkers for Alzheimer's Disease: Unlocking the diagnostic potential in Low- and Middle-Income Countries, focusing on Africa

Luc Nwamekang Belinga[1,2,3] MD, Jeanne Espourteille[I], Yembe Wepnyu Njamnshi [3,4,5] MD, Ariole Zafack Zeukang[3],

Olivier Rouaud[2] MD, Alfred Kongnyu Njamnshi [3,4,6+] MD, Gilles Allali[2+] MD & Kevin Richetin[1,2]* PhD

[1] Department of Psychiatry, Center for Psychiatric Neurosciences, Lausanne University Hospital (CHUV) and University of Lausanne, 1011 Lausanne, Switzerland

[2] Leenaards Memory Center, Department of Clinical Neurosciences, Lausanne University Hospital, University of Lausanne, 1011 Lausanne, Switzerland.

[3] Department of Translational Neuroscience, Brain Research Africa Initiative (BRAIN), 1226 Thonex-Geneva, Switzerland & 25625 Yaoundé, Cameroon

5

6

+

Abstract

Background: Alzheimer's disease (AD) is emerging as a significant public health challenge in Africa, with predictions indicating a tripling in incidence by 2050. The diagnosis of AD on the African continent is notably difficult, leading to late detection that severely limits treatment options and significantly impacts the quality of life for patients and their families.

Summary: This review focuses on the potential of high-sensitivity specific blood biomarkers as promising tools for improving AD diagnosis and management globally, particularly in Africa. These advances are particularly pertinent in the continent, where access to medical and technical resources is often limited.

Key Messages: Identifying precise, sensitive, and specific blood biomarkers could contribute to the biological characterization and management of Alzheimer's disease in Africa. Such advances promise to improve patient care and pave the way for new regional opportunities in pharmaceutical research and drug trials on the continent for Alzheimer's disease. **Introduction**

Alzheimer's disease (AD) is a chronic and debilitating condition characterized by progressive decline in cognitive functions [1]. The impact of AD is significant, affecting approximately 50 million people globally, with over 2 million cases reported for dementia in Africa [2]. The prevalence of AD on the African continent is particularly alarming, rising from 3.6 million cases in 2020 to an estimated 16.2 million by 2050 [3] **(Fig. 1)**. This increasing trend, exacerbated by demographic and epidemiologic transitions coupled with increased life expectancy, is poised to lead to substantial socioeconomic consequences for patients and families, and large pressure on healthcare systems in Africa [2]. Significant advancements have been made since 2011 in the understanding of the pathophysiological mechanisms of AD [4]. These insights have led to considerable progress in diagnostic and treatment approaches. The use of biomarkers, such as tau and amyloid beta, has been instrumental in shifting the focus towards in vivo detection of AD [5]. Despite these advances in vivo AD diagnosis mainly found in high income countries and recent advancements in the development of anti-amyloid drugs that aim to reduce AD morbidity [6]. Africa is far from these current advancements and faces unique and pressing challenges in the diagnosis and management of AD (**Table 1.**) [3]. The African continent faces a shortage of neuroimaging techniques, such as Magnetic Resonance Imaging (MRI) and CT scans, high cost of these equipment, their maintenance and lack of sufficient trained personnel [7,8]. In addition to these challenges, socioeconomic and cultural barriers limit the application of certain diagnostic procedures such as lumbar puncture [2,9]. Therefore, there is a critical need to explore new context-appropriate approaches to enhance AD diagnosis and management in Africa, and one of the most promising approaches could be measure circulating proteins, such as Tau, Amyloid beta, Neurofilament (NfL), and Glial Fibrillary Acidic Protein (GFAP), which are associated with Alzheimer's and related dementia [10]. These proteins, detectable in biofluids such as cerebrospinal fluid (CSF) and blood, could offer a more accessible method for garnering valuable biological insights into AD [10,11]. The implementation of circulating biomarkers could potentialize the current diagnostic process, guide the selection of additional diagnostic tools, and significantly influence patient treatment strategies by contributing to the identification of suitable candidates for anti-amyloid drugs and inform the management of other neurodegenerative diseases. The current lack of biological characterization of AD in low- and middle-income countries (LMICs), particularly Africa, highlights the urgent need to include these regions in ongoing clinical trials [12]. Utilizing circulating biomarkers can provide a more readily available approach for defining the biological aspects of AD in Africa. This review aimed to explore current diagnostic models for AD, discuss selected combined profiles of circulating biomarkers and their potential benefits, and discuss the prerequisites for their implementation in Africa.

2- Current Diagnostic models of Alzheimer's disease (AD) and Application Challenges in Low- and Middle-Income Countries (LMICs).

A Perspective from High-Income Countries: The initial clinical criteria for Alzheimer's disease (AD) have been established since 1984, focusing primarily on clinical symptoms [13]. In 2011, a significant revision was made by the National Institute of Aging (NIA) and Alzheimer's Association (AA), which included definitions of preclinical and mild cognitive impairment (MCI) stages of AD and related disorders [4]. This revision also integrated the biological definition of AD with the inclusion of tau and amyloid CSF biomarkers [14]. These advancements have significantly improved the diagnosis of Alzheimer's disease, transitioning from post-mortem diagnosis to in vivo detection using a combination of clinical and biological markers [15]. The National Institute of Aging (NIA) and Alzheimer's Association (AA) proposed the concept of categorizing the clinical phenotypes of individuals with AD by utilizing biomarker evidence in the cerebrospinal fluid (CSF) and neurodegeneration [16]. This system evaluates the presence of β-amyloid (A), hyperphosphorylated tau (T), and neurodegeneration (N), resulting in 8 possible combinations of biomarkers based on clinical profiles [16]. This classification is based on a comprehensive clinical diagnostic approach that includes neurological and/or psychiatric assessment. Neuroimaging techniques, such as MRI and positron emission tomography (PET), are employed as exploratory tests to support diagnosis by ruling out other conditions or confirming specific clinical features [17]. Alzheimer's diagnosis is confirmed by measuring biomarkers present in the cerebrospinal fluid (CSF), such as the Aβ42/40 ratio, Aβ1-42, P-tau, and total tau [16]. These biomarkers help reduce the diagnostic error rate, which can be as high as 40–45%, when relying solely on clinical-radiological reasoning in cases of degenerative amnesic syndrome, as reported by Landau et al. in 2016 [18]. However, depending on the availability of appropriate health systems and medical resources, the accessibility of this diagnostic procedure is limited in resource-constrained countries, such as those in Africa. The current diagnostic guidelines for Alzheimer's disease without blood biomarkers in clinical settings also warrant reconsideration of the existing NIA-AA criteria, which will hopefully be updated [16].

Evolution of Alzheimer's disease pathology and diagnosis: a historical and contemporary perspective in Africa: In the context of diagnosing Alzheimer's disease in Africa, advancements in biological characterization have presented a limited number of studies focused on Africa's native population, with the majority related to epidemiological investigations [2]. Since 1984, studies such as those by Ogeng'o et al. (1996) paved the way for presenting the first post-mortem characterization of Cerebral Amyloid β Protein Deposits and other Alzheimer's lesions in elderly cohorts from Nairobi and Dar es Salaam [19]. In 2015, Seggane Musisi and Stanley Jacobson's book depicted the radiologic presentation of brain degeneration and dementia in Sub-Saharan Africa [20]. While studies on circulating biomarkers mainly rely on Black American data, Chaudhry et al.'s 2020 meta-analysis highlighted the lack of diverse inclusion, noting disparities in CSF t-tau and p-tau181 levels between African Americans and White Americans, with no studies on native Africans finding [21]. Other significant studies by Oye Gureje et al., 2006 [22], Hendrie et al., 2014 [23], and Naslavsky et al., 2022 [24] showed varying impacts of APOE ε4 on AD depending on ancestry. Kim et al. 2016 identified the risk gene CD2AP in association with plasma homocysteine levels in the African American and Yoruba cohorts [25]. Despite ongoing research by the African Dementia Consortium [26], there are still significant gaps in robust biological AD characterization in Africa, which could be due to a variety of factors, including limited regional and international research funding and challenges in the availability and cost of diagnostic tools. Neuroimaging tools, such as magnetic resonance imaging (MRI) and CT scans, are prohibitively expensive in sub-Saharan Africa, making significant obstacles regarding diagnosis accessibility given the average income in Africa [27]. The lack of universal health coverage in many countries is one of the several factors affecting AD management in Africa [28]. The high costs associated with neuroimaging tools add to the cost of specialized physician consultation, which leads some patients to seek alternative solutions, including traditional medicine or religious practices [2,29,30]. Practitioners in resource-limited settings often resort to less expensive diagnostic modalities based on clinical evaluations and the use of less specific techniques, such as CT scans or EEGs [31]. Although these methods are more accessible, they are not reliable for identifying AD. The challenges in the longitudinal monitoring and evaluation of patients, particularly in the use of cerebrospinal

fluid (CSF), are compounded by ethical considerations regarding techniques such as lumbar puncture, particularly in older patients [9]. In Africa, where life expectancy ranges between 58 and 65 years and treatments are not widely available, families often question the necessity of invasive procedures [9,32]. Cultural beliefs also influence the perceptions of neurocognitive impairment, often seen as a normal part of aging [2,29]. Additionally, the limited availability of multidisciplinary centers and a shortage of trained healthcare professionals significantly impede an effective response to Alzheimer's disease in some countries, such as Cameroon in Africa, which has only approximately 60 psychiatrists and 35 neurologists for a population of over 25 million [33]. Nevertheless, the clinical neuroscience training programs in the Faculty of Medicine and Biomedical Sciences of the University of Yaoundé I are increasing their output of brain health professionals, which could bridge these gaps in care and expertise [33]. There are still African countries that lack adequate neurologists [34]. This shortage of trained healthcare professionals and absence of centers of excellence present significant challenges for community-based AD diagnosis and care. However, these challenges are poised for improvement through initiatives such as task-shifting and outreach programs [35]. These initiatives are expected to be significantly bolstered by the collective efforts of scientists across the continent under the auspices of the Africa Dementia Consortium (ADC) [26]. By combining dementia researchers in a multidisciplinary framework, ADC aims to generate comprehensive clinical and socioeconomic datasets that are crucial for improving the characterization of dementia phenotypes in Africans. These include epidemiological studies focusing on the prevalence, incidence, and risk factors of dementia, genetic and epigenetic research to understand hereditary influences, and identification of unique biomarkers for more precise diagnosis. For future research endeavors, ADC intends to leverage existing resources such as the biobanks of brain samples, cerebrospinal fluid, and blood [36]. This comprehensive approach of ADC is set to fill critical gaps in dementia research and care in Africa, offering hope for improving management and understanding of AD in Africa [26]. In the era of intensive research on anti amyloid drugs that could potentially reduce AD-related morbidity in the coming years, those without biological characterization, such as the native African population, are excluded from current clinical trials [12]. Circulating biomarkers could reduce the diagnostic error rate by as much as 40–45%, as noted by Landau SM et al. in 2016 [18], which relies mainly on clinical-radiological evidence in Africa and could serve as effective preliminary screening tools for AD diagnosis by identifying individuals who are more likely to benefit from further, more expensive, and less accessible diagnostic methods, such as CT scans or MRI, and could open regional anti amyloid clinical trials by detecting amyloid-positive individuals, making suitable candidates for emerging anti-amyloid drugs. This targeted approach could not only optimize the use of context-appropriate diagnostic tools, but also ensure that patients receive care tailored to their specific conditions, contributing to a more efficient, cost effective, and culturally sensitive AD diagnosis and management in Africa. 3- Current Trends of Research on Circulating Biomarkers for Alzheimer's Disease

Circulating biomarkers found in biofluids such as blood provide valuable information regarding the diagnosis and progression of Alzheimer disease [10]. Biomarkers, such as proteins, nucleic acids, microRNAs, and extracellular vesicles, can be measured using minimally invasive blood sampling techniques (subcutaneous venipuncture), offering an alternative to current diagnostic procedures for diseases [37]. Blood sampling is a simple and accessible procedure that can be performed in various healthcare settings with very low levels of health personnel, making it suitable for resource-limited regions such as Africa. The minimally invasive nature of blood biomarkers could reduce the discomfort and lack of accessibility associated with invasive procedures such as lumbar puncture [9].The blood–brain barrier (BBB) has been shown to be affected during Alzheimer's disease [38]. Due to the breach of the BBB, proteins and nanoparticles, including exosomes, can leak into the bloodstream. These biomolecules hold potential for the diagnosis of Alzheimer's **(Fig. 2)** [39,40]. Research on blood biomarkers for Alzheimer's disease has made significant progress, focusing on identifying reliable markers for screening processes in research settings and monitoring clinical trial [10]. The development of highly sensitive devices/systems for detecting these biomarkers in blood has also increased

Some of the most promising biomarkers studied and developed in high-income countries (HICs) are as follows:

· Tau proteins

Tau is a microtubule-binding component that facilitates microtubule polymerization and stability of microtubules [41]. The human tau protein is encoded by MAPT, which is located on chromosome 17 and consists of 16 exons [42]**.** Alternative splicing of exons 2, 3, and 10 generates up to six tau isoform variants in the human brain [43]. In the normal adult human brain, a balanced ratio of 3R and 4R tau isoforms is maintained [44]. However, in Alzheimer's disease and other tauopathies, imbalanced 3R:4R tau isoform ratios in the brain can occur because of altered MAPT pre-mRNA splicing, leading to neurotoxicity [45]. These imbalances adversely affect pre- and postsynaptic compartment synaptosomes, causing a disruption in microtubule assembly, axonal transport, and pre- and postsynaptic functions, eventually leading to neuronal cell death during the later stages of Alzheimer's disease [46]. In AD, tau protein tends to aggregate and become hyperphosphorylated, with several

phosphorylated sites identified [47]. To diagnose AD, researchers often focus on threonine-181 (p-tau181) and ptau 217 as significant tau phosphorylation sites in the CSF. An increase in phosphorylated tau 181 and 217, total Tau in the CSF, and functional neuroimaging are considered the gold standard diagnostic markers for Alzheimer's disease [47]. Recent research in the context of Alzheimer's disease indicates that changes in the levels of total tau and phosphorylated tau isoforms 181 and 217 can be detected in the bloodstream due to neuronal damage and neurodegeneration [48]. A probable practical approach for identifying patients with Alzheimer's disease (AD) using tau blood tests could include setting a high cutoff for the p-tau217/total tau ratio and amyloid 42/total tau ratio in blood tests, which appears to correlate well with neurofibrillary tangles in research settings and could further enhance AD diagnosis in clinical setting [49]. Research on the relevance of tau proteins in the African context is essential to assist in the preliminary process and enhance clinical trial selection and monitoring. This is particularly important given the prevalence of other types of dementia, such as vascular dementia, which could also influence tau measurements. Understanding the specific role and regulation of tau proteins in native African populations will be crucial for developing more accurate biological definitions for Alzheimer's disease and related dementias.

· Beta-Amyloid (Aβ).

Beta-amyloid peptides are essential components of amyloid plaques found in the brains of individuals with Alzheimer's disease [50]. Alzheimer's is characterized by amyloid β-protein (Aβ) deposition plaques within the brain parenchyma and phosphorylated tau in neurofibrillary tangles in neurons [51]. In the past, the diagnosis of Alzheimer's relied on post-mortem brain tissue analysis in the presence of neurofibrillary tangles. Recent advancements in imaging technologies, such as PET for brain Aβ deposition and CSF Aβ biomarkers, have significantly improved diagnosis [52,53]. In exploring Alzheimer's disease biomarkers in biological fluids, particular focus is given to Aβ and tau proteins, which play central roles in AD pathogenesis [54]. Aβ in brain plaques consists of 40–43 amino acids, with Aβ42 and Aβ40 being the primary species generated through proteolysis of amyloid precursor protein (APP) by β- and γ-secretases [55]. Most APP undergo non-amyloidogenic processing by α-secretase, which results in the formation of a non-amyloidogenic fragment called p3. Aβ42 and Aβ43, the longer species, have a high tendency to aggregate and deposit early in the brain, leading to the formation of highly toxic oligomers that harm neurons [56]. In contrast, Aβ40 may have antioxidant and anti-amyloidogenic effects [57]. Dysregulation of amyloid deposition significantly affects glial cells, thereby facilitating detection of Aβ pathology in the brain through plasma Aβ peptides [58]. The biomarker signature of Alzheimer's pathology is characterized by a relative decrease in the Abeta42/40 ratio [59]. This decrease is likely due to the sequestration of Abeta42 in the brain tissue, leading to a lower plasma Abeta42/40 ratio, indicative of Alzheimer's disease pathology in the brain [59]. Recent studies have identified measurable plasma Aβ42 levels in Alzheimer's disease (AD) patients, highlighting their potential as diagnostic biomarkers [60]. However, the

specificity and sensitivity of plasma Aβ42 are somewhat limited, leading to possible false positives in non-AD patients and false negatives in those with Alzheimer's [61]. Ongoing efforts are focused on enhancing the accuracy of plasma Aβ42 as a diagnostic tool [62]. This is crucial to avoid potential overdiagnosis associated with amyloid-positive profiles in normal aging or positivity due to other amyloid pathological processes such as cerebral amyloid angiopathy [63,64].This highlights the importance of a multidisciplinary assessment, combining plasma Aβ42 with other biomarker profiles, such as Tau proteins and other protein related to other neurodegenerative pathways such as NfL could improve diagnostic accuracy for AD and related dementia in Africa [65–67].

· **Neurofilament light (NfL)**

Neurofilament light (NfL) is a prominent protein found in all axons of the neurons in the central nervous system [68]. It forms cylindrical and light subunits, constituting the dynamic network involved in neuronal differentiation and providing structural support to neurons [68]. Neurofilaments play essential roles in axonal growth, stability, maintenance of mitochondrial stability, and microtubule content [69]. Additionally, distinct neurofilament isoforms have been discovered to maintain the structure and function of dendritic spines associated with the synaptic status [70].

Neurofilament light is particularly crucial to study, as it seems to be involved in various pathophysiological processes leading to neurodegeneration [71]. Following axonal damage or neurodegeneration, neurofilaments or their fragments are released from the neurons [72]. The specific peptide species released and the mechanisms responsible for their release have not been clearly characterized [69]. This release can occur actively, for example, through exosomes, or passively due to loss of neuronal membrane integrity [73].

Different supramolecular structures or isoforms of neurofilaments may exhibit different degradation rates [69]. Studies on pathways for trafficking other proteins suggest that degraded neurofilament proteins may enter the peripheral circulation via perivascular drainage along the basement membranes of arteries, eventually reaching the cervical or lumbar lymph nodes and entering the blood [69]. In the central nervous system, NfL (the most soluble and abundant subunit) is likely to be released from damaged neurons into the blood following neurodegeneration or axonal damage [74]. This makes NfL a valuable marker for neuronal damage, especially in brain diseases such as AD, multiple sclerosis or motoneuron disease [75–77]. Recent studies have shown increased NfL levels in the CSF and blood of patients with AD, with significantly higher plasma NfL levels in patients with AD and Mild Cognitive Impairment (MCI) than in controls [78]. These studies have also associated NfL with cognitive, biochemical, and imaging hallmarks of the disease [79]. Consequently, researchers have proposed plasma NfL concentration as a minimally invasive biomarker for assessing neurodegeneration in AD and other brain diseases [80]. Considering the potential of NfL biomarkers in monitoring Alzheimer's disease progression, NfL could be helpful in assessing early neurodegeneration, thus aiding decision-making for the preliminary screening process in Low- and Middle-Income Countries (LMICs). It is crucial to standardize the measurements of NfL biomarkers accurately while also considering potential biases, such as age, dementia staging (non-demented, MCI, dementia), and other neurological disorders, which could significantly impact its biological relevance. Moreover, the general increase in NfL may complement P-tau and Aβ biomarkers, as it captures a broad spectrum of neurodegenerative diseases in Africa. Investigating the relationship between AD specific P-tau217 and the general neurodegeneration marker NfL in Africa could offer a promising direction for molecular epidemiological studies.

· **Glial Fibrillary Acidic Protein (GFAP)**

Astrocyte activation, a principal component of the blood-brain barrier, leads to the secretion of specific proteins including GFAP [81,82]. GFAP exhibits increased expression and concentration in proximity to Aβ plaques [82]. This process contributes to the accumulation of other proteins, such as tau, which further complicates the disease [83]. More recently, Bellaver et al. conducted a multisite study involving three

cohorts, demonstrating that the presence of astrocyte reactivity assessed by plasma GFAP levels could represent a pivotal biomarker abnormality for biologically determining the association between Aβ burden and early tau phosphorylation and aggregation in preclinical AD and for selecting cognitively unimpaired individuals for clinical trials [58]. This finding is particularly significant for identifying cognitively unimpaired individuals who may be potential candidates for clinical trials[58]. This detection is particularly relevant for identifying individuals at high risk of developing amyloid pathology, allowing for timely stratification and intervention [58]. Studies assessing the accuracy of plasma GFAP in the context of Alzheimer's disease, particularly in relation to neuroinflammation induced by comorbidities such as infectious and vascular diseases, could be beneficial in Africa.

- **Combining validation of current circulating biomarkers profiles could offer potential biological evidence of Alzheimer's Disease in native African patients.**

The field of Alzheimer's disease diagnosis through circulating biomarkers is incredibly dynamic, and ongoing research aimed to enhance their accessibility in resource-constraints countries. For Africa which present different comorbidity such as infectious diseases, cardiovascular and metabolic disorders, it could been challenging to define AD limited to A+ T+ profiles pushing us to believe that validation of the combined profiles of biomarkers panels in multidisciplinary approach combining clinical phenotype with biomarkers panel where NfL (indicative of neuronal damage and aspecific neurodegeneration), beta-amyloid ratio (reflecting altered amyloid homeostasis), various forms of P-Tau (signaling disruption of Tau homeostasis), genotyping characterization (African polygenetics risk and epigenetics factor) [84], and GFAP (indicative of altered astrocytic homeostasis) in the context of Alzheimer's disease could be a potential strategy to navigate into biological definition of AD in Africa context strategy [16,58,65–67,85].
For individuals with cognitive impairment or mild cognitive impairment who are plasma biomarker profiles categorized as either Aβ-positive/Tau-negative (A+/T-) or Aβ-positive/Tau-positive (A+/T+), knowing that amyloid presence could be detected in the normal aging state or indicate a preclinical Alzheimer's pathological change without AD symptoms, plasma GFAP levels could indicate Aβ burden and early tau phosphorylation and aggregation, contributing to the assessment of the risk of developing Alzheimer's disease or other types of dementias and for patients presenting clinically with an AD-like phenotype and plasma AD biomarker profiles (A+; T+) [16,58,65–67,85], Neurofilament Light Chain (NfL) can be used to evaluate additional neurodegenerative pathways[80].These efforts aims to mitigate the risk of false-positive biomarkers profiles and also highlight the necessity for a comprehensive evaluation of AD diagnosis by integrating Africa biological data in global AD scope and could be particularly valuable in the selection and expansion of candidate pools for regional clinical trials regarding the hope around anti-amyloid drugs or other current AD drug trial [6,86].

- **Extracellular Vesicles (EVs)**

One of the major challenges associated with highly expressed brain-derived proteins is their low detection in the blood [87]. This is primarily due to the masking effect of overexpressed proteins, such as albumin and immunoglobulins, which can sometimes bias the results [88]. Additionally, the presence of proteases in the blood may contribute to the degradation of key diagnostic proteins [89]. In this context, researchers have focused on circulating EVs in blood as potential carriers of biomarkers [90]. EVs are nanoparticles composed of a lipid bilayer that surrounds various bioactive cargo [90]. For example, EVs can contain lipids, proteins (and protein aggregates), DNA, RNA (including mRNA and miRNA), and functional receptors and organelles secreted by cells [91]. Unlike free proteins, this cargo is shielded from circulating enzymes by a protective lipid bilayer. Under physiological conditions, EVs are involved in intercellular signalling, shuttling of cargo from one cell to another, and the intracellular degradation of debris [92]. They are secreted by all cell types, including the various brain cells. Once secreted, these brain-derived EVs (BD-EV) can remain locally in the interstitial fluid (ISF) of the brain, but they can also cross the choroid plexus to enter the CSF, as well as cross

the BBB to enter the peripheral vasculature [93,94] Therefore, we found that BD-EV circulate among free proteins in the blood.

In the context of Alzheimer's disease, EVs are known to maintain their shuttling capacity, actively transport pathogenic tau, and seed it into recipient cells [93]. It is likely that EVs contain a wide variety of pathogenic cargo related to these disruptions, not limited to tau, which can indicate the pathological state of the brain. In this context, EVs can facilitate a comprehensive search for brain biomarkers in the blood, as the full protein content of these nanoparticles can be studied independently of contaminating blood proteins. Research combining this concept with the measurement of currently established biomarkers could yield powerful diagnostic tools, enabling clearer differentiation between healthy and AD trajectory patients in sub-Saharan Africa.

4- Benefits and challenging perspectives of using These Circulating Biomarkers in Africa

By combining the profiles of these biomarkers, which are commonly used in research settings and drug monitoring trials, their efficiency can be valuable in the decision-making process. These biomarkers aim to provide preliminary biological insights into AD, aiding in the early identification of potential cases, which is crucial in settings where neuroimaging tools are scarce and not widely accessible. Circulating biomarkers are designed to complement traditional diagnostic methods that mostly rely on clinical-radiological evaluations in Africa. Our approach is consistent with the current diagnostic process in Africa; integrating biomarkers as part of a broader assessment strategy could provide several advantages, such as enhancing the screening process and providing an African biological definition of AD. Validating these circulating biomarkers could offer numerous advantages for the diagnosis of AD in African countries.

Accessibility and minimally invasive nature of blood biomarkers: Blood sampling is a straightforward procedure that can be easily conducted in diverse healthcare settings in low- and middle-income countries (LMICs). Additionally, the majority of available quantitative or amplifying protein devices, such as mass spectrometry or SIMOA technology, are semi or not fully semi-automated, opening new opportunities for research capacity building on the continent [95]. In sub-Saharan Africa, the blood is commonly used to diagnose various diseases. This minimally invasive method is more easily integrated in the diagnosis process of diseases on the continent than other techniques such as lumbar puncture [9]. Implementing blood in the screening process for Alzheimer's disease allows for easier and broader implementation, particularly in regions with limited access to specialized facilities or resources.

Orienting the decision-making process: In Africa, AD diagnosis primarily relies on clinical and radiological evidence, with a potential error rate between 40 and 45%, as reported by Landau et al. [18]. Considering Africa's unique health landscape marked by prevalent infectious and non-communicable diseases, we propose a targeted biomarker panel comprising amyloid, P-tau, Total Tau, GFAP, and Neurofilament Light. This selection was guided by the current diagnostic process in Africa, aligned with the current NIA-AA Research Framework AT(N) classification. As already described, plasma GFAP could be particularly valuable in determining the association between the Aβ burden and early tau phosphorylation and aggregation in preclinical AD. Moreover, in patients with strong biological evidence of AD (plasma A+T+), Neurofilament Light can help assess axonal integrity and neurodegeneration beyond AD. In undetermined cases, additional CT scans or MRI can be instrumental in ruling out other neurodegenerative pathways in Africa, reducing the financial burden due to their primary intention use. Combining clinical diagnoses with validated blood biomarkers also aids in timely intervention and improves therapeutic strategies for disease management.

Expanding the Framework of Clinical Trials: Circulating biomarkers offer potential extension of clinical trials for Alzheimer's disease in LMICs, given that current global trends demonstrate the low representation of some

subpopulations, such as native Africans [96]. Expanding clinical trials to diverse populations, including LMICs, is crucial to ensure the generalizability and applicability of ongoing treatment trials [12]. These can serve as measures for monitoring treatment responses, assessing disease progression, and identifying suitable participant candidates for clinical trials in the LMIC regions. Moreover, the potential of African medicinal plants as novel therapeutic approaches to dementia care in these countries can be better studied within the framework of improved traditional medicines for dementia and related disorders [97,98]. The incorporation of blood biomarkers into clinical trial protocols allows for a more diverse population and comprehensive evaluation of therapeutic interventions, facilitating the monitoring and development of effective treatments. Therefore, circulating biomarkers may offer novel regional perspectives for clinical trials. This will enhance the inclusion of underrepresented populations and contribute to the advancement of clinical research, particularly in Africa. **Increasing representation of neglected populations of African ancestry in global genetic research:** Although populations from the African continent have been increasingly included in recent genetic studies, there is still a notable underrepresentation in studies focusing on circulating biomarkers for Alzheimer's Disease (AD) and related dementias. Pioneering initiatives, such as the Human Heredity and Health in Africa (H3Africa), Health and Aging in Africa (HAALSI), and Africa Dementia Consortium (ADC) are crucial in propelling genetic studies on the continent [36]. Assessing the polygenic risk of AD in biofluids could greatly enhance our understanding of the disease and ensure that genetic studies worldwide accurately represent African ancestry populations. This focus is vital in AD research, enabling a more thorough exploration of the disease spectrum, while considering the unique genetic diversity and environmental factors prevalent in African populations.

Addressing Ethical and Cultural Concerns: Practitioners often face ethical dilemmas when dealing with aging patients exhibiting neurocognitive decline, particularly in families that view it as a normal part of aging or through the lens of traditional beliefs [2].Additionally, there is reluctance to label a condition without available treatments or because of the cost of investigation. However, with emerging anti-amyloid drugs, the necessity for screening may be more easily communicated to the patients. Moreover, the lack of strong biological evidence, which can be addressed using blood biomarkers, may help to resolve these ethical and cultural concerns.

5- Requirements before implementing circulating biomarkers in LMICs

Although the potential benefits **(Table 2.)** of using circulating biomarkers for Alzheimer's disease in Africa and other LMICs could be promising, there are several considerations that require further investigation before their clinical application can be piloted and scaled up.

Infrastructure: Infrastructure plays a major role in the successful use of circulating biomarkers for AD diagnosis and research. This requires the availability of equipment, such as proteomic and quantitative amplifying protein detection devices, which are expensive and require the presence of trained bioengineers and other specialized researchers in the region. In addition, the availability of computational devices for analysis and a reliable electricity supply is essential for sample preservation, processing, and analysis. However, overcoming the challenges related to protein/extracellular vesicle extraction, proper sample handling, training national teams, and establishing a robust supply system on the continent is possible in the short term, whereas other aspects can be overcome in the middle and long terms.

Stakeholders: Implementing new initiatives in resource-constrained regions, such as improving the diagnosis of Alzheimer's diseases using circulating biomarkers, could face challenges due to specific regional legislation and regulations. Administrative procedures for ethics in research or clinical applications of research could be long and difficult to obtain, especially when other prevalent diseases with higher epidemiological burdens are prioritized in these countries. Convincing regional healthcare authorities or researchers to adopt new initiatives or deviate from their usual processes may be challenging. Therefore, it is

crucial to include all stakeholders, especially key stakeholders, in the discussion and fully involve them in every project, collaborating with national teams and initiatives to increase their sensitivity, participation, and ownership of change. This approach is vital to advocate for action, policy development, and support in the region regarding the importance and urgency of the diagnosis and management of Alzheimer's disease and related dementias, as was recently declared in Nairobi during the LMIC conference on dementia [36]. Examples of networks and partnerships established by the Africa Dementia Consortium, Africa Biofluid Brain Biobank (A4B), and the Brain Research Africa Initiative (BRAIN) can be very useful in this regard [99].

Standardization of measurement techniques, including sample collection, processing, and analysis methods, is crucial for ensuring consistent and comparable results across different studies and settings. Collaborative efforts among researchers, training of national healthcare professionals, and the creation of regional and subregional centers of excellence for AD research, diagnosis, and management can lead to the establishment of consensus guidelines for standardizing measurement techniques.

Validation:

Validation studies in diverse populations are essential to assess the diagnostic accuracy and clinical utility of circulating biomarkers. These studies should consider various factors, including ethnicity, postmortem brain characterization, neuroimaging (particularly PET amyloid, or tau); CSF circulating biomarkers validation, genetic background, educational level, cultural and linguistic aspects of cognitive assessment, and comorbidities in Africa. These factors can significantly influence and add nuances to the biological interpretation of blood biomarkers during screening. The reliability and applicability of circulating biomarkers can be better understood through studies with a broad range of samples. Subregional and regional dementia initiatives such as the Africa dementia consortium and transnational projects such as the Africa Biofluid and brain biobank (A4B) present valuable opportunities for the validation and implementation of these biomarkers with rigorous study designs, comprehensive data analysis, and careful consideration of covariates that may impact biomarker utilization to ensure the accurate interpretation of results and Diagnosis.

Feasibility studies: Continued research efforts are required to identify novel biomarkers for the diagnosis of neurodegenerative disorders on the continent, not limited to the current candidate**s.** Emerging technologies, such as proteomics, metabolomics, and genomics, can aid in the discovery of new biomarker candidates in different African subpopulations. By exploring these avenues, more specific and sensitive circulating biomarkers can be identified, leading to improved diagnostic accuracy and monitoring of neurodegenerative diseases in Africa and in other LMICs.

Prevention: We firmly believe that implementing risk-reduction strategies even before the onset of dementia symptoms is a valuable and cost-effective approach for integration into the dementia plan framework in the African context. This strategy entails a strong emphasis on potential interventions addressing cerebrovascular risk factors, identification of genetic risks and epigenetic modifications, effective management of comorbidities, consideration of socioeconomic factors, and promotion of education within the region [100] **(Fig. 3)**. Additionally, promoting lifelong cognitive reserve [101], cultivating a resilient environment, promoting brain activity, and necessitating the active participation of practitioners, populations, local associations, government bodies, and all stakeholders to ensure effective communication and comprehensive strategies [101]. Interventions targeting molecular mechanisms related to aging modifications, such as Alzheimer's disease and other related diseases, may be crucial for alleviating the escalating burden of dementia in Africa and other LMICs.

Conclusion

Alzheimer's disease poses significant challenges in low- and middle-income countries, especially in Africa, where the current diagnostic model relies heavily on clinicoradiological evidence. This approach leads to a

high risk of misdiagnosis and excludes many patients from current clinical trials owing to the lack of well-characterized patients or a strong biological definition of AD, which is often hampered by infrastructure limitations, economic burdens, and ethical or cultural discussions. By enhancing the screening process and research in Africa, blood biomarkers could address these challenges. Combining the profiles of biomarkers associated with

neuroinflammation and vascular modulation, such as GFAP, tau, Nfl, and amyloid beta proteins, could provide a minimally invasive, cost-effective, and timely approach for decision making. This method could also filter out patients needing additional investigations, such as CSF or neuroimaging, thereby expanding clinical trial participation in the African population. However, to fully harness the potential of circulating biomarkers in Africa, it is crucial to standardize measurement techniques and conduct validation studies that consider various confounding factors. Ongoing research efforts are essential for identifying novel biomarkers and utilizing emerging technologies for better diagnosis and monitoring of Alzheimer's disease in the African context. This shift in the diagnostic model towards circulating biomarkers could lead to more accessible, cost-effective, and culturally appropriate healthcare in Africa. Funding and collaborative research are vital for validating and integrating these biomarkers into clinical practice, improving patient outcomes, and reducing burden on families and communities.

Acknowledgments

Special thanks go to Dr. Maria C. Carrillo, Ph.D., Chief Science Officer, Medical and Scientific Relations, Alzheimer's Association for pertinent suggestions regarding this manuscript.

Conflict of Interest Statement

The authors have no conflicts of interest to declare.

Funding Sources

The Swiss Confederation, Centre Hospitalier Universitaire Vaudois (CHUV), and Synapsis Foundation, Lawson Foundation and Marina Cuennet-Mauvernay Foundation provided financial support for this project. **Author Contributions**

References

1 Breijyeh Z, Karaman R. Comprehensive Review on Alzheimer's Disease: Causes and Treatment. Molecules. 2020 Dec;25(24). DOI: 10.3390/molecules25245789

2 Akinyemi RO, Yaria J, Ojagbemi A, Guerchet M, Okubadejo N, Njamnshi AK, et al. Dementia in Africa: Current evidence, knowledge gaps, and future directions. Alzheimers Dement. 2022 Apr;18(4):790–809.

3 GBD 2019 Dementia Forecasting Collaborators. Estimation of the global prevalence of dementia in 2019 and forecasted prevalence in 2050: an analysis for the Global Burden of Disease Study 2019. Lancet Public Health.
2022 Feb;7(2): e105–25.

4 Jack CR Jr, Albert MS, Knopman DS, McKhann GM, Sperling RA, Carrillo MC, et al. Introduction to the recommendations from the National Institute on Aging-Alzheimer's Association workgroups on diagnostic guidelines for Alzheimer's disease. Alzheimers Dement. 2011 May;7(3):257–62.

5 Papaliagkas V, Kalinderi K, Vareltzis P, Moraitou D, Papamitsou T, Chatzidimitriou M. CSF Biomarkers in the Early Diagnosis of Mild Cognitive Impairment and Alzheimer's Disease. Int J Mol Sci. 2023 May;24(10). DOI:
10.3390/ijms24108976

6 van Dyck CH, Swanson CJ, Aisen P, Bateman RJ, Chen C, Gee M, et al. Lecanemab in Early Alzheimer's Disease. N Engl J Med. 2023 Jan;388(1):9–21.
7 Naicker S, Eastwood JB, Plange-Rhule J, Tutt RC. Shortage of healthcare workers in sub-Saharan Africa: a nephrological perspective. Clin Nephrol. 2010 Nov;74 Suppl 1: S129–33.
8 Aderinto N, Olatunji D, Abdulbasit M, Edun M. The essential role of neuroimaging in diagnosing and managing cerebrovascular disease in Africa: a review. Ann Med. 2023 Aug;55(2):2251490.
9 Thakur KT, Mateyo K, Hachaambwa L, Kayamba V, Mallewa M, Mallewa J, et al. Lumbar puncture refusal in sub-Saharan Africa: A call for further understanding and intervention. Neurology. 2015 May;84(19):1988–90.
10 Bermudez C, Graff-Radford J, Syrjanen JA, Stricker NH, Algeciras-Schimnich A, Kouri N, et al. Plasma biomarkers for prediction of Alzheimer's disease neuropathologic change. Acta Neuropathol. 2023 Jul;146(1):13– 29.
11 Karikari TK, Pascoal TA, Ashton NJ, Janelidze S, Benedet AL, Rodriguez JL, et al. Blood phosphorylated tau 181 as a biomarker for Alzheimer's disease: a diagnostic performance and prediction modelling study using data from four prospective cohorts. Lancet Neurol. 2020 May;19(5):422–33.
12 Clark LT, Watkins L, Piña IL, Elmer M, Akinboboye O, Gorham M, et al. Increasing Diversity in Clinical Trials:
Overcoming Critical Barriers. Curr Probl Cardiol. 2019 May;44(5):148–72.
13 McKhann G, Drachman D, Folstein M, Katzman R, Price D, Stadlan EM. Clinical diagnosis of Alzheimer's disease: report of the NINCDS-ADRDA Work Group under the auspices of Department of Health and Human Services Task Force on Alzheimer's Disease. Neurology. 1984 Jul;34(7):939–44.
14 Lee JC, Kim SJ, Hong S, Kim Y. Diagnosis of Alzheimer's disease utilizing amyloid and tau as fluid biomarkers. Exp Mol Med. 2019 May;51(5):1–10.
15 Leuzy A, Heurling K, Ashton NJ, Schöll M, Zimmer ER. In vivo Detection of Alzheimer's Disease. Yale J Biol Med. 2018 Sep;91(3):291–300.
16 Jack CR Jr, Bennett DA, Blennow K, Carrillo MC, Dunn B, Haeberlein SB, et al. NIA-AA Research Framework:
Toward a biological definition of Alzheimer's disease. Alzheimers Dement. 2018 Apr;14(4):535–62.
17 Del Sole A, Malaspina S, Magenta Biasina A. Magnetic resonance imaging and positron emission tomography in the diagnosis of neurodegenerative dementias. Funct Neurol. 2016 Oct/Dec;31(4):205–15.
18 Landau SM, Horng A, Fero A, Jagust WJ, Alzheimer's Disease Neuroimaging Initiative. Amyloid negativity in patients with clinically diagnosed Alzheimer disease and MCI. Neurology. 2016 Apr;86(15):1377–85.
19 Ogeng'o JA, Cohen DL, Sayi JG, Matuja WB, Chande HM, Kitinya JN, et al. Cerebral amyloid beta protein deposits and other Alzheimer lesions in non-demented elderly east Africans. Brain Pathol. 1996 Apr;6(2):101–7.
20 Musisi S, Jacobson S. Brain Degeneration and Dementia in Sub-Saharan Africa. Springer New York; 2015.
DOI: 10.1007/978-1-4939-2456-1
21 Chaudhry A, Rizig M. Comparing fluid biomarkers of Alzheimer's disease between African American or Black African and white groups: A systematic review and meta-analysis. J Neurol Sci. 2021 Feb; 421:117270.
22 Gureje O, Ogunniyi A, Baiyewu O, Price B, Unverzagt FW, Evans RM, et al. APOE epsilon4 is not associated with Alzheimer's disease in elderly Nigerians. Ann Neurol. 2006 Jan;59(1):182–5.

23 Hendrie HC, Murrell J, Baiyewu O, Lane KA, Purnell C, Ogunniyi A, et al. APOE ε4 and the risk for Alzheimer disease and cognitive decline in African Americans and Yoruba. Int Psychogeriatr. 2014 Jun;26(6):977–85.

24 Naslavsky MS, Suemoto CK, Brito LA, Scliar MO, Ferretti-Rebustini RE, Rodriguez RD, et al. Global and local ancestry modulate APOE association with Alzheimer's neuropathology and cognitive outcomes in an admixed sample. Mol Psychiatry. 2022 Nov;27(11):4800–8.

25 Kim S, Nho K, Ramanan VK, Lai D, Foroud TM, Lane K, et al. Genetic Influences on Plasma Homocysteine Levels in African Americans and Yoruba Nigerians. J Alzheimers Dis. 2016;49(4):991–1003.

26 Akinyemi RO, Owolabi MO, Okubadejo N, Ogunniyi A, Kalaria RN, African Dementia Consortium. The African Dementia Consortium. Lancet Neurol. 2023 Jan;22(1):28–9.

27 Chancel L, Cogneau D, Gethin A, Myczkowski A, Robilliard A-S. Income inequality in Africa, 1990–2019:
Measurement, patterns, determinants. World Dev. 2023 Mar; 163:106162.

28 Azevedo MJ. The State of Health System(s) in Africa: Challenges and Opportunities. In: Azevedo MJ, editor. Historical Perspectives on the State of Health and Health Systems in Africa, Volume II: The Modern Era.
Cham: Springer International Publishing; 2017; pp 1–73.

29 Adebisi AT, Salawu MA. Misconception of dementia-related disorders in Sub-Saharan Africa. Front Neurol.
2023 Apr; 14:1148076.

30 Yenet A, Nibret G, Tegegne BA. Challenges to the Availability and Affordability of Essential Medicines in African Countries: A Scoping Review. Clinicoecon Outcomes Res. 2023 Jun;15:443–58.

31 Chávez-Fumagalli MA, Shrivastava P, Aguilar-Pineda JA, Nieto-Montesinos R, Del-Carpio GD, PeraltaMestas A, et al. Diagnosis of Alzheimer's Disease in Developed and Developing Countries: Systematic Review and Meta-Analysis of Diagnostic Test Accuracy. J Alzheimers Dis Rep. 2021 Jan;5(1):15–30.

32 Salami D, Shaaban AN, Oliveira Martins M Do R. Africa Rising, a Narrative for Life Expectancy Gains? Evidence from a Health Production Function. Ann Glob Health. 2019 Apr;85(1). DOI: 10.5334/aogh.2307

33 Njamnshi AK. Looking back into the future of the neurosciences in Cameroon and Sub-Saharan Africa.
Health Sci Dis. 2022;23(10 Suppl 1). DOI: 10.5281/hsd. v23i10 Suppl 1.4444

34 Kissani N, Liqali L, Hakimi K, Mugumbate J, Daniel GM, Ibrahim EAA, et al. Why does Africa have the lowest number of Neurologists and how to cover the Gap? J Neurol Sci. 2022 Mar; 434:120119.

35 Njamnshi AK, Chokote E-S, Ngarka L, Nfor LN, Tabah EN, Atchou JGB, et al. Epilepsy-associated neurocognitive disorders (EAND) in an onchocerciasis-endemic rural community in Cameroon: A population-based case-control study. Epilepsy Behav. 2020 Nov; 112:107437.

36 Maestre G, Carrillo M, Kalaria R, Acosta D, Adams L, Adoukonou T, et al. The Nairobi Declaration-Reducing the burden of dementia in low- and middle-income countries (LMICs): Declaration of the 2022 Symposium on
Dementia and Brain Aging in LMICs. Alzheimers Dement. 2023 Mar DOI: 10.1002/alz.13025

37 Luzzatto L, Fasola F, Tshilolo L. Haematology in Africa. Br J Haematol. 2011 Sep;154(6):777–82.

38 Carvey PM, Hendey B, Monahan AJ. The blood-brain barrier in neurodegenerative disease: a rhetorical perspective. J Neurochem. 2009 Oct;111(2):291–314.

39 Ramos-Zaldívar HM, Polakovicova I, Salas-Huenuleo E, Corvalán AH, Kogan MJ, Yefi CP, et al. Extracellular vesicles through the blood-brain barrier: a review. Fluids Barriers CNS. 2022 Jul;19(1):60.

40 Klyucherev TO, Olszewski P, Shalimova AA, Chubarev VN, Tarasov VV, Attwood MM, et al. Advances in the development of new biomarkers for Alzheimer's disease. Transl Neurodegener. 2022 Apr;11(1):25.

41 Barbier P, Zejneli O, Martinho M, Lasorsa A, Belle V, Smet-Nocca C, et al. Role of Tau as a MicrotubuleAssociated Protein: Structural and Functional Aspects. Front Aging Neurosci. 2019 Aug;11:204.

42 Corsi A, Bombieri C, Valenti MT, Romanelli MG. Tau Isoforms: Gaining Insight into MAPT Alternative Splicing. Int J Mol Sci. 2022 Dec;23(23). DOI: 10.3390/ijms232315383

43 Liu F, Gong C-X. Tau exon 10 alternative splicing and tauopathies. Mol Neurodegener. 2008 Jul; 3:8.

44 Gambardella JC, Schoephoerster W, Bondarenko V, Yandell BS, Emborg ME. Expression of tau and phosphorylated tau in the brain of normal and hemiparkinsonian rhesus macaques. J Comp Neurol. 2023 Aug;531(11):1198–216.

45 Lacovich V, Espindola SL, Alloatti M, Pozo Devoto V, Cromberg LE, Čarná ME, et al. Tau Isoforms Imbalance Impairs the Axonal Transport of the Amyloid Precursor Protein in Human Neurons. J Neurosci. 2017 Jan;37(1):58–69.

46 Jellinger KA. Basic mechanisms of neurodegeneration: a critical update. J Cell Mol Med. 2010 Mar;14(3):457–87.

47 Iqbal K, Liu F, Gong C-X, Grundke-Iqbal I. Tau in Alzheimer disease and related tauopathies. Curr Alzheimer Res. 2010 Dec;7(8):656–64.

48 Suárez-Calvet M, Karikari TK, Ashton NJ, Lantero Rodríguez J, Milà-Alomà M, Gispert JD, et al. Novel tau biomarkers phosphorylated at T181, T217 or T231 rise in the initial stages of the preclinical Alzheimer's continuum when only subtle changes in Aβ pathology are detected. EMBO Mol Med. 2020 Dec;12(12): e12921.

49 Jonaitis EM, Janelidze S, Cody KA, Langhough R, Du L, Chin NA, et al. Plasma phosphorylated tau 217 in preclinical Alzheimer's disease. Brain Commun. 2023 Mar;5(2): fcad057.

50 Sadigh-Eteghad S, Sabermarouf B, Majdi A, Talebi M, Farhoudi M, Mahmoudi J. Amyloid-beta: a crucial factor in Alzheimer's disease. Med Princ Pract. 2015;24(1):1–10.

51 Murphy MP, LeVine H 3rd. Alzheimer's disease and the amyloid-beta peptide. J Alzheimers Dis. 2010;19(1):311–23.

52 Ruan D, Sun L. Amyloid-β PET in Alzheimer's disease: A systematic review and Bayesian meta-analysis. Brain Behav. 2023 Jan;13(1): e2850.

53 DeTure MA, Dickson DW. The neuropathological diagnosis of Alzheimer's disease. Mol Neurodegener. 2019 Aug;14(1):32.

54 O'Brien RJ, Wong PC. Amyloid precursor protein processing and Alzheimer's disease. Annu Rev Neurosci. 2011; 34:185–204.

55 Chow VW, Mattson MP, Wong PC, Gleichmann M. An overview of APP processing enzymes and products. Neuromolecular Med. 2010 Mar;12(1):1–12.

56 Wang D, Chen F, Han Z, Yin Z, Ge X, Lei P. Relationship Between Amyloid-β Deposition and Blood-Brain Barrier Dysfunction in Alzheimer's Disease. Front Cell Neurosci. 2021 Jul; 15:695479.

57 Ono K, Hamaguchi T, Naiki H, Yamada M. Anti-amyloidogenic effects of antioxidants: implications for the prevention and therapeutics of Alzheimer's disease. Biochim Biophys Acta. 2006 Jun;1762(6):575–86.

58 Bellaver B, Povala G, Ferreira PCL, Ferrari-Souza JP, Leffa DT, Lussier FZ, et al. Astrocyte reactivity influences amyloid-β effects on tau pathology in preclinical Alzheimer's disease. Nat Med. 2023 Jul;29(7):1775– 81.

59 Pérez-Grijalba V, Romero J, Pesini P, Sarasa L, Monleón I, San-José I, et al. Plasma Aβ42/40 Ratio Detects Early Stages of Alzheimer's Disease and Correlates with CSF and Neuroimaging Biomarkers in the AB255 Study. J Prev Alzheimers Dis. 2019;6(1):34–41.

60 Brand AL, Lawler PE, Bollinger JG, Li Y, Schindler SE, Li M, et al. The performance of plasma amyloid beta measurements in identifying amyloid plaques in Alzheimer's disease: a literature review. Alzheimers Res Ther.
2022 Dec;14(1):195.

61 Ashton NJ, Janelidze S, Mattsson-Carlgren N, Binette AP, Strandberg O, Brum WS, et al. Differential roles of Aβ42/40, p-tau231 and p-tau217 for Alzheimer's trial selection and disease monitoring. Nat Med. 2022 Dec;28(12):2555–62.

62 Klafki H-W, Vogelgsang J, Manuilova E, Bauer C, Jethwa A, Esselmann H, et al. Diagnostic performance of automated plasma amyloid-β assays combined with pre-analytical immunoprecipitation. Alzheimers Res Ther.
2022 Sep;14(1):127.

63 Coria F, Castaño EM, Frangione B. Brain amyloid in normal aging and cerebral amyloid angiopathy is antigenically related to Alzheimer's disease beta-protein. Am J Pathol. 1987 Dec;129(3):422–8.

64 Vergallo A, Mégret L, Lista S, Cavedo E, Zetterberg H, Blennow K, et al. Plasma amyloid β 40/42 ratio predicts cerebral amyloidosis in cognitively normal individuals at risk for Alzheimer's disease. Alzheimers Dement.
2019 Jun ;15(6) :764–75.

65 Martínez-Dubarbie F, Guerra-Ruiz A, López-García S, Lage C, Fernández-Matarrubia M, Infante J, et al. Accuracy of plasma Aβ40, Aβ42, and p-tau181 to detect CSF Alzheimer's pathological changes in cognitively unimpaired subjects using the Lumipulse automated platform. Alzheimers Res Ther. 2023 Oct;15(1):163.

66 Höglund K, Kern S, Zettergren A, Börjesson-Hansson A, Zetterberg H, Skoog I, et al. Preclinical amyloid pathology biomarker positivity: effects on tau pathology and neurodegeneration. Transl Psychiatry. 2017 Jan;7(1): e995.

67 Ashton NJ, Brum WS, Di Molfetta G, Benedet AL, Arslan B, Jonaitis E, et al. Diagnostic Accuracy of a Plasma Phosphorylated Tau 217 Immunoassay for Alzheimer Disease Pathology. JAMA Neurol. 2024 Jan DOI:
10.1001/jamaneurol.2023.5319

68 Narayanan S, Shanker A, Khera T, Subramaniam B. Neurofilament light: a narrative review on biomarker utility. Fac Rev. 2021 May; 10:46.

69 Gafson AR, Barthélemy NR, Bomont P, Carare RO, Durham HD, Julien J-P, et al. Neurofilaments: neurobiological foundations for biomarker applications. Brain. 2020 Jul;143(7):1975–98.

70 Gürth C-M, do Rego Barros Fernandes Lima MA, Macarrón Palacios V, Cereceda Delgado AR, Hubrich J, D'Este E. Neurofilament Levels in Dendritic Spines Associate with Synaptic Status. Cells. 2023 Mar;12(6). DOI:
10.3390/cells12060909

71 Yuan A, Nixon RA. Neurofilament Proteins as Biomarkers to Monitor Neurological Diseases and the Efficacy of Therapies. Front Neurosci. 2021 Sep;15:689938.

72 Yuan A, Rao MV, Veeranna, Nixon RA. Neurofilaments and Neurofilament Proteins in Health and Disease.
Cold Spring Harb Perspect Biol. 2017 Apr;9(4). DOI: 10.1101/cshperspect. a018309

73 Huo L, Du X, Li X, Liu S, Xu Y. The Emerging Role of Neural Cell-Derived Exosomes in Intercellular Communication in Health and Neurodegenerative Diseases. Front Neurosci. 2021 Aug; 15:738442.

74 Ferreira-Atuesta C, Reyes S, Giovanonni G, Gnanapavan S. The Evolution of Neurofilament Light Chain in Multiple Sclerosis. Front Neurosci. 2021 Apr ;15 :642384.

75 Andersson E, Janelidze S, Lampinen B, Nilsson M, Leuzy A, Stomrud E, et al. Blood and cerebrospinal fluid neurofilament light differentially detect neurodegeneration in early Alzheimer's disease. Neurobiol Aging. 2020 Nov; 95:143–53.
76 Kouchaki E, Dashti F, Mirazimi SMA, Alirezaei Z, Jafari SH, Hamblin MR, et al. Neurofilament light chain as a biomarker for diagnosis of multiple sclerosis. EXCLI J. 2021 Aug; 20:1308–25.
77 Behzadi A, Pujol-Calderón F, Tjust AE, Wuolikainen A, Höglund K, Forsberg K, et al. Neurofilaments can differentiate ALS subgroups and ALS from common diagnostic mimics. Sci Rep. 2021 Nov;11(1):22128.
78 Fan Z, Liu X, Liu J, Chen C, Zhou M. Neurofilament Light Chain as a Potential Biomarker in Plasma for Alzheimer's Disease and Mild Cognitive Impairment: A Systematic Review and a Meta-Analysis. J Integr Neurosci. 2023 Jun;22(4):85.
79 Mattsson N, Andreasson U, Zetterberg H, Blennow K, Alzheimer's Disease Neuroimaging Initiative. Association of Plasma Neurofilament Light with Neurodegeneration in Patients with Alzheimer Disease. JAMA Neurol. 2017 May;74(5):557–66.
80 Beydoun MA, Noren Hooten N, Beydoun HA, Maldonado AI, Weiss J, Evans MK, et al. Plasma neurofilament light as a potential biomarker for cognitive decline in a longitudinal study of middle-aged urban adults. Transl Psychiatry. 2021 Aug;11(1):436.
81 Wang P, Ye Y. Astrocytes in Neurodegenerative Diseases: A Perspective from Tauopathy and αSynucleinopathy. Life. 2021 Sep;11(9). DOI: 10.3390/life11090938
82 Asken BM, Elahi FM, La Joie R, Strom A, Staffaroni AM, Lindbergh CA, et al. Plasma Glial Fibrillary Acidic Protein Levels Differ Along the Spectra of Amyloid Burden and Clinical Disease Stage. J Alzheimers Dis. 2020;78(1):265–76.
83 Fleeman RM, Proctor EA. Astrocytic Propagation of Tau in the Context of Alzheimer's Disease. Front Cell Neurosci. 2021 Mar; 15:645233.
84 Fatumo S, Sathan D, Samtal C, Isewon I, Tamuhla T, Soremekun C, et al. Polygenic risk scores for disease risk prediction in Africa: current challenges and future directions. Genome Med. 2023 Oct;15(1):87.
85 Kim KY, Shin KY, Chang K-A. GFAP as a Potential Biomarker for Alzheimer's Disease: A Systematic Review and Meta-Analysis. Cells. 2023 May;12(9). DOI: 10.3390/cells12091309
86 Addressing Diversity in Alzheimer's Clinical Trials [Internet]. AAIC. [cited 2024 Feb 13]. Available from: https://aaic.alz.org/releases_2021/clinical-trial-diversity.asp
87 Delaby C, Hirtz C, Lehmann S. Overview of the blood biomarkers in Alzheimer's disease: Promises and challenges. Rev Neurol. 2023 Mar;179(3):161–72.
88 Schenk S, Schoenhals GJ, de Souza G, Mann M. A high confidence manually validated human blood plasma protein reference set. BMC Med Genomics. 2008 Sep; 1:41.
89 López-Otín C, Bond JS. Proteases: multifunctional enzymes in life and disease. J Biol Chem. 2008 Nov;283(45):30433–7.
90 Di Bella MA. Overview and Update on Extracellular Vesicles: Considerations on Exosomes and Their Application in Modern Medicine. Biology. 2022 May;11(6). DOI: 10.3390/biology11060804
91 Welsh JA, Goberdhan DCI, O'Driscoll L, Buzas EI, Blenkiron C, Bussolati B, et al. Minimal information for studies of extracellular vesicles (MISEV2023): From basic to advanced approaches. J Extracell Vesicles. 2024 Feb;13(2): e12404.
92 Berumen Sánchez G, Bunn KE, Pua HH, Rafat M. Extracellular vesicles: mediators of intercellular communication in tissue injury and disease. Cell Commun Signal. 2021 Oct;19(1):104.
93 Eshraghi M, Adlimoghaddam A, Mahmoodzadeh A, Sharifzad F, Yasavoli-Sharahi H, Lorzadeh S, et al.

Alzheimer's Disease Pathogenesis: Role of Autophagy and Mitophagy Focusing in Microglia. Int J Mol Sci. 2021 Mar;22(7). DOI: 10.3390/ijms22073330

94 Perbet R, Zufferey V, Leroux E, Parietti E, Espourteille J, Culebras L, et al. Tau Transfer via Extracellular Vesicles Disturbs the Astrocytic Mitochondrial System. Cells. 2023 Mar;12(7). DOI: 10.3390/cells12070985

95 2014 Nov;16(6):1175–

96 Mora J, Given Chunyk A, Dysinger M, Purushothama S, Ricks C, Osterlund K, et al. Next generation ligand binding assays-review of emerging technologies' capabilities to enhance throughput and multiplexing. AAPS J. 84.

Morris JC, Schindler SE, McCue LM, Moulder KL, Benzinger TLS, Cruchaga C, et al. Assessment of Racial Disparities in Biomarkers for Alzheimer Disease. JAMA Neurol. 2019 Mar;76(3):264–73.

97 Njamnshi AK, Ahidjo N, Ngarka L, Nfor LN, Mengnjo MK, Njamnshi WY, et al. Characterization of the Cognitive and Motor Changes Revealed by the Elevated Plus Maze in an Experimental Rat Model of RadiationInduced Brain Injury. Adv Biomed Res. 2020 Nov; 9:72.

98 Ahidjo N, Ngarka L, Seke Etet PF, Njamnshi WY, Nfor LN, Mengnjo MK, et al. Garcinia kola improves cognitive and motor function of a rat model of acute radiation syndrome in the elevated plus maze. Brain Commun. 2021 Jul;3(3): fcab170.

Figure legends

Fig. 1. Alarming Surge in Alzheimer's Disease Cases Expected in Africa by 2050. (A) Diagram illustrating the projected increase in AD across the continents. (B) Map displaying doctor-to-population z-scores by country. (C) Histogram showing the average MRI densities (z-score) by continent in 2019. The data for this figure were obtained from the WHO Health Organization website (https://www.who.int).

Fig. 2. Brain Secretome: A Promising Diagnostic Tool for Alzheimer's disease. This illustration depicts the various proteins increased (arrow up) and decreased (arrow down) in the brain of an Alzheimer's patient, which are secreted into biofluids such as cerebrospinal fluid (CSF) and blood in free form (circulating Brain-Derived protein) or in extracellular vesicles (circulating Brain-derived EV).* for P-Tau include : pTau-181, pTau-199 , pTau-

202, pTau-205, pTau-217, pTau-231 and pTau-396

Fig. 3. Summary of possible areas of intervention for dementia prevention in Africa. This illustration describes the areas of intervention essential for preserving cognitive health in Africa's diverse landscapes. From community education to targeted healthcare, these strategies address the unique challenges faced by the continent in its fight against dementia.

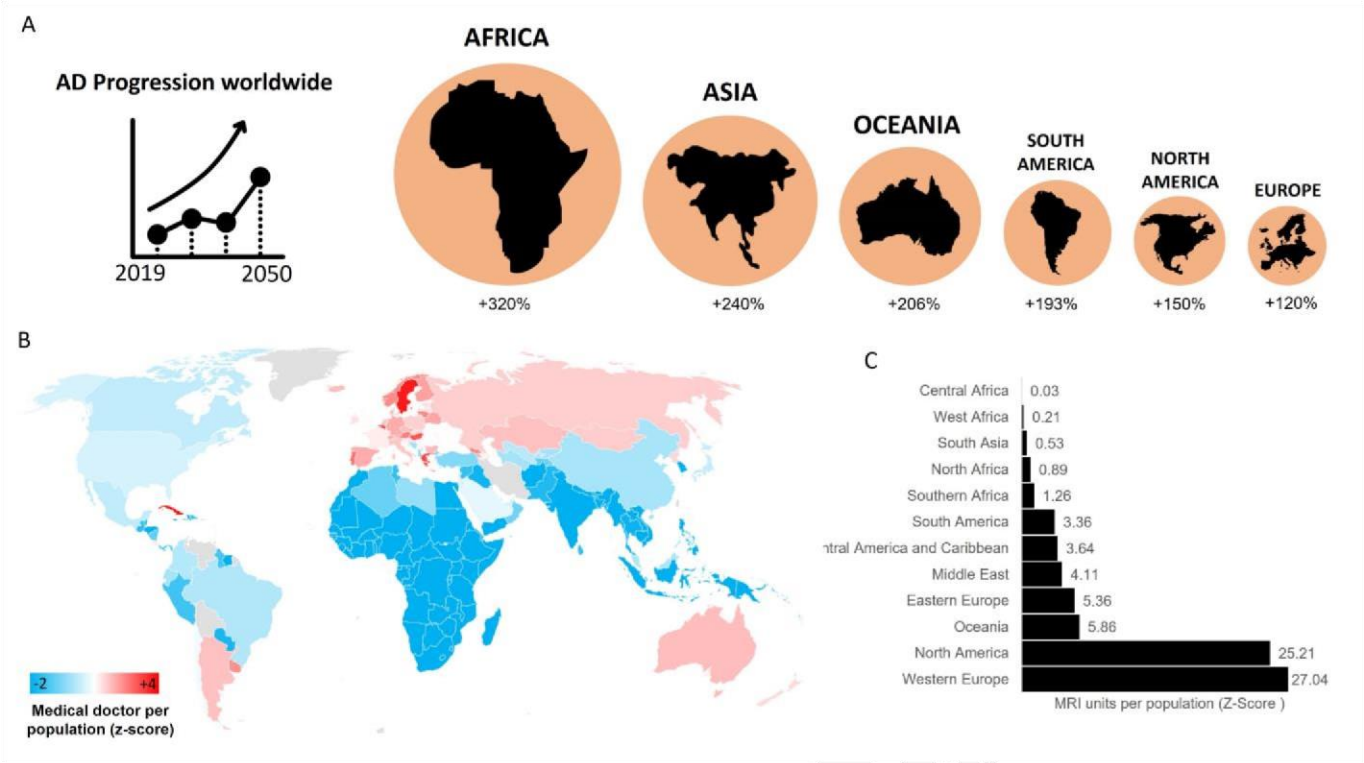

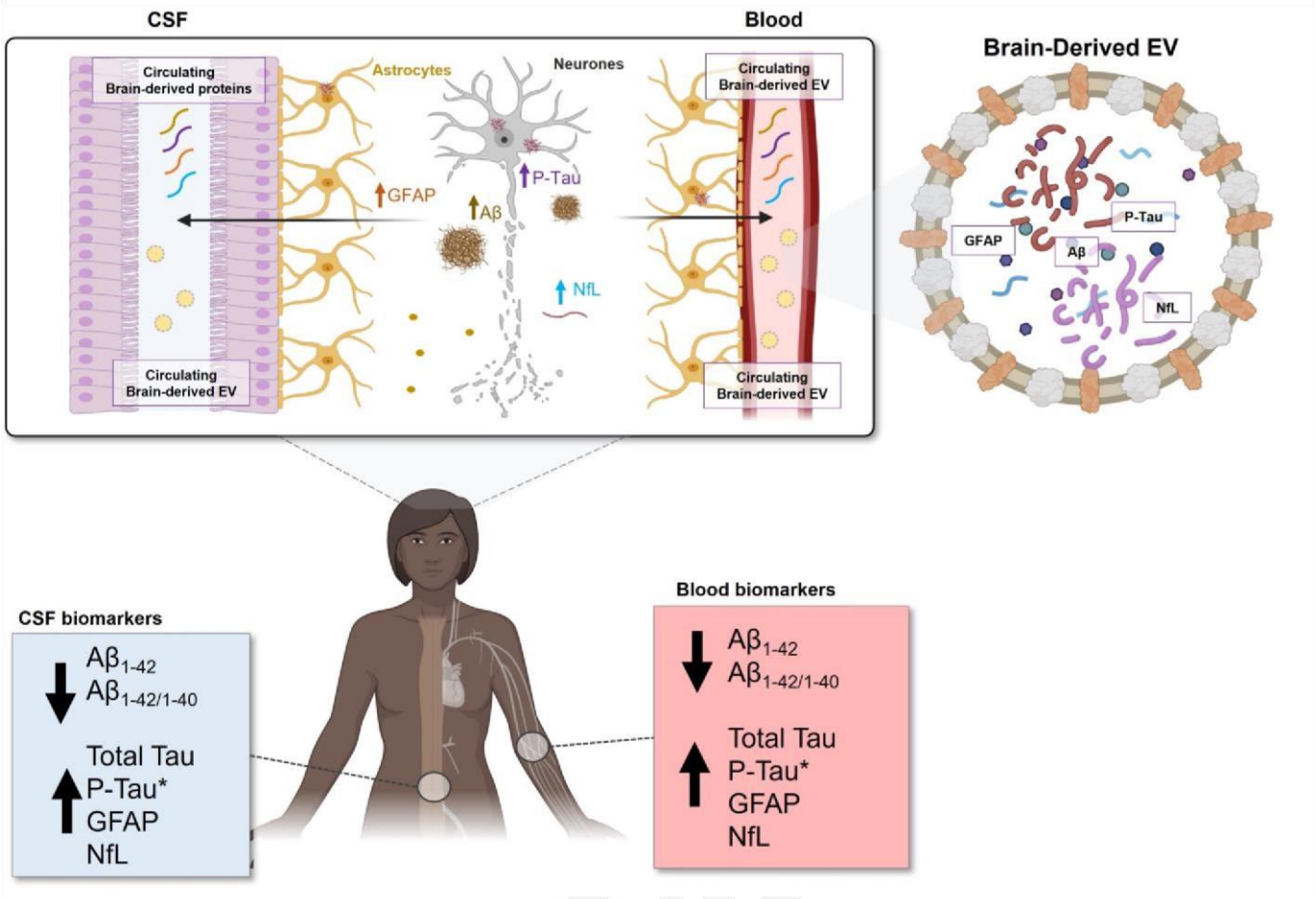

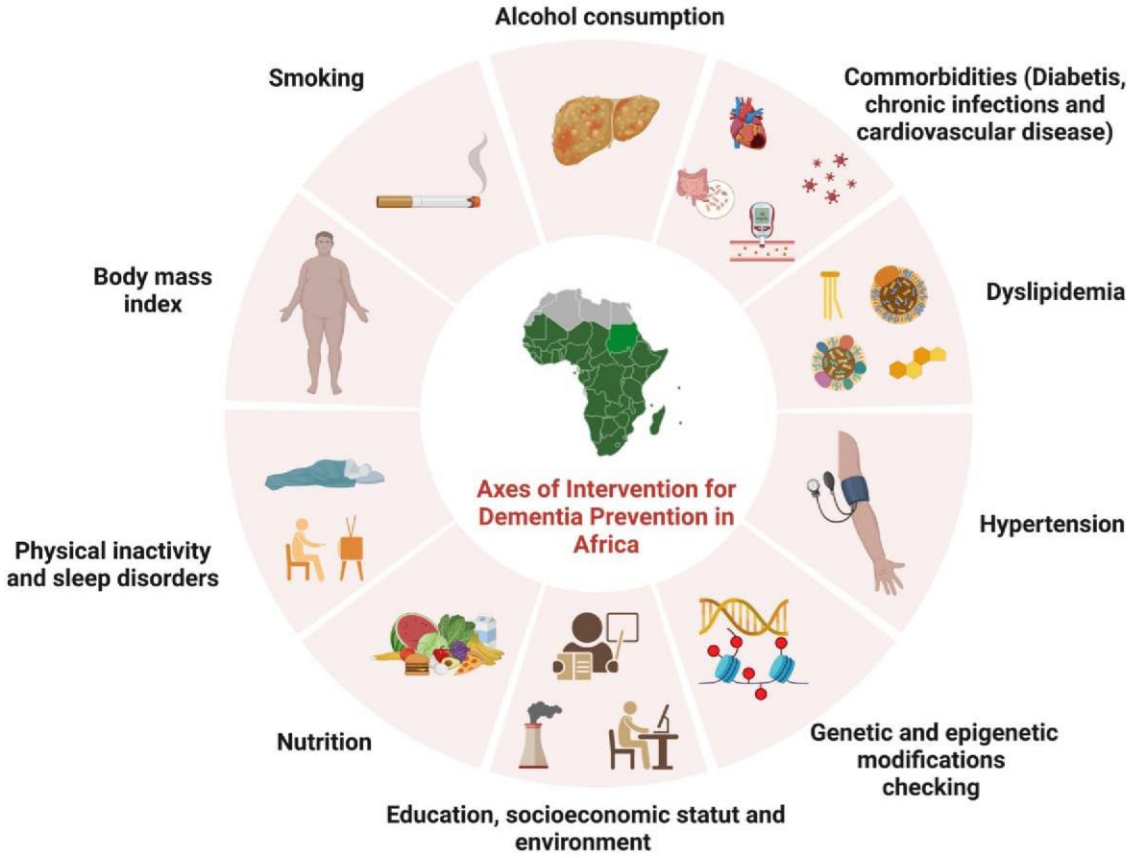

Table 1. Summary of the different challenges related to diagnosis access for Alzheimer's disease in Africa.

Not enough healthcare resources
Concerns about certain diagnostic methods
Not enough specialized doctors or centers
Inadequate healthcare coverage
Expensive diagnostic tools
Unsuitable nature of tools to local culture and education levels
high economic burden, along with other health priorities
Lack of data on dementia and CSF biomarkers.

Table 2. Summary of the benefits of using circulating biomarkers for Alzheimer's disease in Africa.

Providing biological support for the screening process
Expanding clinical trials with diverse participants
Inclusion of populations of African ancestry in genetic studies
Dealing with ethical and cultural issues
Establishing patient cohorts for disease monitoring over time
Speeding up diagnosis confirmation talks
Improving patient counseling and support
Demystifying disease misconceptions using evidence
Using easy and appropriate technology for biomarker measurement
Cost-effective and minimally invasive approaches
Increasing global biomarker data
Supporting evidence-informed policy.

Annex 5

Inverse and Postponed Impacts of Extracellular Tau PHF on Astrocytes and Neurons' Mitochondrial Function

Valentin Zufferey[1], Enea Parietti[1], Aatmika Barve[1], Jeanne Espourteille[1], Yvan Varisco[2], Kerstin Fabbri[2], Francesca Capotosti[2], Nicolas Preitner[2], Kevin Richetin[1,3*]

[1] Centre des Neurosciences Psychiatriques (CNP), Centre Hospitalier Universitaire Vaudois (CHUV) - Université de Lausanne (UNIL)

[2] AC Immune SA, Lausanne, Switzerland

[3] Centre Leenaards de la memoire, Centre Hospitalier Universitaire Vaudois (CHUV) - Université de Lausanne (UNIL)

Corresponding author: Dr. Richetin Kevin (kevin.richetin@chuv.ch)

Keywords: Tau, mitochondria, astrocytes, neurons, synapses, live imaging microscopy

Abstract

Background: Tauopathies encompass a spectrum of neurodegenerative disorders which are marked by the pathological aggregation of tau protein into paired helical filaments (PHF-tau), neurofibrillary tangles (NFTs) and Glial-fibrillary tangles (GFTs). These aggregates impair cellular, mitochondrial, and synaptic functions. The emergence of extracellular tau (ePHF-tau), featuring a myriad of isoforms and phosphorylation states, presents a challenge in comprehending its nuanced effects on neural cells, particularly concerning synaptic and mitochondrial integrity.

Methods: We studied the impact of ePHF-tau (2N4R) on different states and ages of primary cultures of rat neuroglia. Using confocal microscopy and proteomic analysis of synaptosomes, we studied the impact of ePHF-tau on neurite and synapse number. We monitored mitochondrial responses in neurons and astrocytes over 72 hours using advanced fluorescence microscopy for dynamic, high-throughput analysis.

Results: Treatment with ePHF-tau has a strong effect on the neurites of immature neurons, but its toxicity is negligible when the neurons are more mature. At the mature stage of their development, we observed a substantial increase in the density of the PSD-95/vGlut1 zone in neurite, suggesting altered synaptic connectivity and ePHF-tau excitotoxicity. Proteomics revealed significant changes in mitochondrial protein in synaptosomes following exposure to ePHF-tau. In the neuronal compartment, real-time imaging revealed rapid and persistent mitochondrial dysfunction, increased ATP production, and reduced mitochondrial turnover. In contrast, we observed increased mitochondrial turnover and filamentation after treatment in the astrocyte processes, indicating cell-specific adaptive responses to ePHF-tau.

Conclusions: This study sheds light on the intricate effects of extracellular tau aggregates on neuronal and astrocytic mitochondrial populations, highlighting how tau pathology can lead to mitochondrial disturbances and synaptic alterations. By delineating the differential responses of neurons and astrocytes to ePHF-tau, our findings pave the way for developing targeted therapeutic interventions to mitigate the detrimental impacts of tau aggregates in neurodegenerative diseases.

Background

Under healthy conditions, the tau protein plays a crucial role in stabilizing microtubules within neurons, which is vital for preserving cellular architecture and facilitating intracellular transport mechanisms [1]. However, as individuals age, the brain may exhibit abnormal accumulations of tau protein, forming insoluble paired helical filaments (PHF-tau). These can further aggregate into neurofibrillary tangles (NFTs), which are composed of various phosphorylated tau species. This phenomenon underpins the pathology of a diverse group of disorders known as tauopathies, which encompass more than 20 diseases, such as Alzheimer's disease (A.D.), progressive supranuclear palsy (PSP), and frontotemporal dementia (FTD) [2]. Despite the common feature of tau accumulation in tauopathies, significant distinctions exist regarding the distribution of tau pathology, the occurrence of tau inclusions in glial cells, the association with other neuropathological features such as amyloid deposits or Lewy bodies, and the specific tau isoforms and aggregates present [3].

Much research has focused on the deleterious effects of intracellular Tau aggregation, particularly concerning synaptic functions and mitochondrial integrity. Various tau species, including extracellular NFTs and PHF-tau (ePHF-tau), can be released into the extracellular space during neurodegenerative states. This process of cell-to-cell transmission has been thoroughly investigated, revealing how it facilitates the spread of tau pathology by compromising the function of endogenous tau in neighboring neurons [4,5]. Studies have shown that extracellular paired helical filaments (PHFs) can trigger extensive tau accumulation within neurites, mainly affecting postmitotic neurons [6]. It has also been suggested that PHFs indirectly interfere with dynein/kinesin-mediated axonal transport, underscoring the intricate impact of tau on neuronal function [7]. The wide variability of extracellular tau, including differences in isoform and phosphorylation levels, complicates our understanding of its exact pathophysiological consequences on synaptic structures.

Although most of the related work has focused on understanding the deleterious effects of various forms of tau on neurons, several studies have recently demonstrated that glial cells, particularly astrocytes, are capable of accumulating tau in its hyperphosphorylated and aggregated form in different contexts and pathologies. In this context, we previously demonstrated that the mitochondrial system is particularly susceptible to the different forms of 3R and 4R Tau that accumulate or recover [8,9]. To further extend our understanding of the cellular and mitochondrial impacts of Tau pathology, we explored the impact of ePHF aggregates on 2D pure neuron rat primary cultures and 3D neuro-glia rat primary cultures. We aimed to decipher the mechanisms by which ePHF influences cell function through an integrative approach combining confocal imaging, real-time fluorescence imaging and proteomics analysis of synaptosomes. We shed light on the complexity and temporality of the effect of ePHFs on different synaptic compartments, with a particular focus on the mitochondrial system of neurites and astrocytic processes. This work reveals the subtle perturbations induced by ePHF-tau and its ability to modulate synaptic architecture through its differential effects on the mitochondria of neurons and astrocytes.

Methods

Isolation of human brain derived PHF

Tau paired-helical filaments (PHF) were isolated from post-mortem frontal cortex tissue of an Alzheimer's disease (A.D.) patient (purchased from Tissue Solution). The enrichment procedure was modified from Jicha et al, 1997 and Rostagno and Ghiso, 2009. Briefly, approximately 15 g of frontal cortex tissue were thawed on ice and homogenized using a glass Dounce homogenizer in 50 mL of a homogenization buffer consisting of 0.75 M NaCl, 100 mM (MES) pH 6.8, 1 mM EGTA, 0.5 mM MgSO4, 2 mM DTT, and protease inhibitors (Complete; Roche 11697498001). The homogenate was then incubated at 4°C for 20 min for microtubule depolymerization, before being transferred into polycarbonate centrifuge bottles (16 x 76 mm; Beckman 355603) and centrifuged at 11,000 g (12,700 RPM) in an ultracentrifuge (Beckman, XL100K) for 20 min at 4°C using the pre-cooled 70.1 rotor (Beckman, 342184). Pellets were kept on ice. Supernatants were pooled into polycarbonate bottles and centrifuged again at 100,000 g (38,000 RPM) for 1 h at 4°C in the 70.1 Ti rotor to isolate PHF-rich pellets, whereas soluble tau remained in the supernatants. The pellets from the first and second centrifugations were resuspended in 120 mL of extraction buffer [10 mM Tris-HCl pH 7.4, 10% sucrose, 0.85 M NaCl, 1% protease inhibitor (Calbiochem 539131), 1 mM EGTA, 1% phosphatase inhibitor (Sigma P5726 and P0044)]. The solution was then transferred into polycarbonate centrifuge bottles (16 x 76 mm; Beckman 355603) and centrifuged at 15,000 g (14,800 RPM) in an ultracentrifuge (Beckman, XL100K) for 20 min at 4°C using the 70.1 Ti rotor. In the presence of 10% sucrose and at low-speed centrifugation, most PHF remained in the supernatant whereas intact or fragmented NFTs and larger PHF aggregates were pelleted. The pellets were discarded. 30% Sarkosyl (Sigma L7414-10ML) was added to the supernatants to a final concentration of 1% and stirred at R.T. for 1 h. This solution was then centrifuged in polycarbonate bottles at 100,000 g (38,000 RPM) for 1 h at 4°C in the 70.1 Ti rotor, and the pellets containing PHF-rich material were resuspended in 50ul PBS/ 1g of brain tissue. The resuspended PHF was then sonicated on ice for 60s with 1s-on/1s-off cycles at 20% amplitude. Aliquots were snap frozen and stored at -80°C.

Preparation of Tau aggregates

Tau PHF isolated from Human A.D. brain was used as seed to induce the templated aggregation of human full length 2N4R Tau monomers (35uM, Biotechne in a 72h incubation at 37C on a shaker at 1000 rpm . These aggregates were stored at -20°C. Three days before the treatment of neurons, these aggregates were thawed

and used as seeds (1:200) in a secondary aggregation reaction in the presence of 10 µM tau monomers (72h at 37C, 1000 rpm).

Lentiviral vector production and infection

The L.V.s were pseudotyped as vesicular stomatitis virus glycoprotein G (VSV-G). LV-PGK-MitoTimer and LV-PGK-MitoGoTeam2 (G1B3 promoter instead of PGK for astrocytes) were produced by transfection of human embryonic kidney (HEK) *293T* cells (mycoplasma-negative, ATCC, LGC Standards GmbH, Germany). L.V.s were concentrated by ultracentrifugation and resuspended in phosphate-buffered saline (dPBS, Gibco, Life Technologies, Zug, Switzerland) supplemented with 1% bovine serum albumin (BSA, Sigma□Aldrich, Buchs, Switzerland). The viral particle content in each batch was determined using a p24 antigen enzyme-linked immunosorbent assay (p24 ELISA, RETROtek; Kampenhout, Belgium). The stocks were stored at −80°C until use and diluted to 100,000 ng/ml in PBS/1% BSA. For neuronal expression of mitochondrial biosensors, cells were infected at DIV 5 with lentiviral vectors (L.V.s) expressing reporter genes, mainly in neurons. The LV-PGK vectors used in this study have been previously described by Schwab and colleagues [10]. The reporter gene contained a woodchuck hepatitis virus B postregulatory element (WPRE) and the mouse PGK promoter. Astrocytes were infected at 8 DIV with lentiviral vectors (LV) expressing the mitochondrial reporter gene. The gfaABC1D promoter was ligated to enhancer B(3) to generate the G1B3 promoter, which was subsequently cloned and inserted into the SIN-cPPT-gateway-WPRE-miR124T transfer plasmid, which contains four copies of the neuron-specific miRNA-124 target sequence (miR124T; full homology) to repress transgene expression in neurons, WPRE and the central polypurin tract (cPPT) to increase transgene expression and a 400-nucleotide deletion in the long 3' terminal repeat (self-inactivating vector) to increase biosafety.

2D Primary pure neuron culture

Rat primary cortical cultures were prepared from Sprague-Dawley rats (Charles River Laboratories L'Arbresle, France) at postnatal day 1. The neocortex and hippocampus were isolated by removing the dura, brainstem, olfactory bulbs and subcortical regions. Isolated cortex and hippocampus were cut into small pieces and dissociated by enzymatic digestion for 30 minutes at 37°C in dissociation buffer (papaine, CaCl2, EDTA, and HEPES; all from Invitrogen, Carlsbad, CA, USA). DNase (Invitrogen, Basel, Switzerland) was added, and the mix was incubated for another 30 min at 37C. After mechanical dissociation consisting in pipetting the tissue up and down, the cell suspension was passed through a cell strainer and dispersed cells were plated onto 96-well tissue culture plates coated with poly-D-Lysine (Corning, 3841) at 30K cells/well. Cells were plated in Neurobasal medium (Invitrogen, Basel, Switzerland) without phenol red, with the addition of L-glutamine (2

mM; Sigma, Buchs, Switzerland), 10% FCS (Invitrogen, Basel, Switzerland), and penicillin/streptomycin (Sigma, Buchs, Switzerland) and incubated at 37C in the presence of 5% CO2. 1.5 hours after plating the cells, the medium was replaced with Neurobasal medium containing 2mM L-Glutamine, B-27TM (Gibco, 17504-044), and penicillin/streptomycin. After 4 days in culture, cell proliferation was blocked by treatment with 2.5 µM cytosine arabinoside (Invitrogen, Basel, Switzerland).

3D Primary neuron-glial cultures

For 3D culture, hippocampus of E17 Wistar rat embryos was dissected, and the cells were dissociated with a neuronal dissociation kit (130-092-628). Mixed cells were plated at a density of 30K cells/cm2 in 24-well or 96-well glass-bottom plates (Ibidi 82426, Corning™ 356234) coated with Matrigel in 200 µM DMEM (Gibco 41965-039, 25 mM glucose) supplemented with 0.25% L-glutamine (Gibco, 25030081), 1% penicillin/streptomycin (Thermo Fisher Scientific 15140-122) and 2% B27 (17504044, Gibco) and incubated at 37°C and 5% CO2.

Immunofluorescent stainings

Three days after treatment, cells were fixed with 4% PFA (Sigma, 158127-500G) for 15 min at 37°C and stored in PBS at 4°C for further analysis. All the incubations and extractions were carried out in PBST (10010-015, Gibco), 0.3% Triton X-100 (Sigma–Aldrich, X100-100ML), and 3% NHS (Gibco, 16050-122). Primary antibody incubation was performed overnight with rabbit anti-VGlut1 (Cell Signaling Technology, 1230.31; 1:500), chicken anti MAP2 (Abcam, ab5392, 1:1'000), goat anti-PSD95 (Abcam, ab12093; 1:500), or mouse anti-NeuN (Chemicon, MAB337) and anti-GFAP (Dako, GA52461-2) antibodies. Secondary antibody incubation was conducted for 60 min at room temperature with Alexa Fluor 488-, 555- or 647-conjugated highly cross-adsorbed donkey anti-goat, donkey anti-rabbit or donkey anti-chicken antibodies, respectively (1:500; Invitrogen A31573, Invitrogen A11055, Jackson IR 703-545-155). After additional incubation in DAPI (Merck, 268298; 1:5,000), the cells were stored at 4 °C in PBS.

Microscopy and image acquisition

In this study, 2D cultures (Fig.1) and live imaging (Fig. 4-5) were acquired with an inverted microscope (Nikon Eclipse Ti-2) equipped with an Okolab cage incubator (H201-T-UNIT), the Perfect Focus System (PFS), CFI Plan Apochromat Lambda D 40X and 60X Oil, and Lumencor SPECTRA X Light Engine. 3D culture (Fig.2) were acquired with fully motorized model Ni-E equipped with spinning-disk confocal technology (CrestOptic, X-Light V3) and CFI Plan Apochromat Lambda D 40X and 60X Oil. All images were acquired with Nikon's software suite NIS HC v.5.42.

Images analysis

Images were analyzed using Nikon NIS AI or H.C. v.5.42 and the General analysis 3 (GA3) module of this software. For 2D culture analysis, 8000x8000 pixels mosaic images of each well were analyzed to quantify the number of DAPI-labeled cells and neuritic segments, using MAP2 labeling reconstruction. MAP2 was segmented and skeletonized to measure total branch length. MAP2 in the vicinity of DAPI+ nuclei was excluded by subtraction of dilated the DAPI objects.

For synapse analysis all images were enhanced AI-denoising tool. VGlut1+ and PSD-95+ labeled puncta were quantified in regions of interest free of cell nuclei. Synaptic markers were analyzed using a spot detection algorithm. Overlay points between spots were quantified to detect vGlut1/PSD-95 active areas. All data were normalized by the MAP2 area per ROI. The GA3 analysis script used is accessible in the supplementary material. For the analysis of 3D cultures, confocal acquisitions at 60X were performed on approximately 30 focal sections of 0.3 µm of 2048x2048 pixels. Between 5 and 10 volumes of interest located in proximal neurites emanating from neurospheroids were selected to quantify vGlut1 and PSD95 in three dimensions. Volumes corresponding to PSD95 were used to create three-dimensional objects, while a spot detection algorithm was used to identify vGlut1 puncta. To include only vGlut1 volumes in contact with PSD-95, the PSD95 volume was dilated by 0.1 µm. The sum of the volumes of vGlut1 spots in the dilated volume of PSD95 (PSD-95 shell) was then calculated. All GA3 analysis scripts are available in the data repository.

Mitochondrial live monitoring of morphology and turnover was conducted as previously described [8,9] at 40x magnification. We acquired images before treatment as a baseline (B.L) and then every 2 h for 3 days. Live Mitotimer analysis was conducted within a small ROI placed on distal cell processes to ensure the selection of cellular endpoints. A minimum of 12 processes were analyzed for each image sequence. Briefly, Total mitotimer was obtained from the two fluorescent channels and used for segmentation. Only individual and well reconstructed mitochondria were considered for measurements of morphology and fluorescence intensity values (Red and Green intensities, red/green ratio, elongation, area, length, skeleton branches, junctions, circularity, diameter, surface, shape factor, and mitochondria number). Finally, after log transformation and averaging by frame, a score was calculated a the fold-change relatively to the first frame (baseline). To analyze mitochondrial ATP levels in neurons with neuronal Go-ATeam2 [11] expression, single mitochondrial units were semi manually segmented into 12 axons per replicate to conduct ratio measurements. The measurements were further processed like Mitotimer.

Synaptosome extraction

The cells were rinsed several times, collected, and snap-frozen. Homogenization was performed on ice in PBS. The samples were centrifuged at 1300 × g for 3 min at 4° C to pull down the membrane fragments, nuclei, and cells. The supernatant was coupled with Anti-tomm22 micro-Beats (30min at 4° C) to remove free mitochondria through Magnetic-assisted cell sorting (MACS) (Miltenyi Biotec, 130-096-946, 130-042-401). The mitochondria-depleted flow-through was centrifuged at 13,000 × g for 10 min at 4° C to pellet synaptosomes (100ul of PBS resuspension, stored frozen until further analysis).

Synaptosomes proteomic mass spectrometry

(1) Protein digestion: Synaptosomal fractions were digested according to a modified version of the iST method 80 (named miST method). Briefly, 50 µl solution of PBS was supplemented with 50 µl miST lysis buffer (1% sodium deoxycholate, 100 mM Tris pH 8.6, 10 mM DTT) and heated at 95°C for 5 min. Samples were then diluted 1:1 (v:v) with water, and reduced disulfides were alkylated by adding ¼ vol of 160 mM chloroacetamide (final 32 mM) and incubating at 25°C for 45 min in the dark. Samples were adjusted to 3 mM EDTA and digested with 0.5 µg Trypsin/LysC mix (Promega #V5073) for 1h at 37°C, followed by a second 1h digestion with a second and identical aliquot of proteases. To remove sodium deoxycholate and desalt peptides, two sample volumes of isopropanol containing 1% TFA were added to the digests, and the samples were desalted on a strong cation exchange (SCX) plate (Oasis MCX; Waters Corp., Milford, MA, USA) by centrifugation. After washing with isopropanol/1%TFA, peptides were eluted in 250 µl of 80% MeCN, 19% water, and 1% (v/v) ammonia; **(2)** Liquid chromatography-tandem mass spectrometry: Eluates after SCX desalting were frozen, dried, and resuspended in variable volumes of 0.05% trifluoroacetic acid and 2% acetonitrile to equilibrate concentrations. Approximately 1 µg of each sample was injected into the column for nanoLC-MS analysis. **(3)** M.S. and M.S. data analysis: Dependent LC-MS/MS analysis of the TMT sample was performed on a Fusion Tribrid Orbitrap mass spectrometer (Thermo Fisher Scientific) interfaced through a nano-electrospray ion source to an Ultimate 3000 RSLCnano HPLC system (Dionex). Peptides were separated on a reversed-phase custom-packed 40 cm C18 column (75 µm ID, 100 Å, Reprosil Pur 1.9 µm particles, Dr. Maisch, Germany) with a 4-76% acetonitrile gradient in 0.1% formic acid (total time 140 min). Full MS survey scans were performed at 120'000 resolution. A data-dependent acquisition method controlled by the Xcalibur 4.2 software (Thermo Fisher Scientific) was used to optimize the number of precursors selected ("top speed") of charge 2+ to 5+ while maintaining a fixed scan cycle of 1.5s. The precursor isolation window used was 0.7 Th. Full survey scans were performed at a 120'000 resolution, and a top speed precursor selection strategy was applied to maximize acquisition of peptide tandem M.S. spectra with a maximum cycle time of 0.6s. HCD

fragmentation mode was used at a normalized collision energy of 32% with a precursor isolation window of 1.6 m/z, andthe MS/MS spectra were acquired in the ion trap. The peptides selected for MS/MS were excluded from further fragmentation for 60s. Tandem MS data were processed using MaxQuant software (version 1.6.3.4) 81 incorporating the Andromeda search engine 82. UniProt reference proteome (RefProt) databases for Homo sapiens and mice were used, supplemented with sequences of common contaminants. Trypsin (cleavage at K, R) was used as the enzyme definition, allowing for two missed cleavages. The carbamidomethylation of cysteine was specified as a fixed modification. N-terminal acetylation of proteins and oxidation of methionine are specified as variable modifications.

Proteomic data analysis

MaxQuant data were further processed using the Perseus software[12] and Microsoft Excel. We used a cutoff for the presence of a protein in a sample such as Razor Peptide Score >2 and MS/MS Count >2; 29% of the proteins were discarded in this process. IBAQ values are the sum of the intensities of all unique peptides for a protein divided by the number of theoretical tryptic peptides between six and 30 amino acids in length[17]. LFQ were calculated according to the number of unique peptides of a protein on the total number of peptides. The relative protein abundance was calculated as the sum of the relative intensity-based absolute quantification (rIBAQ) of all selected proteins that were independently present in each replicate. Protein Annotation was conducted in Perseus using the Gene Ontology databases (Biological Process (B.P.), Cellular Compartment (CC), Molecular Function (M.F.)) [13,14] and MitoCarta3.0 [15,16] databases for mitochondrial protein localization and pathway ontologies. 2D enrichment analysis of annotations was performed in Perseus to assess synaptosomal extraction quality and identify differentially enriched ontologies. We used the MitoCarta annotation to filter the mitochondrial proteins and generate subsets per localization. We conducted a Pearson correlation analysis of the LFQs of mitochondrial proteins in relation to tau protein. We then selected the results with a cutoff of 0.5 on the absolute Pearson coefficient to form groups of positively and negatively correlating (or uncorrelated) proteins. The overrepresentation of pathways at each mitochondrial localization was estimated as the fold-change between the pathway distribution observed from the total Mitocarta database and the distribution observed in the mitochondrial protein subset.

Statistical analysis:

Values are presented as the mean ± SEM; Statistical analyses were performed on raw data with Graphpad Prism software, Shapiro-Wilk tests were performed to test distribution normality. The level of significance was set to $P < 0.05$. Mitochondrial biosensor data were log-transformed, and multiple t-tests for control versus

ePHF conditions were performed at each time point. Mass spectrometry data analysis: 2D annotation enrichment analysis was performed using Benjamini-Hochberg FDR Truncation with a 2% cutoff[18]. Pearson's correlation analysis was used to evaluate the correlation of proteins MAPT amounts. A cutoff with a correlation coefficient ≥0.5 was used to select correlating proteins for further analysis. Synapse active zone analysis: Comparison of counts, surfaces, and volumes was performed with t-tests or Mann-Whitney, respectively, for normal and non-normal distribution of data. Immunohistochemical analysis: one-way ANOVA of optical densities and mitochondrial data.

Results

Impact of ePHF-tau on neurites and synapse development.

In this study, we first isolated PHF-tau from the insoluble sarkosylated fraction extracted from the frontal cortex of Alzheimer's patients. This human PHF-tau was combined with a high amount of monomeric 2N4R tau to generate PHF-tau(2N4R), subsequently referred to as ePHF-tau, following the methodology developed by Courade et al [19]. To further our understanding of the impact of ePHF on neurites and synapses, pure neuronal cultures were exposed to various concentrations of ePHF-tau over different periods of days in vitro (DIV) and for different durations (**Fig.1 a**). Our previous work mentioned that these rat neuronal cultures develop extensive interconnected 2D neuronal networks (**Fig. 1 b**). During this phase, neurite maturation takes place over the first three weeks, while excitatory synaptic maturation is established from the third week [20–22]. We found that prolonged exposure (14 days) to ePHF-tau on early maturing neurons (DIV7) resulted in a significant reduction in both cell density (**Fig. 1c**) and the extent of the neuritic network (**Fig. 1d**), even at a dose of 0.5uM. However, short-term treatment of mature neurons (DIV22), even at high doses of 1.5uM, did not appear to affect cell density (**Fig. 1e**) or neural network complexity (**Fig. 1f**). Subsequently, in order to assess the impact of PHF-tau on synaptic integration, we measured the density of presynaptic (puncta vGlut1+), postsynaptic (puncta PSD-95+) proteins, as well as excitatory active zones defined by the number of pairs of puncta vGlut1+ and PSD-95+ (**Fig. 1g**). Three days of ePHF-tau in the culture medium of mature neurons (DIV22) did not alter the densities of vGlut1+, PSD-95+ or the number of excitatory active zones (**Fig. 1g-j**). However, when cultures were subjected to the same treatment but at a later time (DIV25), we observed that PHF-tau induced a notable increase in the number of vGlut1+ puncta and PSD-95+ puncta, increasing the number of potentially active excitatory synapses (**Fig. 1g, k-m**).

To deepen our analysis of the impact of ePHF-tau on brain cells, We opted to complement our results with mixed neuron-glial 3D cultures **(Fig. 2a)**. These mixed three-dimensional systems offer an organization closer to brain physiology, favoring faster electrical maturation and increased resilience to nerve agents, compared with pure 2D neuronal cultures **(Fig. 2b)** [20]. We observed that culture constitutes an assembly of neurospheroids enriched in neurons (NeuN) and astrocytes (GFAP), and endowed with neurites (NFL) interconnecting spheroids **(Fig. 2b)**. ePHF treatment at a concentration of 0.5 µM does not affect the formation of neurospheroid (**Fig. 2c**), the density of neurons (**Fig. 2d**) and the amount of neurofibrillary fibers that compose them (**Fig. 2e**). Using confocal microscopy imaging and three-dimensional reconstruction of the neurospheroids, we quantified the volumes of vGlut1 and PSD-95 in the proximal neurites to the

neurospheroids (**Fig. 2f-g**). We revealed that exposure to ePHF-tau for three days did not change PSD-95 density (**Fig. 2g-h**) or vGlut1 (**Fig. 2g,i**) volumes. However, the volume of overlap between vGlut1 and PSD-95 is significantly increased by ePHF treatment, suggesting an increase in the number of excitatory active synaptic sites **(Fig. 2g-j)**. These results illustrate how exposure to ePHF-tau affects neurons differently depending on their stage of maturation and organiszation, reducing neurite density and complexity in immature neurons while increasing of excitatory active zone and potential excitotoxicity.

Extracellular PHF-tau impacts the mitochondrial composition of synaptosomes.

To better understand how ePHF-tau treatment could induce potential excitotoxicity, we isolated synaptosomes from 3D cultures 3 days after treatment with ePHF-tau and analyzed using proteomics. (**Fig. 3a**). Enrichment analysis revealed that most proteins were associated with synaptic terms, confirming the quality of the synaptosome isolation (**Fig. 3b**). ePHF-tau treatment affected numerous G.O. terms that were notably related to mitochondrial respiratory chain and regulation of mitochondrial membrane potential (**Fig. 3b**). Interestingly, consistent with our microscopy data (**Fig. 1-2**), another most differentially enriched G.O. terms were associated with intracellular transport and glutamate metabolism (**Fig. 3b**). In synaptosomes, we have observed that the amount of tau protein is highly correlated with the presence of mitochondrial protein from the inner membrane (I.M.) and intermembrane space (IMS), (**Fig. 3c**). Among these mitochondrial proteins found in synaptosomes we found a significant (8-fold) increase in the number of "central dogma" pathway proteins in the 19 IMS-associated proteins and a 4-fold increase in the number of proteins involved in "signaling" in the 40 mitochondrial matrix proteins (**Fig. 3e**). Together, these results suggest that treatment with ePHF-tau alone can induce significant activation of mitochondrial functions in synapses, which may be responsible for the increase in active zone and potential excitotoxicity.

Mitochondrial monitoring revealed reversed and delayed effects of ePHF-tau on neurons and astrocytes.

The primary challenge with the findings related to mitochondrial disruption at synapses when toxic substances are present extracellularly is the complexity of discerning whether this disruption is a direct effect on neurons, astrocytes, or a secondary response to the disturbance of either population. To improve this understanding, a continuous monitoring of the dynamic effects of ePHF-tau on mitochondrial function in different cell subpopulation may provide many clues. In this context, we employed lentivirus-mediated expression of MitoTimer and MitoGo-ATeam2 biosensors, which specifically target neurons or astrocytes [8,9]. We monitored the mitochondrial dynamics within neurites (**Fig. 4**) and astrocytic fine processes (**Fig. 5**) over a 72-hour

posttreatment period using advanced fluorescence microscopy equipped for high-throughput acquisition and analysis. Observations were conducted at 2-hour intervals, amounting to approximately 35 timepoints. As previously described, each measured parameter is normalized with reference to its base state obtained in the first acquisition [9,21].

In neurites (Fig. 4), we revealed that treatment with ePHF-tau induced significant, rapid (from 10 h) and lasting (over 70 h) changes in neurite mitochondria (**Fig. 4a-k**). We observed a significant increase in mitochondrial ATP production **(Fig. 4d)** and mitochondrial oxidation **(Fig. 4f-g).** The primary contributor to mitochondrial oxidation (**Fig. 4e**) was an increase in the level of oxidized complexes (red color from Mitotimer) (**Fig. 4f**) rather than a reduction in mitochondrial biogenesis (green color from Mitotimer) (**Fig. 4g**). Moreover, ePHF-tau induced mitochondrial enlargement with a swollen morphology **(Fig. 4h-k).** Mitochondrial swelling in neurites is characterized by increased diameter, surface area, and length (**Fig. 4h-j**). Additionally, we observed a significant decrease in the shape factor of mitochondria (**Fig. 4k**), suggesting structural modifications with decreased convexity. Despite being administered in a single dose, the treatment progressively escalated toward increased stress conditions over time. In astrocytes processes (**Fig 5a-c**), we found no alterations in the mitochondrial redox state **(Fig 5d, e-g)** or mitochondrial morphology **(Fig 5d, h-k)** within the first 36 hours of treatment. However, significant deviations were observed beyond this period: mitochondrial processes display stronger fluorescence in the greens (**Fig. 5c, d**), corresponding to a decrease in the mitotimer ratio and suggesting increased mitochondrial turnover caused by increased biogenesis. Morphologically **(Fig. 5c, g),** despite the lack of significance, we observed a trend toward mitochondrial filamentation (fusion>fission). These results suggest that neurons are very rapidly sensitive to the effects of ePHF-tau, which will induce strong activation of the mitochondrial system and ultimately its functional disruption, whereas the effect on astrocytes is cocomitant with the neuronal problems and appears more as an increase in biogenesis and dynamics.

Discussion

This study highlights the complexity of the toxic effect of extracellular tau aggregates on mitochondrial and synaptic function. This toxicity affects the mitochondria of neurons both rapidly and progressively, while the mitochondrial system of astrocytes does not appear to be immediately sensitive to these aggregated forms of tau but is stimulated a few days later. At the synaptic level, the effect of ePHF-tau on different synaptic behaviors induces an increase in neuronal excitability, potentially explained by cytotoxicity. Our study used Tau aggregates extracted from the brains of patients diagnosed with A.D. but standardized with tau 2N4R in

monomeric form. Reverse and delayed astrocytic mitochondria responses to ePHF-tau treatment highlight cell-specific vulnerabilities and adaptation mechanisms to mitochondrial stress. Indeed, neurons show very rapid mitochondrial modification, which will lead to severe alteration in the long term. Astrocytes, on the other hand, show a significantly delayed response, synchronized with neuronal alterations, suggesting that the cells are rather reacting than suffering. These results underline the importance of considering the distinct roles and responses of different CNS cell types when exploring the pathophysiology of extracellular forms of tau.

Recent in-depth studies on the consequences of insoluble tau protein deposits in neurons, a characteristic marker of tauopathies, have highlighted the ability of these deposits to generate complex dysfunctions within various signaling pathways. These dysfunctions frequently translate into significant alterations in synaptic function, highlighting the major impact of these aggregates on fundamental neuronal mechanisms [22]. Indeed, soluble tau aggregates have been shown to significantly inhibit long-term depression (LTD) in the dorsal hippocampus of anesthetized rats, revealing their direct influence on synaptic plasticity [23]. The mechanism involves the binding of tau to synaptic vesicles via its N-terminal domain, which disrupts presynaptic functions, including synaptic vesicle mobility and release rate, effectively reducing neurotransmission [24]. Our results revealed that even nonhyperphosphorylated ePHF-tau can significantly increase synaptic active zones. In addition, our proteomic analyses revealed a notable reduction in proteins associated with the conversion of glutamate to GABA in synaptosomes, suggesting a decrease in inhibitory potential, a finding that could partly explain the observed imbalance in inhibitory potential. Previous work has also demonstrated that tau aggregates can alter the function of postsynaptic receptors, such as NMDA and AMPA receptors, contributing to the dysregulation of intracellular calcium homeostasis and increased neurotoxicity [25]. Furthermore, neuronal hyperexcitability and changes in presynaptic markers highlight a loss of balance between excitation and inhibition in neuronal networks [26], an imbalance potentially responsible for the cognitive and behavioral deficits observed in tauopathies [27]. Although the exact mechanisms underlying this synaptic disruption were not directly addressed in our study, our findings reinforce the idea that the effect of tau aggregates does not depend exclusively on the presence of hyperphosphorylated forms, and the strong association with mitochondrial proteins suggests that mitochondrial dysfunction could be one of the earliest signs of synaptic disruption.

The accumulation of tau protein in synapses plays a significant role in the disruption of mitochondrial function, contributing to the neuronal dysfunction characteristic of neurodegenerative pathologies such as A.D. Our study revealed that the mere presence of extracellular tau can significantly affect mitochondrial homeostasis in a very short time. Given the considerable size of ePHFs, our observations suggest two plausible hypotheses:

first, specific fragments of tau, such as the N-terminal region, can detach and infiltrate synapses, rapidly influencing mitochondria; second, the aggregate itself can activate extracellular receptors that modulate mitochondrial homeostasis. Previous studies have shown that the truncated NH2 fragment of tau, 20-22 kDa in size, is mainly present in the mitochondria of cryopreserved synaptosomes from brains affected by A.D. This same Tau NH2 fragment has also been identified in other non-AD tauopathies, indicating its potential role in exacerbating synaptic degeneration in these diseases [28]. Our synaptosome analyses revealed a significant correlation between the amount of tau and the disruption of essential mitochondrial functions. However, our data show no specific enrichment of N-ter or C-ter fragments of human tau in synaptosomes following treatment, suggesting that the disruption is not solely due to these fragments. Research in mouse models has shown that mitochondrial distribution is gradually altered in neurites containing tau aggregates. It has also been established that aggregated tau can inhibit mitochondrial calcium efflux via the mitochondrial Na+/Ca2+ exchanger (NCLX), thus affecting neurons [29]. Our study highlights that the mere presence of ePHF is sufficient to induce a rapid and marked increase in ATP production by mitochondria in neurites, subsequently leading to extensive fragmentation and oxidation of mitochondria. These findings suggest potential underlying mechanisms by which neurons release Tau aggregates, raising crucial questions about the relevance of specific treatments currently in phase 2 and 3 clinical trials.

Astrocytes play an essential role in the evolution of tauopathies, influencing the progression of these diseases through their accumulation of tau and their ability to capture and diffuse pathological tau. Changes in their phenotype in the context of tauopathies can lead to dysfunctions that compromise their support of neurons or cause neurotoxicity [30]. Furthermore, specific expression of Tau 4R in mice expressing human tau has been shown to worsen seizure severity and increase phosphorylated Tau deposition without inducing neuronal or synaptic loss [31]. Our research revealed that only the accumulation of Tau 3R, not Tau 4R, in dentate gyrus astrocytes led to mitochondrial disruption, neuronal dysfunction, and memory deficits in mice[8]. Our recent studies also indicated that mitochondria from iPSC-derived astrocytes accelerate turnover and increase filamentation when exposed to extracellular vesicles from neurons that accumulate tau 1N4Rs, whereas they fragment and oxidize in response to those from neurons that accumulate tau 1N3Rs [9].

In our experiment with 2N4R tau aggregates on astrocytes, we also observed a significant increase in mitochondrial turnover and filamentation, although these changes took longer to appear as with 4R neuron-derived E.V.s. Initially, the mitochondrial system of astrocytes shows few changes in the first two days after exposure to PHF-tau 2N4R, suggesting that filamentation and increased mitochondrial turnover might indicate a proinflammatory profile [32,33]. This observation raises the hypothesis that astrocytes and their

mitochondrial system might be less sensitive to these forms of 2N4R aggregates than to those present in or on extracellular vesicles. In this study, we did not explore the mechanisms underlying these effects, particularly the potential for capture by the LRP1 protein which is present in astrocytes and plays a crucial role in eliminating certain forms of amyloid aggregates. It is difficult to determine whether this cellular adaptation results from a response to distress in neighboring neurons or whether astrocytes have captured forms of tau that have activated them. Another hypothesis beside usual signal of stress transmission to glia, could be that neurons transfer dysfunctional mitochondria to astrocytes, as recently demonstrated in different brain injury contexts [34] and to microglia [35].

Conclusion

This study highlights the variability of the response of the mitochondrial system to tau aggregates, emphasizing that this reaction depends on the cell type involved. This discovery could shed light on some of the obstacles encountered by clinical trials in their quest for drugs and antibodies capable of reducing the pathological burden of tau. This study also highlights the crucial importance of considering tau's different forms and isoforms in the design of future preclinical drug trials. This perspective emphasizes the need for a more nuanced and personalized approach in the search for effective treatments for tauopathy diseases, reflecting the inherent complexity of these pathologies and the diversity of cellular responses they engender. Ultimately, our results reinforce the idea that the fight against tauopathies requires an in-depth understanding of the molecular mechanisms specific to each cellular context, paving the way for more targeted and potentially more effective therapeutic strategies.

List of abbreviations

A.D.: Alzheimer's disease

ePHF-tau: extracellular paired helical filaments of tau

FTD: Frontotemporal dementia

LV: Lentiviral Vector

NFT: Neurofibrillary tangles of tau

PHF-tau: paired helical filaments of tau.

PSP: progressive supranuclear palsy

ROI: Region of interest

VOI: Volume of interest

Acknowledgments

The authors thank Maria Rey and Nicole Déglon, Lausanne University Hospital (CHUV) and University of Lausanne (UNIL), Department of Clinical Neurosciences (DNC), and Laboratory of Cellular and Molecular Neurotherapies (LCMN) for their help in the production of lentiviral vectors.

Funding

This work was supported by the Synapsis Foundation, Novartis Foundation, MCM and an A.C. Immune Research Fund.

Author contributions

Study design and conceptualization: K.R. Writing, review, and editing: K.R, V.Z. Support for manuscript editing: N.P. Experimentation: E.P, V.Z, A.B, Y.V, K.F. Funding acquisition: K.R, F.C. Supervision: K.R. All authors have read and agreed to the published version of the manuscript.

Ethics declarations

For murine-derived primary cultures, experiments were performed according to an ethics protocol approved by our institutional review committee CER-VD 2018-01622, Lausanne, Switzerland.

References

1. Pidara I, Yamada K. The Structure of Tau Proteins and Its Role in Neurodegenerative Disease. FASEB J [Internet]. 2022;36. Available from: https://onlinelibrary.wiley.com/doi/full/10.1096/fasebj.2022.36.S1.R4663

2. Olfati N, Shoeibi A, Litvan I. Clinical Spectrum of Tauopathies. Front Neurol [Internet]. 2022;13. Available from: https://pubmed.ncbi.nlm.nih.gov/35911892/

3. Rösler TW, Tayaranian Marvian A, Brendel M, Nykänen NP, Höllerhage M, Schwarz SC, et al. Four-repeat tauopathies. Prog Neurobiol [Internet]. 2019 [cited 2020 Jul 7];180:101644. Available from: https://pubmed.ncbi.nlm.nih.gov/31238088/

4. Gerando AM De, Welikovitch LA, Khasnavis A, Commins C, Glynn C, Chun JE, et al. Tau seeding and spreading in vivo is supported by both AD-derived fibrillar and oligomeric tau. Acta Neuropathol. 2023;146:191.

5. Vogel JW, Iturria-Medina Y, Strandberg OT, Smith R, Levitis E, Evans AC, et al. Spread of pathological tau proteins through communicating neurons in human Alzheimer's disease. Nat Commun. 2020;11.

6. Varghese M, Santa-Maria I, Ho L, Ward L, Yemul S, Dubner L, et al. Extracellular Tau Paired Helical Filaments Differentially Affect Tau Pathogenic Mechanisms in Mitotic and Post-Mitotic Cells: Implications for Mechanisms of Tau Propagation in the Brain. J Alzheimers Dis. 2016;54:477–96.

7. Tejeda HA, Wu J, Kornspun AR, Pignatelli M, Kashtelyan V, Krashes MJ, et al. Pathway- and Cell-Specific Kappa-Opioid Receptor Modulation of Excitation-Inhibition Balance Differentially Gates D1 and D2 Accumbens Neuron Activity. Neuron [Internet]. 2017;93:147–63. Available from: https://pubmed.ncbi.nlm.nih.gov/28056342/

8. Richetin K, Steullet P, Pachoud M, Perbet R, Parietti E, Maheswaran M, et al. Tau accumulation in astrocytes of the dentate gyrus induces neuronal dysfunction and memory deficits in Alzheimer's disease. Nat Neurosci. 2020;23:1567–79.

9. Perbet R, Zufferey V, Leroux E, Parietti E, Espourteille J, Culebras L, et al. Tau Transfer via Extracellular Vesicles Disturbs the Astrocytic Mitochondrial System. Cells [Internet]. 2023;12. Available from: /pmc/articles/PMC10093208/

10. Schwab LCCL, Richetin K, Barker RARARA, Déglon N, D??glon N, Déglon N. Formation of hippocampal mHTT aggregates leads to impaired spatial memory, hippocampal activation and adult neurogenesis. Neurobiol Dis [Internet]. 2017;102:105–12. Available from: http://linkinghub.elsevier.com/retrieve/pii/S0969996117300529

11. Nakano M, Imamura H, Nagai T, Noji H. Ca(2+) regulation of mitochondrial ATP synthesis visualized at the single cell level. ACS Chem Biol [Internet]. 2011;6:709–15. Available from: http://dx.doi.org/10.1021/cb100313n

12. Tyanova S, Temu T, Sinitcyn P, Carlson A, Hein MY, Geiger T, et al. The Perseus computational platform for comprehensive analysis of (prote)omics data. Nat Methods. 2016;13:731–40.

13. Aleksander SA, Balhoff J, Carbon S, Cherry JM, Drabkin HJ, Ebert D, et al. The Gene Ontology knowledgebase in 2023. Genetics. 2023;224.

14. Ashburner M, Ball CA, Blake JA, Botstein D, Butler H, Cherry JM, et al. Gene ontology: tool for the unification of biology. The Gene Ontology Consortium. Nat Genet. 2000;25:25–9.

15. Rath S, Sharma R, Gupta R, Ast T, Chan C, Durham TJ, et al. MitoCarta3.0: an updated mitochondrial proteome now with sub-organelle localization and pathway annotations. Nucleic Acids Res [Internet]. 2021;49:D1541–7. Available from: https://pubmed.ncbi.nlm.nih.gov/33174596/

16. Calvo SE, Clauser KR, Mootha VK. MitoCarta2.0: an updated inventory of mammalian mitochondrial proteins. Nucleic Acids Res [Internet]. 2016;44:D1251–7. Available from: https://pubmed.ncbi.nlm.nih.gov/26450961/

17. Schwanhüusser B, Busse D, Li N, Dittmar G, Schuchhardt J, Wolf J, et al. Global quantification of mammalian gene expression control. Nature [Internet]. 2011;473:337–42. Available from: https://pubmed.ncbi.nlm.nih.gov/21593866/

18. Cox J, Mann M. 1D and 2D annotation enrichment: a statistical method integrating quantitative proteomics with

complementary high-throughput data. BMC Bioinformatics. 2012;13 Suppl 1.

19. Courade J-P, Angers R, Mairet-Coello G, Pacico N, Tyson K, Lightwood D, et al. Epitope determines efficacy of therapeutic anti-Tau antibodies in a functional assay with human Alzheimer Tau. 2018;136:729–45.

20. Karahuseyinoglu S, Sekerdag E, Aria MM, Cetin Tas Y, Nizamoglu S, Solaroglu I, et al. Three-dimensional neuron–astrocyte construction on matrigel enhances establishment of functional voltage-gated sodium channels. J Neurochem. 2021;156:848–66.

21. Espourteille J, Zufferey V, Laurent J-H, Richetin K. Live-imaging of Mitochondrial System in Cultured Astrocytes. J Vis Exp [Internet]. 2021 [cited 2022 Jan 28]; Available from: https://pubmed.ncbi.nlm.nih.gov/34866623/

22. Robbins M, Clayton E, Kaminski Schierle GS. Synaptic tau: A pathological or physiological phenomenon? Acta Neuropathol Commun. 2021;9:1–30.

23. Ondrejcak T, Hu NW, Qi Y, Klyubin I, Corbett GT, Fraser G, et al. Soluble tau aggregates inhibit synaptic long-term depression and amyloid β-facilitated LTD in vivo. Neurobiol Dis. 2019;127:582–90.

24. Zhou L, Mcinnes J, Wierda K, Holt M, Herrmann AG, Jackson RJ, et al. ARTICLE Tau association with synaptic vesicles causes presynaptic dysfunction. Nat Commun [Internet]. 2017 [cited 2024 Mar 4];8. Available from: www.nature.com/naturecommunications

25. Italia M, Ferrari E, Diluca M, Gardoni F. NMDA and AMPA Receptors at Synapses: Novel Targets for Tau and α□Synuclein Proteinopathies. Biomedicines. 2022;10.

26. Tai HC, Wang BY, Serrano-Pozo A, Frosch MP, Spires-Jones TL, Hyman BT. Frequent and symmetric deposition of misfolded tau oligomers within presynaptic and postsynaptic terminals in Alzheimer's disease. Acta Neuropathol Commun. 2014;2:1–14.

27. García-Cabrero AM, Guerrero-López R, Giráldez BG, Llorens-Martín M, Ávila J, Serratosa JM, et al. Hyperexcitability and epileptic seizures in a model of frontotemporal dementia. Neurobiol Dis. 2013;58:200–8.

28. Amadoro G, Corsetti V, Stringaro A, Colone M, D'Aguanno S, Meli G, et al. A NH 2 Tau Fragment Targets Neuronal Mitochondria at A.D. Synapses: Possible Implications for Neurodegeneration. J Alzheimer's Dis. 2010;21:445–70.

29. Britti E, Ros J, Esteras N, Abramov AY. Tau inhibits mitochondrial calcium efflux and makes neurons vulnerable to calcium-induced cell death. Cell Calcium. 2020;86:102150.

30. Reid MJ, Beltran-Lobo P, Johnson L, Perez-Nievas BG, Noble W. Astrocytes in Tauopathies. Front Neurol [Internet]. 2020 [cited 2024 Mar 4];11:572850. Available from: www.frontiersin.org

31. Ezerskiy LA, Schoch KM, Sato C, Beltcheva M, Horie K. Jciinsight-7-152012. :1–18.

32. Göbel J, Motori E, Bergami M. Spatiotemporal control of mitochondrial network dynamics in astroglial cells. Biochem Biophys Res Commun [Internet]. 2017;1–9. Available from: http://linkinghub.elsevier.com/retrieve/pii/S0006291X17313220

33. Motori E, Puyal J, Toni N, Ghanem A, Angeloni C, Malaguti M, et al. Inflammation-induced alteration of astrocyte mitochondrial dynamics requires autophagy for mitochondrial network maintenance. Cell Metab [Internet]. 2013 [cited 2017 Aug 23];18:844–59. Available from: http://linkinghub.elsevier.com/retrieve/pii/S1550413113004543

34. Hayakawa K, Esposito E, Wang X, Terasaki Y, Liu Y, Xing C, et al. Transfer of mitochondria from astrocytes to neurons after stroke. Nature [Internet]. 2016;539:551–5. Available from: http://www.nature.com/doifinder/10.1038/nature19805

35. Scheiblich H, Dansokho C, Mercan D, Schmidt S V., Bousset L, Wischhof L, et al. Microglia jointly degrade fibrillar alpha-synuclein cargo by distribution through tunneling nanotubes. Cell [Internet]. 2021;184:5089-5106.e21. Available from: https://doi.org/10.1016/j.cell.2021.09.007

Figures legends

Figure 1: ePHF-tau affects neurites development and synapse maturation. (a) Scheme of the experimental design for tau aggregate treatment in pure neuron cultures. (b) Illustration of a fluorescence micrographs of dapi (DNA) and map2 (neurites) staining, and of the segmentation of neurites and nuclei. (blue squares indicates an examples ROI for subsequent synapses analysis). (c-f) Bar plots of the quantifications of cell numbers (c, e) and neurites total length (d, f), respectively with early or late treatment. (g) Examples ROI image used for synapses marker analysis (PSD-95, vGlut1). White squares correspond to the insets shown on the right, in which examples of the segmentation used for analysis are depicted. (h-J) Bar plots of the control normalized counts of pre-synaptic (h), post-synaptic (i) and associated markers (j) (medians) with early treatment. (k-m) Same as (h-j) for later treatment. (N = 3 cultures, 2 replicates per conditions, 1 large image per replicate, and 3 ROIs per image for synapse analysis; **** $p < 0.0001$).

Figure 2: ePHF-tau induces modifications in synaptic markers in mixed cultures. (a) Scheme of the experimental design for tau aggregate treatment in mixed cultures. (b) Micrographs of a large section of culture depicting neurospheroids in bighfield. Examples of stainings for nucleis, glial and neuronal markers (Dapi, GFAP, NeuN, NFL) . (c-e) Bar plots of the quantification of neuropheroid density (c), as well as NeuN (d) and neurofilament (e) coverage of neurospheroids. (f) Illustration of neurospheroid stained for synaptic markers with example of an analyzed volume depicted with a white rectangle and illustrated in the center. Overlayed white objects (e.g. white arrow) correspond to the identified active zones. On the right, a small diagram illustrating how the active zone object were reconstructed from PSD-95 and vGlut1 signals. (g) Detailed examples of pre and post synaptic markers images (top) and associated 3D reconstruction (bottom). (h-j) Bar plots of the total PSD-95 (h) and vGlut1 (i) volumes (medians), and active zone volume per surface of PSD95. (N = 3 cultures, total of 25 neurospheroids scanned, and 5 neurites VOIs analyzed per image; *** $p < 0.001$).

Figure 3: Effect of ePHF-tau on synaptic mitochondrial composition. (a) Scheme of the experimental design for synaptosome proteomics. (b) Two-dimensional (2D) annotation term enrichment analysis using LFQ as a quantitative indicator of protein abundance. Enrichment scores in the CTRL and ePHF-tau groups are shown on the X- and Y-axes, respectively. The table shows the enriched terms with the top five score differences (red: enriched with tau, blue: depleted). (c) Stacked bar plot of the distribution of mitochondrial proteins in each sublocalization, grouped by the values of their correlation with tau protein levels. (d) Scheme of a mitochondrion labeled with the Mitocarta 3.0 annotations of sublocalization. (e) Heatmap of the over-/underrepresentation of pathways in each subcompartment for mitochondrial-correlated proteins when normalized to the proportions obtained from the total MitoCarta database. Crossed-out cells indicated that these ontologies did not occur in Mitocarta. (N = 3 cultures per condition).

Figure 4: ePHF-tau negatively affects mitochondrial turnover in neurites. (a) Scheme of the experimental design: primary mixed cultures were equipped with mitochondrial sensors and imaged over time in the presence of ePHF-tau. (b) Fluorescence microscopy images of Mitotimer in neurites of the CTRL and ePHF-tau treatment groups at baseline, 24 h and 72 h and a diagram of the analyzed region and the observed mitochondrial effect. (c) Heatmap of p values obtained for the comparison of scores between the CTRL and ePHF-tau treatment groups over time (0-72 h) (multiple t tests; red values indicate p values<0.05). (d-k) Line plots of time series showing significant differences in the mitochondrial ATP content concerning the Mito-GoATeam2 ratio (R/R0, up to 24 h). (d) Mitotimer red (555 nm)/green (488 nm) redox state ratio (e) red (555 nm) fluorescence intensity (f) and green (488 nm) fluorescence intensity (g) and mitochondrial morphology with diameter (h), surface (i), length (j), and shape factor (k). (N = 3 cultures; 24 neurites analyzed per culture, *: p value<0.05, **: p value<0.01.)

Figure 5: ePHF-tau positively affects mitochondrial turnover in astrocytes. (a) Scheme of the experimental design: primary mixed cultures were equipped with specific mitochondrial sensors and imaged over time in the presence of ePHF-tau. (b) Fluorescence microscopy images of astrocyte mitochondria from the CTRL and ePHF-tau treatment groups at baseline and late time points. Single mitochondria on cellular extensions were sampled for analysis. The diagram summarizes the observations. (d) Heatmap of p values obtained for the comparison of scores between the CTRL and ePHF-tau treatment groups over time (0-72 h) (multiple t tests; red values indicate p values<0.05). (e-k) Line plots of time series showing significant differences in mitochondrial features mesures with MitoTimer in astrocytes. (e) Mitotimer Red (555 nm)/Green (488 nm) redox state ratio. (f) Red (555 nm) fluorescence intensity. (g) Green (488 nm) fluorescence intensity of MitoTime. Mitochondrial morphology with diameter (h), surface (i), length (j), and shape factor (k). (N = 3 cultures; 140-150 cells analyzed per culture), *: p value<0.05, **: p value<0.01.

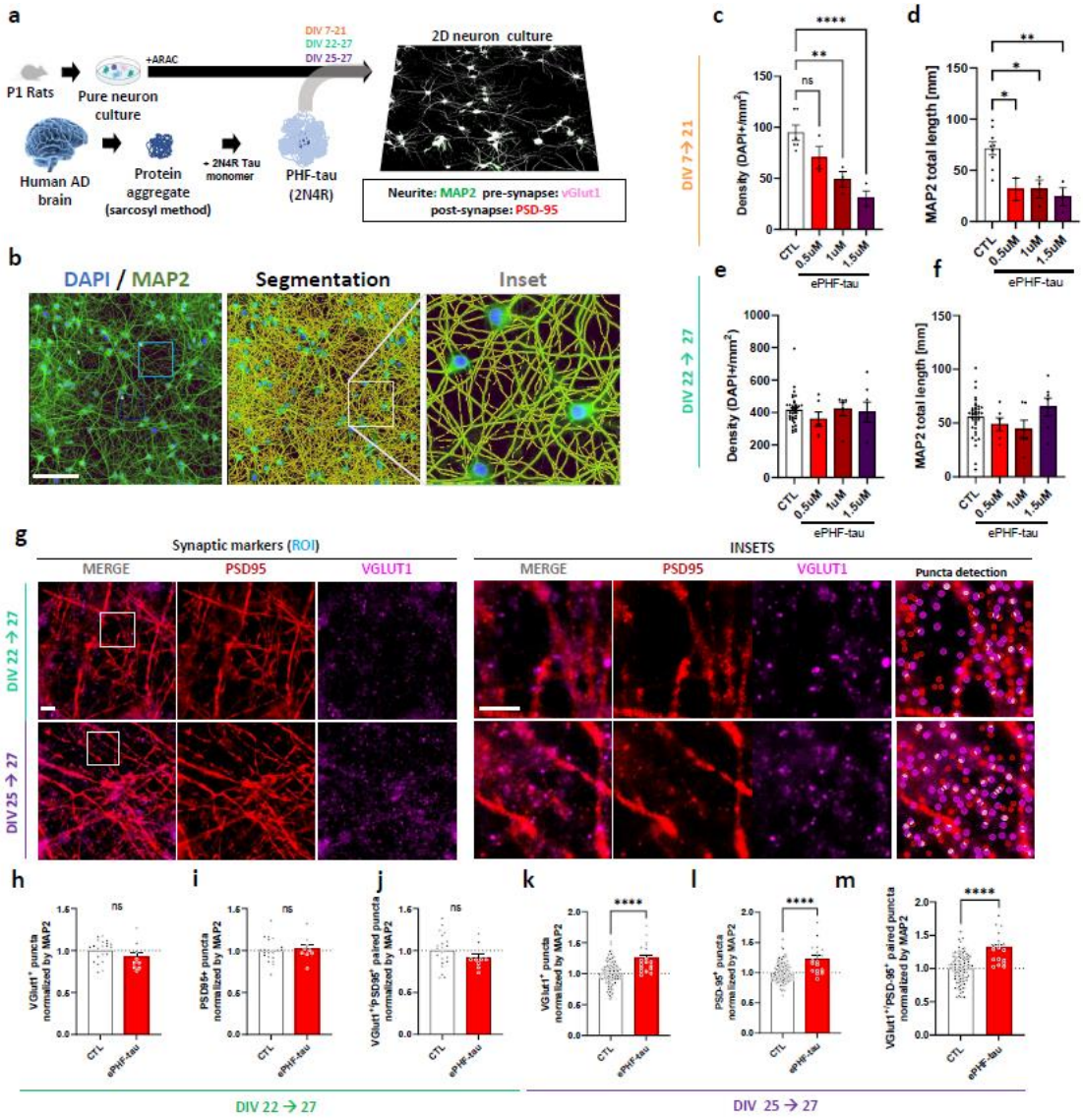
a
P1 Rats
+ARAC
Pure neuron culture
DIV 7-21
DIV 22-27
DIV 25-27
2D neuron culture
Human AD brain
Protein aggregate (sarcosyl method)
+ 2N4R Tau monomer
PHF-tau (2N4R)
Neurite: MAP2 pre-synapse: vGlut1 post-synapse: PSD-95
b
DAPI / MAP2
Segmentation
Inset
c
DIV 7→21
Density (DAPI+/mm²)
CTL
0.5uM
1uM
1.5uM
ePHF-tau
d
MAP2 total length [mm]
e
DIV 22→27
f
g
Synaptic markers (ROI)
INSETS
MERGE
PSD95
VGLUT1
Puncta detection
DIV 22→27
DIV 25→27
h
i
j
k
l
m
ns
DIV 22→27
DIV 25→27

Figure 1

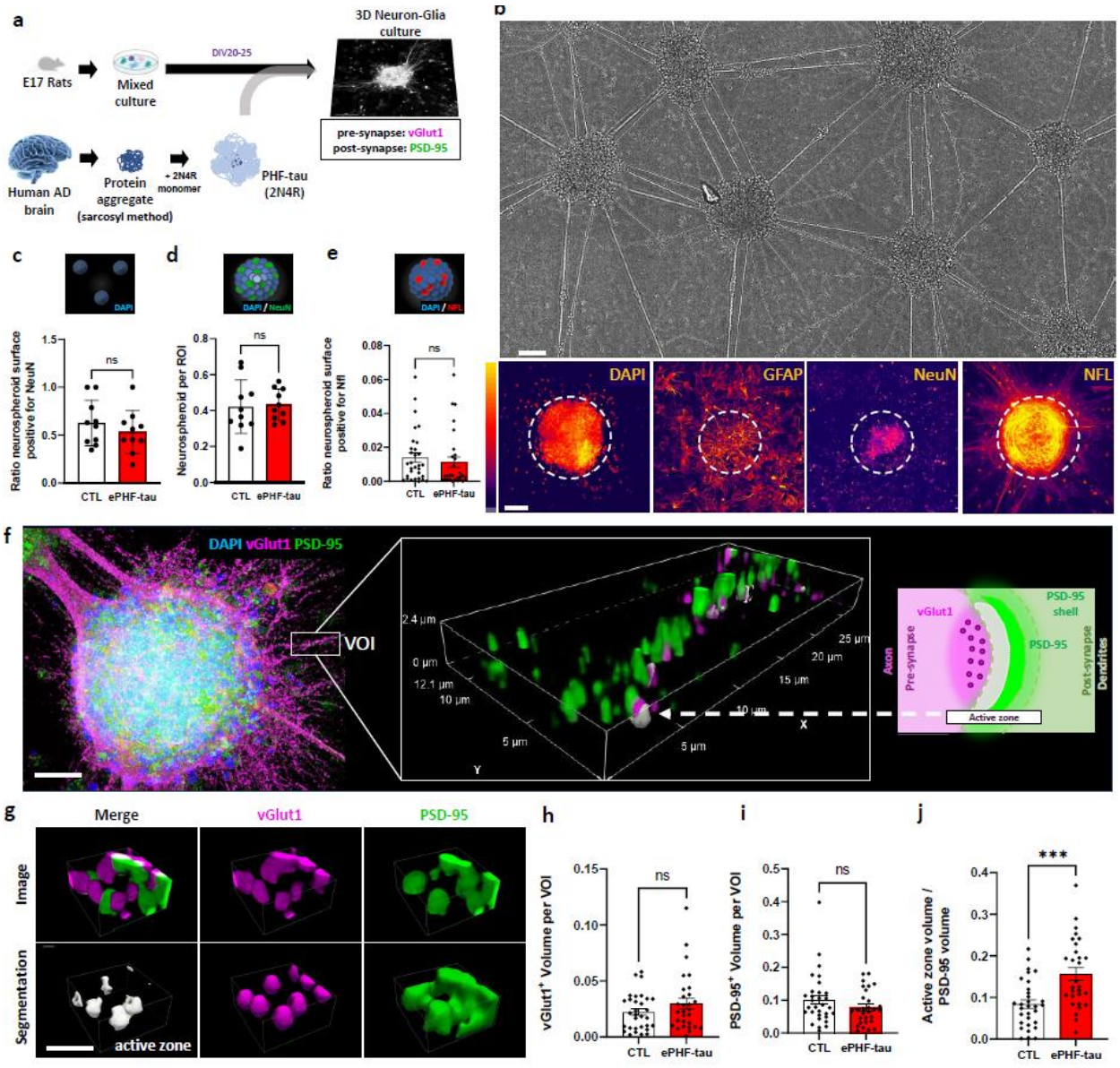
a
E17 Rats
Mixed culture
DIV20-25
3D Neuron-Glia culture
pre-synapse: vGlut1
post-synapse: PSD-95
Human AD brain
Protein aggregate (sarcosyl method)
+ 2N4R monomer
PHF-tau (2N4R)
b
DAPI
GFAP
NeuN
NFL
c
d
e
Ratio neurospheroid surface positive for NeuN
Neurospheroid per ROI
Ratio neurospheroid surface positive for Nfl
ns
CTL
ePHF-tau
f
DAPI vGlut1 PSD-95
VOI
2.4 µm
0 µm
12.1 µm
10 µm
5 µm
25 µm
20 µm
15 µm
10 µm
X
Y
vGlut1
PSD-95 shell
PSD-95
Pre-synapse
Post-synapse
Axon
Dendrites
Active zone
g
Merge
vGlut1
PSD-95
Image
Segmentation
active zone
h
vGlut1+ Volume per VOI
i
PSD-95+ Volume per VOI
j
Active zone volume / PSD-95 volume
***

Figure 2

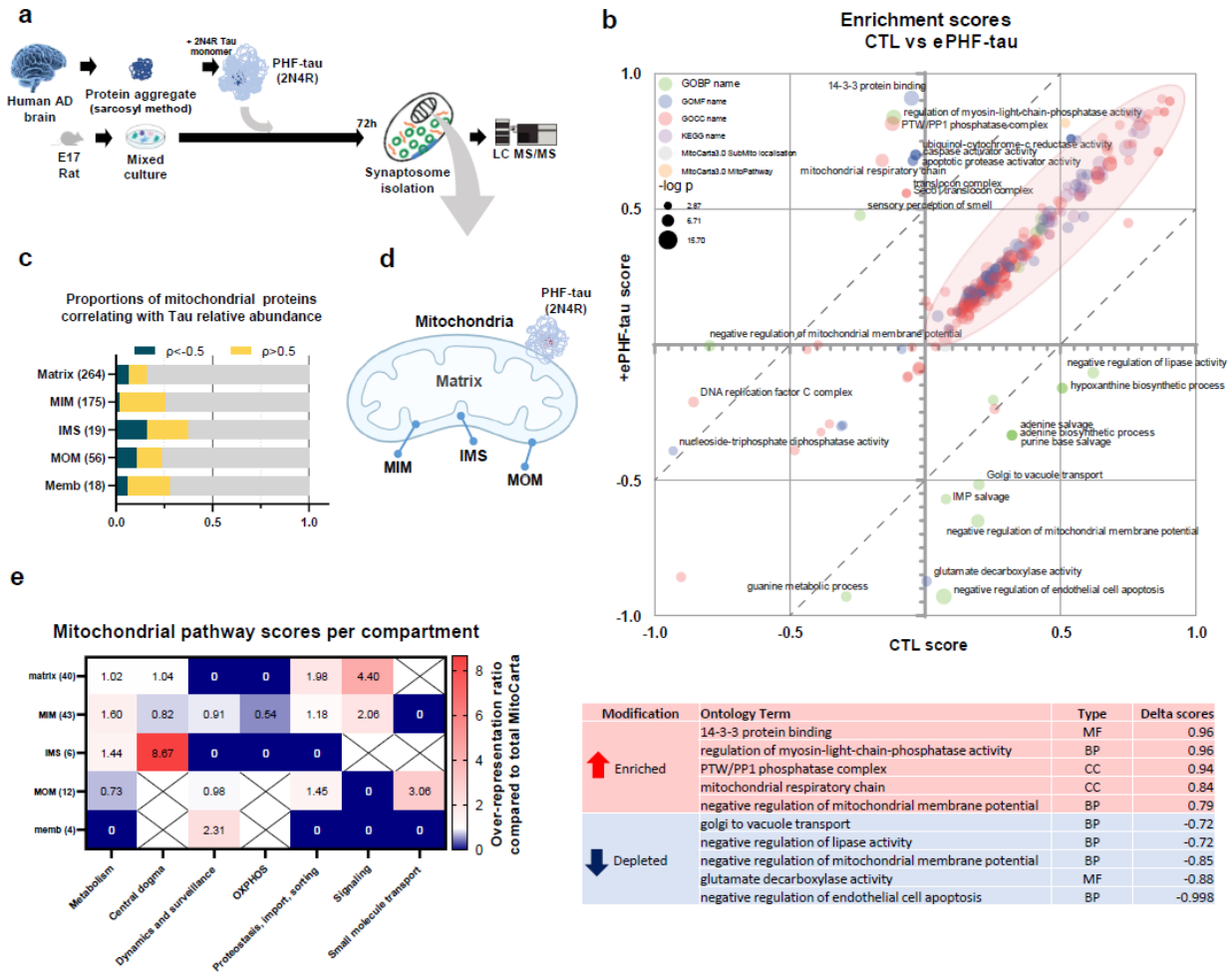

Modification	Ontology Term	Type	Delta scores
Enriched	14-3-3 protein binding	MF	0.96
	regulation of myosin-light-chain-phosphatase activity	BP	0.96
	PTW/PP1 phosphatase complex	CC	0.94
	mitochondrial respiratory chain	CC	0.84
	negative regulation of mitochondrial membrane potential	BP	0.79
Depleted	golgi to vacuole transport	BP	-0.72
	negative regulation of lipase activity	BP	-0.72
	negative regulation of mitochondrial membrane potential	BP	-0.85
	glutamate decarboxylase activity	MF	-0.88
	negative regulation of endothelial cell apoptosis	BP	-0.998

Figure 3

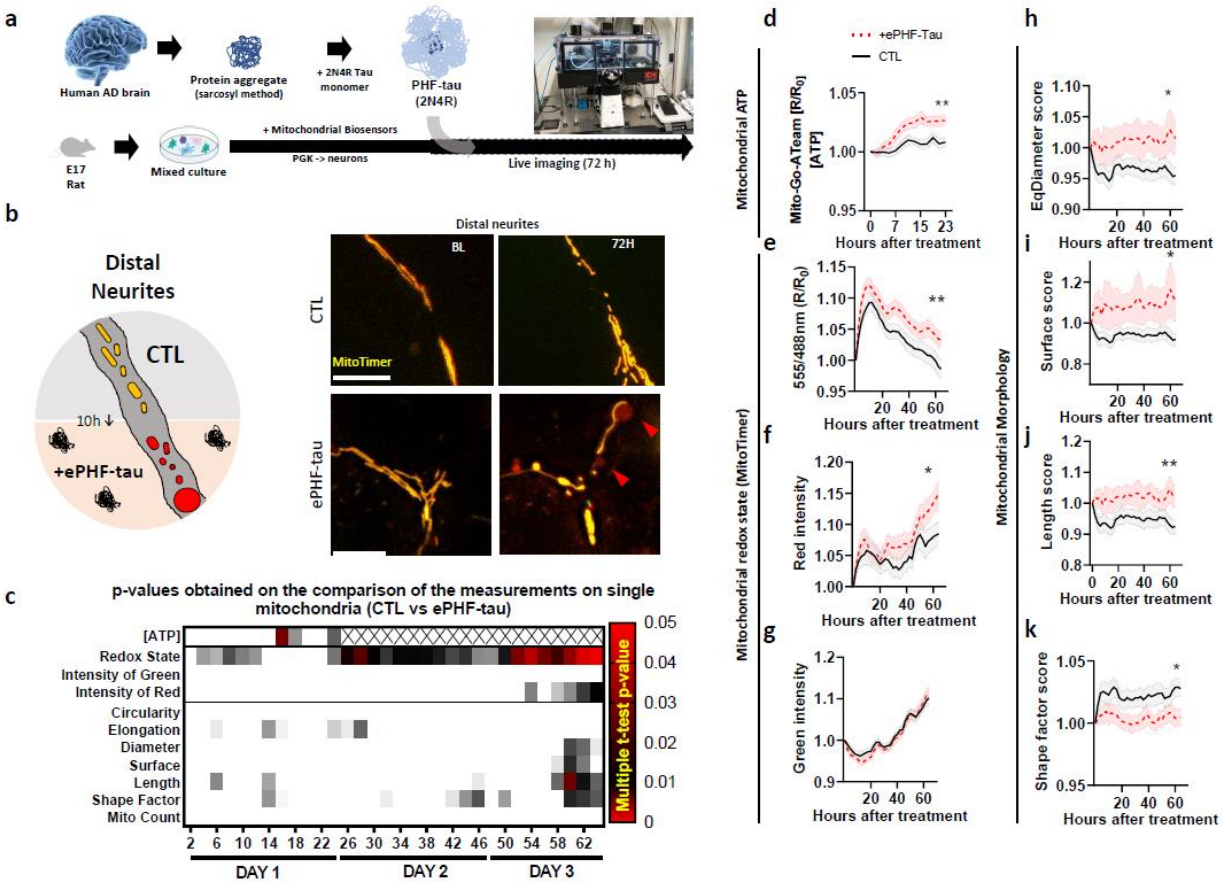
a
Human AD brain
Protein aggregate (sarcosyl method)
+ 2N4R Tau monomer
PHF-tau (2N4R)
E17 Rat
Mixed culture
+ Mitochondrial Biosensors
PGK -> neurons
Live imaging (72 h)
b
Distal Neurites
CTL
10h
+ePHF-tau
Distal neurites
BL
72H
CTL
ePHF-tau
MitoTimer
c
p-values obtained on the comparison of the measurements on single mitochondria (CTL vs ePHF-tau)
[ATP]
Redox State
Intensity of Green
Intensity of Red
Circularity
Elongation
Diameter
Surface
Length
Shape Factor
Mito Count
Multiple t-test p-value
DAY 1
DAY 2
DAY 3
d
+ePHF-Tau
CTL
Mitochondrial ATP
Mito-Go-ATeam [R/R0] [ATP]
Hours after treatment
e
555/488nm (R/R0)
Mitochondrial redox state (MitoTimer)
f
Red intensity
g
Green intensity
h
Mitochondrial Morphology
EqDiameter score
i
Surface score
j
Length score
k
Shape factor score

Figure 4

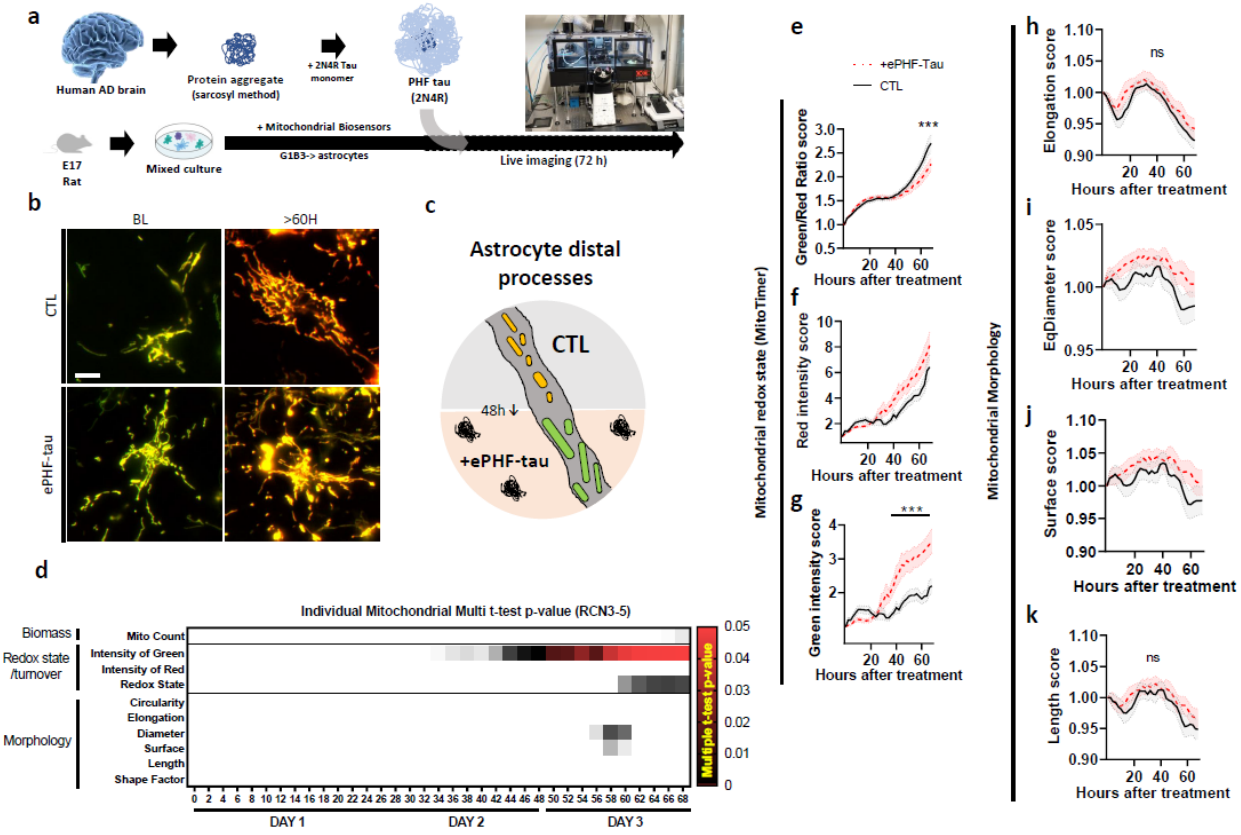
a
Human AD brain
Protein aggregate (sarcosyl method)
+ 2N4R Tau monomer
PHF tau (2N4R)
E17 Rat
Mixed culture
+ Mitochondrial Biosensors
G1B3-> astrocytes
Live imaging (72 h)
b
BL
>60H
CTL
ePHF-tau
c
Astrocyte distal processes
CTL
48h
+ePHF-tau
d
Individual Mitochondrial Multi t-test p-value (RCN3-5)
Biomass
Redox state /turnover
Morphology
Mito Count
Intensity of Green
Intensity of Red
Redox State
Circularity
Elongation
Diameter
Surface
Length
Shape Factor
Multiple t-test p-value
DAY 1
DAY 2
DAY 3
e
+ePHF-Tau
CTL
Green/Red Ratio score
Hours after treatment
f
Red intensity score
Hours after treatment
g
Green intensity score
Hours after treatment
Mitochondrial redox state (MitoTimer)
Mitochondrial Morphology
h
Elongation score
ns
Hours after treatment
i
EqDiameter score
Hours after treatment
j
Surface score
Hours after treatment
k
Length score
ns
Hours after treatment

Figure 5

References

1. Elahi, F. M. & Miller, B. L. A clinicopathological approach to the diagnosis of dementia. *Nat. Rev. Neurol.* **13**, 457–476 (2017).
2. Ciurea, A. V. *et al.* Unraveling Molecular and Genetic Insights into Neurodegenerative Diseases: Advances in Understanding Alzheimer's, Parkinson's, and Huntington's Diseases and Amyotrophic Lateral Sclerosis. *Int. J. Mol. Sci.* **24**, (2023).
3. Wilson, D. M. *et al.* Hallmarks of neurodegenerative diseases. *Cell* **186**, 693–714 (2023).
4. Phatnani, H. & Maniatis, T. Astrocytes in neurodegenerative disease. *Cold Spring Harb. Perspect. Biol.* **7**, 1–18 (2015).
5. Colin, M. *et al.* From the prion-like propagation hypothesis to therapeutic strategies of anti-tau immunotherapy. *Acta Neuropathologica* at https://doi.org/10.1007/s00401-019-02087-9 (2020).
6. Venkatramani, A. & Panda, D. Regulation of neuronal microtubule dynamics by tau: Implications for tauopathies. *Int. J. Biol. Macromol.* **133**, 473–483 (2019).
7. Kent, S. A., Spires-Jones, T. L. & Durrant, C. S. The physiological roles of tau and Aβ: implications for Alzheimer's disease pathology and therapeutics. *Acta Neuropathol.* **140**, 417–447 (2020).
8. Guha, S., Johnson, G. V. W. & Nehrke, K. The Crosstalk Between Pathological Tau Phosphorylation and Mitochondrial Dysfunction as a Key to Understanding and Treating Alzheimer's Disease. *Mol. Neurobiol.* **57**, 5103–5120 (2020).
9. Guo, T., Noble, W. & Hanger, D. P. Roles of tau protein in health and disease. *Acta Neuropathol.* **133**, 665–704 (2017).
10. Sealey, M. A. *et al.* Distinct phenotypes of three-repeat and four-repeat human tau in a transgenic model of tauopathy. *Neurobiol. Dis.* **105**, 74–83 (2017).
11. Zabik, N. L., Imhof, M. M. & Martic-Milne, S. Structural evaluations of tau protein conformation: methodologies and approaches. *Biochem. Cell Biol.* **95**, 338–349 (2017).
12. Espíndola, S. L. *et al.* Modulation of Tau Isoforms Imbalance Precludes Tau Pathology and Cognitive Decline in a Mouse Model of Tauopathy. *Cell Rep.* **23**, 709–715 (2018).
13. Duquette, A., Pernègre, C., Veilleux Carpentier, A. & Leclerc, N. Similarities and Differences in the Pattern of Tau Hyperphosphorylation in Physiological and Pathological Conditions: Impacts on the Elaboration of Therapies to Prevent Tau Pathology. *Front. Neurol.* **11**, (2021).
14. Dujardin, S. *et al.* Different tau species lead to heterogeneous tau pathology propagation and misfolding. *Acta Neuropathol. Commun.* **6**, 132 (2018).
15. Kovacs, G. G. Astroglia and Tau: New Perspectives. *Front. Aging Neurosci.* **12**, (2020).
16. Strang, K. H., Golde, T. E. & Giasson, B. I. MAPT mutations, tauopathy, and mechanisms of neurodegeneration. *Lab. Investig.* **99**, 912–928 (2019).
17. Kovacs, G. G. Invited review: Neuropathology of tauopathies: Principles and practice. *Neuropathol. Appl. Neurobiol.* **41**, 3–23 (2015).
18. Zhang, Y., Wu, K. M., Yang, L., Dong, Q. & Yu, J. T. Tauopathies: new perspectives and challenges. *Mol. Neurodegener.* **17**, 1–29 (2022).
19. Orr, M. E., Sullivan, A. C. & Frost, B. A Brief Overview of Tauopathy: Causes, Consequences, and Therapeutic Strategies. *Trends in Pharmacological Sciences* at https://doi.org/10.1016/j.tips.2017.03.011 (2017).
20. Coughlin, D. & Irwin, D. J. Emerging Diagnostic and Therapeutic Strategies for Tauopathies. *Curr. Neurol. Neurosci. Rep.* **17**, 72 (2017).

21. Cummings, J., Lee, G., Zhong, K., Fonseca, J. & Taghva, K. Alzheimer's disease drug development pipeline: 2021. *Alzheimer's Dement. Transl. Res. Clin. Interv.* **7**, (2021).

22. Olfati, N., Shoeibi, A. & Litvan, I. Clinical Spectrum of Tauopathies. *Front. Neurol.* **13**, (2022).

23. Riley, K. J., Graner, B. D. & Veronesi, M. C. The tauopathies: Neuroimaging characteristics and emerging experimental therapies. *J. Neuroimaging* **32**, 565–581 (2022).

24. VandeVrede, L., Ljubenkov, P. A., Rojas, J. C., Welch, A. E. & Boxer, A. L. Four-Repeat Tauopathies: Current Management and Future Treatments. *Neurotherapeutics* **17**, 1563–1581 (2020).

25. Irwin, D. J. Tauopathies as clinicopathological entities. *Park. Relat. Disord.* **22**, S29–S33 (2016).

26. Hosseini, A. A. *et al.* Clinical Utility of Cerebrospinal Fluid Aβ42and Tau Measures in Diagnosing Mild Cognitive Impairment in Early Onset Dementia. *J. Alzheimer's Dis.* **87**, 771–780 (2022).

27. Zetterberg, H. & Blennow, K. Moving fluid biomarkers for Alzheimer's disease from research tools to routine clinical diagnostics. *Mol. Neurodegener.* **16**, 10 (2021).

28. Jack, C. R. *et al.* NIA-AA Research Framework: Toward a biological definition of Alzheimer's disease. *Alzheimer's Dement.* **14**, 535–562 (2018).

29. Salvadó, G. *et al.* Specific associations between plasma biomarkers and postmortem amyloid plaque and tau tangle loads. *EMBO Mol. Med.* **15**, 1–16 (2023).

30. Garcia-Escobar, G. *et al.* Blood Biomarkers of Alzheimer's Disease and Cognition: A Literature Review. *Biomolecules* **14**, 1–18 (2024).

31. Milà-Alomà, M. *et al.* Plasma p-tau231 and p-tau217 as state markers of amyloid-β pathology in preclinical Alzheimer's disease. *Nat. Med.* **28**, 1797–1801 (2022).

32. Maschio, C. & Ni, R. Amyloid and Tau Positron Emission Tomography Imaging in Alzheimer's Disease and Other Tauopathies. *Front. Aging Neurosci.* **14**, (2022).

33. Nwamekang Belinga, L. *et al.* Circulating Biomarkers for Alzheimer's Disease: Unlocking the diagnostic potential in Low-and Middle-Income Countries, focusing on Africa. *Neurodegener. Dis.* (2024) doi:10.1159/000538623.

34. Kim, K. Y., Shin, K. Y. & Chang, K. A. GFAP as a Potential Biomarker for Alzheimer's Disease: A Systematic Review and Meta-Analysis. *Cells* **12**, (2023).

35. Leuzy, A. *et al.* Tau PET imaging in neurodegenerative tauopathies—still a challenge. *Mol. Psychiatry* **24**, 1112–1134 (2019).

36. Hu, X., Meier, M. & Pruessner, J. Challenges and opportunities of diagnostic markers of Alzheimer's disease based on structural magnetic resonance imaging. *Brain Behav.* 1–10 (2023) doi:10.1002/brb3.2925.

37. Zecha, J. *et al.* TMT labeling for the masses: A robust and cost-efficient, in-solution labeling approach. *Mol. Cell. Proteomics* **18**, 1468–1478 (2019).

38. Kyalu Ngoie Zola, N. *et al.* Specific post-translational modifications of soluble tau protein distinguishes Alzheimer's disease and primary tauopathies. *Nat. Commun.* **14**, 1–17 (2023).

39. Dang, X. T. T., Kavishka, J. M. & Zhang, D. X. Extracellular Vesicles as an E ffi cient and Versatile. *Cells* **9**, 2191 (2020).

40. Doyle, L. & Wang, M. Overview of Extracellular Vesicles, Their Origin, Composition, Purpose, and Methods for Exosome Isolation and Analysis. *Cells* **8**, 727 (2019).

41. Borges, F. T., Reis, L. A. & Schor, N. Extracellular vesicles: structure, function, and potential clinical uses in renal diseases. *Brazilian J. Med. Biol. Res.* **46**, 824–830 (2013).

42. Kalluri, R. & LeBleu, V. S. The biology, function, and biomedical applications of exosomes. *Science* at https://doi.org/10.1126/science.aau6977 (2020).

43. Yáñez-Mó, M. *et al.* Biological properties of extracellular vesicles and their physiological functions. *J. Extracell. Vesicles* **4**, (2015).

44. Hadizadeh, N. *et al.* Extracellular vesicles biogenesis, isolation, manipulation and genetic engineering for potential in vitro and in vivo therapeutics: An overview. *Front. Bioeng. Biotechnol.* **10**, (2022).

45. Liang, W. *et al.* Mitochondria are secreted in extracellular vesicles when lysosomal function is impaired. *Nat. Commun.* **14**, 1–18 (2023).

46. Crewe, C. *et al.* Extracellular vesicle-based interorgan transport of mitochondria from energetically stressed adipocytes. *Cell Metab.* **33**, 1853-1868.e11 (2021).

47. Veziroglu, E. M. & Mias, G. I. Characterizing Extracellular Vesicles and Their Diverse RNA Contents. *Front. Genet.* **11**, 1–30 (2020).

48. Edelmann, M. J. & Kima, P. E. Current Understanding of Extracellular Vesicle Homing/Tropism. *Zoonoses* **2**, (2022).

49. Fitzner, D. *et al.* Selective transfer of exosomes from oligodendrocytes to microglia by macropinocytosis. *J. Cell Sci.* **124**, 447–458 (2011).

50. Pedrioli, G. & Paganetti, P. Hijacking Endocytosis and Autophagy in Extracellular Vesicle Communication: Where the Inside Meets the Outside. *Front. Cell Dev. Biol.* **8**, (2021).

51. Wu, D. *et al.* Profiling surface proteins on individual exosomes using a proximity barcoding assay. *Nat. Commun.* **10**, 1–10 (2019).

52. Hallal, S., Tűzesi, Á., Grau, G. E., Buckland, M. E. & Alexander, K. L. Understanding the extracellular vesicle surface for clinical molecular biology. *J. Extracell. Vesicles* **11**, (2022).

53. Heidarzadeh, M., Zarebkohan, A., Rahbarghazi, R. & Sokullu, E. Protein corona and exosomes: new challenges and prospects. *Cell Commun. Signal.* **21**, 1–15 (2023).

54. Théry, C. *et al.* Minimal information for studies of extracellular vesicles 2018 (MISEV2018): a position statement of the International Society for Extracellular Vesicles and update of the MISEV2014 guidelines. *J. Extracell. Vesicles* **7**, 1535750 (2018).

55. Monguió-Tortajada, M., Gálvez-Montón, C., Bayes-Genis, A., Roura, S. & Borràs, F. E. Extracellular vesicle isolation methods: rising impact of size-exclusion chromatography. *Cell. Mol. Life Sci.* **76**, 2369–2382 (2019).

56. Shi, M., Sheng, L., Stewart, T., Zabetian, C. P. & Zhang, J. New windows into the brain: Central nervous system-derived extracellular vesicles in blood. *Prog. Neurobiol.* **175**, 96–106 (2019).

57. Kumar, A., Nader, M. A. & Deep, G. Emergence of Extracellular Vesicles as “Liquid Biopsy” for Neurological Disorders: Boom or Bust. *Pharmacol. Rev.* **76**, 199–227 (2024).

58. Van Niel, G., D’Angelo, G. & Raposo, G. Shedding light on the cell biology of extracellular vesicles. *Nature Reviews Molecular Cell Biology* at https://doi.org/10.1038/nrm.2017.125 (2018).

59. Lopez, K., Lai, S. W. T., Lopez Gonzalez, E. D. J., Dávila, R. G. & Shuck, S. C. Extracellular vesicles: A dive into their role in the tumor microenvironment and cancer progression. *Front. Cell Dev. Biol.* **11**, 1–18 (2023).

60. Hou, P. pei & Chen, H. zi. Extracellular vesicles in the tumor immune microenvironment. *Cancer Lett.* **516**, 48–56 (2021).

61. Guo, S. *et al.* The role of extracellular vesicles in circulating tumor cell-mediated distant metastasis. *Mol. Cancer* **22**, 1–18 (2023).

62. Wang, S. E. Extracellular vesicles and metastasis. *Cold Spring Harb. Perspect. Med.* **10**, 1–18 (2020).

63. Majood, M., Rawat, S. & Mohanty, S. Delineating the role of extracellular vesicles in cancer metastasis: A comprehensive review. *Front. Immunol.* **13**, 1–17 (2022).

64. Chatterjee, S., Kordbacheh, R. & Sin, J. Extracellular Vesicles: A Novel Mode of Viral Propagation Exploited by Enveloped and Non-Enveloped Viruses. *Microorganisms* **12**, (2024).

65. Xia, X., Wang, Y. & Zheng, J. C. Extracellular vesicles, from the pathogenesis to the therapy of neurodegenerative diseases. *Transl. Neurodegener.* **11**, 1–31 (2022).

66. Leroux, E. *et al.* Extracellular vesicles: Major actors of heterogeneity in tau spreading among human tauopathies. *Mol. Ther.* **30**, 782–797 (2022).

67. Chung, D. eun C., Roemer, S., Petrucelli, L. & Dickson, D. W. Cellular and pathological heterogeneity of primary tauopathies. *Mol. Neurodegener.* **16**, 1–20 (2021).

68. Perbet, R. *et al.* Tau Transfer via Extracellular Vesicles Disturbs the Astrocytic Mitochondrial System. *Cells* **12**, 985 (2023).

69. Li, Q., Babinchak, W. M. & Surewicz, W. K. Cryo-EM structure of amyloid fibrils formed by the entire low complexity domain of TDP-43. *Nat. Commun.* **12**, (2021).

70. Natale, F., Fusco, S. & Grassi, C. Dual role of brain-derived extracellular vesicles in dementia-related neurodegenerative disorders: cargo of disease spreading signals and diagnostic-therapeutic molecules. *Transl. Neurodegener.* **11**, 50 (2022).

71. You, Y. *et al.* Human neural cell type-specific extracellular vesicle proteome defines disease-related molecules associated with activated astrocytes in Alzheimer's disease brain. *J. Extracell. Vesicles* **11**, (2022).

72. Allen, N. J. & Lyons, D. A. Glia as architects of central nervous system formation and function. *Science (80-.).* **362**, 181–185 (2018).

73. Kierdorf, K. & Prinz, M. Microglia in steady state. *J. Clin. Invest.* **127**, 3201–3209 (2017).

74. Taverna, E., Götz, M. & Huttner, W. B. The cell biology of neurogenesis: toward an understanding of the development and evolution of the neocortex. *Annu. Rev. Cell Dev. Biol.* **30**, 465–502 (2014).

75. Lawal, O., Ulloa Severino, F. P. & Eroglu, C. The role of astrocyte structural plasticity in regulating neural circuit function and behavior. *Glia* **70**, 1467–1483 (2022).

76. Beard, E., Lengacher, S., Dias, S., Magistretti, P. J. & Finsterwald, C. Astrocytes as Key Regulators of Brain Energy Metabolism: New Therapeutic Perspectives. *Front. Physiol.* **12**, (2022).

77. Cassé, F., Richetin, K. & Toni, N. Astrocytes' contribution to adult neurogenesis in physiology and Alzheimer's disease. *Front. Cell. Neurosci.* **12**, 1–13 (2018).

78. Shan, L., Zhang, T., Fan, K., Cai, W. & Liu, H. Astrocyte-Neuron Signaling in Synaptogenesis. *Front. Cell Dev. Biol.* **9**, (2021).

79. Baldwin, K. T. & Eroglu, C. Molecular mechanisms of astrocyte-induced synaptogenesis. *Curr. Opin. Neurobiol.* **45**, 113–120 (2017).

80. Escalada, P., Ezkurdia, A., Ramírez, M. J. & Solas, M. Essential Role of Astrocytes in Learning and Memory. *Int. J. Mol. Sci.* **25**, 1–15 (2024).

81. Buskila, Y., Bellot-Saez, A. & Morley, J. W. Generating Brain Waves, the Power of Astrocytes. *Front. Neurosci.* **13**, (2019).

82. Allen, N. J. & Eroglu, C. Cell Biology of Astrocyte-Synapse Interactions. *Neuron* **96**, 697–708 (2017).

83. Liu, C. Y., Yang, Y., Ju, W. N., Wang, X. & Zhang, H. L. Emerging roles of astrocytes in neuro-vascular

unit and the tripartite synapse with emphasis on reactive gliosis in the context of alzheimer's disease. *Front. Cell. Neurosci.* **12**, 1–12 (2018).

84. Zhang, W., Xiao, D., Mao, Q. & Xia, H. Role of neuroinflammation in neurodegeneration development. *Signal Transduct. Target. Ther.* **8**, (2023).

85. Bustos, L. M. & Sattler, R. The Fault in Our Astrocytes - cause or casualties of proteinopathies of ALS/FTD and other neurodegenerative diseases? *Front. Mol. Med.* **3**, 1–17 (2023).

86. Smethurst, P., Franklin, H., Clarke, B. E., Sidle, K. & Patani, R. The role of astrocytes in prion-like mechanisms of neurodegeneration. *Brain* **145**, 17–26 (2022).

87. Lana, D., Ugolini, F., Nosi, D., Wenk, G. L. & Giovannini, M. G. The Emerging Role of the Interplay Among Astrocytes, Microglia, and Neurons in the Hippocampus in Health and Disease. *Front. Aging Neurosci.* **13**, (2021).

88. Lawrence, J. M., Schardien, K., Wigdahl, B. & Nonnemacher, M. R. Roles of neuropathology-associated reactive astrocytes: a systematic review. *Acta Neuropathol. Commun.* **11**, 1–28 (2023).

89. Amro, Z., Yool, A. J. & Collins-Praino, L. E. The potential role of glial cells in driving the prion-like transcellular propagation of tau in tauopathies. *Brain, Behav. Immun. - Heal.* **14**, 100242 (2021).

90. Fleeman, R. M. & Proctor, E. A. Astrocytic Propagation of Tau in the Context of Alzheimer's Disease. *Front. Cell. Neurosci.* **15**, 1–9 (2021).

91. Reid, M. J., Beltran-Lobo, P., Johnson, L., Perez-Nievas, B. G. & Noble, W. Astrocytes in Tauopathies. *Front. Neurol.* **11**, (2020).

92. Richetin, K. *et al.* Tau accumulation in astrocytes of the dentate gyrus induces neuronal dysfunction and memory deficits in Alzheimer's disease. *Nat. Neurosci.* **23**, 1567–1579 (2020).

93. Knox, E. G., Aburto, M. R., Clarke, G., Cryan, J. F. & O'Driscoll, C. M. The blood-brain barrier in aging and neurodegeneration. *Mol. Psychiatry* **27**, 2659–2673 (2022).

94. Sanghai, N. & Tranmer, G. K. Biochemical and Molecular Pathways in Neurodegenerative Diseases: An Integrated View. *Cells* **12**, 1–20 (2023).

95. Rayaprolu, S. *et al.* Systems-based proteomics to resolve the biology of Alzheimer's disease beyond amyloid and tau. *Neuropsychopharmacology* **46**, 98–115 (2021).

96. Espourteille, J., Zufferey, V., Laurent, J.-H. & Richetin, K. Live-imaging of Mitochondrial System in Cultured Astrocytes. *J. Vis. Exp.* (2021) doi:10.3791/62957.

97. Zufferey, V. *et al.* Inverse and Postponed Impacts of Extracellular Tau PHF on Astrocytes and Neurons' Mitochondrial Function. *bioRxiv* 2024.03.19.585791 (2024) doi:10.1101/2024.03.19.585791.

98. Cario, A. & Berger, C. L. Tau, microtubule dynamics, and axonal transport: New paradigms for neurodegenerative disease. *BioEssays* **45**, 1–10 (2023).

99. Barbier, P. *et al.* Role of tau as a microtubule-associated protein: Structural and functional aspects. *Front. Aging Neurosci.* **10**, 1–14 (2019).

100. Sferra, A., Nicita, F. & Bertini, E. Microtubule dysfunction: A common feature of neurodegenerative diseases. *Int. J. Mol. Sci.* **21**, 1–36 (2020).

101. Olney, N. T., Spina, S. & Miller, B. L. Frontotemporal Dementia. *Neurol. Clin.* **35**, 339–374 (2017).

102. Kovacs, G. G. *et al.* Distribution patterns of tau pathology in progressive supranuclear palsy. *Acta Neuropathol.* **140**, 99–119 (2020).

103. Stoothoff, W. *et al.* Differential effect of three-repeat and four-repeat tau on mitochondrial axonal transport. *J. Neurochem.* **111**, 417–427 (2009).

104. Kapogiannis, D. *et al.* Association of Extracellular Vesicle Biomarkers with Alzheimer Disease in the Baltimore Longitudinal Study of Aging. *JAMA Neurol.* (2019) doi:10.1001/jamaneurol.2019.2462.

105. Gualerzi, A. *et al.* Extracellular Vesicles as Biomarkers for Parkinson's Disease: How Far from Clinical Translation? *Int. J. Mol. Sci.* **25**, (2024).

106. Dar, G. H. *et al.* Extracellular vesicles: A new paradigm in understanding, diagnosing and treating neurodegenerative disease. *Front. Aging Neurosci.* **14**, 1–13 (2022).

107. Fowler, S. L. *et al.* Extracellular vesicles derived from postmortem human brain tissue contain seed-competent C-terminal tau fragments, and provide proteomic clues to the identity of selectively vulnerable cell populations in human tauopathies. *Alzheimer's Dement.* **16**, 1–2 (2020).

108. Li, T. R. *et al.* Extracellular vesicles as an emerging tool for the early detection of Alzheimer's disease. *Mech. Ageing Dev.* **184**, 111175 (2019).

109. Regalado-Reyes, M. *et al.* Phospho-tau changes in the human CA1 during Alzheimer's disease progression. *J. Alzheimer's Dis.* **69**, 277–288 (2019).

110. Goedert, M., Jakes, R. & Vanmechelen, E. Monoclonal antibody AT8 recognises tau protein phosphorylated at both serine 202 and threonine 205. *Neurosci. Lett.* **189**, 167–170 (1995).

111. Braak, F., Braak, H. & Mandelkow, E.-M. A sequence of cytoskeleton changes related to the formation of neurofibrillary tangles and neuropil threads. *Acta Neuropathol.* **87**, 554–567 (1994).

112. Bertrand, J., Plouffe, V., Sénéchal, P. & Leclerc, N. The pattern of human tau phosphorylation is the result of priming and feedback events in primary hippocampal neurons. *Neuroscience* **168**, 323–334 (2010).

113. Kimura, T. *et al.* Sequential Changes of Tau-Site-Specific Phosphorylation during Development of Paired Helical Filaments. *Dement. Geriatr. Cogn. Disord.* **7**, 177–181 (1996).

114. Su, J. H., Cummings, B. J. & Cotman, C. W. Early phosphorylation of tau in Alzheimer's disease occurs at Ser-202 and is preferentially located within neurites. *Neuroreport* **5**, 2358–2362 (1994).

115. Luna-Muñoz, J., Chávez-Macías, L., García-Sierra, F. & Mena, R. Earliest Stages of Tau Conformational Changes are Related to the Appearance of a Sequence of Specific Phospho-Dependent Tau Epitopes in Alzheimer's Disease1. *J. Alzheimer's Dis.* **12**, 365–375 (2007).

116. McKenzie, A. T. *et al.* Brain Cell Type Specific Gene Expression and Co-expression Network Architectures. *Sci. Rep.* (2018) doi:10.1038/s41598-018-27293-5.

117. Uhlén, M. *et al.* Tissue-based map of the human proteome. *Science (80-.).* **347**, (2015).

118. Dalfó, E., Martinez, A., Muntané, G. & Ferrer, I. Abnormal α-synuclein solubility, aggregation and nitration in the frontal cortex in Pick's disease. *Neurosci. Lett.* **400**, 125–129 (2006).

119. Mori, F. *et al.* Pick's disease: α- and β-synuclein-immunoreactive Pick bodies in the dentate gyrus. *Acta Neuropathol.* **104**, 455–461 (2002).

120. Popescu, A., Lippa, C. F., Lee, V. M.-Y. & Trojanowski, J. Q. Lewy Bodies in the Amygdala. *Arch. Neurol.* **61**, (2004).

121. Wang, P. *et al.* α-Synuclein-carrying astrocytic extracellular vesicles in Parkinson pathogenesis and diagnosis. *Transl. Neurodegener.* **12**, 1–20 (2023).

122. Stuendl, A. *et al.* α-Synuclein in Plasma-Derived Extracellular Vesicles Is a Potential Biomarker of Parkinson's Disease. *Mov. Disord.* **36**, 2508–2518 (2021).

123. Lin, J. *et al.* Plasma glial fibrillary acidic protein as a biomarker of disease progression in Parkinson's disease: a prospective cohort study. *BMC Med.* **21**, 1–14 (2023).

124. Bettcher, B. M. *et al.* Astrogliosis and episodic memory in late life: higher GFAP is related to worse

memory and white matter microstructure in healthy aging and Alzheimer's disease. *Neurobiol. Aging* **103**, 68–77 (2021).

125. Ruan, Z. Extracellular vesicles drive tau spreading in Alzheimer's disease. *Neural Regen. Res.* **17**, 328–329 (2022).

126. Polanco, J. C., Scicluna, B. J., Hill, A. F. & Götz, J. Extracellular vesicles isolated from the brains of rTg4510 mice seed tau protein aggregation in a threshold-dependent manner. *J. Biol. Chem.* (2016) doi:10.1074/jbc.M115.709485.

127. Hagel, L., Östberg, M. & Andersson, T. Apparent pore size distributions of chromatography media. *J. Chromatogr. A* **743**, 33–42 (1996).

128. Kulak, N. A., Pichler, G., Paron, I., Nagaraj, N. & Mann, M. Minimal, encapsulated proteomic-sample processing applied to copy-number estimation in eukaryotic cells. *Nat. Methods* **11**, 319–324 (2014).

129. Cox, J. & Mann, M. MaxQuant enables high peptide identification rates, individualized p.p.b.-range mass accuracies and proteome-wide protein quantification. *Nat. Biotechnol.* **26**, 1367–1372 (2008).

130. Cox, J. *et al.* Andromeda: A peptide search engine integrated into the MaxQuant environment. *J. Proteome Res.* **10**, 1794–1805 (2011).

131. Ashburner, M. *et al.* Gene Ontology: tool for the unification of biology. *Nat. Genet.* **25**, 25–29 (2000).

132. Aleksander, S. A. *et al.* The Gene Ontology knowledgebase in 2023. *Genetics* **224**, 1–14 (2023).

133. Langfelder, P. & Horvath, S. WGCNA: An R package for weighted correlation network analysis. *BMC Bioinformatics* **9**, (2008).

134. Zambon, A. C. *et al.* GO-Elite: A flexible solution for pathway and ontology over-representation. *Bioinformatics* **28**, 2209–2210 (2012).

135. Seyfried, N. T. *et al.* The AMP-AD Consortium. **4**, 60–72 (2018).

136. Dammer, E. CellTypeFET. at https://github.com/edammer/CellTypeFET (2023).

137. Pedregosa, F. *et al.* Scikit-learn: Macihne Learning in Python. *J. Mach. Learn. Res.* **12**, 2825–2830 (2011).

138. Krishnapuram, B. *et al.* KDD '16: Proceedings of the 22nd ACM SIGKDD International Conference on Knowledge Discovery and Data Mining. in *KDD '16: Proceedings of the 22nd ACM SIGKDD International Conference on Knowledge Discovery and Data Mining* (Association for Computing Machinery, 2016). doi:10.1145/2939672.

139. Malia, T. J. *et al.* Epitope mapping and structural basis for the recognition of phosphorylated tau by the anti-tau antibody AT8. *Proteins Struct. Funct. Bioinforma.* **84**, 427–434 (2016).

140. Allen, B. *et al.* Abundant tau filaments and neurodegeneration in mice transgenic for human P301S tau. *J. Neuropathol. Exp. Neurol.* **22**, 9340–9351 (2002).

141. Zheng-Fischhöfer, Q. *et al.* Sequential phosphorylation of Tau by glycogen synthase kinase-3β and protein kinase A at Thr212 and Ser214 generates the Alzheimer-specific epitope of antibody AT100 and requires a paired-helical-filament-like conformation. *Eur. J. Biochem.* **252**, 542–552 (1998).

142. Yoshida, H. & Goedert, M. Sequential phosphorylation of tau protein by cAMP-dependent protein kinase and SAPK4/p38δ or JNK2 in the presence of heparin generates the AT100 epitope. *J. Neurochem.* **99**, 154–164 (2006).

143. Saint-Pol, J., Gosselet, F., Duban-Deweer, S., Pottiez, G. & Karamanos, Y. Targeting and Crossing the Blood-Brain Barrier with Extracellular Vesicles. *Cells* vol. 9 at https://doi.org/10.3390/cells9040851 (2020).

144. Ramos-Zaldívar, H. M. *et al.* Extracellular vesicles through the blood–brain barrier: a review. *Fluids*

Barriers CNS **19**, 1–15 (2022).

145. Lista, S., Faltraco, F. & Hampel, H. Biological and methodical challenges of blood-based proteomics in the field of neurological research. *Prog. Neurobiol.* **101–102**, 18–34 (2013).

146. Reseco, L. *et al.* Characterization of Extracellular Vesicles from Human Saliva: Effects of Age and Isolation Techniques. *Cells* **13**, (2024).

147. Cvjetkovic, A. *et al.* Detailed Analysis of Protein Topology of Extracellular Vesicles–Evidence of Unconventional Membrane Protein Orientation. *Sci. Rep.* **6**, 36338 (2016).

148. Diaz, G. *et al.* Protein digestion, ultrafiltration, and size exclusion chromatography to optimize the isolation of exosomes from human blood plasma and serum. *J. Vis. Exp.* **2018**, 1–6 (2018).

149. Manouchehri Doulabi, E. *et al.* Surface protein profiling of prostate-derived extracellular vesicles by mass spectrometry and proximity assays. *Commun. Biol.* **5**, 1–13 (2022).

150. Belov, L. *et al.* Extensive surface protein profiles of extracellular vesicles from cancer cells may provide diagnostic signatures from blood samples. *J. Extracell. Vesicles* **5**, 1–12 (2016).

151. Löf, L. *et al.* Detecting individual extracellular vesicles using a multicolor in situ proximity ligation assay with flow cytometric readout. *Sci. Rep.* **6**, 1–9 (2016).

152. Woud, W. W. *et al.* An imaging flow cytometry-based methodology for the analysis of single extracellular vesicles in unprocessed human plasma. *Commun. Biol.* **5**, 1–14 (2022).

153. Marchisio, M. *et al.* Flow cytometry analysis of circulating extracellular vesicle subtypes from fresh peripheral blood samples. *Int. J. Mol. Sci.* **22**, 1–18 (2021).

154. Corso, G. *et al.* Systematic characterization of extracellular vesicles sorting domains and quantification at the single molecule–single vesicle level by fluorescence correlation spectroscopy and single particle imaging. *J. Extracell. Vesicles* **8**, (2019).

155. Han, C. *et al.* Single-vesicle imaging and co-localization analysis for tetraspanin profiling of individual extracellular vesicles. *J. Extracell. Vesicles* **10**, (2021).

156. Ma, B. *et al.* Optical Imaging of Single Extracellular Vesicles: Recent Progress and Prospects. *Chem. Biomed. Imaging* **2**, 27–46 (2024).

157. Amrhein, K. *et al.* Dual Imaging Single Vesicle Surface Protein Profiling and Early Cancer Detection. *ACS Appl. Mater. Interfaces* **15**, 2679–2692 (2022).

158. Zhang, X. M. *et al.* Current progression in application of extracellular vesicles in central nervous system diseases. *Eur. J. Med. Res.* **29**, 1–14 (2024).

159. Xu, X. *et al.* Brain-derived extracellular vesicles: Potential diagnostic biomarkers for central nervous system diseases. *Psychiatry Clin. Neurosci.* **78**, 83–96 (2024).

160. Wang, X., Yang, H., Liu, C. & Liu, K. A new diagnostic tool for brain disorders: extracellular vesicles derived from neuron, astrocyte, and oligodendrocyte. *Front. Mol. Neurosci.* **16**, 1–11 (2023).

161. Nogueras-Ortiz, C. J. *et al.* Astrocyte- and Neuron-Derived Extracellular Vesicles from Alzheimer's Disease Patients Effect Complement-Mediated Neurotoxicity. *Cells* **9**, 1618 (2020).

162. Goetzl, E. J. *et al.* Decreased synaptic proteins in neuronal exosomes of frontotemporal dementia and Alzheimer's disease. *FASEB J.* **30**, 4141–4148 (2016).

163. Guha, D. *et al.* Proteomic analysis of cerebrospinal fluid extracellular vesicles reveals synaptic injury, inflammation, and stress response markers in HIV patients with cognitive impairment. *J. Neuroinflammation* **16**, (2019).

164. Ohmichi, T. *et al.* Quantification of brain-derived extracellular vesicles in plasma as a biomarker to diagnose Parkinson's and related diseases. *Park. Relat. Disord.* **61**, 82–87 (2019).

165. Goetzl, E. J. *et al.* Cargo proteins of plasma astrocyte-derived exosomes in Alzheimer's disease. *FASEB J.* **30**, 3853–3859 (2016).

166. Goetzl, E. J., Schwartz, J. B., Abner, E. L., Jicha, G. A. & Kapogiannis, D. High complement levels in astrocyte-derived exosomes of Alzheimer disease. *Ann. Neurol.* **83**, 544–552 (2018).

167. Lemaire, Q. *et al.* Isolation of microglia-derived extracellular vesicles: Towards miRNA signatures and neuroprotection. *J. Nanobiotechnology* **17**, 1–21 (2019).

168. Winston, C. N., Sarsoza, F., Spencer, B. & Rissman, R. A. Characterizing blood-based, microglial derived exosomes (MDEs) as biomarkers for Alzheimer's disease. *Alzheimer's Dement.* **17**, (2021).

169. Visconte, C. *et al.* Plasma microglial-derived extracellular vesicles are increased in frail patients with Mild Cognitive Impairment and exert a neurotoxic effect. *GeroScience* **45**, 1557–1571 (2023).

170. López-Guerrero, J. A., Ripa, I., Andreu, S. & Bello-Morales, R. The role of extracellular vesicles in demyelination of the central nervous system. *Int. J. Mol. Sci.* **21**, 1–18 (2020).

171. Norman, M. *et al.* L1CAM is not associated with extracellular vesicles in human cerebrospinal fluid or plasma. *Nat. Methods* **18**, 631–634 (2021).

172. Buzas, E. I. Opportunities and challenges in studying the extracellular vesicle corona. *Nat. Cell Biol.* **24**, 1322–1325 (2022).

173. Nguyen, V. H. & Lee, B. J. Protein corona: A new approach for nanomedicine design. *Int. J. Nanomedicine* **12**, 3137–3151 (2017).

174. Tóth, E. *et al.* Formation of a protein corona on the surface of extracellular vesicles in blood plasma. *J. Extracell. Vesicles* **10**, (2021).

175. Mangolini, V. *et al.* Biochemical Characterization of Human Salivary Extracellular Vesicles as a Valuable Source of Biomarkers. *Biology (Basel).* **12**, (2023).

176. Singh, P. *et al.* Removal and identification of external protein corona members from RBC-derived extracellular vesicles by surface manipulating antimicrobial peptides. *J. Extracell. Biol.* **2**, (2023).

177. Omasits, U., Ahrens, C. H., Müller, S. & Wollscheid, B. Protter: Interactive protein feature visualization and integration with experimental proteomic data. *Bioinformatics* **30**, 884–886 (2014).

178. D'Acunzo, P. *et al.* Mitovesicles are a novel population of extracellular vesicles of mitochondrial origin altered in down syndrome. *Sci. Adv.* **7**, (2021).

179. Emelyanov, A. *et al.* Cryo-electron microscopy of extracellular vesicles from cerebrospinal fluid. *PLoS One* **15**, 1–11 (2020).

180. Matthies, D. *et al.* Microdomains form on the luminal face of neuronal extracellular vesicle membranes. *Sci. Rep.* **10**, 1–9 (2020).

181. Rani, K. *et al.* Neuronal exosomes in saliva of Parkinson's disease patients: A pilot study. *Park. Relat. Disord.* **67**, 21–23 (2019).

182. Xie, X. *et al.* Urinary Astrocyte-derived Extracellular Vesicles: A Non-invasive Tool for Capturing Human In Vivo Molecular "Movies" of Brain. *medRxiv* 2024.01.12.24301104 (2024) doi:10.1101/2024.01.12.24301104.

183. Wu, J., Liu, G., Jia, R. & Guo, J. Salivary Extracellular Vesicles: Biomarkers and Beyond in Human Diseases. *Int. J. Mol. Sci.* **24**, (2023).